
Advanced State Transition Matrix Computation Algorithms

Trabajo Fin de Máster

Máster Universitario en Ingeniería Aeronáutica

Escuela Técnica Superior de Ingeniería
Aeronáutica y del Espacio

Universidad Politécnica de Madrid



UNIVERSIDAD
POLITÉCNICA
DE MADRID



Autor: Rodrigo Fernández Matilla

Tutor profesional: Víctor Manuel Moreno Villa

Tutor académico: Manuel Pérez Cortés

Marzo 2023

Agradecimientos.

Uno no tiene muchas oportunidades en la vida de plasmar en un papel oficial su gratitud hacia todas las personas que le han ayudado durante el camino, por largo o corto que sea. Bien, pues no desaprovecharé la mía.

Quiero dar las gracias a Víctor y a Thomas, mis tutores y maestros en este proyecto, por toda la confianza, apoyo y conocimiento que me han transmitido. Estoy enormemente agradecido por esta oportunidad. Sólo espero haber estado a la altura, y hacer que todo el tiempo que habéis dedicado a enseñarme, ayudarme y motivarme merezca la pena. Gracias también al equipo de HERA y al resto de la unidad de FSR por el buen rollo, por la predisposición a ayudar a la gente nueva y por ser más que compañeros de trabajo.

En la esfera más personal, quiero mostrar mi agradecimiento a mis padres, Gonzalo y Ángeles, por el ánimo en cada cosa que haga, por aguantar mis numerosos errores y por darme la oportunidad de seguir formándome como persona e ingeniero. El objetivo no ha dejado nunca de ser que estéis orgullosos de mi, sea en la faceta de la vida que sea. Gracias a mi hermano Gonzalo por su la sabiduría que cada día me transmite, y por seguir siendo el ejemplo al que, en algún momento de mi vida, me quiero parecer. Gracias a mi hermana Sofía, a mi abuela Ángela, a Gema y también, por qué no, a mi ahijado Santiago. Gracias por supuesto a Paula, por haberme aguantado estos años, y por tranquilizarme y ayudarme tanto cuando las cosas van mal. Gracias a mis amigos y amigas, sean de Bembibre, de Madrid o de Aquisgrán. Todos habéis formado parte de mi vida durante este período y, en mayor o menor medida, me habéis ayudado a llegar hasta aquí. Una parte de este humilde proyecto os pertenece, y estoy orgulloso de que así sea.

Rodrigo Fernández Matilla

9 de marzo de 2023

Resumen.

Las matrices de transición de estado constituyen una herramienta muy útil para el análisis de movimiento relativo entre vehículos espaciales. El hecho de ser formas lineales y además de soluciones semianalíticas se plasma en las siguientes ventajas:

- a. Dan lugar a un coste computacional razonable, sin comprometer en exceso la precisión numérica.
- b. Su carácter analítico permite extraer conclusiones interesantes sobre el funcionamiento del sistema.

Los modelos linealizados generalmente permiten obtener mejores resultados mediante una mejor modelización del sistema. En el caso de la dinámica espacial relativa, el análisis y la implementación de perturbaciones son vitales, al ser la parte normalmente despreciada y más difícil de modelar del problema. Uno de los efectos más comúnmente analizados en el caso de órbitas terrestres es el campo gravitatorio no esférico, debido esencialmente a ser el más relevante en magnitud en órbitas bajas. La expansión del potencial gravitatorio en armónicos esféricos permite obtener una aproximación ciertamente precisa del mismo, aunque, en función de cómo se aborde, su manejo analítico puede resultar altamente complejo.

Este trabajo trata de proporcionar una visión general sobre la dinámica relativa linealizada entre vehículos espaciales, analizando modelos progresivamente más complejos y precisos, así como introduciendo teorías de perturbaciones – cuyo uso último es la construcción de modelos para dinámica relativa. El concepto de seguridad orbital también es abordado, debido a su vital importancia en el movimiento relativo en cercanía (p.ej., vuelo en formación, *rendez-vous*...).

Abstract.

State Transition Matrices are a very useful and widely used tool for the analysis of linearised spacecraft relative motion. Their closed-form and linear characters bear two main advantages:

- a. A quite good computational cost is achieved, without compromising accuracy more than desired.
- b. Highly insightful knowledge about the dynamics of the system is obtained.

Linearised models return better outcomes the truer-to-life they are. With this in mind, the analysis and implementation of perturbations play an important role, as it is one of the main ways to achieve high accuracy. Earth's non-spherical gravity field is by far the most usually analysed perturbation in Earth orbits, as it has generally the biggest effect (in value). The way in which this perturbation is approached allows for a better or worse reliability of the results.

This thesis intends to provide an outlook on linearised relative motion, evaluating increasingly more complex motion models, and also analysing perturbation theories, whose ulterior use is relative motion. Orbit safety is also recurrently tackled, due to the vital role it plays in close-proximity relative motion.

Contents

Resumen.	v
Abstract.	vii
Nomenclature	xv
Introduction.	xxi
1 General concepts on spacecraft relative dynamics and STMs.	1
1.1 Spacecraft relative dynamics.	1
1.1.1 Rendez-vous.	2
1.1.2 Formation flying.	3
1.2 State transition matrices.	4
1.2.1 Concept: System dynamics.	4
1.2.2 Applications of STMs in celestial mechanics.	6
2 Relative dynamics around a near-circular unperturbed reference orbit.	11
2.1 Introduction.	11
2.2 Motion model: Hill equations.	11
2.2.1 Equations of motion of a spacecraft.	11
2.2.2 Forces in the spacecraft motion problem.	12
2.2.3 Two-body problem.	13
2.2.4 Three-body problem.	15
2.2.5 Differential equations of proximity relative motion.	15
2.2.6 Hill equations.	17
2.3 Solutions of Hill equations.	18
2.3.1 Direct numerical integration.	19
2.3.2 Clohessy-Wiltshire solution and STM.	19
2.3.3 State transition matrix propagation.	21
2.3.4 Jordan canonical decomposition.	22
2.3.5 Results: Comparison against High-Fidelity.	28

2.4	Orbit safety in near-circular orbits.	33
2.4.1	Orbit safety concept.	33
2.4.2	Eccentricity-inclination vector separation strategy.	34
3	Relative dynamics around elliptic reference orbits.	43
3.1	Introduction.	43
3.2	Motion model and STM.	44
3.2.1	Simplification of equations of motion: Yamanaka-Ankersen solution.	44
3.2.2	Yamanaka-Ankersen STM and integration constants.	47
3.2.3	Results: Comparison with HCW and Hi-Fi propagation.	51
3.3	Orbit safety in eccentric, unperturbed orbits.	56
3.3.1	Relative motion description in TAN frame.	56
3.3.2	General trajectories and safe orbits.	58
4	Perturbations: Non-spherical gravity.	65
4.1	Introduction.	65
4.1.1	Relevant perturbations in spacecraft motion.	66
4.1.2	Variational formulation of perturbed motion: Averaging methods.	68
4.2	Non-spherical gravity: General concepts.	73
4.3	J_2 effect analysis.	74
4.3.1	Mean and osculating elements	74
4.3.2	Brouwer's theory.	74
4.3.3	STM approach.	80
4.3.4	Validation.	80
4.4	Kaula's theory.	85
4.4.1	Approach: \mathbf{V}_{lm} function rearrangement.	86
4.4.2	Subfunctions \mathbf{F}_{lmp} , \mathbf{G}_{lpq} and \mathbf{S}_{lmpq}	87
4.4.3	Implementation.	97
4.4.4	Validation.	101
5	Perturbed relative motion.	115
5.1	Introduction.	115
5.1.1	Relative orbit propagation in perturbed relative motion.	115

5.2	Gim-Alfriend STM.	117
5.2.1	Gim-Alfriend STM structure.	117
5.2.2	Linearised mean to osculating transformation.	118
5.2.3	Inverse transformation.	119
5.3	State-of-the art perturbed STMs.	120
5.4	Orbit safety in perturbed motion.	122
5.4.1	Equivalence of cartesian coordinates and relative OEs.	122
5.4.2	Effect of non-spherical gravity field: J_2	126
6	Conclusions and research outlook.	131
A	Absolute and relative orbital element sets.	133
A.1	Introduction.	133
A.2	Absolute element sets.	133
A.2.1	Workflow for transformations between absolute element sets.	133
A.2.2	Element sets.	134
A.3	Relative sets.	138
A.3.1	Workflow for transformations between ROEs.	138
A.3.2	Element sets.	141
B	Cartesian reference systems.	145
B.1	Introduction.	145
B.1.1	Inertial and rotating reference frames.	145
B.1.2	Absolute and relative frames.	145
B.2	Transformations between reference systems.	145
B.2.1	Direct analytical differentiation.	147
B.2.2	Classical motion composition.	148
B.3	Absolute reference systems.	150
B.3.1	Earth-Centered-Inertial reference system (ECI).	150
B.3.2	Earth-Centered, Earth-Fixed reference system (ECEF).	151
B.3.3	Perifocal (PQW) reference frame.	155
B.4	Relative reference systems.	158
B.4.1	RTN reference frame.	158

B.4.2	LVLH reference frame.	160
B.4.3	TAN reference frame.	162
B.5	Conversions from OEs to cartesian coordinates.	164
B.5.1	Keplerian OEs to ECI and vice versa.	164
B.5.2	Relative Keplerian OEs to RTN.	166
C	Analytical mechanics applied to the two-body problem.	169
C.1	Introduction.	169
C.2	Lagrangian formulation.	169
C.2.1	Generalized coordinates & energy of a dynamical system.	169
C.2.2	Lagrangian function.	169
C.2.3	Lagrange equations.	170
C.3	Hamiltonian formulation.	170
C.3.1	Hamiltonian function.	170
C.3.2	Hamilton equations.	170
C.3.3	Canonical transformations.	170
C.3.4	Hamilton-Jacobi theory.	172
C.4	Application to the two-body problem.	173
D	Software & simulator.	175
D.1	Software tool: MATLAB	175
D.2	Code repository.	175
D.2.1	Purpose and approach.	175
D.2.2	General structure.	176
D.2.3	General orbit propagation workflow.	178
D.2.4	High-Fidelity simulator.	179
D.2.5	MATLAB Exchange libraries.	180
E	Miscellaneous	181
E.1	State Transition Matrices.	181
E.1.1	STM for circular, unperturbed reference orbit.	181
E.1.2	STM for elliptic, unperturbed reference orbit.	181
E.1.3	STM for elliptic, J2-perturbed orbit.	182

E.2 Variational equations.	182
E.2.1 Lagrange Planetary Equations.	183
E.2.2 Gauss Variational Equations.	186
E.3 Elliptic anomaly mapping.	187
E.3.1 Angles.	187
E.3.2 Angle rates.	189
E.3.3 Relative anomalies.	189
E.4 Kaula's functions.	190
E.5 Series expansions for β and e/β	195
E.5.1 β series expansion.	195
E.5.2 e/β series expansion.	195
Bibliography	197
General	197
Eccentric Dynamics	198
Perturbations	199
MATLAB Exchange libraries	200
Websites & others	201

Nomenclature

Acronyms

BF	Body-Fixed frame
CR3BP	Circular Restricted Three Body Problem
CW	Clohessy-Wiltshire
ECEF	Earth-Centered Earth-Fixed frame
ECI	Earth-Centered Inertial frame
GA	Gim-Alfriend
HCW	Hill/Clohessy-Wiltshire
Hi-Fi	High-Fidelity
ICs	Initial Conditions
IP	In-plane
IVP	Initial Value Problem
KOE	Keplerian OEs vector
LEO	Low Earth Orbit
LVLH	Local-Vertical, Local-Horizontal frame
MOD	Mean-of-Date frame
NSG	Non-spherical gravity
ODE	Ordinary Differential Equation
OEs	Orbital Elements
OOP	Out-of-plane
PBF	Pseudo-Body-Fixed frame
RTN	Radial-Transverse-Normal frame
SRP	Solar Radiation Pressure
STM	State Transition Matrix
TOD	True-of-Date frame
YA	Yamanaka-Ankersen

General

μ	Gravitational parameter of a celestial body	$\left[\frac{m^3}{s^2} \right]$
\underline{a}_i	Acceleration on body i	$\left[\frac{m}{s^2} \right]$
\underline{F}_i	Force on body i	[N]
a_e	Equatorial radius of a celestial body	[m]
m_i	Mass off body i	[kg]
Mathematics		
$\Delta\bullet$	Variation or increment of a quantity	
$\delta\bullet$	Relative quantity (deputy's minus chief's value)	
Λ	Real or complex eigenvalue matrix	
\mathbb{I}	Identity matrix	
$\Phi(t, t_0)$	State Transition Matrix	
J	Jordan form	
V	Real or complex eigenvector matrix	
\mathbf{A}	System's matrix of a system of ODEs	
\underline{f}	Dynamics function of a system	
$\underline{u}, \underline{y}$	State vector of a system of ODEs	
Orbital elements		
λ	Mean argument of latitude	[rad]
Ω	Right Ascension of Ascending Node	[rad], [deg]
ω	Argument of periapsis	[rad], [deg]
θ	True anomaly	[rad], [deg]
a	Semimajor axis	[m]
E	Eccentric anomaly	[rad]
e	Eccentricity	[--]
F	Eccentric argument of latitude	[rad]
i	Inclination	[rad], [deg]
M	Mean anomaly	[rad]

u	True argument of latitude	$[rad], [deg]$	Subindices
Perturbations			
\overline{OE}	Mean orbital element vector	\bullet_0	Variable at $t = t_0$
\underline{OE}	Osculating orbital element vector	\bullet_C	Variable from the chief spacecraft
ε	Small parameter	\bullet_D	Variable from the deputy spacecraft
H	Hamiltonian of the system	$[- - -]$	
K	Modified Hamiltonian of the system	$ _i$	Expressed in frame i
Useful expressions			
p_i, P_i	Generalized momentum (original or transformed)	$\eta = \sqrt{1 - e^2}$	$[- - -]$
q_i, Q_i	Generalized coordinate (original or transformed)	ϕ, λ	Geodetic latitude and longitude $[rad], [deg]$
R	Disturbing function	? $\rho = 1 + e \cos \theta$	$[- - -]$
S, W	Generating function of the transformation	h	Orbit altitude or orbit momentum $[m]$ or $\left[\frac{m^2}{s} \right]$

List of Figures

1.1	Distributed space systems classification.	2
1.2	Docking and berthing [1].	3
1.3	Covariance ellipsoid evolution along a radial hop.	8
2.1	Difference in relative distance between HCW methods and Hi-Fi (V-bar approach).	30
2.2	x-z trajectory comparison between STM propagation (HCW) and High-Fidelity.	31
2.3	Difference in relative distance between HCW methods and Hi-Fi (R-bar approach).	32
2.4	x-z trajectory comparison between STM propagation (HCW) and High-Fidelity (R-bar approach).	33
2.5	Effect of δr and δu in radial and along-track distances.	35
2.6	Inclination vector and cross-track distance.	37
2.7	Relative motion in RTN frame for $\delta a = 0$ and a general $\delta e - \delta i$ alignment.	40
2.8	Relative motion for parallel and antiparallel $\delta e/\delta i$ vectors.	41
3.1	Workflow of the propagation with YA STM.	51
3.2	Scenario 1($e = 0.1$): Comparison between Hi-Fi, HCW and YA.	53
3.3	Scenario 2 ($e = 0.7$): Comparison between Hi-Fi, HCW and YA.	55
3.4	Safe orbit family: Scenario 1 ($C_1 = 0$).	61
3.5	Safe orbit family: Scenario 2 ($C_1 = C_m$).	62
3.6	Comparison between Peters-Noomen approach and High-Fidelity propagation.	63
4.1	Order of magnitude of various perturbations of a satellite orbit. [3]	67
4.2	Mean to osculating theory versus High-Fidelity propagation.	84
4.3	Workflow of the computation of V_{lm} .	98
4.4	Workflow of the computation of F_{lmp} .	99
4.5	Workflow of the computation of G_{lpq} through Kaula's approach.	100
4.6	Results of Kaula's conversion for scenario 1 ($e = 0.1$).	110
4.7	Results of Kaula's conversion for scenario 2 ($e = 0.01$).	112
4.8	Results of Kaula's conversion for scenario 3 ($e = 0.001$).	114
5.1	Workflow of mean element propagation from and to cartesian states.	116

5.2	Workflows of the conversions from cartesian states to mean elements and vice versa.	116
5.3	Workflow of iterative osculating-to-mean transformation.	120
5.4	J_2 effect on the relative eccentricity and inclination vectors.	130
A.1	Workflow for transforming between two arbitrary absolute element sets.	134
A.2	Frame rotation from inertial to perifocal frame.	135
A.3	Workflow for transforming any relative set into KOE.	140
A.4	Workflow for transforming RKOE into any other set.	141
A.5	Relative eccentricity & inclination vectors.	142
B.1	Absolute and relative frames.	146
B.2	ECI and ECEF reference frames.	151
B.3	Nutation and precession motion [44].	153
B.4	RTN frame [38].	158
B.5	Relative reference frames.	163
D.1	Workflow of the High-Fidelity propagator.	179
D.2	Workflow of the relative dynamics computation through the Hi-Fi simulator.	180
E.1	Workflow of the relative anomaly transformation (eccentric to mean).	190

List of Tables

2.1	Testing scenarios for Hill equations validation [12].	29
2.2	Elapsed time for the computation of V-bar scenario through each HCW method.	31
2.3	Elapsed time for the computation of R-bar scenario through each HCW method.	33
3.1	Testing scenarios for YA STM [4].	52
3.2	Correspondence between QNS and C ROEs.	57
3.3	Parameters of an orbit family.	59
3.4	Testing scenarios for safe orbit implementation [21].	60
4.1	Results of the mean to osculating transformation for both surveyed methods.	81
4.2	Approximations of the J_2 term of the geopotential expansion.	103
4.3	Scenarios for testing Kaula's theory.	108
C.1	Canonical transformation relations [9].	171
E.1	Inclination functions $F_{lmp}(i)$	191
E.2	Derivatives of the inclination functions $dF_{lmp}/di(i)$	192
E.3	Eccentricity functions and its derivatives $G_{lpq}(e)$	194

Introduction.

Spacecraft relative motion is an essential part of distributed space systems analysis. It focuses on the dynamics of two or more vehicles, whose relative position (and generally attitude) should be controlled or at least monitored. Rendez-vous operations, formation flying and satellite constellations are three examples of relative motion, all of them being present in contemporary and past missions. Its relevance cannot be underestimated, and its complexity leads to the currently non-existent quorum on its modelling. However, it is quite widely accepted that linear models using State Transition Matrices (*i.e.* STMs onwards) provides a comforting balance between accuracy and computational cost. One could think that, given the huge computational resources that most people have access to, computational efficiency should not even be a concern. Be that as it may, satellites on-board computers have limited resources, both computational and energy-related. Any reduction in any activity is greatly welcomed, and that naturally includes the GNC computation. That is the reason why this thesis focuses on the review, analysis and implementation of STM models of relative motion.

A bottom-up approach to this topic is herewith followed, starting from the simplest relative motion model (HCW), building up complexity with elliptic models (YA) and finally reaching state-of-the-art perturbed models. With respect to perturbations, non-spherical gravity arises as the main concern, due to its prevailing effect over the other sources - third bodies and drag among others - for the Earth-centered orbits (excluding very low LEO orbits or very high orbits, like GEO).

Chapter 1 provides a brief description of the roots of this thesis. Relative motion and its main branches are firstly described, to then continue with STMs and its applications.

Chapter 2 starts with the development of the equations of relative motion, eventually reaching Hill equations, which model the linearised equations for circular unperturbed reference orbits. Several approaches to its solution are detailed, performing then a small trade-off analysis between them. Finally, orbit safety is presented, to be then applied to the circular, unperturbed case.

Chapter 3 looks for extending the analysis to elliptic (still unperturbed) reference orbits. The state-of-the-art Yamanaka-Ankersen model is developed and tested against a High-Fidelity propagator. To end this chapter, the safe orbit theory is also extended to this elliptic case, through the usage of an analogue set of relative orbital elements and a slightly different relative reference frame.

Chapter 4 tackles the analysis of propagation theory. A brief analysis of averaging methods is discussed, including Von Zeipel's and Lie series' approach. Afterwards, the spotlight is turned on the non-spherical gravity field modelling. The classical Brouwer's theory is first briefed, to then move on to probably the main topic of the thesis: Kaula's theory, which tries to develop a general approach to the spherical harmonic description of the gravity field.

After this theoretical analysis, **chapter 5** moves back to the relative motion field, considering perturbations in this case. An implementation of Brouwer's theory is drafted through Gim-Alfriend STM, after which a survey of the state of the art of perturbed relative motion is presented. To conclude, perturbed orbit safety is simply sketched out.

The pure content of the thesis is then followed by a set of appendices to provide some background in certain relevant topics, if that is required or desired by the reader.

Appendix A provides a comprehensive review and description of the main orbital element sets.

In a somewhat parallel fashion, **appendix B** focuses on the reference systems used or mentioned throughout the thesis, as well as the transformations between them and from/to orbital elements.

The variational formulation of the spacecraft equations of motion is introduced in **appendix C**, providing context for some subjects of perturbation theory.

Appendix D is devoted to the software approach and structure of the developed content during the thesis.

Finally, **appendix E** contains several relevant topics that are not big enough to be included in an individual appendix, and do not fully fit into the existing ones.

The goal of this thesis is then to provide an educated outlook on the linearised formulation of spacecraft relative motion, building up complexity as it unfolds, eventually reaching state-of-the-art models which are actually used in operational missions. Due to the structure of this field, this finds a niche in the manipulation and understanding of perturbations; as a result of which a considerable part of the thesis is devoted to it. The validation and trade-off evaluation of said models is naturally an essential part of this work as well. However, this thesis is not a result-based work: it is rather a knowledge, analysis-based project, which should be kept in mind along its reading.

General concepts on spacecraft relative dynamics and STMs.

1.1 Spacecraft relative dynamics.

Spacecraft relative dynamics is a vast, very relevant and ever-increasing branch of celestial mechanics. It tries to analyze, rather than the motion around a central body, that of a secondary body (or set of bodies) around a primary, assuming that neither of them generate a gravitational effect on each other. This discipline hence focuses on analyzing how a certain force field – which may include different influences – differentially affects two or more different spacecrafts in a mostly common orbit.

Relative dynamics models are regularly reached through the manipulation of the absolute dynamics of each of the spacecrafts, although they come in all kinds of flavours. Some of them may be formulated through variational mechanics, while others are directly derived from Newton's equations of motion. Naturally, there is a variety also in the kind of variables they use, mainly being orbital elements or cartesian coordinates. When the spacecrafts are close enough together, the linearization of the equations becomes a common procedure, simplifying and increasing the efficiency of the formulation at the expense of accuracy. The trade-off between these two figures of merit will be a recurring topic along this thesis.

Spacecraft relative dynamics is embedded in the Distributed Space Systems discipline. A Distributed Space System is a system composed of two or more satellites that work together to accomplish an objective, impossible using a single spacecraft. A diagram of the different sub-groups of missions is shown in figure 1.1. Along this thesis, only proximity motion is considered. Hence, only two branches will be analyzed: rendez-vous and formation flying.

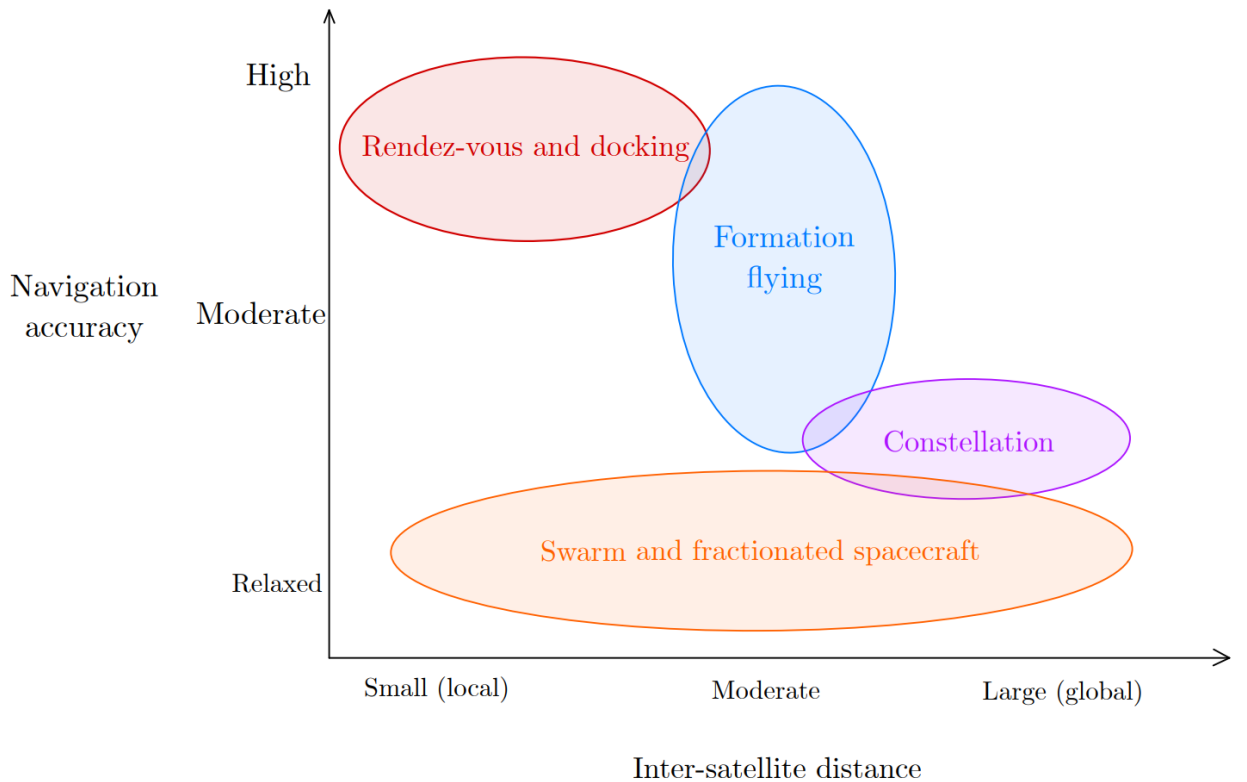


Figure 1.1: Distributed space systems classification.

1.1.1 Rendez-vous.

A rendez-vous flight is basically an operation or a mission in which a spacecraft (chaser or deputy) approaches another one (target or chief) [1]. It is normally followed by a mating procedure, after which both spacecrafts are connected by a rigid link. The final goal of this kinds of missions may be “simply” meet the chief spacecraft (*e.g.* reaching the International Space Station for research purposes), station keeping (*e.g.* maintaining nominal conditions on the orbit of a passive spacecraft through impulses), on-orbit servicing or, lately, debris removal.

A general rendez-vous mission generally consists of the following stages [1]:

- 1st Launch phase and injection: This phase begins with the lift-off, greatly influenced by the launch window, and ends with the chaser vehicle in an injection orbit, considerably below and behind the target.
- 2nd Phasing: This stage aims to reduce the phase angle between the spacecrafts, which is achieved by exploiting the higher orbital rate of lower orbits. This phase ends with the acquisition of either an aim point or an entry gate, which marks the starting point of the rendez-vous procedure.

Two main constraints are usually considered: the phasing constraint (arriving at the correct relative position) and the scheduling constraint (arriving at the correct time).

3rd Far-range rendez-vous: The tasks of this phase are (a) the reduction of approach velocity (b) the synchronisation of the mission timeline and (c) lead the chaser to close proximity. It begins with said vehicle at the aim point and ends with it at the final approach hold point.

4th Close-range rendez-vous: This stage is subdivided into a preparation phase (*i.e.* closing phase) and the final approach. The first one basically is devoted to a controlled range reduction (as well as obtaining the conditions for the final approach) while the latter is aimed to end with mating conditions (axis alignment, etc.). Depending on the kind of mating procedure (docking or berthing, see phase 5th), these conditions differ.

5th Mating: This phase aims to achieve a certain connection between both spacecrafts. There are two main procedures for this purpose: Docking and berthing, which are shown in figure 1.2. The connection, besides structural, usually involves power, data and possibly fluids. It is important to note that residual relative motion must be attenuated.

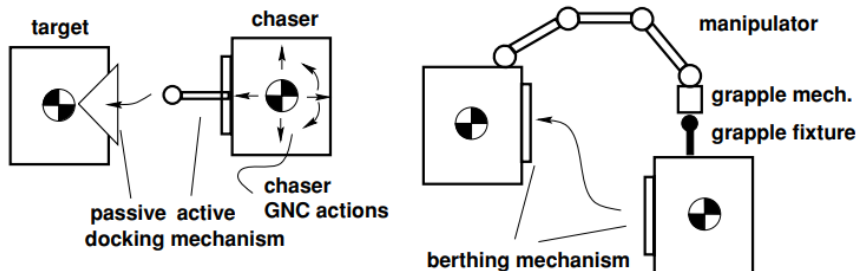


Figure 1.2: Docking and berthing [1].

1.1.2 Formation flying.

Formation flying does not have a specially precise definition, varying from institution to institution. However, NASA's Goddard Space Flight Center provides a definition to which most of the space community would agree, defining it as the tracking or maintenance of a desired relative separation, orientation or position between or among spacecraft [2]. It involves longer-term planning and operations than rendez-vous, hence usually requiring or being further rewarded by the usage of more accurate models. Fuel consumption becomes an even more critical concern, depending on several factors such as mission requirements, initial conditions, drag or thrusting errors.

Missions involving spacecraft formation flying have been certainly infrequent. The required knowledge about control, measurement and modeling have turned some groundbreaking projects down due to their costs. Nonetheless, there are current missions such as CLUSTER and GRACE which feature concepts closely related to the discipline. Furthermore, missions like PRISMA or the upcoming Proba-3 and LISA are the main bids to develop the involved methodologies and technologies of formation flying.

A very important concern about formation flying is orbit safety, being very tightly related to formation control. This will be a recurrent topic along the thesis, analyzing state-of-the-art methodologies and practical examples of greater or smaller complexities.

1.2 State transition matrices.

Orbit propagation is a very wide and varied field. It comprises many different approaches and methods to obtain more or less accurate results, with a higher or lower computational cost. Some examples are the numerical integration of the equations of motion in cartesian coordinates, the numerical integration of the variational equations (*i.e.* equations of motion expressed in OEs) and the development of closed-form solutions by simplifying the problem. Within this last group, State Transition Matrices arise.

The State Transition Matrix is a linearization procedure of a nonlinear dynamical system. It is used to approximate the dynamics of said system over short periods of time, allowing for a lower computational cost while maintaining an acceptable accuracy. This concept is not restricted to orbital mechanics, although it is one of the main fields in which it is used [3].

This section intends to provide some background in (a) its mathematical formulation and (b) its applications in orbit theory.

1.2.1 Concept: System dynamics.

Consider the uncontrolled, nonlinear dynamic system that is characterized through the state vector $\underline{y} = [y_1, y_2, \dots, y_n]$. The Initial Value Problem (IVP) for this system may be expressed as:

$$[P] \equiv \begin{cases} \text{Eq. } \frac{d\underline{y}}{dt} = \mathbf{F}(\underline{y}, t) \\ \text{ICs. } \underline{y}(t_0) = \underline{y}_0 \end{cases} \quad (1.1)$$

where $\mathbf{F}(\underline{y}, t)$ represents the nonlinear dynamics of the system. This problem is unsolvable in general, mainly due to its nonlinearity. In the context of orbit propagation, the state vector \underline{y} might be the

position and velocity (be it relative or absolute) of the celestial body, and the dynamics function \mathbf{F} contains the considered force model. In order to arrive at a closed-form, solvable problem, it is assumed that the solution $\underline{y}(t)$ can be expressed as:

$$\underline{y}(t) = \Phi(t, t_0) \underline{y}(t_0) \quad (1.2)$$

where $\Phi(t, t_0)$ is the State Transition Matrix (STM) of the system. This matrix allows the state vector at a certain epoch t to be calculated as the product of the matrix times the initial condition. This expression is obviously very favorable, but the question now is how does one compute it. Its actual definition can be easily derived from (1.2) as:

$$\Phi(t, t_0) \equiv \frac{\partial \underline{y}}{\partial \underline{y}_0} \quad (1.3)$$

Yet again, how to compute it is not clear at all. There are three main options, depending on the situation:

- A. If the nonlinear solution as a function of the initial condition is known, then the expression (1.3) is directly applied. This is an uncommon case, although simplified examples exist in the orbit propagation field. For example, the Keplerian motion equations expressed in Keplerian orbital elements (OEs) can be solved this way, due to the trivial remaining equations. Another example is the Clohessy-Wiltshire solution, from which the STM can be directly obtained. This process is detailed later on in section 2.3.2.
- B. The nonlinear solution is unknown in the original state space, but can be calculated in a different space through a transformation. Mathematically, this can be written as:

$$\Phi_y(t, t_0) = \frac{\partial \underline{y}}{\partial \underline{y}_0} = \frac{\partial \underline{y}}{\partial \underline{u}} \frac{\partial \underline{u}}{\partial \underline{u}_0} \frac{\partial \underline{u}_0}{\partial \underline{y}_0} \equiv W(t) \Phi_u(t, t_0) (W(t_0))^{-1} \quad (1.4)$$

where $W(t)$ is the transformation matrix, where it is assumed that the transformation $\underline{y} = h(\underline{u})$ is known. An example of this kind of approach is the transformation of the Cartesian equations of motion into the Keplerian OEs, whose solution is known, as mentioned in A.. This is a very commonly used method in relative orbit propagation, as in [4, 5].

- C. If none of the above can be performed, then the STM can be integrated itself, to be then used to calculate the state vector. This starts by differentiating (1.1) with respect to the initial condition

\underline{y}_0 , leading to:

$$\begin{aligned} \bullet \quad & \frac{\partial}{\partial \underline{y}(t_0)} \frac{d\underline{y}(t)}{dt} = \frac{d}{dt} \frac{\partial \underline{y}(t)}{\partial \underline{y}(t_0)} = \frac{d}{dt} \Phi(t, t_0) \\ \bullet \quad & \frac{\partial \mathbf{F}(t, \underline{y})}{\partial \underline{y}(t_0)} = \frac{\partial \mathbf{F}(t, \underline{y})}{\partial \underline{y}(t)} \frac{\partial \underline{y}}{\partial \underline{y}(t_0)} = \mathbf{A}\Phi(t, t_0) \\ \Rightarrow [P] \equiv & \begin{cases} \text{Eq. } \frac{d}{dt} \Phi(t, t_0) = \mathbf{A}\Phi(t, t_0) \\ \text{IC } \Phi(t_0, t_0) = \mathbb{I}_{n \times n} \end{cases} \end{aligned} \quad (1.5)$$

This last method is a bit unrewarding, as it forces one to integrate an IVP. However, the problem in terms of $\Phi(t, t_0)$ (eq. (1.5)) might be simpler or more efficient than the original (eq. (1.1)), although it is rare. An example of this approach is shown later in section 2.3.3.

1.2.2 Applications of STMs in celestial mechanics.

State Transition Matrices can be useful in a wide range of spacecraft dynamics applications. Some of the most important are [6]:

A. Precise Orbit Determination.

Precise Orbit Determination (POD) is a method through which the orbit of a flying spacecraft can be determined with a high accuracy [7]. This estimation is performed using general orbit determination algorithms, such as Kalman filtering or a batch least squares. It requires both high-precision geodetic receivers and high-precision dynamics models, where STMs comes to play. POD usually requires all typically important perturbations, such as non-spherical gravity, drag, tidal forces ...

B. Guidance, Navigation and Control (GNC).

GNC deals with the design the systems to control the spacecraft. It involves the determination of the desired trajectory (guidance), the instantaneous determination of the spacecraft's position (navigation) and the manipulation of the controllers to execute guidance commands (control). STMs become very useful specially in situations in which the linearization error is small, such as in rendez-vous, station-keeping or formation flying operations. They prove to be useful in all three branches:

- Guidance: STMs are a lightweight yet precise tool to generate reference trajectories.
- Navigation: Signal filtering makes extensive use of STMs for the propagation of the estimated state. This is certainly one of the most relevant applications.
- Control: Algorithms like robust online optimal control involve state propagation, using the STM.

C. Orbit design.

Alternatively, rather than propagating already defined orbits, it may be useful to solve the inverse problem: that is, find the orbit that satisfies a set of conditions (*e.g.* optimality). This is specially relevant for the Circular Restricted Three Body Problem (CR3BP), or its particular case of Halo orbits (periodic 3D orbit near one of the Lagrange libration points). STMs are quite useful to determine an initial solution for said Halo orbits, and can also be used to evaluate the effect of a deviation in initial conditions or other parameters.

D. Covariance matrix propagation.

Some degree of uncertainty will always be assumed in the estimation of a spacecraft's position and velocity. This matter becomes really important in the context of collision avoidance, where ideally, said uncertainty would be exactly calculated. However, these values are usually not something inherently worrying. What is worrying indeed is that this uncertainty may propagate in a divergent fashion, leading to unbounded trajectories with its inherent collision risk.

Here is where the covariance matrix comes to light. Conceptually, it can be seen as an entity which indicates how certain are each of the components of the state vector. That is represented by their variances and covariances. Mathematically, it is defined as:

$$P(t) = E \left[(\hat{x} - \underline{x}) (\hat{x} - \underline{x})^T \right]$$

If one knew the covariance at a certain epoch t_j , it is possible to map it to a different epoch t_k (latter or earlier) through the STM, that is:

$$\begin{aligned} P(t_k) &= E \left[(\hat{x}_k - \underline{x}_k) (\hat{x}_k - \underline{x}_k)^T \right] = E \left[\Phi(t_k, t_j) (\hat{x}_j - \underline{x}_j) (\hat{x}_j - \underline{x}_j)^T \Phi^T(t_k, t_j) \right] \\ &\Rightarrow P(t_k) = \Phi(t_k, t_j) P(t_j) \Phi^T(t_k, t_j) \end{aligned}$$

Now, once the mathematical formalism has been stated, it is time to apply it to the situation at hand. Spacecraft state uncertainty has essentially two sources: estimation error (associated to navigation) and execution error (associated to control/manoeuvres).

In a fairly relaxed approach (*i.e.* assuming the state variables be decoupled), the covariance matrix associated to the estimation error has the following shape:

$$P_{est} = \begin{bmatrix} \delta x^2 & 0 & 0 & 0 & 0 & 0 \\ 0 & \delta y^2 & 0 & 0 & 0 & 0 \\ 0 & 0 & \delta z^2 & 0 & 0 & 0 \\ 0 & 0 & 0 & \delta v_x^2 & 0 & 0 \\ 0 & 0 & 0 & 0 & \delta v_y^2 & 0 \\ 0 & 0 & 0 & 0 & 0 & \delta v_z^2 \end{bmatrix} \quad (1.6)$$

where $\delta\psi$ indicates the standard deviation of the variable ψ . An useful way to visualize the covariance is the probability ellipsoid, defined by:

$$\begin{bmatrix} \tilde{x} & \tilde{y} & \tilde{z} \end{bmatrix} P_{xyz}^{-1} \begin{bmatrix} \tilde{x} \\ \tilde{y} \\ \tilde{z} \end{bmatrix} = l^2$$

where $\tilde{x}, \tilde{y}, \tilde{z}$ are the coordinates of a point of the ellipsoid (referred to its center), P_{xyz} is the partition of the covariance matrix related to the position and l is the sigma coefficient. That is, for $l = 2$, the equation represents the ellipsoid in which the spacecraft will be found with a 2σ probability. An example of the evolution of this ellipsoid can be seen for a small radial hop in figure 1.3.

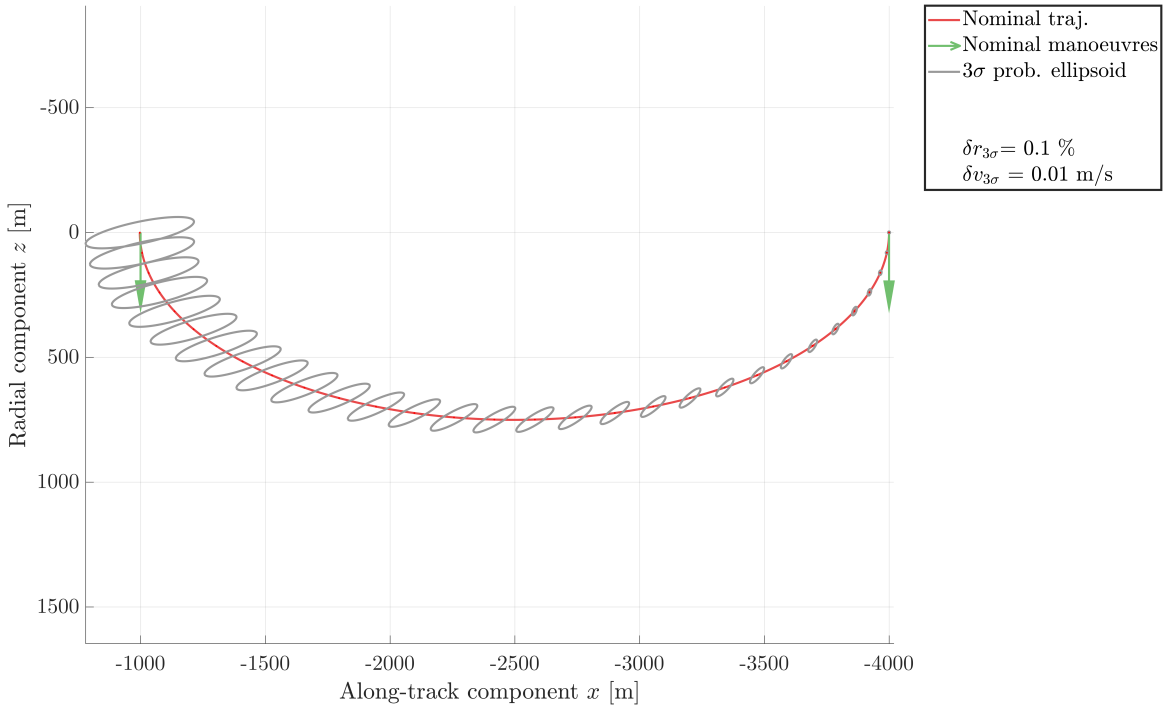


Figure 1.3: Covariance ellipsoid evolution along a radial hop.

Most of these concepts lie out of the thesis' scope. However, it is important to know that the STMs developed or quoted throughout this thesis can be used in many different fields of celestial mechanics.

Relative dynamics around a near-circular unperturbed reference orbit.

2.1 Introduction.

Relative dynamics may involve different degrees of complexity, which depends basically on the considered model and the scenario to simulate. During this thesis, the approach will be to incrementally increase this complexity, starting from the simplest, less accurate models all the way to the more convoluted, realistic ones.

With this in mind, the least complicated scenario is the near-circular unperturbed reference orbit. This simplifies greatly the mathematical involvement, as it (a) neglects any perturbation and (b) yields a chief spacecraft with a constant velocity and orbital radius. It makes sense then that this was the first relative dynamics model ever created and hence used for rendez-vous and formation flying operations.

This chapter firstly focuses on the derivation of the linearized Hill equations [8], starting from the most general form of the equations of motion of a spacecraft. Afterwards, some implementations of said equations are analyzed and compared with a High-Fidelity propagation. Lastly, the concept of orbit safety will be introduced, and safety strategies will be also studied.

2.2 Motion model: Hill equations.

2.2.1 Equations of motion of a spacecraft.

This section intends to briefly note the general equations of motion of a certain spacecraft. From these, several simplifications may follow.

Any spacecraft is subject mainly to gravitational forces. Nonetheless, many other forces may be relevant, such as drag, solar radiation pressure or thrust. Newton's equation, with its respective initial conditions, would then take the following form:

$$[P] \equiv \begin{cases} \text{Eq. } m_i \ddot{\underline{r}}_i = \underline{F}_{g,i} + \underline{T}_i + \underline{F}_{\text{other}, i} \\ \text{ICs } \begin{cases} \underline{r}_i(t = t_0) = \underline{r}_{i,0} \\ \dot{\underline{r}}_i(t = t_0) = \dot{\underline{r}}_{i,0} \end{cases} \end{cases} \quad (2.1)$$

where \underline{r}_i denotes the i^{th} spacecraft position vector with respect to an inertial frame. Obtaining an analytical solution for this problem is almost impossible for most of the cases, as forces may depend on the position, velocity and control variables of the spacecraft, as well as time. Numerical integration becomes an option, though it leads to barely no knowledge and a high computational cost. Our goal is then to find semi-analytical solutions, that is, analytical solutions of a modelled, simplified version of the problem. This does give an insight into the physical problem, enabling the possibility of further understanding of it. These solutions can be implemented in an incremental way, namely, increasing in difficulty and incorporating elements progressively less relevant.

A description of each of the forces that show up in equation (2.1).

2.2.2 Forces in the spacecraft motion problem.

I. Gravitational forces

This term includes the effect of the gravity generated by all the considered bodies. Generally, the considered bodies are a primary (much more massive than any other), the spacecraft set (of negligible gravitational effects) and possibly, third bodies, which fall in between the former (relevant effect but far from that of the primary body).

The effect of each celestial body in the considered spacecraft can be modelled differently. For example, the Earth can be considered to be a perfect sphere (central body acceleration) or, in other modelizations, some of its shape irregularities can be taken into account. As one moves further away from any celestial body, its gravity field tends to that of a central body, which is why third bodies' fields are modelled as central bodies. In a latter chapter, an outlook on how this asphericity is modelled and how it affects the dynamics of any given spacecraft will be provided.

One can then decompose the gravitational force on the spacecraft i as:

$$\underline{F}_{g,i} = \underline{F}_{\text{primary},i} + \underline{F}_{\text{third bodies},i} = \underline{F}_{\text{primary, CB}, i} + \underline{F}_{\text{primary, NSG}, i} + \underline{F}_{\text{third bodies},i}$$

where CB and NSG refer to Central Body and Non-Spherical Gravity, respectively.

II. Thrust

With the purpose of controlling the trajectory and attitude of the spacecraft, thrusters are usually installed and actuated. This has obviously to be taken into account when integrating the motion of any spacecraft, though in this thesis this will not be the case: only uncontrolled motion will be analyzed.

III. Other forces

Logically, interplanetary trajectories take place in a much different environment compared to Earth orbits. Hence, different perturbation forces must be taken into account in each case. For example, in the case of low Earth orbits (LEOs), tidal forces become relevant, as well as drag and even the solar albedo. Conversely, in a interplanetary transfer orbit, solar radiation pressure might be taken into account. The key here is to establish a threshold of which effects to take into account and then start modelling those which rise above it.

2.2.3 Two-body problem.

As stated before, semi-analytical solutions are to be found. The simplest and most widely studied simplification of equation (2.1) is the two-body problem. As the name suggests, it only considers a primary and a secondary body, and the goal is to obtain the motion of the latter around the former.

The equations of motion of the Keplerian two-body problem are obtained under the so-called Hill assumptions [2]:

- I. Gravity is the only internal or external force.
- II. Gravity fields come from spherical bodies.
- III. Gravitational forces are Newtonian.
- IV. There are no tidal forces.
- V. The mass of the primary body is much larger than the orbiting body's.

The equations of the two-body problem can be then written as:

$$[P] \equiv \begin{cases} \text{Eq.} & \ddot{\underline{r}} = -\frac{\mu \underline{r}}{r^3} \\ \text{ICs} & \begin{cases} \underline{r}(t = t_0) = \underline{r}_0 \\ \dot{\underline{r}}(t = t_0) = \dot{\underline{r}}_0 \end{cases} \end{cases} \quad (2.2)$$

The solution of (2.2) is known as Keplerian motion, and is universally known. There are many ways to obtain it, such as the one shown in [2], section 2.2. That development is merely quoted, as it does not lie within the scope of the thesis.

2.2.3.1 Perturbed two-body problem.

With the two-body solution in mind, some problems can be modelled as a perturbed version of it. The Keplerian motion can then be seen as a *first order* solution of the problem at hand, from which the perturbed problem slightly deviates. This deviation may be approached through several ways [9].

A direct integration of the equation is again possible, though knowledge acquisition will again be null. Furthermore, many of the significant figures will simply reproduce the two-body solution - which is already known- leading to computational inefficiency. This brute force approach is commonly referred to as Cowell's method.

Another numeric approach is to expand the perturbed solution around the original, thus integrating only the perturbation. This is the so-called Encke's method. Though this leads to a better computational efficiency and accuracy, still no further understanding is gained.

The last main option is to integrate the Gauss Variational Equations (see E.2). These equations actually provide some knowledge of the perturbed problem, and are quite computationally efficient. This fact is due to (a) the slow time-varying character of the OEs, allowing for a greater time-step and (b) the possibility of substituting the two-body problem solution in the right-side of the equations.

Whatever the approach is, the perturbed two-body problem can be written as:

$$[P] \equiv \begin{cases} \text{Eq.} & \ddot{\underline{r}} = -\frac{\mu \underline{r}}{r^3} + \underline{a}_P \\ \text{ICs} & \begin{cases} \underline{r}(t = t_0) = \underline{r}_0 \\ \dot{\underline{r}}(t = t_0) = \dot{\underline{r}}_0 \end{cases} \end{cases} \quad (2.3)$$

where \underline{a}_P is the perturbation acceleration.

2.2.4 Three-body problem.

The three-body problem considers the motion of three bodies: a primary and two secondaries. It can be understood as an extension of the two-body problem, where a third body appears and perturbs the motion of the pre-existing secondary body. This problem lacks a general, closed-form solution. Nonetheless, some approximations have been developed.

One approach to this problem is to consider the gravitational effect of the third body on the secondary body as a perturbation with respect to the two body problem. This approach is actually a particularization of the perturbed two-body problem, which is developed in detail in chapter 4.

2.2.4.1 Reduced three-body problem.

Another further simplification of the three-body problem is obtained by assuming that the two secondary bodies do not cause a gravitational effects on each other. This is commonly referred to as the reduced three-body problem, being actually the set of equations that describe spacecraft formation flying. This and further simplifications will be analyzed in the following section.

2.2.5 Differential equations of proximity relative motion.

As the proximity assumption ($\|\underline{r}\| \ll \|\underline{R}\|$) is quite widely common and valid for a fair range of operations, it is interesting to describe them here briefly, following [4]. Consider the motion of two spacecrafts, namely, chief and deputy. The general equations of motion for each of them can be written as:

$$\text{Chief} \Rightarrow \ddot{\underline{R}} = -\mu \frac{\underline{R}}{\|\underline{R}\|^3} + \underline{a}_{C,d} \quad (2.4)$$

$$\text{Deputy} \Rightarrow \ddot{\underline{R}} + \ddot{\underline{r}} = -\mu \frac{\underline{R} + \underline{r}}{\|\underline{R} + \underline{r}\|^3} + \underline{a}_{D,d} + \underline{a}_f \quad (2.5)$$

where \underline{R} and \underline{r} are the chief's absolute position vector and the deputy's relative position vector, respectively. $\underline{a}_{\bullet,d}$ is the disturbing acceleration on each spacecraft, while \underline{a}_f denotes the thrust vector of the deputy. In order to facilitate the linearization, the orbital radius of the deputy can be rewritten as:

$$\|\underline{R} + \underline{r}\| = [(\underline{R} + \underline{r})^T(\underline{R} + \underline{r})]^{1/2} = \|\underline{R}\| \left(1 + 2 \frac{\underline{R}^T \underline{r}}{\|\underline{R}\|^2} + \frac{\|\underline{r}\|^2}{\|\underline{R}\|^2} \right)^{1/2}$$

then, the effect of the gravity field on the deputy can be expressed as:

$$\frac{\underline{R} + \underline{r}}{\|\underline{R} + \underline{r}\|^3} = \frac{\underline{R} + \underline{r}}{\|\underline{R}\|^3} \left(1 + 2 \frac{\underline{R}^T \underline{r}}{\|\underline{R}\|^2} + \frac{\|\underline{r}\|^2}{\|\underline{R}\|^2} \right)^{-\frac{3}{2}}$$

Assuming that the relative distance is much smaller than the chief's orbital radius:

$$\frac{\underline{R} + \underline{r}}{\|\underline{R} + \underline{r}\|^3} \underset{\|\underline{r}\| \ll \|\underline{R}\|}{\approx} \frac{\underline{R} + \underline{r}}{\|\underline{R}\|^3} \left[1 - \frac{3}{2} \left(2 \frac{\underline{R}^T \underline{r}}{\|\underline{R}\|^2} + \frac{\|\underline{r}\|^2}{\|\underline{R}\|^2} \right) \right] \approx \frac{1}{\|\underline{R}\|^3} \left(\underline{R} + \underline{r} - 3 \frac{\underline{R}^T \underline{r}}{\|\underline{R}\|^2} \underline{R} \right) \quad (2.6)$$

If (2.6) is now substituted in the difference (2.5) minus (2.4):

$$\ddot{\underline{r}} = -\frac{\mu}{\|\underline{R}\|^3} \left(\underline{r} - 3 \frac{\underline{R}^T \underline{r}}{\|\underline{R}\|^2} \underline{R} \right) + \underline{a}_f + \underline{a}_{D,d} - \underline{a}_{C,d} \quad (2.7)$$

Experience shows it is convenient to express equation (2.7) in a chief-centered frame, for example, the LVLH frame (see section B.4.2). This leads to the need of applying Coriolis' Theorem twice, so as to get the non-inertial effects derived from describing the motion in a rotating frame. The equations of motion take now the following form:

$$\ddot{\underline{r}} = -\frac{\mu}{\|\underline{R}\|^3} \left(\underline{r} - 3 \frac{\underline{R}^T \underline{r}}{\|\underline{R}\|^2} \underline{R} \right) - 2\underline{\omega} \times \dot{\underline{r}} - \dot{\underline{\omega}} \times \underline{r} - \underline{\omega} \times (\underline{\omega} \times \underline{r}) + \underline{a}_f + \underline{a}_{D,d} - \underline{a}_{C,d} \quad (2.8)$$

where $\underline{\omega}$ is the target orbital rate. Expressing each vector in the LVLH frame:

$$\underline{\omega} = \begin{Bmatrix} 0 \\ -\omega \\ 0 \end{Bmatrix} \quad \underline{R} = \begin{Bmatrix} 0 \\ 0 \\ -R \end{Bmatrix} \quad \underline{r} = \begin{Bmatrix} x \\ y \\ z \end{Bmatrix} \quad (2.9)$$

leading to the next expressions for the terms in equation (2.8):

$$\begin{aligned} \underline{\omega} \times \dot{\underline{r}} &= \begin{Bmatrix} \omega \dot{z} \\ 0 \\ \omega \dot{x} \end{Bmatrix} & \dot{\underline{\omega}} \times \underline{r} &= \begin{Bmatrix} -\dot{\omega} z \\ 0 \\ \dot{\omega} x \end{Bmatrix} \\ \underline{\omega} \times (\underline{\omega} \times \underline{r}) &= \begin{Bmatrix} -\omega^2 x \\ 0 \\ -\omega^2 z \end{Bmatrix} & \underline{r} - 3 \frac{\underline{R}^T \underline{r}}{\|\underline{R}\|^2} \underline{R} &= \begin{Bmatrix} x \\ y \\ -2z \end{Bmatrix} \end{aligned}$$

and introducing these results into (2.8), it follows:

$$\begin{Bmatrix} \ddot{x} \\ \ddot{y} \\ \ddot{z} \end{Bmatrix} = \begin{Bmatrix} -k\omega^{3/2}x + 2\omega\dot{z} + \dot{\omega}z + \omega^2x \\ -k\omega^{3/2}y \\ 2k\omega^{3/2}z - 2\omega\dot{x} - \dot{\omega}x + \omega^2z \end{Bmatrix} + \underline{a}_f + \underline{a}_{D,d} - \underline{a}_{C,d} \quad (2.10)$$

finally, considering Keplerian motion:

$$\begin{Bmatrix} \ddot{x} \\ \ddot{y} \\ \ddot{z} \end{Bmatrix} = \begin{Bmatrix} -k\omega^{3/2}x + 2\omega\dot{z} + \dot{\omega}z + \omega^2x \\ -k\omega^{3/2}y \\ 2k\omega^{3/2}z - 2\omega\dot{x} - \dot{\omega}x + \omega^2z \end{Bmatrix} \quad (2.11)$$

where k is a constant defined by

$$\frac{\mu}{R^3} = \frac{\mu}{h^{3/2}} \equiv k\omega^{3/2} \Leftrightarrow k \equiv \frac{\mu}{h^{3/2}}$$

and $h = \omega R^2$ is the chief's angular momentum.

2.2.6 Hill equations.

It is convenient to summarize the path followed up until now. The starting point was the equations of motion of a spacecraft, in which many effects appear. From there, the perturbed two-body problem followed, which is actually a reformulation rather than a simplification. After that, the differential equations for relative motion between two spacecrafts were derived, which were finally simplified under the assumptions that motion was unperturbed and that the spacecrafts were in close proximity.

Now, it is turn to do the last simplification: the assumption of near-circular or circular orbits ($e \ll 1$). The derived equations are the so-called Hill equations [8], or, in some references, the Clohessy-Wiltshire equations (though these are presented later in (2.19))

If the reference orbit is near-circular, the orbital radius and hence the velocity is constant along time. This leads to the angular rate ω to be constant, and equal to:

$$\omega = \sqrt{\frac{\mu}{a^3}}$$

hence:

$$k\omega^{3/2} = \frac{\mu}{a^3} = \omega^2 \quad (2.12)$$

The equations (2.11) simplify to:

$$\begin{Bmatrix} \ddot{x} \\ \ddot{y} \\ \ddot{z} \end{Bmatrix} = \begin{Bmatrix} 2\omega\dot{z} \\ -\omega^2 y \\ 3\omega^2 z - 2\omega\dot{x} \end{Bmatrix} \quad (2.13)$$

which can be expressed as a set of first-order ordinary differential equations:

$$\begin{Bmatrix} \dot{x} \\ \dot{y} \\ \dot{z} \\ \ddot{x} \\ \ddot{y} \\ \ddot{z} \end{Bmatrix} = \left[\begin{array}{ccc|ccc} 0 & 0 & 0 & 1 & 0 & 0 \\ 0 & 0 & 0 & 0 & 1 & 0 \\ 0 & 0 & 0 & 0 & 0 & 1 \\ \hline 0 & 0 & 0 & 0 & 0 & 2\omega \\ 0 & \omega^2 & 0 & 0 & 0 & 0 \\ 0 & 0 & 3\omega^2 & -2\omega & 0 & 0 \end{array} \right] \begin{Bmatrix} x \\ y \\ z \\ \dot{x} \\ \dot{y} \\ \dot{z} \end{Bmatrix} \quad (2.14)$$

Equation (2.14) are the so-called Hill equations, which can also be decoupled into in-plane ($x-z$) and out-of-plane motion (y). They can be rewritten in a more compact form through the coefficient matrix \mathbf{A} , as:

$$\begin{Bmatrix} \dot{x} \\ \dot{y} \\ \dot{z} \\ \ddot{x} \\ \ddot{y} \\ \ddot{z} \end{Bmatrix} = \left[\begin{array}{c|c} \mathbb{O}_{3x3} & \mathbb{I}_{3x3} \\ \hline \mathbf{G} & \boldsymbol{\Omega} \end{array} \right] \begin{Bmatrix} x \\ y \\ z \\ \dot{x} \\ \dot{y} \\ \dot{z} \end{Bmatrix} \quad (2.15)$$

$$\Rightarrow \mathbf{A} = \left[\begin{array}{c|c} \mathbb{O}_{3x3} & \mathbb{I}_{3x3} \\ \hline \mathbf{G} & \boldsymbol{\Omega} \end{array} \right] \quad (2.16)$$

2.3 Solutions of Hill equations.

The goal now is to analyze which solution does this simplified set of equations lead to, which will be done through several methods. Once all of them have been presented, they will be compared between themselves and with respect to a High-Fidelity solution for some circular orbit scenarios.

2.3.1 Direct numerical integration.

The first option that may come to mind is to simply numerically integrate equation (2.14), being somewhat efficient, as the coefficient matrix can be computed once for all iterations. In this case, the numerical integration was done using a four-step Runge-Kutta method, due to its good balance between performance, stability and complexity. A constant timestep of 10 seconds is imposed. No sensitivity analysis has been done to this respect, though results show that it is a good enough value.

This approach, as all computational approaches, does not yield any real knowledge: it is just “cranking the numbers”. That is why other methods are thereupon described.

2.3.2 Clohessy-Wiltshire solution and STM.

In order to get a reasonable insight into the behaviour of the relative dynamics, the Clohessy-Wiltshire (CW) solution will be developed [1]. Firstly, recalling the expression for Laplace transforms of derivatives:

$$\begin{aligned}\mathcal{L}(\dot{f}(t)) &= sF(s) - f(0_+) \\ \mathcal{L}(\ddot{f}(t)) &= s^2F(s) - sf(0_+) - \dot{f}(0_+)\end{aligned}$$

where $F(s) = \mathcal{L}(f(t))$. Taking that into consideration, the Laplace transform of the equations (2.13) becomes:

$$\left\{ \begin{array}{l} s^2X(s) - sx_0 - \dot{x}_0 - 2\omega sZ(s) + 2\omega z_0 = 0 \end{array} \right. \quad (2.17a)$$

$$\left\{ \begin{array}{l} s^2Y(s) - sy_0 - \dot{y}_0 + \omega^2 sY(s) = 0 \end{array} \right. \quad (2.17b)$$

$$\left\{ \begin{array}{l} s^2Z(s) - sz_0 - \dot{z}_0 + 2\omega sX(s) - 2\omega x_0 - 3\omega^2 Z(s) = 0 \end{array} \right. \quad (2.17c)$$

Solving for $X(s)$, $Y(s)$ and $Z(s)$ in (2.17), the solution in the Laplace domain is reached:

$$\left\{ \begin{array}{l} X(s) = x_0 \frac{1}{s} + (\dot{x}_0 - 2\omega z_0) \frac{1}{s^2} + 2\omega z_0 \frac{1}{s^2 + \omega^2} + 2\omega \dot{z}_0 \frac{1}{s(s^2 + \omega^2)} \\ \quad + 2\omega (4\omega^2 z_0 - 2\omega \dot{x}_0) \frac{1}{s^2(s^2 + \omega^2)} \end{array} \right. \quad (2.18a)$$

$$\left\{ \begin{array}{l} Y(s) = y_0 \frac{s}{s^2 + \omega^2} + \dot{y}_0 \frac{1}{s^2 + \omega^2} \end{array} \right. \quad (2.18b)$$

$$\left\{ \begin{array}{l} Z(s) = z_0 \frac{s}{s^2 + \omega^2} + \dot{z}_0 \frac{1}{s^2 + \omega^2} + (4\omega^2 z_0 - 2\omega \dot{x}_0) \frac{1}{s(s^2 + \omega^2)} \end{array} \right. \quad (2.18c)$$

In order to obtain the time domain solution, the inverse Laplace transform is applied, leading to the Clohessy-Wiltshire (CW) solution [10]:

$$\begin{cases} x(t) = \left(\frac{4\dot{x}_0}{\omega} - 6z_0 \right) \sin(\omega\tau) - \frac{2\dot{z}_0}{\omega} \cos(\omega\tau) + (6\omega z_0 - 3\dot{x}_0) \tau + \left(x_0 + \frac{2\dot{z}_0}{\omega} \right) \end{cases} \quad (2.19a)$$

$$\begin{cases} y(t) = y_0 \cos(\omega\tau) + \frac{\dot{y}_0}{\omega} \sin(\omega\tau) \end{cases} \quad (2.19b)$$

$$\begin{cases} z(t) = \left(\frac{2\dot{x}_0}{\omega} - 3z_0 \right) \cos(\omega\tau) + \frac{\dot{z}_0}{\omega} \sin(\omega\tau) + \left(4z_0 - \frac{2\dot{x}_0}{\omega} \right) \end{cases} \quad (2.19c)$$

where $\tau = t - t_0$ is the elapsed time since the initial condition. A comprehensive survey of the different simple trajectories that can be derived from (2.19) is shown in [1], chapter 3.

2.3.2.1 Clohessy-Wiltshire STM.

Once the CW solution has been developed, an equivalent STM can be derived. The expression one is looking for is:

$$\underline{y}(t) = \Phi(t, t_0) \underline{y}(t_0)$$

where $\underline{y}(t) = \{\underline{r}, \dot{\underline{r}}\}^T$ denotes the state vector of the deputy, expressed in the chief's LVLH frame. The computation of the STM $\Phi(t, t_0)$ can be carried out in two ways:

A. Differentiating (2.19) with respect to the initial state vector $\underline{y}(t_0) = \{x_0, y_0, z_0, \dot{x}_0, \dot{y}_0, \dot{z}_0\}^T$.

B. Using the general expression $\Phi(t, t_0) = \exp(\mathbf{A}(t - t_0))$.

As the actual explicit relationship $\underline{y}(t) = f(t, \underline{y}(t_0))$ is known, the first option is selected. The second one will be developed in a latter section, following a Jordan Canonical Decomposition.

The CW STM takes then the following form:

$$\Phi(t, t_0) = \begin{bmatrix} 1 & 0 & 6(\omega\tau - \sin \omega\tau) & \frac{4}{\omega} \sin \omega\tau - 3\tau & 0 & \frac{2}{\omega}(1 - \cos \omega\tau) \\ 0 & \cos \omega\tau & 0 & 0 & \frac{1}{\omega} \sin \omega\tau & 0 \\ 0 & 0 & 4 - 3 \cos \omega\tau & \frac{2}{\omega}(\cos \omega\tau - 1) & 0 & \frac{1}{\omega} \sin \omega\tau \\ 0 & 0 & 6\omega(1 - \cos \omega\tau) & 4 \cos \omega\tau - 3 & 0 & 2 \sin \omega\tau \\ 0 & -\omega \sin \omega\tau & 0 & 0 & \cos \omega\tau & 0 \\ 0 & 0 & 3\omega \sin \omega\tau & -2 \sin \omega\tau & 0 & \cos \omega\tau \end{bmatrix} \quad (2.20)$$

where the gray shaded part of the matrix corresponds to the out-of-plane dynamics, which are completely decoupled from the in-plane (rest of the matrix). This shape suggests that, if reshaped, the

matrix could show this decoupling in a more intuitive and visual manner. This will be somehow carried out later on with the Jordan Canonical decomposition.

Now the state vector at a given epoch can be easily calculated, being a function only of the elapsed time τ and the chief's semimajor axis a (through ω).

2.3.3 State transition matrix propagation.

Another alternative approach considers the propagation of the actual state transition matrix. Following Montenbruck [3, section 7.2.1], the initial value problem (IVP) for the state vector propagation can be written as:

$$[P] \equiv \begin{cases} \text{Eq. } \frac{d\underline{y}}{dt} = \underline{f}(t, \underline{y}) \\ \text{ICs } \underline{y}(t = t_0) = \underline{y}_0 \end{cases} \quad (2.21)$$

where $\underline{f} = \{\dot{\underline{r}}, \ddot{\underline{r}}\}$ is a generally non-linear function. Nonetheless, this problem can be linearized, arriving to:

$$[P] \equiv \begin{cases} \text{Eq. } \frac{d\underline{y}}{dt} = \mathbf{A}\underline{y} \\ \text{ICs } \underline{y}(t = t_0) = \underline{y}_0 \end{cases} \quad (2.22)$$

where $\mathbf{A} = \frac{\partial f(t, y)}{\partial y}$. This coefficient matrix A can be calculated as:

$$\mathbf{A} = \frac{\partial \{\dot{\underline{r}}, \ddot{\underline{r}}\}^T}{\partial \{\underline{r}, \dot{\underline{r}}\}^T} = \left[\begin{array}{c|c} \frac{\partial \dot{\underline{r}}}{\partial \underline{r}} & \frac{\partial \dot{\underline{r}}}{\partial \dot{\underline{r}}} \\ \hline \frac{\partial \ddot{\underline{r}}}{\partial \underline{r}} & \frac{\partial \ddot{\underline{r}}}{\partial \dot{\underline{r}}} \end{array} \right] = \left[\begin{array}{c|c} \mathbb{O}_{3x3} & \mathbb{I}_{3x3} \\ \hline \mathbf{G} & \mathbf{\Omega} \end{array} \right] \quad (2.23)$$

It is no coincidence that this \mathbf{A} matrix is (when under the Hill assumptions) identical to the one already defined in (2.16). The approach followed through equations (2.21), (2.22) and (2.23) is an equally valid way of obtaining the Hill equations. The procedure followed in section 2.2.6 starts from the already linearised differential equations for proximity relative motion, which are then simplified with Hill's assumptions. This leads to a constant-coefficient system of ODEs, in which the \mathbf{A} matrix can be deducted. The perspective outlined in this section develops a general, linearized form, in which the \mathbf{A} matrix is first defined and then simplified, in a more inductive fashion.

After this incise, it is time to transform a state vector IVP into a STM IVP. Firstly, the derivative of (2.21) with respect to the initial state vector $\underline{y}(t_0)$ is taken. Manipulating the derivative of each

member of said equation, it follows that:

$$\begin{aligned} \bullet \quad & \frac{\partial}{\partial \underline{y}(t_0)} \frac{d\underline{y}(t)}{dt} = \frac{d}{dt} \frac{\partial \underline{y}(t)}{\partial \underline{y}(t_0)} = \frac{d}{dt} \Phi(t, t_0) \\ \bullet \quad & \frac{\partial \underline{f}(t, \underline{y})}{\partial \underline{y}(t_0)} = \frac{\partial \underline{f}(t, \underline{y})}{\partial \underline{y}(t)} \frac{\partial \underline{y}}{\partial \underline{y}(t_0)} = \mathbf{A} \Phi(t, t_0) \\ \frac{\partial(2.21)}{\partial \underline{y}(t_0)} \Rightarrow [P] \equiv & \begin{cases} \text{Eq. } \frac{d}{dt} \Phi(t, t_0) = \mathbf{A} \Phi(t, t_0) \\ \text{ICs } \Phi(t, t_0)(t = t_0) = \mathbb{I}_{6 \times 6} \end{cases} \end{aligned} \quad (2.24)$$

The problem (2.24) can now be integrated, having then the value of the STM at any time epoch. The state vector would be simply calculated through the STM definition, that is, $\underline{y}(t) = \Phi(t, t_0)\underline{y}(t_0)$.

2.3.4 Jordan canonical decomposition.

As stated earlier, the most general way of obtaining the state transition matrix of a system involves calculating the exponential of the coefficient matrix \mathbf{A} . This can be easily derived from equation (2.22) as:

$$\begin{aligned} \frac{d\underline{y}}{dt} = \mathbf{A}\underline{y} \rightarrow \underline{y}(t) &= \exp[\mathbf{A}(t - t_0)]\underline{y}(t_0) \equiv \Phi(t, t_0)\underline{y}(t_0) \\ \Rightarrow \Phi(t, t_0) &= \exp[\mathbf{A}(t - t_0)] \end{aligned} \quad (2.25)$$

In order to compute the matrix exponential, a Jordan Canonical Decomposition will be performed. This procedure consists basically in applying eigenspace theory to decompose \mathbf{A} into elements whose exponential can be easily calculated. Firstly, a real diagonal form of \mathbf{A} will be obtained. Once the desired shape has been achieved, the exponential of the diagonal matrix will be calculated. Finally, a rearrangement of the matrices will be done, and the meaning of each will be duly explained.

2.3.4.1 Jordan canonical forms of \mathbf{A} .

A. Complex Jordan form.

For the sake of simplicity, only the in-plane part of the matrix \mathbf{A} will be analyzed. The goal is to achieve the components of the following expression:

$$\mathbf{A} = VJV^{-1}$$

where V is the eigenvector matrix (*i.e.* each column is an eigenvector of \mathbf{A}) and J is the Jordan matrix. The eigenvalues of \mathbf{A} are first computed as:

$$\det(\mathbf{A} - \lambda \mathbb{I}_{4 \times 4}) = \begin{vmatrix} -\lambda & 0 & 1 & 0 \\ 0 & -\lambda & 0 & 1 \\ 0 & 0 & -\lambda & 2\omega \\ 0 & 3\omega^2 & -2\omega & -\lambda \end{vmatrix} = 0 \Rightarrow \lambda^2(\lambda^2 + 1) = 0$$

$$\left\{ \begin{array}{ll} \lambda_1 = 0 & \Rightarrow \text{Double real eigenvalue} \\ \lambda_3 = \pm i\omega & \Rightarrow \text{Complex eigenvalue} \end{array} \right. \quad (2.26)$$

It is necessary to check if the matrix can be diagonalized. For that to happen, the algebraic and geometric multiplicities of each eigenvalue must be equal, so that the nullspace of \mathbf{A} can be fully generated.

- Eigenvalue λ_1 :

$$\text{nullspace}(\mathbf{A} - \lambda_1 \mathbb{I}_{4 \times 4}) = \text{nullspace}(\mathbf{A}) = \mathcal{L} \left(\begin{Bmatrix} 1 \\ 0 \\ 0 \\ 0 \end{Bmatrix} \right)$$

As the nullspace of \mathbf{A} is generated by only one eigenvector, the geometric multiplicity of λ_1 is 1.

As the algebraic multiplicity is 2, the matrix cannot be diagonalized. In order to get the second eigenvector associated to λ_1 , the nullspace of $(\mathbf{A} - \lambda_1 \mathbb{I}_{4 \times 4})^2$ must be calculated:

$$\text{nullspace}(\mathbf{A} - \lambda_1 \mathbb{I}_{4 \times 4})^2 = \text{nullspace}(\mathbf{A}^2) = \mathcal{L} \left(\begin{Bmatrix} 1 \\ 0 \\ 0 \\ 0 \end{Bmatrix}, \begin{Bmatrix} 0 \\ \frac{2}{3\omega} \\ 1 \\ 0 \end{Bmatrix} \right)$$

The eigenvectors associated to λ_1 are then:

$$\begin{cases} \underline{v}_2 = \left\{ 0 \quad \frac{2}{3\omega} \quad 1 \quad 0 \right\}^T & \text{as } \underline{v}_2 \in \text{nullspace}(\mathbf{A}^2) \quad \text{and} \quad \underline{v}_2 \notin \text{nullspace}(\mathbf{A}) \end{cases} \quad (2.27a)$$

$$\underline{v}_1 = \mathbf{A}\underline{v}_2 = \left\{ 1 \quad 0 \quad 0 \quad 0 \right\}^T \quad \text{as } \mathbf{A}^2\underline{v}_2 = 0 = \mathbf{A}(\mathbf{A}\underline{v}_2) \equiv \mathbf{A}\underline{v}_1 \quad (2.27b)$$

- Eigenvalue λ_3 :

$$\text{nullspace } (\mathbf{A} - \lambda_3 \mathbb{I}_{4 \times 4}) = \mathcal{L} \left(\begin{Bmatrix} -\frac{2}{\omega} \\ \frac{i}{\omega} \\ 2i \\ 1 \end{Bmatrix} \right)$$

$$\text{nullspace } (\mathbf{A} - \lambda_4 \mathbb{I}_{4 \times 4}) = \mathcal{L} \left(\begin{Bmatrix} -\frac{2}{\omega} \\ -\frac{i}{\omega} \\ -2i \\ 1 \end{Bmatrix} \right)$$

In this case, the algebraic and geometric multiplicity match, so no further calculations are to be made. The vectors \underline{v}_3 take then the following form:

$$\underline{v}_3 = \left\{ -\frac{2}{\omega}, \pm \frac{i}{\omega}, \pm 2i, 1 \right\}^T \quad (2.28)$$

Rescaling ($\times (-3)$) the eigenvectors (2.27) and merging with (2.28), the Jordan complex eigenvector matrix can be built as:

$$V = \begin{bmatrix} -3 & 0 & -\frac{2}{\omega} & -\frac{2}{\omega} \\ 0 & -\frac{2}{\omega} & \frac{i}{\omega} & -\frac{i}{\omega} \\ 0 & -3 & 2i & -2i \\ 0 & 0 & 1 & 1 \end{bmatrix}$$

with the complex Jordan matrix J being:

$$J = V^{-1} \mathbf{A} V = \begin{bmatrix} 0 & 1 & 0 & 0 \\ 0 & 0 & 0 & 0 \\ 0 & 0 & -i\omega & 0 \\ 0 & 0 & 0 & i\omega \end{bmatrix} \quad (2.29)$$

B. Real Jordan form.

In order to get rid of the complex numbers from the matrices V and J , a complex-to-real diagonal form transformation can be performed. This consists in a modification of the eigenvector definition, and consequently, a reformulation of the eigenvalue matrix. In general, the transformation converts both matrices as [11]:

$$J|_{complex} = \begin{bmatrix} \lambda_1 & & & \\ & a + bi & & \\ & & a - bi & \\ & & & c + di \\ & & & c - di \\ & & & \dots \end{bmatrix} \xrightarrow{cdf2rdf} J|_{real} = \begin{bmatrix} \lambda_1 & & & \\ & a & b & \\ & -b & a & \\ & c & d & \\ & -d & c & \\ & & & \dots \end{bmatrix} \quad (2.30)$$

$$V|_{complex} = \left[\underline{v}_1 \mid Re(\underline{v}_2) + iIm(\underline{v}_2) \mid Re(\underline{v}_2) - iIm(\underline{v}_2) \mid Re(\underline{v}_3) + iIm(\underline{v}_3) \mid Re(\underline{v}_3) - iIm(\underline{v}_3) \mid \dots \right]$$

$$\xrightarrow{cdf2rdf} V|_{real} = \left[\underline{v}_1 \mid Re(\underline{v}_2) \mid Im(\underline{v}_2) \mid Re(\underline{v}_3) \mid Im(\underline{v}_3) \mid \dots \right] \quad (2.31)$$

This transformation is based in that the nullspace generated by the complex eigenvectors (\underline{v}_3 and \underline{v}_4 in this case) can also be generated by two linear combinations of both. For this case, the real eigenvector matrix becomes:

$$V = \begin{bmatrix} -3 & 0 & -\frac{2}{\omega} & 0 \\ 0 & -\frac{2}{\omega} & 0 & \frac{1}{\omega} \\ 0 & -3 & 0 & 2 \\ 0 & 0 & 1 & 1 \end{bmatrix} \quad (2.32)$$

The real Jordan matrix is computed again as:

$$J = \begin{bmatrix} 0 & 1 & 0 & 0 \\ 0 & 0 & 0 & 0 \\ 0 & 0 & 0 & \omega \\ 0 & 0 & -\omega & 0 \end{bmatrix} \quad (2.33)$$

2.3.4.2 Exponential of the Jordan matrix.

Up until now, the coefficient matrix \mathbf{A} has been decomposed into the following product:

$$\mathbf{A} = VJV^{-1}$$

where V and J are given by equations (2.32) and (2.33) respectively. Now it is turn to compute the exponential itself, which satisfies:

$$\exp [A(t - t_0)] = V \exp (J(t - t_0)) V^{-1} \quad (2.34)$$

The new target is then to compute $\exp [J(t - t_0)]$. Recalling that the exponential of a matrix is calculated as:

$$\exp [A(t - t_0)] = \sum_{n=0}^{\infty} \frac{(t - t_0)^n A^n}{n!}$$

Due to the structure of J , the summation has a finite number of non-zero terms. Still, it is convenient to separate J in two components: the periodic part J_p and the time-proportional part J_t . These take the following form:

$$J_t = \begin{bmatrix} 0 & 1 & 0 & 0 \\ 0 & 0 & 0 & 0 \\ 0 & 0 & 0 & 0 \\ 0 & 0 & 0 & 0 \end{bmatrix} \quad (2.35a) \qquad J_p = \begin{bmatrix} 0 & 0 & 0 & 0 \\ 0 & 0 & 0 & 0 \\ 0 & 0 & 0 & \omega \\ 0 & 0 & -\omega & 0 \end{bmatrix} \quad (2.35b)$$

Now, the exponential of the Jordan matrix can be expressed as:

$$K \equiv \exp (J(t - t_0)) = K_p(t) K_t(t - t_0) (K_p(t_0))^{-1} \quad (2.36)$$

where:

$$K_p(t) = \exp J_p t \quad (2.37a)$$

$$K_t(t) = \exp J_t t \quad (2.37b)$$

The actual expressions for K , K_p and K_t are:

$$K_p(t) = \begin{bmatrix} 1 & 0 & 0 & 0 \\ 0 & 1 & 0 & 0 \\ 0 & 0 & C_{\omega t} & S_{\omega t} \\ 0 & 0 & -S_{\omega t} & C_{\omega t} \end{bmatrix} \quad (2.38a) \qquad K_t(t) = \begin{bmatrix} 1 & t & 0 & 0 \\ 0 & 1 & 0 & 0 \\ 0 & 0 & 1 & 0 \\ 0 & 0 & 0 & 1 \end{bmatrix} \quad (2.38b)$$

$$K(t) = \begin{bmatrix} 1 & t & 0 & 0 \\ 0 & 1 & 0 & 0 \\ 0 & 0 & C_{\omega t} & S_{\omega t} \\ 0 & 0 & -S_{\omega t} & C_{\omega t} \end{bmatrix} \quad (2.38c)$$

where $C_{\omega t} = \cos \omega t$ and $S_{\omega t} = \sin \omega t$.

III. Final expression of the in-plane motion STM.

Substituting (2.36) into (2.34), it follows that:

$$\Phi(t, t_0) = \exp(\mathbf{A}(t - t_0)) = V K_p(t) K_t(t - t_0) (K_p(t_0))^{-1} V^{-1} \quad (2.39)$$

Equation (2.39) can be yet again reframed as:

$$\Phi(t, t_0) = B(t) \Phi_{E\lambda}(t, t_0) (B(t_0))^{-1} \quad (2.40)$$

where $B(t) = V K_p(t)$ and $\Phi_{E\lambda}(t, t_0) = K_t(t - t_0)$. The propagation can now be understood as the composition of three operations:

1st Conversion of the initial cartesian state vector to the eigenspace $E\lambda$.

2nd Propagation of the eigenspace state vector through the $\Phi_{E\lambda}(t, t_0)$ STM.

3rd Back-transformation of the eigenspace state vector at the final epoch to the cartesian space.

The matrices B and $\Phi_{E\lambda}$ can be calculated from (2.32),(2.38a) and (2.38b). The final result is:

$$\Phi_{IP}(t, t_0) = \begin{bmatrix} 1 & 6(\omega\tau - \sin \omega\tau) & \frac{4}{\omega} \sin \omega\tau - 3\tau & \frac{2}{\omega}(1 - \cos \omega\tau) \\ 0 & 4 - 3 \cos \omega\tau & \frac{2}{\omega}(\cos \omega\tau - 1) & \frac{1}{\omega} \sin \omega\tau \\ 0 & 6\omega(1 - \cos \omega\tau) & 4 \cos \omega\tau - 3 & 2 \sin \omega\tau \\ 0 & 3\omega \sin \omega\tau & -2 \sin \omega\tau & \cos \omega\tau \end{bmatrix} \quad (2.41)$$

Which is identical to the in-plane part of (2.20).

IV. Out-of-plane motion STM.

The out-of-plane counterpart can be equally calculated, but in this case, only the results will be shown. The procedure is exactly the same as done with the in-plane, but with a simpler mathematical

manipulation:

$$V_{complex} = \begin{bmatrix} \frac{i}{2n} & \frac{i}{2n} \\ \frac{1}{2} & \frac{1}{2} \end{bmatrix} \quad (2.42a)$$

$$V = \begin{bmatrix} 0 & \frac{1}{2} \\ \frac{n}{2} & 0 \end{bmatrix} \quad (2.42b)$$

$$K(t) = \begin{bmatrix} C_{\omega t} & S_{\omega t} \\ -S_{\omega t} & C_{\omega t} \end{bmatrix} \quad (2.42c) \quad K_p(t) = \begin{bmatrix} C_{\omega t} & S_{\omega t} \\ -S_{\omega t} & C_{\omega t} \end{bmatrix} \quad (2.42d) \quad K_t(t) = \begin{bmatrix} 1 & S_{\omega t} \\ -S_{\omega t} & 1 \end{bmatrix} \quad (2.42e)$$

$$\Phi_{OOP}(t, t_0) = \begin{bmatrix} \cos \omega(t - t_0) & \frac{\sin \omega(t - t_0)}{\omega} \\ -\omega \sin \omega(t - t_0) & \cos \omega(t - t_0) \end{bmatrix} \quad (2.43)$$

The combination of (2.41) and (2.43) lead to the exact same expression as (2.20). Alternatively, the Jordan Canonical Decomposition could be carried out for the full system, though it would be of more cumbersome manipulation.

2.3.5 Results: Comparison against High-Fidelity.

Once all these methods have been duly developed, it is time to test them between themselves and against the High-Fidelity propagation. This will be done for two simple, very typical scenarios: V-bar and R-bar approach, both provided in [12], page 367. The V-bar approach is an along-track approach, which means that the orbital rate is equal for both spacecrafts. The R-bar approach is a radial approach, in which the deputy, who is in a lower orbit, features a higher orbital rate.

Wakker [12] only specifies the orbit height, which is not a problem for the Hill equations propagation. Conversely, the Hi-Fi propagator requires the whole set of the Keplerian OEs, which is why the rest of them are set to zero (for pure simplicity). Table 2.1 shows the full setup of the scenario.

Parameter	Value
Chief's orbit	
Height	$h = 400 \text{ km}$
Deputy's relative state (LVLH frame)	
Scenario 1) V-bar approach.	
Initial position	$(x, y, z) = (-200, 0, 0) \text{ m}$
Initial velocity	$(\dot{x}, \dot{y}, \dot{z}) = (0.2, 0, 0) \text{ m/s}$
Scenario 2) R-bar approach.	
Initial position	$(x, y, z) = (0, 0, -200) \text{ m}$
Initial velocity	$(\dot{x}, \dot{y}, \dot{z}) = (0, 0, 0.2) \text{ m/s}$
Propagation parameters	
Propagation time	$N_{\text{orbits}} = 10$

Table 2.1: Testing scenarios for Hill equations validation [12].

2.3.5.1 Scenario 1: V-Bar approach.

Figure 2.1(a) shows the relative error of the described Hill equations approaches with respect to High-Fidelity in relative distance, for the V-Bar approach. This allows to select the most accurate method, which turns out to be the STM propagation. The error is nonetheless quite close in all surveyed methods. It is possible now to compare every other method with STM integration, which is shown in figure 2.1(b). As it could be expected, direct integration and STM propagation yield really similar results, as they are two completely equivalent formulations. On the other hand, CW solution and Jordan Decomposition yield also the same result, as again, they use exactly the same STM (decomposed or not).

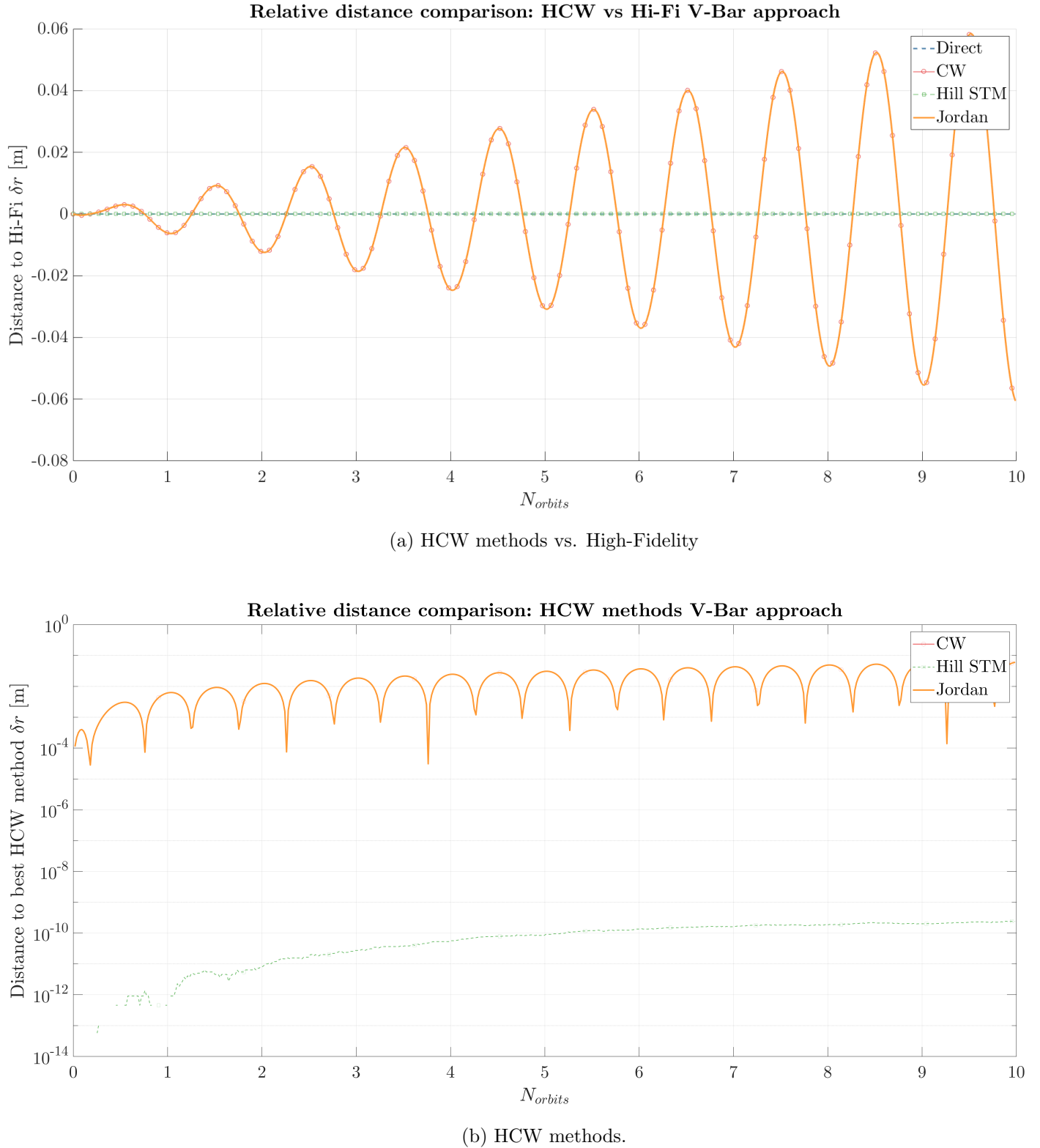


Figure 2.1: Difference in relative distance between HCW methods and Hi-Fi (V-bar approach).

This is only one side of the sword. Besides accuracy, computational efficiency is another concern, which can be analysed through the elapsed time. Table 2.2 represents these results, which show a big difference between the two numerical methods and the analytical ones (around one order of magnitude). As a scale, the time required for High-Fidelity propagation is also provided, which doubles any of the HCW methods.

Method	Direct integration	CW solution	STM propagation	Jordan Decomposition	High-Fidelity
Elapsed time [s]	1.8697	0.1407	2.1526	0.2881	3.9657

Table 2.2: Elapsed time for the computation of V-bar scenario through each HCW method.

Figure 2.2 shows the in-plane motion for this scenario as integrated by Hi-Fi and HCW. A drift in radial direction is seen as the main difference between them, which is due to Hill assumptions and the close-proximity simplification.

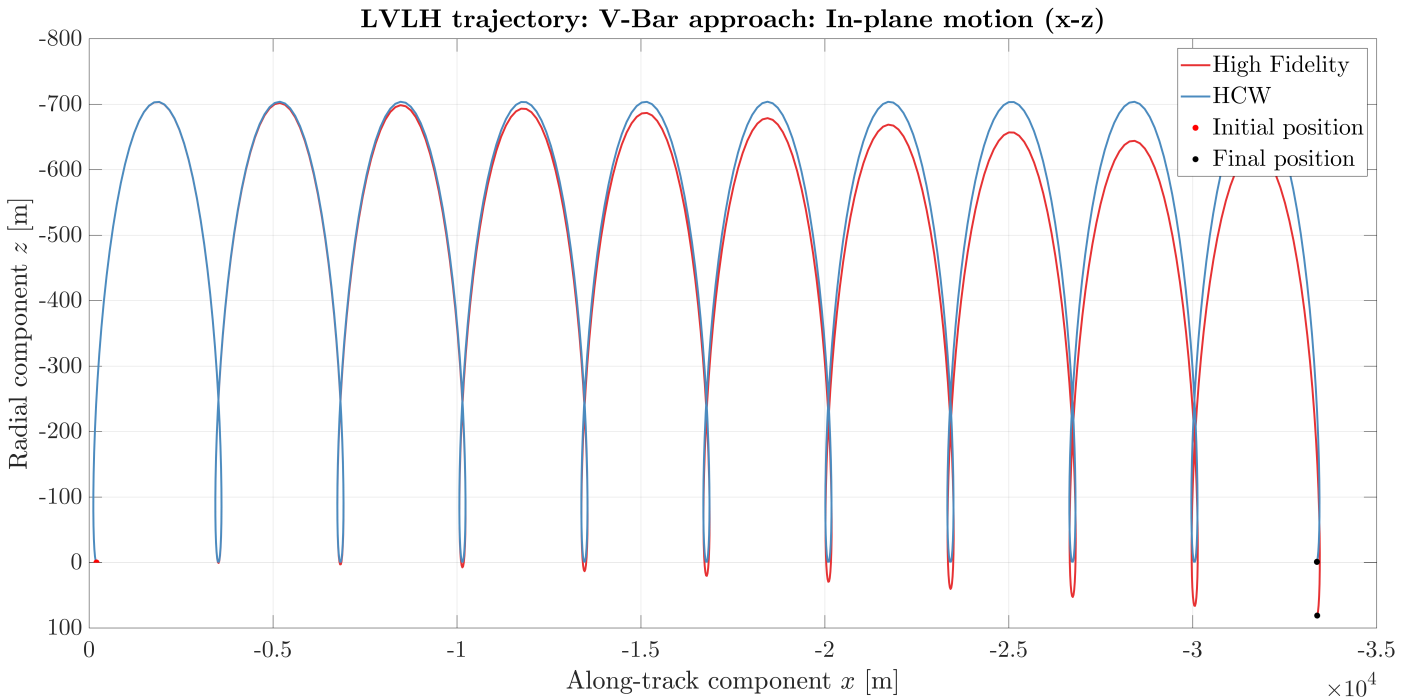


Figure 2.2: x-z trajectory comparison between STM propagation (HCW) and High-Fidelity.

2.3.5.2 Scenario 2: R-Bar approach.

The same procedure is here reproduced for the R-bar approach. No further comments are to be made, as the same behaviour is repeated: STM propagation is the most accurate, numerical methods are much more expensive and a similar drift in radial coordinate is again present.

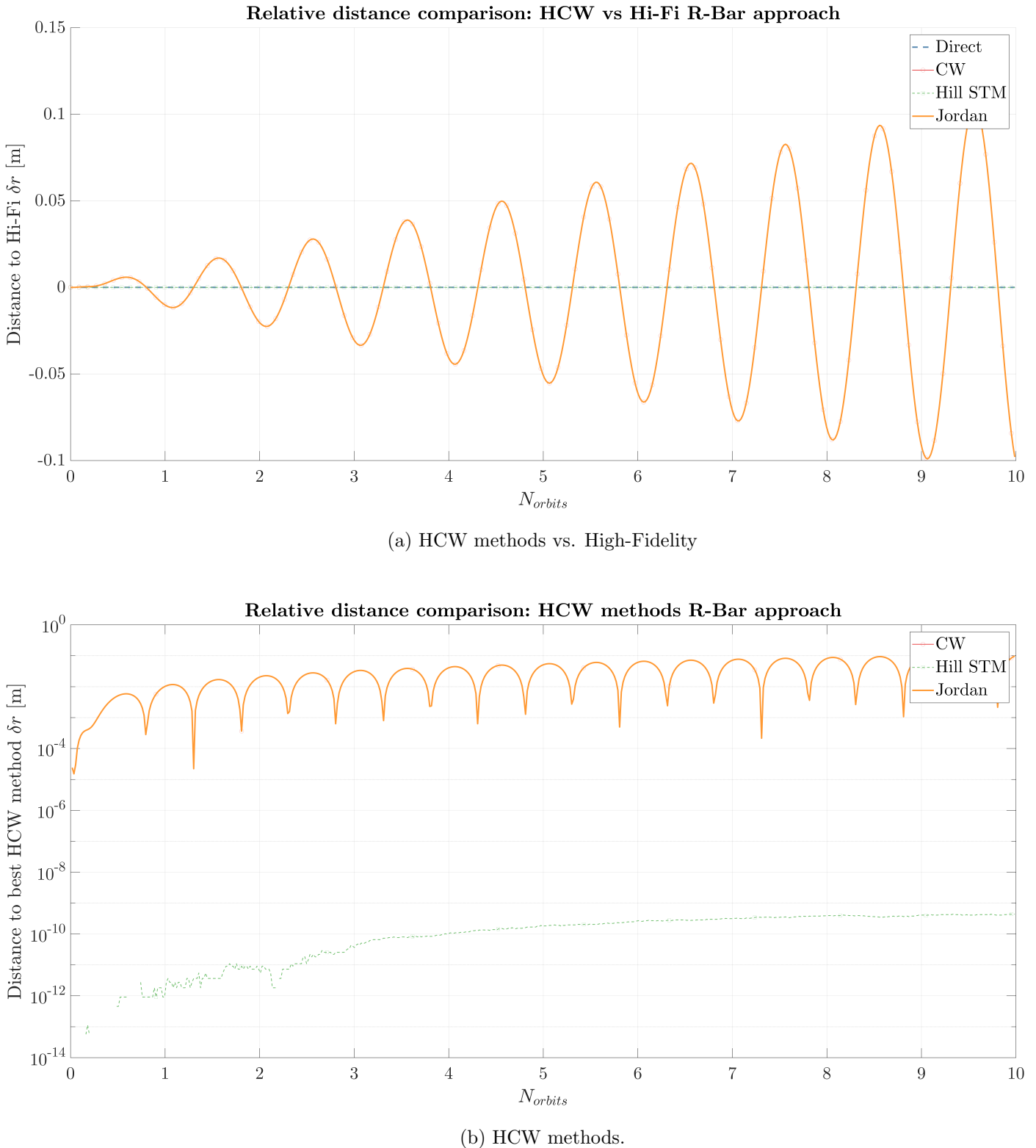


Figure 2.3: Difference in relative distance between HCW methods and Hi-Fi (R-bar approach).

Method	Direct integration	CW solution	STM propagation	Jordan Decomposition	High-Fidelity
Elapsed time [s]	1.9224	0.1486	2.2159	0.2984	4.1314

Table 2.3: Elapsed time for the computation of R-bar scenario through each HCW method.

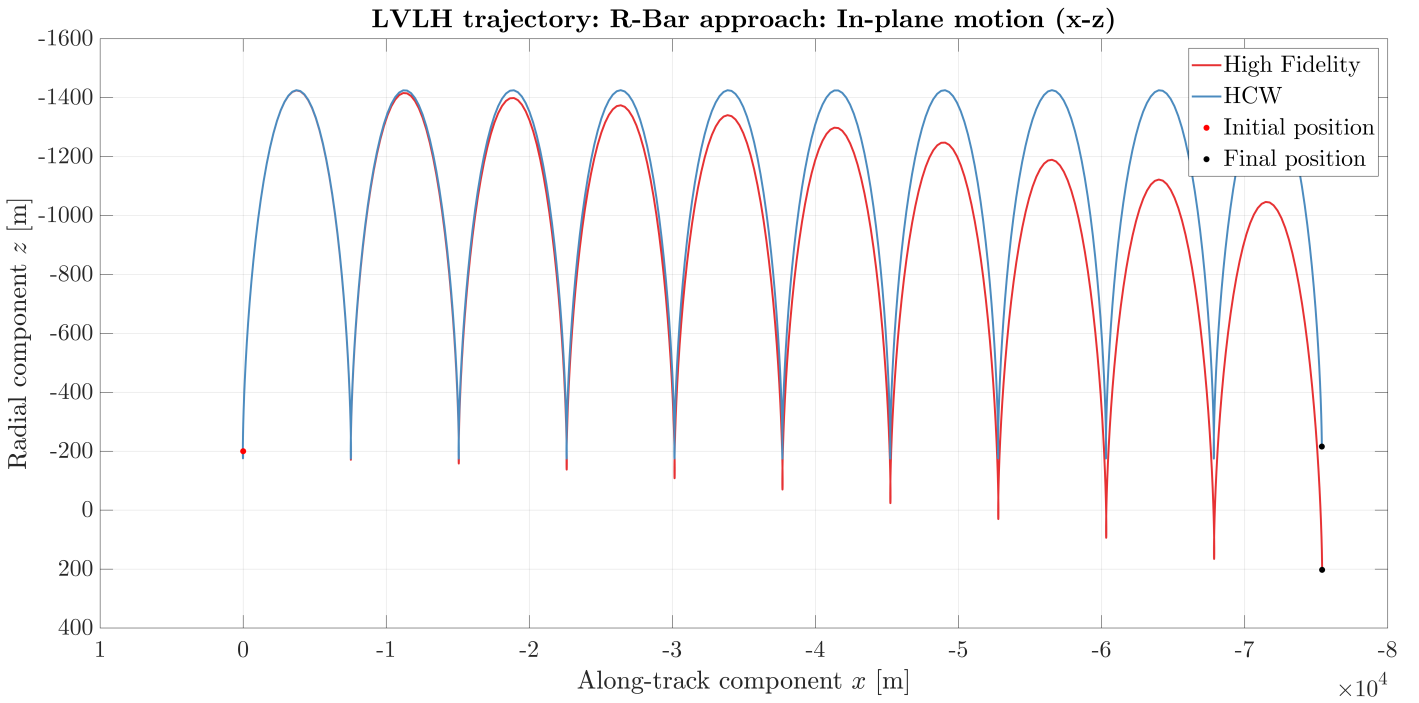


Figure 2.4: x-z trajectory comparison between STM propagation (HCW) and High-Fidelity (R-bar approach).

2.4 Orbit safety in near-circular orbits.

2.4.1 Orbit safety concept.

Orbit or trajectory safety can be understood as how protected from danger or risk a spacecraft formation is. It is essentially a kinematic condition, being closely related to the notions of relative position and velocity, and how these vary over time. Both branches of relative motion (*i.e.* rendez-vous and formation flying) are subject to this concept.

One of the biggest concerns about orbit safety is trajectory uncertainty. If one knew the exact position of each spacecraft, safety margins could be lowered down to almost zero, but, unfortunately, that is not the case. For this reason, distance margins have to be established. Relative motion is usually decomposed in three components: radial, along-track and cross-track. The most susceptible one to estimation errors is the along-track component, due to the high influence of the semimajor axis on the angular rate, thus on the angular position [13]. Hence, along-track uncertainty will always tend

to be much higher than either radial or cross-track.

With this fact in mind, it seems logical to try and separate the spacecrafts in radial or cross-track components, as motion can be more accurately predicted in those directions. It is here where the eccentricity/inclination vector separation concept arises, as an approach to describe the periodic relative motion that takes place in said components. In the following section, its grounds and applications will be discussed, both in general terms and applied to near-circular reference orbits.

2.4.2 Eccentricity-inclination vector separation strategy.

2.4.2.1 Eccentricity and inclination vectors.

The eccentricity and inclination vectors constitute an interesting way to parametrize relative motion. This description was firstly introduced by Eckstein [13], aimed initially at geostationary orbits. Later on, it was extended to proximity LEO operations [14], which is today's main scope of application.

This approach to orbit safety will be treated recurrently along the thesis, being progressively extended as the orbits grow in complexity. In this section, the basics of this concept will be described, starting with the parametrization of proximity relative motion in terms of the eccentricity and inclination vectors (see section A.3.2.1). After that, the two feasible setups of δ_e and δ_i are discussed.

2.4.2.2 Linearized equations of relative motion in terms of δ_e and δ_i .

The target is to obtain an expression which relates the eccentricity and inclination vector components to the radial, along-track and cross-track distances. This can be done by applying some transformations to the already available Keplerian OE set to RTN (see B.5.2), or through a geometric analysis of the motion. As the first one is almost trivial (considered said section), the second one will be tackled, as explained in more detail in [15]:

I. Effect of relative eccentricity vector δ_e .

The relative eccentricity vector accounts for the variation in the eccentricity value and the argument of perigee. Assuming no other variation in any element, it can be projected on the chief's orbital plane, leading to:

$$\underline{e} = \begin{Bmatrix} e_x \\ e_y \end{Bmatrix} = e \begin{Bmatrix} \cos \omega \\ \sin \omega \end{Bmatrix} \Rightarrow \delta\underline{e} = \begin{Bmatrix} \delta e_x \\ \delta e_y \end{Bmatrix} = \delta e \begin{Bmatrix} \cos \varphi \\ \sin \varphi \end{Bmatrix}$$

where φ is usually referred to as the argument of perigee of the relative orbit. The relative eccentricity has an effect on the in-plane motion (*i.e.* on the radial and along-track components). In order to get these, one must first derive some expressions for the orbital radius r and the difference $\theta - M$.

The orbital radius for near-circular orbits ($e \ll 1$) can be expressed as:

$$\begin{aligned} \frac{r}{a} &= 1 - e \cos E \underset{e \ll 1}{\approx} 1 - e \cos M = 1 - e \cos(\lambda - \omega) = 1 - e \cos \omega \cos \lambda + e \sin \lambda \sin \omega \\ &\Rightarrow \frac{r}{a} \approx 1 - e_x \cos \lambda - e_y \sin \lambda \end{aligned} \quad (2.44)$$

where λ is the mean argument of latitude, which embodies the time-varying element of the E/I element set. The second auxiliary expression $\theta - M$ can be obtained in many handbooks, by looking for the series expansion of the mean anomaly in terms of the true [16]:

$$M = \theta + 2 \sum_{n=1}^{\infty} (-1)^n \left(\frac{1}{n} + \sqrt{1-e^2} \right) \beta^n \sin n\theta \underset{e \ll 1}{\approx} \theta - 2e \sin \theta$$

$$\Rightarrow \theta - M = 2e \sin M = 2e \sin(\lambda - \omega) = 2e (\sin \lambda \cos \omega - \cos \lambda \sin \omega) = 2e_x \sin \lambda - 2e_y \cos \lambda \quad (2.45)$$

Assuming that both spacecrafts have the same mean argument of latitude and semimajor axis, the radial and along-track distance (δr_R , δr_T) between chief and deputy are due to (a) the difference in orbital radius δr and (b) the difference in true argument of latitude $\delta u = \delta\theta + \delta\omega$. With this in mind, a graphical representation of the situation can be drafted, as shown in 2.5.

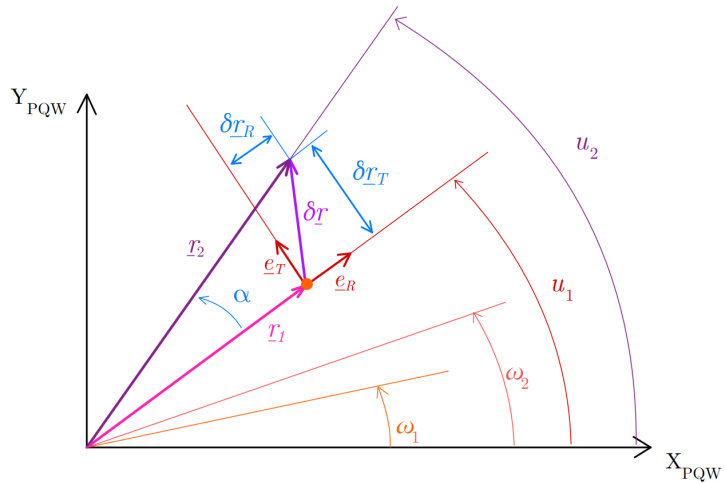


Figure 2.5: Effect of δr and δu in radial and along-track distances.

The angle α can be developed in terms of known magnitudes, that is:

$$\begin{aligned}\alpha &= u_2 - u_1 = (\lambda_2 - \lambda_1) + (\theta_2 - M_2) - (\theta_1 - M_1) = \\ 0 + 2e_2 \sin M_2 - 2e_1 \sin M_1 &= 2\delta e_x \sin \lambda - 2\delta e_y \cos \lambda = \mathcal{O}(\delta e) \\ \Rightarrow \alpha &= \mathcal{O}(\delta e) \sim 10^{-3}\end{aligned}\tag{2.46}$$

I.A. Effect of $\underline{\delta e}$ in δr_R .

Radial distance can be derived from figure 2.5 as:

$$\delta r_R = r_2 \cos \alpha - r_1 \underset{|\alpha| \ll 1}{\approx} r_2 - r_1 = \delta r$$

In virtue of equation (2.44):

$$\begin{aligned}\delta r_R &= \delta r = a (e_1 \cos M_1 - e_2 \cos M_2) \\ \frac{\delta r_R}{a} &= e_1 (\cos \lambda \cos \omega_1 - \sin \lambda \sin \omega_1) - e_2 (\cos \lambda \cos \omega_2 - \sin \lambda \sin \omega_2) = \\ &= \cos \lambda (e_{x1} - e_{x2}) - \sin \lambda (e_{y1} - e_{y2}) \\ \Rightarrow \frac{\delta r_R}{a} \Big|_{\delta e} &\approx -\delta e_y \sin \lambda - \delta e_x \cos \lambda\end{aligned}\tag{2.47}$$

I.B. Effect of $\underline{\delta e}$ in δr_T .

The along-track distance can be computed in a similar manner, neglecting terms of order $e \delta e$ and higher:

$$\begin{aligned}\delta r_T &= r_2 \sin \alpha \underset{|\alpha| \ll 1}{\approx} a (1 - e_2 \cos M_2) \alpha \underset{|e \delta e| \ll |\delta e|}{\approx} a \alpha \\ \Rightarrow \frac{\delta r_T}{a} \Big|_{\delta e} &\approx \alpha = 2\delta e_x \sin \lambda - 2\delta e_y \cos \lambda\end{aligned}\tag{2.48}$$

II. Effect of relative inclination vector $\underline{\delta i}$.

As presented in section A.3.2.1, the relative inclination vector takes the following form:

$$\delta \underline{i} = \sin \delta i \begin{Bmatrix} \cos \psi \\ \sin \psi \end{Bmatrix} \approx \begin{Bmatrix} \delta i \\ \sin i \delta \Omega \end{Bmatrix}$$

where ψ is referred to as the ascending node of the relative orbit. Its effect on the cross-track distance can be derived from the spherical triangle in figure 2.6, applying the law of sines as:

$$\frac{\sin(u_2 - \psi)}{\sin \frac{\pi}{2}} = \frac{\sin \frac{\delta r_N}{a}}{\sin \delta i} \Rightarrow \sin \frac{\delta r_N}{a} \underset{\delta r_N \ll a}{\approx} \frac{\delta r_N}{a} = \sin \delta i \sin(u_2 - \psi) \quad (2.49)$$

However, an expression with the mean argument of latitude instead of the true counterpart is needed. As only first-order terms are to be retained:

$$\begin{aligned} \sin(u - \psi) &= \sin[(\lambda - \psi) + (u - \lambda)] = \sin(\lambda - \psi) \cos(u - \lambda) + \cos(\lambda - \psi) \sin(u - \lambda) = \\ &= \sin(\lambda - \psi) \cos(2e \sin \theta) + \cos(\lambda - \psi) \sin(2e \sin \theta) \approx \\ &\underset{|2e \sin \theta| \ll 1}{\approx} \sin(\lambda - \psi) \left(1 - \frac{(2e \sin \theta)^2}{2}\right) + \cos(\lambda - \psi) 2e \sin \theta = \sin(\lambda - \psi) + \mathcal{O}(e) \end{aligned}$$

$$\sin(u - \psi) \Big|_{|2e \sin \theta| \ll 1} \underset{|2e \sin \theta| \ll 1}{\approx} \sin(\lambda - \psi) \quad (2.50)$$

Substituting (2.50) into (2.49):

$$\begin{aligned} \frac{\delta r_N}{a} &\approx \sin \delta i \sin(\lambda - \psi) = \sin \delta i \cos \psi \sin \lambda - \sin \delta i \sin \theta \cos \lambda \\ &\Rightarrow \frac{\delta r_N}{a} \Big|_{\delta i} \approx \delta i_x \sin \lambda - \delta i_y \cos \lambda \end{aligned} \quad (2.51)$$

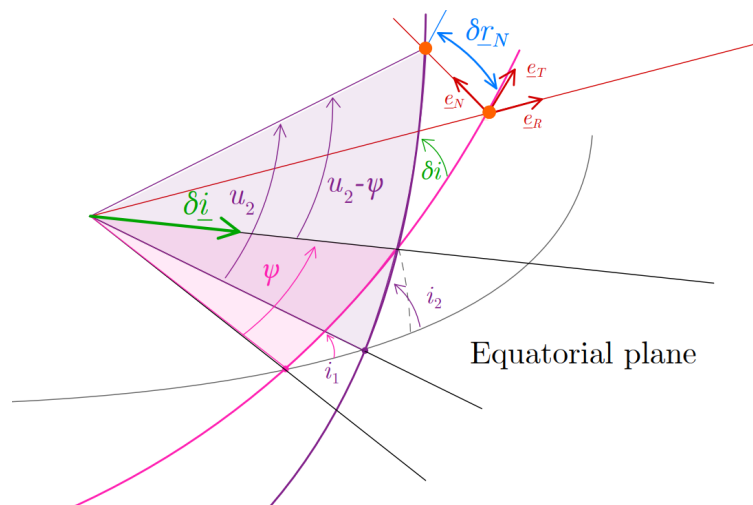


Figure 2.6: Inclination vector and cross-track distance.

III. Effect of relative semimajor axis and mean argument of latitude δa , $\delta \lambda$.

As previously stated, the relative semimajor axis has a crucial influence on the relative dynamics, varying the angular rate of the orbit and thus to an unbounded along-track drift. Consequently, the effect of a relative semimajor axis δa in the angular rate $\dot{\lambda}$ is expanded up to first-order as:

$$\begin{aligned}\dot{\lambda}(a) &= \dot{\omega} + \dot{M}(a) = \dot{M}(a) = n = \sqrt{\frac{\mu}{a^3}} \\ \Rightarrow \delta\dot{\lambda}_{\delta a} &= \dot{\lambda}(a + \delta a) - \dot{\lambda}(a) = \sqrt{\frac{\mu}{(a + \delta a)^3}} - \sqrt{\frac{\mu}{a^3}} \\ \Rightarrow \delta\dot{\lambda}_{\delta a} &= \sqrt{\frac{\mu}{a^3}} \left[\frac{1}{(1 + \frac{\delta a}{a})^{3/2}} - 1 \right] \underset{|\frac{\delta a}{a}| << 1}{\approx} -\frac{3}{2} \frac{\delta a}{a} n \\ \delta\lambda|_{\delta a} &= \int_{t_0}^t \delta\dot{\lambda} dt = -\frac{3}{2} \frac{\delta a}{a} n(t - t_0) = -\frac{3}{2} \frac{\delta a}{a} (M - M_0) = -\frac{3}{2} \frac{\delta a}{a} (\lambda - \lambda_0)\end{aligned}\tag{2.52}$$

III.A. Effect of δa , $\delta \lambda$ in δr_R .

The expression for the radial distance induced by δa is, assuming a constant mean argument of latitude λ and argument of perigee ω :

$$\begin{aligned}\delta r_R &\approx r_2 - r_1 \approx (a + \delta a)(1 - e_2 \cos M_2) - a(1 - e_1 \cos M_1) \approx \delta a \\ \Rightarrow \frac{\delta r_R}{a} \Big|_{\delta a} &\approx \frac{\delta a}{a}\end{aligned}\tag{2.53}$$

where it is assumed that the relative mean argument of latitude has no effect on it.

III.B. Effect of δa , $\delta \lambda$ in δr_T .

The effect in along-track distance is due to both δa and $\delta \lambda$, as λ is intrinsically affected by δa (see eq. (2.52)). Without further ado:

$$\begin{aligned}\delta r_T &= r_2 \sin(u_2 - u_1) \underset{(2.52)}{\approx} r_2 \sin(\lambda_2 - \lambda_1) \underset{|\lambda_2 - \lambda_1| << 1}{\approx} (a + \delta a) (1 - e_2 \cos M_2) (\lambda_2 - \lambda_1) \\ &\rightarrow \delta r_T \underset{e << 1}{\approx} (a + \delta a) \left[\delta \lambda - \frac{3}{2} \frac{\delta a}{a} (\lambda - \lambda_0) \right] \\ \Rightarrow \frac{\delta r_T}{a} \Big|_{\delta a \delta \lambda} &\approx \delta \lambda - \frac{3}{2} \frac{\delta a}{a} (\lambda - \lambda_0)\end{aligned}\tag{2.54}$$

IV. Final set of linearized equations.

Now, considering all the previous effects, a compact set of equations can be reached [14]:

$$\begin{Bmatrix} \delta r_R \\ \delta r_T \\ \delta r_N \end{Bmatrix} = \begin{Bmatrix} \delta a \\ \delta \lambda - \frac{3}{2} \frac{\delta a}{a} (\lambda - \lambda_0) \\ 0 \end{Bmatrix} + a \delta e \begin{Bmatrix} -\cos(\lambda - \varphi) \\ 2 \sin(\lambda - \varphi) \\ 0 \end{Bmatrix} + a \delta i \begin{Bmatrix} 0 \\ 0 \\ \sin(\lambda - \psi) \end{Bmatrix} \quad (2.55)$$

$$\Leftrightarrow \begin{Bmatrix} \delta r_R \\ \delta r_T \\ \delta r_N \end{Bmatrix} = \begin{bmatrix} \delta a/a & 0 & -\delta e_x & -\delta e_y \\ \delta \lambda & -\frac{3}{2} \delta a/a & -2\delta e_y & 2\delta e_x \\ 0 & 0 & -\delta i_y & \delta i_x \end{bmatrix} \begin{Bmatrix} 1 \\ \lambda - \lambda_0 \\ \cos \lambda \\ \sin \lambda \end{Bmatrix} \quad (2.56)$$

A comparison of 2.56 and the analytical solution of the HCW equations show a complete correspondence of individual terms, hence proving the mathematical equivalence of both formulations. This equation can also be understood as a linearized approach to the Gauss Variational Equations (see E.2), and finally, as an alternative to the mapping provided in B.5.2.

2.4.2.3 Collision avoidance for bounded trajectories: $\delta e/\delta i$ separation.

The previous equations can be particularized for the bounded trajectory case. This means that there is no mutual drift, hence relative semimajor axis drops to zero. The equations for the relative distances between both spacecrafts can be expressed as:

$$\begin{cases} \frac{\delta r_R}{a} = -\delta e \cos(\lambda - \varphi) \end{cases} \quad (2.57a)$$

$$\begin{cases} \frac{\delta r_T}{a} = 2\delta e \sin(\lambda - \varphi) \end{cases} \quad (2.57b)$$

$$\begin{cases} \frac{\delta r_N}{a} = \delta i \sin(\lambda - \psi) \end{cases} \quad (2.57c)$$

This formulation indeed facilitates the safety analysis. In order to avoid collision hazard, considering along-track position uncertainties, a proper separation in radial and cross-track components must be set up. As shown in [17], two possible strategies to achieve this are (a) a parallel alignment of δe and δi and (b) an antiparallel (orthogonal) arrangement.

Before discussing these alternatives, it is useful to do a quick analysis of the relevant positions that may arise from (2.57). If $\lambda = \varphi$, tangential distance vanishes, that is, the deputy is right below the chief (at a certain cross-track distance). Conversely, if $\lambda = \varphi + \frac{\pi}{2}$, radial distance vanishes, and the deputy comes just in front of the chief. Similar statements can be made with the out-of-plane

motion. A graphical representation of the mentioned geometry is shown in figure 2.7.

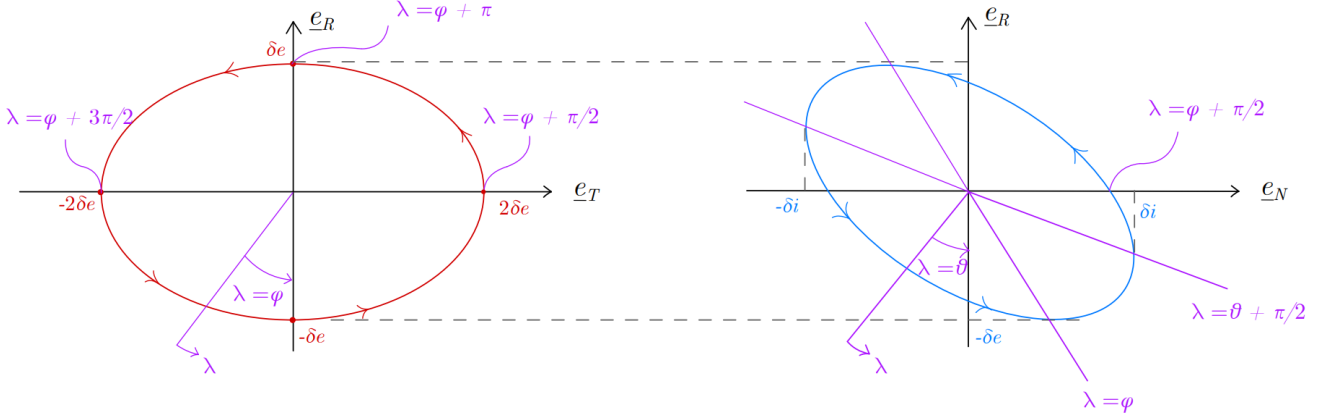


Figure 2.7: Relative motion in RTN frame for $\delta a = 0$ and a general $\delta \underline{e} - \delta \underline{i}$ alignment.

A. Parallel configuration.

If the relative eccentricity and inclination vectors are parallel, it follows that.

$$\delta \underline{e} \parallel \delta \underline{i} \Rightarrow \delta \underline{e} \cdot \delta \underline{i} = \delta e \delta i \begin{Bmatrix} \cos \varphi & \sin \varphi \end{Bmatrix} \begin{Bmatrix} \cos \psi \\ \sin \psi \end{Bmatrix} = \delta e \delta i \cos(\varphi - \psi) \underset{\delta \underline{e} \parallel \delta \underline{i}}{=} 1$$

$$\implies \varphi = \psi + 2\pi k, \quad k \in \mathbb{Z} \quad (2.58)$$

For this configuration, the radial and cross-track distances never drop to zero simultaneously.

In fact, if $\delta r_R = 0$, then δr_N is maximum, and viceversa. Hence, minimum separation satisfies:

$$\|\delta \underline{r}\| \geq \min(a \delta e, a \delta i)$$

In conclusion, separation between the spacecrafts is ensured, even if tangential distance is null.

A graphical representation of this configuration can be seen in figure 2.8(a).

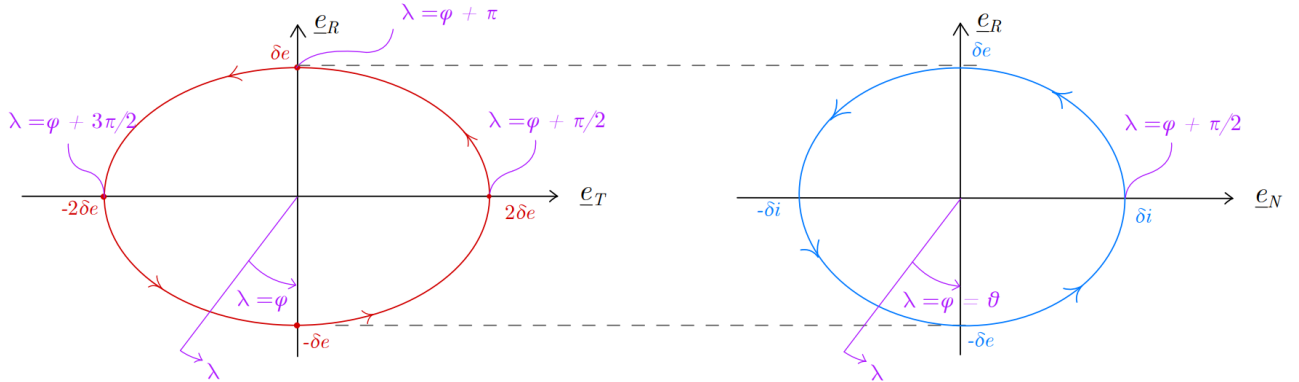
B. Antiparallel configuration.

The condition for antiparallel configuration can be expressed as:

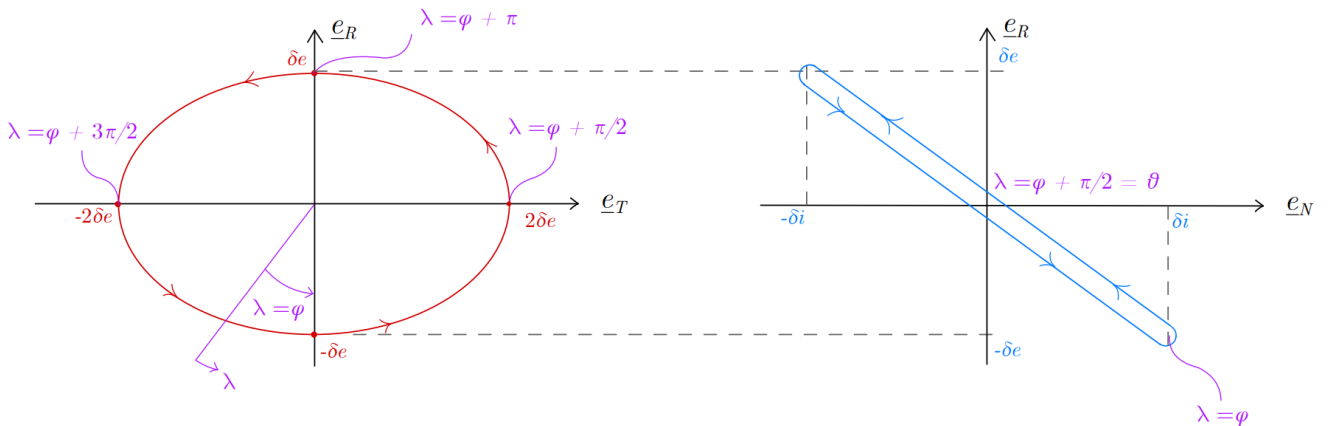
$$\delta \underline{e} \perp \delta \underline{i} \Rightarrow \delta \underline{e} \cdot \delta \underline{i} = \delta e \delta i \begin{Bmatrix} \cos \varphi & \sin \varphi \end{Bmatrix} \begin{Bmatrix} \cos \psi \\ \sin \psi \end{Bmatrix} = \delta e \delta i \cos(\varphi - \psi) \underset{\delta \underline{e} \perp \delta \underline{i}}{=} 0$$

$$\implies \varphi = \psi + (2k+1)\frac{\pi}{2}, \quad k \in \mathbb{Z} \quad (2.59)$$

This configuration can also be seen in 2.8(b).



(a) Parallel configuration.



(b) Antiparallel configuration.

Figure 2.8: Relative motion for parallel and antiparallel $\delta\underline{e}/\delta\underline{i}$ vectors.

The right diagram of figure 2.8(b) shows exactly the predicted behaviour: normal and radial distance vanish simultaneously for $\lambda = \varphi + \pi/2$, which may endanger the formation if the along-track separation is not big enough.

In conclusion, parallel E/I vector configuration is a very much feasible option. This will be later extended to elliptic (see 3.3.2.2) and perturbed reference orbits (see 5.4).

Relative dynamics around elliptic reference orbits.

3.1 Introduction.

In the previous chapter, the Clohessy-Wiltshire set of equations of motion has been analysed. Getting them from Newton's law required the fulfilment of two assumptions. Firstly, the distance between deputy and chief must be negligible compared to either spacecraft's orbital radius. This is usually the case when dealing both with formation flying and rendez-vous manoeuvres. The second assumption is that both orbits are near-circular ($e \ll 1$), which is not as acceptable as the first one. This is specially relevant on formation flying, as the timescale is usually large enough to experience sensible deviations.

Conceptually, there are some obvious differences between near-circular and eccentric orbits. Firstly, orbital radius varies over time for non-null eccentricity, which means that, at every point, the spacecraft is radially closing or moving away from the central body (*i.e.* the Earth). But more importantly, the angular velocity is no longer constant, which means that the non-inertial effects when analysing the relative motion are not constant. That will surely make it harder -yet not impossible- to get analytical expressions, though through some simplifications, it may be done.

For this reason, several motion models for elliptic orbits have been developed [18]. Both linear and nonlinear models are present in the literature, though the first ones are the most usually employed. Tschauner and Hempel [19] developed a linear, first-order model through the truncation of the Taylor series expansion of the differential gravity. The so-called Tschauner-Hempel equations were widely used at the time, as they are consistent with the Hill/Clohessy-Wiltshire (HCW) model. Nonetheless, they were subsequently improved, due to the existence of singularities in the in-plane motion. Carter [20] provides a non-singular solution for this issue.

Instead of these solutions, the motion model used for elliptic, unperturbed orbits in this thesis was developed by Yamanaka and Ankersen [4] (YA onwards). It results in a fairly simpler STM, which

is generally considered the state-of-the-art solution for linear propagation of the relative position and velocity in eccentric orbits. It will actually be used in the PROBA-3 mission, which flies in a highly eccentric elliptical orbit.

During this chapter, YA's approach for the motion model and their proposed solution for it will be firstly developed. This enables in turn to develop the YA STM, which will be duly tested with their own scenarios. Lastly, orbit safety concerns will be approached, extending the prior knowledge from near-circular orbits to arbitrarily elliptical, as done by Peters and Noomen [21].

3.2 Motion model and STM.

3.2.1 Simplification of equations of motion: Yamanaka-Ankersen solution.

As developed in section 2.2.5, the differential equations for proximity relative motion are:

$$\begin{Bmatrix} \ddot{x} \\ \ddot{y} \\ \ddot{z} \end{Bmatrix} = \begin{Bmatrix} -k\omega^{3/2}x + 2\omega\dot{z} + \dot{\omega}z + \omega^2x \\ -k\omega^{3/2}y \\ 2k\omega^{3/2}z - 2\omega\dot{x} - \dot{\omega}x + \omega^2z \end{Bmatrix} + \underline{a}_f + \underline{a}_{D,d} - \underline{a}_{C,d} \quad (3.1)$$

In this chapter, only the unperturbed version of this problem will be approached, that is, $\underline{a}_f = \underline{a}_{D,d} = \underline{a}_{C,d} = \underline{0}$. A slightly more general approach is to assume that, if dealing with perturbed motion, the perturbation acceleration is equal on either body. The main difference now with respect to Hill equations (see 2.2.6) is that the angular rate ω is now time-varying, whereas before it was constant ($\omega = n = \text{const.}$). This fact completely changes the character of the mathematical problem: the coefficient matrix is no longer constant.

It is here where Yamanaka and Ankersen, following Carter's approach, implement two changes. Firstly, chief's true anomaly θ is adopted as the independent variable instead of time. That changes the derivative definition, and for a certain variable ξ , the conversion from time to true anomaly derivatives is as follows:

$$\frac{d\xi}{dt} = \frac{d\xi}{d\theta} \frac{d\theta}{dt} = \omega \frac{d\xi}{d\theta} \Rightarrow \dot{\xi} = \omega \xi' \quad (3.2a)$$

$$\frac{d^2\xi}{dt^2} = \frac{d}{dt} \left(\frac{d\xi}{dt} \right) = \omega \frac{d\omega}{d\theta} \frac{d\xi}{d\theta} + \omega^2 \frac{d^2\xi}{dt^2} \Rightarrow \ddot{\xi} = \omega^2 \xi'' + \omega \omega' \xi' \quad (3.2b)$$

where ω' is calculated by simply using the angular momentum definition:

$$\omega = \frac{h}{R^2} = \frac{h}{p^2} (1 + e \cos \theta)^2 = k^2 \rho^2 \Rightarrow \omega' = 2k^2 \rho \rho' = -2k^2 e \sin \theta \rho \quad (3.3)$$

Substituting (3.2a), (3.2b) and (3.3) into (3.1) yields:

$$\begin{cases} \rho x'' - 2e \sin \theta x' - e \cos \theta x = 2\rho z' - 2e \sin \theta z \\ \rho y'' - 2e \sin \theta y' = -y \end{cases} \quad (3.4a)$$

$$\begin{cases} \rho z'' - 2e \sin \theta z' - (3 + e \cos \theta)z = -2\rho x' + 2e \sin \theta x \end{cases} \quad (3.4b)$$

$$\begin{cases} \rho z'' - 2e \sin \theta z' - (3 + e \cos \theta)z = -2\rho x' + 2e \sin \theta x \end{cases} \quad (3.4c)$$

Once this change of variable has been applied, the following transformation is performed:

$$\begin{Bmatrix} \tilde{x} \\ \tilde{y} \\ \tilde{z} \end{Bmatrix} = (1 + e \cos \theta) \begin{Bmatrix} x \\ y \\ z \end{Bmatrix} \quad (3.5)$$

which, if substituted in (3.4), lead to the rather simple following set of equations:

$$\begin{cases} \tilde{x}'' = 2\tilde{z}' \\ \tilde{y}'' = -\tilde{y} \end{cases} \quad (3.6a)$$

$$\begin{cases} \tilde{y}'' = -\tilde{y} \end{cases} \quad (3.6b)$$

$$\begin{cases} \tilde{z}'' = 3\frac{\tilde{z}}{\rho} - 2\tilde{x}' \end{cases} \quad (3.6c)$$

The initial conditions that complete the initial value problem (IVP) can be written as:

$$\begin{Bmatrix} \tilde{x} \\ \tilde{y} \\ \tilde{z} \end{Bmatrix}(\theta_0) = \begin{Bmatrix} \tilde{x}_0 \\ \tilde{y}_0 \\ \tilde{z}_0 \end{Bmatrix} = (1 + e \cos \theta_0) \begin{Bmatrix} x_0 \\ y_0 \\ z_0 \end{Bmatrix}$$

Solution of the simplified set of equations.

It is rather obvious that equations (3.6a), (3.6b), (3.6c) feature a decoupling between in-plane components (x-z) and out-of-plane (y). The latter can easily be solved as:

$$\tilde{y} = K_{y1} \sin \theta + K_{y2} \cos \theta \quad (3.7)$$

while for the in-plane motion, equation (3.6a) must be first integrated, then introduced into (3.6c), yielding:

$$\tilde{z}'' + \left(4 - \frac{3}{\rho}\right) \tilde{z} = -2K_{x1} \quad (3.8)$$

with \tilde{x} calculated from \tilde{z} as:

$$\tilde{x}' = 2\tilde{z} + K_{x1} \quad (3.9)$$

where K_i is the set of integration constants, derived from the prescribed initial conditions. The relation between them will be later described.

The task at hand now is to solve (3.8). Yamanaka and Ankersen propose a new solution to it, whose mathematical development is detailed in [4]. Bottom line is that, the solution for \tilde{z} is:

$$\tilde{z} = K_{z1}\rho \sin \theta + \left(K_{z2} - \frac{K_{x1}}{e} \right) \rho \cos \theta - K_{z2}e (2 - 3e\rho \sin \theta J) \quad (3.10)$$

where:

$$J = k^2(t - t_0)$$

Substituting into (3.9) and integrating:

$$\tilde{x} = K_{x2} - K_{z1} \cos \theta (\rho + 1) + \left(K_{z2} - \frac{K_{x1}}{e} \right) \sin \theta (\rho + 1) - 3K_{z2}e\rho^2 J \quad (3.11)$$

Redefining the integral constants for simplicity as:

$$K_1 \equiv K_{x2} \quad K_2 \equiv K_{z1} \quad K_3 = \left(K_{z2} - \frac{K_{x1}}{e} \right) \quad K_4 = -K_{z2}e$$

and using the following simplified notation

$$s = \rho \sin \theta \quad c = \rho \cos \theta$$

the solution of the in-plane dynamics turns fairly simpler:

$$\begin{cases} \tilde{x} = K_1 - K_2c \left(1 + \frac{1}{\rho} \right) + K_3s \left(1 + \frac{1}{\rho} \right) + 3K_4\rho^2 J \\ \tilde{z} = K_2s + K_3c + K_4(2 - 3esJ) \end{cases} \quad (3.12a)$$

$$(3.12b)$$

By simply differentiating (3.12a) and (3.12b), the in-plane velocity components can be obtained. Considering both position and velocity, a simple matrix form can be achieved:

$$\begin{Bmatrix} \tilde{x} \\ \tilde{z} \\ \tilde{v}_x \\ \tilde{v}_z \end{Bmatrix} = \begin{bmatrix} 1 & -c(1 + \rho^{-1}) & s(1 + \rho^{-1}) & 3\rho^2 J \\ 0 & s & c & (2 - 3esJ) \\ 0 & 2s & 2c - e & 3(1 - 2esJ) \\ 0 & s' & c' & -3e(s'J + s/\rho^2) \end{bmatrix} \begin{Bmatrix} K_1 \\ K_2 \\ K_3 \\ K_4 \end{Bmatrix} \equiv \Phi_\theta|_{IP} \underline{K}_{IP} \quad (3.13)$$

where:

$$s' = \cos \theta + e \cos 2\theta \quad c' = -(\sin \theta + e \sin 2\theta)$$

The out-of-plane problem can be expressed in this form as well:

$$\begin{Bmatrix} \tilde{y} \\ \tilde{v}_y \end{Bmatrix} = \begin{bmatrix} \cos \theta & \sin \theta \\ -\sin \theta & \cos \theta \end{bmatrix} \begin{Bmatrix} \tilde{y}_0 \\ \tilde{v}_{y0} \end{Bmatrix} \equiv \Phi_\theta|_{OOP} \underline{K}_{OOP} \quad (3.14)$$

3.2.2 Yamanaka-Ankersen STM and integration constants.

The target is to obtain a state transition matrix, that is, a matrix which when fed a state vector at a given time, returns the state vector at a latter epoch. Generally speaking, said entity is built as:

$$\Phi_{\theta_0}^\theta = \Phi_\theta \Phi_{\theta_0}^{-1} \Rightarrow \underline{x}(\theta) = \Phi_{\theta_0}^\theta \underline{x}(\theta_0)$$

where θ can be substituted by any independent variable, such as time. Yamanaka and Ankersen propose to merge the second part of the STM and the initial state vector, leading to the so-called pseudoinitial state vector, defined by:

$$\bar{\underline{x}}_0 = \Phi_{\theta_0}^\theta \underline{x}(\theta_0)$$

which is also called the Yamanaka-Ankersen element set. With this in mind, the goal now is to obtain both matrices, which in fact can be built from the in- and out-of-plane parts, previously defined in (3.13) and (3.14).

3.2.2.1 In-plane motion.

The first component Φ_θ was already defined as (3.13):

$$\Phi_\theta|_{IP} = \begin{bmatrix} 1 & -c(1 + \rho^{-1}) & s(1 + \rho^{-1}) & 3\rho^2 J \\ 0 & s & c & (2 - 3esJ) \\ 0 & 2s & 2c - e & 3(1 - 2esJ) \\ 0 & s' & c' & -3e(s'J + s/\rho^2) \end{bmatrix} \quad (3.15)$$

In order to get $\Phi_{\theta_0}|_{IP}^{-1}$, note that $J(\theta_0) = J(t_0) = 0$. Once applied that, the inverse is not so hard to compute, namely:

$$\Phi_{\theta_0}|_{IP}^{-1} = \frac{1}{1 - e^2} \begin{bmatrix} 1 - e^2 & 3e(s/\rho)(1 + \rho^{-1}) & -es(1 + \rho^{-1}) & 2 - ec \\ 0 & -3(s/\rho)(1 + e^2/\rho) & s(1 + \rho^{-1}) & c - 2e \\ 0 & -3(e + c/\rho) & c(1 + \rho^{-1}) + e & -s \\ 0 & 3\rho + e^2 - 1 & -\rho^2 & es \end{bmatrix}_{\theta_0} \quad (3.16)$$

3.2.2.2 Out-of-plane motion.

The out-of-plane equations are identical to those of the harmonic oscillator, whose solution is trivial. However, and so as to build an STM solution, the first step is to divide the full STM in (3.14) into the two subcomponents by substituting θ for $\theta - \theta_0$. Then, using trigonometric relations for the sum of sines and cosines, it is easy to pull both matrices apart as:

$$\Phi_{\theta_0}^\theta = \begin{bmatrix} \cos(\theta - \theta_0) & \sin(\theta - \theta_0) \\ -\sin(\theta - \theta_0) & \cos(\theta - \theta_0) \end{bmatrix} = \begin{bmatrix} \cos \theta & \sin \theta \\ -\sin \theta & \cos \theta \end{bmatrix} \begin{bmatrix} \cos \theta_0 & -\sin \theta_0 \\ \sin \theta_0 & \cos \theta_0 \end{bmatrix} \equiv \Phi_\theta \Phi_{\theta_0}^{-1} \quad (3.17)$$

3.2.2.3 Full matrices.

By simply but carefully placing the elements of (3.15), (3.16), and (3.17) in a 6x6 matrix, the full matrices are reached:

$$\Phi_\theta = \begin{bmatrix} 1 & 0 & -c(1 + \rho^{-1}) & s(1 + \rho^{-1}) & 0 & 3\rho^2 J \\ 0 & \cos \theta & 0 & 0 & \sin \theta & 0 \\ 0 & 0 & s & c & 0 & 2 - 3esJ \\ 0 & 0 & 2s & 2c - e & 0 & 3(1 - 2esJ) \\ 0 & -\sin \theta & 0 & 0 & \cos \theta & 0 \\ 0 & 0 & s' & c' & 0 & -3e(s'J + s/\rho^2) \end{bmatrix} \quad (3.18)$$

$$\Phi_{\theta_0}^{-1} = \frac{1}{1 - e^2} \times \begin{bmatrix} 1 - e^2 & 0 & 3e(s/\rho)(1 + \rho^{-1}) & -es(1 + \rho^{-1}) & 0 & 2 - ec \\ 0 & (1 - e^2)\cos \theta & 0 & 0 & -(1 - e^2)\sin \theta & 0 \\ 0 & 0 & -3(s/\rho)(1 + e^2/\rho) & s(1 + \rho^{-1}) & 0 & c - 2e \\ 0 & 0 & -3(c/\rho + e) & c(1 + \rho^{-1}) + e & 0 & -s \\ 0 & (1 - e^2)\sin \theta & 0 & 0 & (1 - e^2)\cos \theta & 0 \\ 0 & 0 & 3\rho + e^2 - 1 & -\rho^2 & 0 & es \end{bmatrix} \quad (3.19)$$

3.2.2.4 Pseudo-initial state vector.

Finally, the so-called pseudoinitital conditions are computed as defined before, namely:

$$\left\{ \begin{array}{l} \bar{x}_0 \\ \bar{y}_0 \\ \bar{z}_0 \\ \bar{v}_{x0} \\ \bar{v}_{y0} \\ \bar{v}_{z0} \end{array} \right\} = \Phi_{\theta_0}^{-1} \tilde{x}_0 = \frac{1}{1 - e^2} \times$$

$$\begin{bmatrix} 1 - e^2 & 0 & 3e(s/\rho)(1 + \rho^{-1}) & -es(1 + \rho^{-1}) & 0 & 2 - ec \\ 0 & (1 - e^2)C\theta & 0 & 0 & -(1 - e^2)S\theta & 0 \\ 0 & 0 & -3(s/\rho)(1 + e^2/\rho) & s(1 + \rho^{-1}) & 0 & c - 2e \\ 0 & 0 & -3(c/\rho + e) & c(1 + \rho^{-1}) + e & 0 & -s \\ 0 & (1 - e^2)S\theta & 0 & 0 & (1 - e^2)C\theta & 0 \\ 0 & 0 & 3\rho + e^2 - 1 & -\rho^2 & 0 & es \end{bmatrix} \begin{Bmatrix} \tilde{x}_0 \\ \tilde{y}_0 \\ \tilde{z}_0 \\ \tilde{v}_{x0} \\ \tilde{v}_{y0} \\ \tilde{v}_{z0} \end{Bmatrix} \quad (3.20)$$

where $C = \cos$ and $S = \sin$. Nonetheless, the right hand side vector $\tilde{\underline{x}}$ is actually a transformation of a genuine LVLH state vector (see (3.5)), which is the true input of our relative dynamics problem. For that reason, it is necessary to map the transformed state vector $\tilde{\underline{x}}$ from and to the original one \underline{x} . This is done through the matrix T_θ as follows:

$$\tilde{\underline{x}} = T_\theta \underline{x} \Rightarrow \begin{Bmatrix} \tilde{r} \\ \tilde{v} \end{Bmatrix} = \begin{bmatrix} \rho \mathbb{I}_{3 \times 3} & \mathbb{O}_{3 \times 3} \\ -e \sin \theta \mathbb{I}_{3 \times 3} & \frac{1}{k^2 \rho} \mathbb{I}_{3 \times 3} \end{bmatrix} \begin{Bmatrix} r \\ v \end{Bmatrix} \quad (3.21)$$

The combination of (3.20) and (3.21) leads to a transformation between a LVLH state vector and the so-called Yamanaka-Ankersen element set, through the transformation matrix $T_{LVLH \rightarrow YA}$:

$$\underline{x} \equiv \underline{x}_{YA} = \Phi_{\theta_0}^{-1} T_\theta \underline{x}_{LVLH} = \frac{1}{1 - e^2} \times$$

$$\begin{bmatrix} 1 - e^2 & 0 & 3e(s/\rho)(1 + \rho^{-1}) & -es(1 + \rho^{-1}) & 0 & 2 - ec \\ 0 & (1 - e^2) \cos \theta & 0 & 0 & -(1 - e^2) \sin \theta & 0 \\ 0 & 0 & -3(s/\rho)(1 + e^2/\rho) & s(1 + \rho^{-1}) & 0 & c - 2e \\ 0 & 0 & -3(c/\rho + e) & c(1 + \rho^{-1}) + e & 0 & -s \\ 0 & (1 - e^2) \sin \theta & 0 & 0 & (1 - e^2) \cos \theta & 0 \\ 0 & 0 & 3\rho + e^2 - 1 & -\rho^2 & 0 & es \end{bmatrix} \times$$

$$\begin{bmatrix} \rho & 0 & 0 \\ 0 & \rho & 0 \\ 0 & 0 & \rho \\ -e \sin \theta & 0 & 0 \\ 0 & -e \sin \theta & 0 \\ 0 & 0 & -e \sin \theta \end{bmatrix} \underline{x}_{LVLH} \quad (3.22)$$

3.2.2.5 Solution scheme.

The target is to compute the relative state vector at a certain time epoch, given the following inputs:

- $\underline{x}_{LVLH}|_0$: Initial LVLH relative state vector (see section B.4.2).
- $\underline{KOE}_C|_0$: Initial chief's Keplerian OE set (see section A.2.2.1).
- t : Time elapsed from the initial time epoch to the desired one.

With all the operations and transformations previously described, this process is graphically described in 3.1.

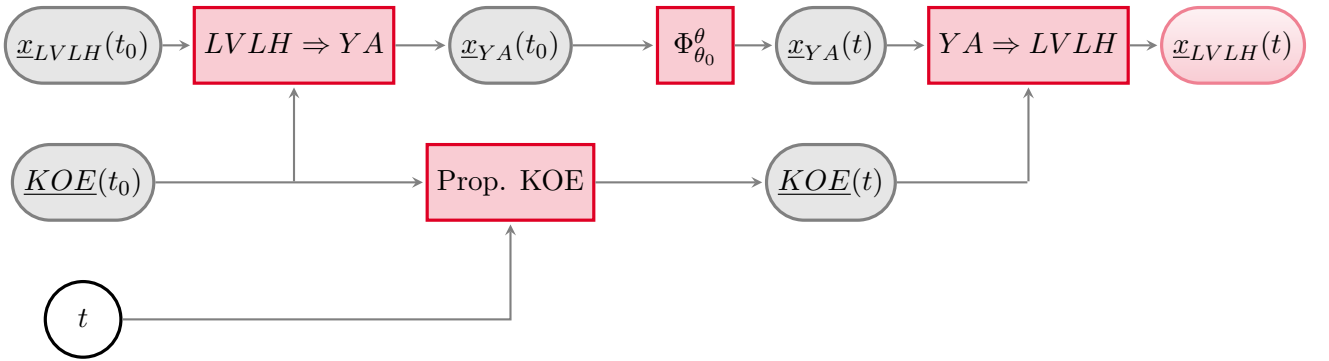


Figure 3.1: Workflow of the propagation with YA STM.

3.2.3 Results: Comparison with HCW and Hi-Fi propagation.

Once the complete model for orbit propagation has been defined, it is turn to discuss how does it compare with respect to the previous solution (HCW) and the High-Fidelity propagation (see D.2.4)

Now, it is turn to define (rather cite) a scenario to test this method. In order to be able to compare the results with the method source, the scenarios defined by Yamanaka and Ankersen will be used [4]. If no body-dependent perturbations are considered, a scenario is completely defined by:

- Chief's reference orbit (Keplerian OEs)
- Deputy's relative position and velocity with respect to chief (LVLH frame)
- Propagation values: Time elapsed and numerical method for high-fidelity propagation(algorithm, timestep ...)

In this case, Yamanaka and Ankersen define them as:

Parameter	Value
Chief's orbit	
Eccentricity	$e_1 = 0.1, e_2 = 0.7$
Perigee height	$h_p = 500 \text{ km}$
Inclination	$i = 30^\circ$
RAAN	$\Omega = 0^\circ$
Argument of perigee	$\omega = 0^\circ$
True anomaly at $t = 0$	$\theta = 45^\circ$
Deputy's relative position (LVLH frame)	
Initial position	$\{x, y, z\} = [100, 10, 10] \text{ m}$
Initial velocity	$\{\dot{x}, \dot{y}, \dot{z}\} = [0.1, 0.1, 0.1] \text{ m/s}$
Propagation parameters	
Propagation time	$N_{\text{orbits}} = 2$
Numerical method	Fourth order Runge-Kutta

Table 3.1: Testing scenarios for YA STM [4].

Nonetheless, one must get the set of Keplerian OEs as defined in A.2.2.1. Firstly, the semimajor axis is computed from the perigee height h_p as:

$$h_p = a(1 - e) \Rightarrow a = \frac{h_p}{1 - e}$$

Secondly, the mean anomaly is computed from the true anomaly and the eccentricity, as explained in section E.3.1.3. Then, the Keplerian OEs for both scenarios are:

$$\left\{ \begin{array}{l} \underline{KOE}_1 = (7.61861333 \cdot 10^6, 0.1, \pi/6, 0, 0, 0.65125326) \quad [\text{m}, -, \text{rad}, \text{rad}, \text{rad}, \text{rad}] \end{array} \right. \quad (3.23a)$$

$$\left\{ \begin{array}{l} \underline{KOE}_2 = (2.28558400 \cdot 10^7, 0.7, \pi/6, 0, 0, 0.10811191) \quad [\text{m}, -, \text{rad}, \text{rad}, \text{rad}, \text{rad}] \end{array} \right. \quad (3.23b)$$

3.2.3.1 Scenario 1: $e = 0.1$.

Figure 3.2 shows the in-plane and out-of-plane motion for the low eccentricity case. The correlation between the YA model and the High-Fidelity is almost perfect, with the HCW falling quite behind (more and more as the orbit continues).

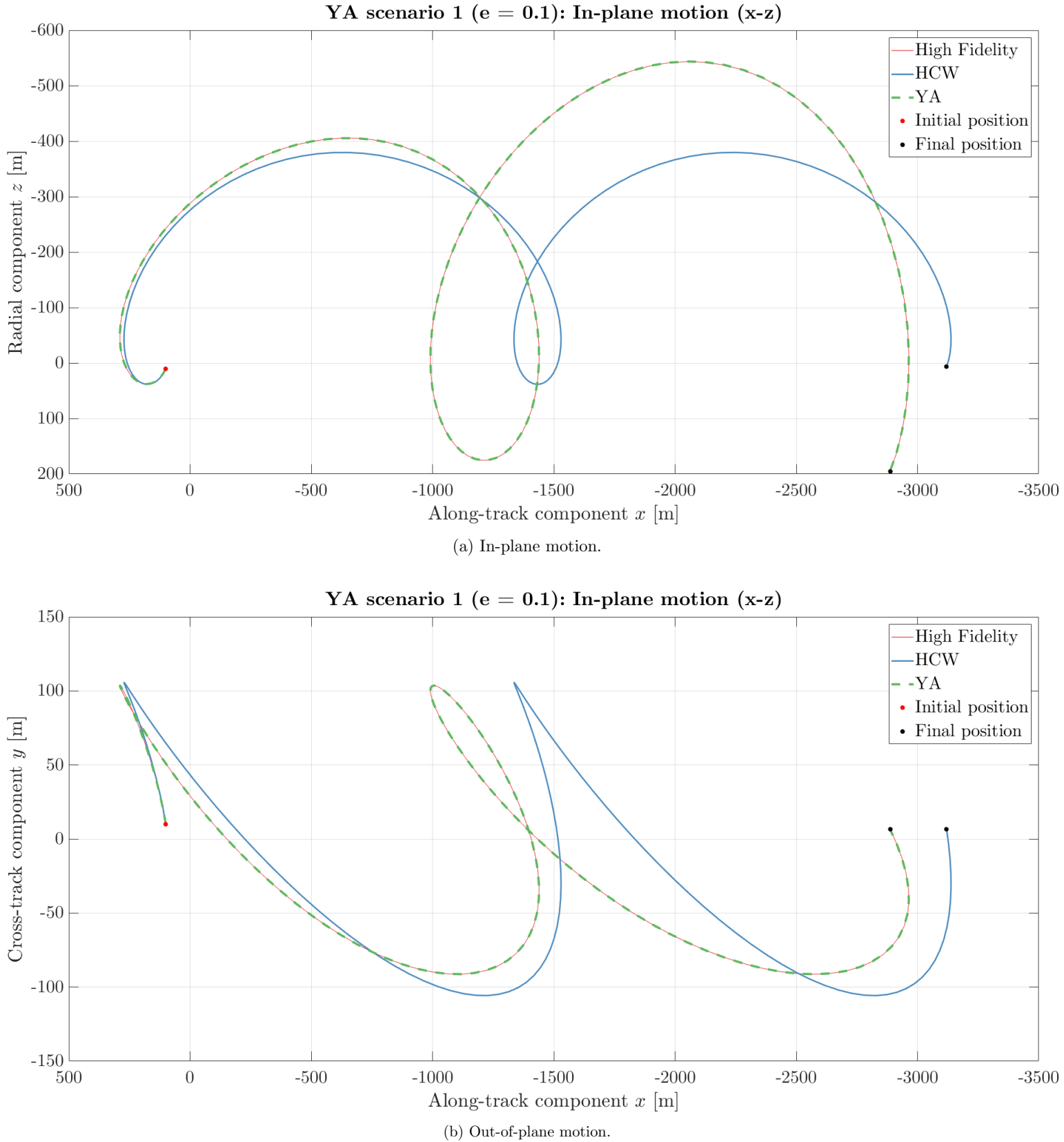


Figure 3.2: Scenario 1($e = 0.1$): Comparison between Hi-Fi, HCW and YA.

3.2.3.2 Scenario 2: $e = 0.7$.

Again, the matching between the YA solution and the eccentric is quite flawless both in-plane (3.3(a)) and out-of-plane (3.3(b)). The difference between them and the circular model is specially big in the OOP, being unacceptable from the very beginning.

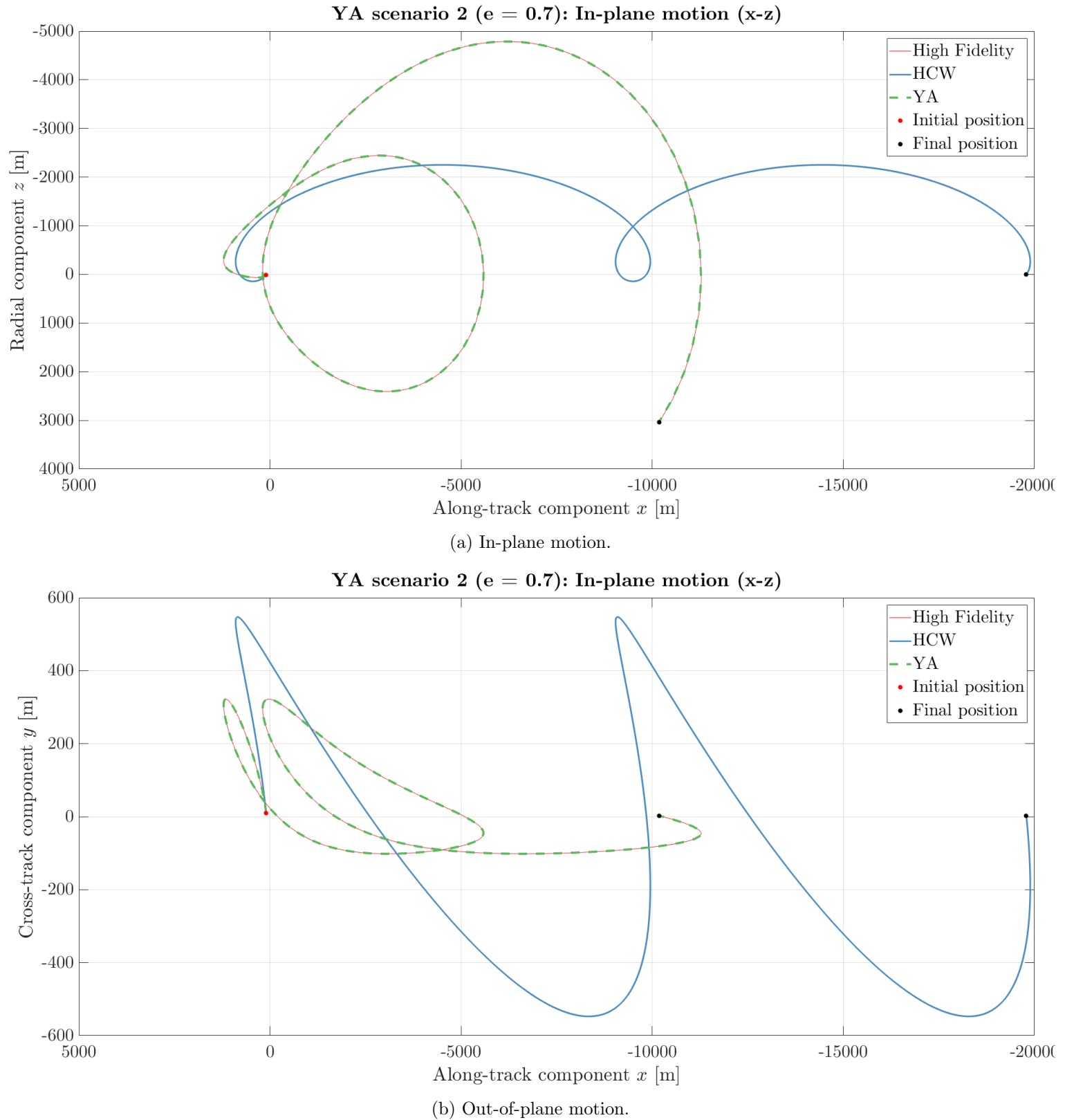


Figure 3.3: Scenario 2 ($e = 0.7$): Comparison between Hi-Fi, HCW and YA.

3.3 Orbit safety in eccentric, unperturbed orbits.

As orbit safety has already been introduced in section 2.4.1, just an extension to eccentric orbits has to be made. This is neatly presented in [21], whose main concern is linear cotangential transfers. As a quick summary, trajectory safety is tightly related to the notions of relative position, looking for avoiding collision by maintaining a certain distance and orientation between the spacecrafts.

As stated before, one substantial fact that differentiates eccentric and circular orbits is that orbital radius is no longer constant. As a consequence, orbital velocity is also time-varying. These two facts lead to the definition of the TAN frame (see B.4.3), which embodies a set of characteristics that allow for a much simpler description of the relative motion. That is to say, as for near-circular orbits the LVLH frame was employed, the TAN frame will be now used to describe the relative motion. Later on, said advantages will be duly looked at.

This section starts by giving a brief description of the parametrization of the relative motion in the TAN frame. Secondly, general relative trajectories for eccentric reference orbits will be discussed, and finally, safe orbit families will be defined and represented, extending as well the eccentricity-inclination vector separation strategy.

3.3.1 Relative motion description in TAN frame.

In order to properly follow the herewith developed relations, it is recommended to first understand sections A.3.2.2 and B.4.3. As already explained, the radial and cross-track coordinates are analysed to ensure orbit safety, as along-track uncertainty is much larger. The target is then to describe the relative motion in TAN frame, that is, to have a description of (y_{TAN}, z_{TAN}) in terms of some relative orbital elements, in a somewhat analog manner compared to 2.4.1.

The QNS relative OE set is quite useful in near-circular orbits, greatly simplifying the relative motion description. Nonetheless, this simplicity fades away for elliptic reference orbits. This is where the C relative OE set becomes useful. The elements C_1 , C_2 and C_3 will somehow describe the radial coordinate, while C_4 is associated with the along-track position. Finally, C_5 and C_6 describe the cross-track relative motion. A one-to-one relation between the QNS ROEs and the C ROEs can be drafted, as shown in table 3.2.

	Near-circular (RQNSOE)	Elliptic (C ROE)
Radial	δa	$\xrightarrow[\text{corresponds to}]{} C_1$
	δe_x	$\xrightarrow[\text{corresponds to}]{} C_2$
	δe_y	$\xrightarrow[\text{corresponds to}]{} C_3$
Along-track	$\delta \lambda$	$\xrightarrow[\text{corresponds to}]{} C_4$
Cross-track	δi_x	$\xrightarrow[\text{corresponds to}]{} C_5$
	δi_y	$\xrightarrow[\text{corresponds to}]{} C_6$

Table 3.2: Correspondence between QNS and C ROEs.

I. Parameter reformulation.

The description reached at 2.4.1 (see equation 2.57) depended on the relative inclination and eccentricity δi and δe and the angles φ and θ . The complete $y - z$ motion in LVLH frame was then determined by four parameters: The amplitude of two oscillations and their respective phase angles. A similar formulation can be developed here for the C ROE set. To start, C_2 and C_3 are converted into a radial amplitude C_m and a radial phase angle α as shown in [21]:

$$\left\{ \begin{array}{l} C_m = \sqrt{C_2^2 + C_3^2} \\ \alpha = \text{atan2}(C_3, C_2) \end{array} \right. \quad (3.24a)$$

$$\left\{ \begin{array}{l} C_2 = C_m \cos \alpha \\ C_3 = C_m \sin \alpha \end{array} \right. \quad (3.24b)$$

that is,

$$\left\{ \begin{array}{l} C_2 = C_m \cos \alpha \end{array} \right. \quad (3.25a)$$

$$\left\{ \begin{array}{l} C_3 = C_m \sin \alpha \end{array} \right. \quad (3.25b)$$

Now it is turn to do the same for the cross-track component. The cross-track amplitude is defined by the ratio Λ , hand in hand with the cross-track phase β :

$$\left\{ \begin{array}{l} \Lambda C_m = \sqrt{C_5^2 + C_6^2} \end{array} \right. \quad (3.26a)$$

$$\left\{ \begin{array}{l} \beta = \text{atan2}(C_6, C_5) \end{array} \right. \quad (3.26b)$$

that is,

$$\begin{cases} C_5 = \Lambda C_m \cos \beta \\ C_6 = \Lambda C_m \sin \beta \end{cases} \quad (3.27a)$$

$$(3.27b)$$

With these expressions at hand, the description turns easier and parallel to the developed for near-circular orbits.

II. Radial and cross-track coordinates.

The TAN coordinates can be easily obtained from the C ROE set and the true anomaly of the chief θ as [21, appendix B]:

$$\begin{cases} \hat{y}_{TAN} = \rho y_{TAN} = C_5 \sin \theta - C_6 \cos \theta \\ \hat{z}_{TAN} = \rho \Theta z_{TAN} = - (C_1 + C_2 \cos \theta + C_3 \sin \theta) \end{cases} \quad (3.28a)$$

$$(3.28b)$$

where the variables with a hat denote the scaled variables (unlike the regular, unscaled ones). ρ (defined as before) and $\Theta = \sqrt{2\rho - \eta^2}$ are the scaling factors. Substituting (3.25) and (3.27) into (3.28) and applying trigonometric relations, it follows that:

$$\begin{cases} \hat{y}_{TAN} = \Lambda C_m \sin (\tau - \tau_0) \\ \hat{z}_{TAN} = C_m \cos \tau - C_1 \end{cases} \quad (3.29a)$$

$$(3.29b)$$

where $\tau = \theta - \alpha$ is the radial phase referred to the maximum radial separation and $\tau_0 = \beta - \alpha$ is the relative phase between radial and cross-track motion. This is a very similar expression compared to (2.57), especially considering that, for bounded trajectories, $C_1 = 0$. From a very primitive analysis, it is seen that τ_0 will determine the shape of the $y-z$ motion, similarly to what $\varphi-\psi$ did in near-circular orbits.

3.3.2 General trajectories and safe orbits.

3.3.2.1 Orbit families.

In this context, an orbit family is a set of relative orbits who share most of the defining elements (in particular, C_1 , C_m , e and τ_0), being differenced just by the phase angle α (anomaly at which radial distance is maximum). Scaled variables are actually independent of α , conversely to the unscaled

ones. This will be later graphically portrayed. As a summary, table 3.3 shows the different elements which define an orbit family.

	Parameter	Meaning	Units
Fixed for each family	e	Chief's orbit eccentricity	[–]
	C_1	Relative radial offset	[m]
	C_m	Radial motion amplitude	[m]
	Λ	Cross-track/radial amplitude ratio	[–]
	τ_0	Cross-track/radial relative phase	[rad]
Member parameter	α	Radial motion phase	[rad]
Propagation parameter	θ	Chief's true anomaly	[rad]

Table 3.3: Parameters of an orbit family.

3.3.2.2 Eccentricity/inclination vector separation in eccentric orbits.

By simply looking at equation (3.29), it is clear that τ_0 will determine the eccentricity/inclination vector relative orientation. As for the near-circular case, the parallel configuration takes place when both phases have the same value, that is:

$$\beta = \alpha \Rightarrow \tau_0 = 0$$

In that case, the scaled coordinates behave as:

$$\begin{cases} \hat{y}_{TAN} = \Lambda C_m \sin \tau \\ \hat{z}_{TAN} = C_m \cos \tau - C_1 \end{cases} \quad (3.30a)$$

$$\begin{cases} \hat{y}_{TAN} = \Lambda C_m \sin \tau \\ \hat{z}_{TAN} = C_m \cos \tau - C_1 \end{cases} \quad (3.30b)$$

which is the equation of an ellipse with center at $(0, -C_1)$, a semimajor axis C_m and semiminor axis ΛC_m . An antiparallel configuration is obtained if $\tau_0 = \pi$, exactly as for near-circular reference orbits. Nonetheless, the useful configuration is the parallel one, which is now analysed.

I. Scenario definition.

The goal is to propagate a family of safe orbits, defined by (a) the chief's orbit and (b) the amplitudes and phase angles of the radial and cross-track components. In fact, only the eccentricity of the chief's orbit is required. Table 3.4 shows the two scenarios that have been chosen for this validation, as well as the different values of α within each family.

Parameter	Value
Chief's orbit	
Eccentricity	$e = 0.1$
Deputy's relative position (LVLH frame)	
Radial amplitude	$C_m = 10 \text{ m}$
Radial phase	$\alpha = \frac{i}{4}2\pi, \quad i = 0, 1, 2, 3, 4$
Radial offset	$C_1 _1 = 0, \quad C_1 _2 = C_m = 10 \text{ m}$
Amplitude ratio	$\Lambda = 1$
Relative phase	$\tau_0 = \beta - \alpha = 0$
Propagation parameters	
Propagation time	$N_{orbits} = 1$

Table 3.4: Testing scenarios for safe orbit implementation [21].

II. A. Bounded trajectory case ($C_1 = 0$).

Figure 3.4 shows the scaled coordinates, the unscaled coordinates (one for each α value) and the lower and upper boundaries of the relative motion. They can be easily obtained from the scaled variables by applying the maximum and minimum scaling factors, respectively. That is:

$$\begin{cases} y_{TAN,LB} = \frac{1}{\rho(\theta=0)} \Lambda C_m \sin \tau & = \frac{\Lambda C_m}{1+e} \sin \tau \\ z_{TAN,LB} = \frac{1}{\rho(\theta=0)\Theta(\theta=0)} C_m \cos \tau & = \frac{C_m}{(1+e)^2} \cos \tau \end{cases} \quad (3.31)$$

$$\begin{cases} y_{TAN,UB} = \frac{1}{\rho(\theta=\pi)} \Lambda C_m \sin \tau & = \frac{\Lambda C_m}{1-e} \sin \tau \\ z_{TAN,UB} = \frac{1}{\rho(\theta=\pi)\Theta(\theta=\pi)} C_m \cos \tau & = \frac{C_m}{(1-e)^2} \cos \tau \end{cases} \quad (3.32)$$

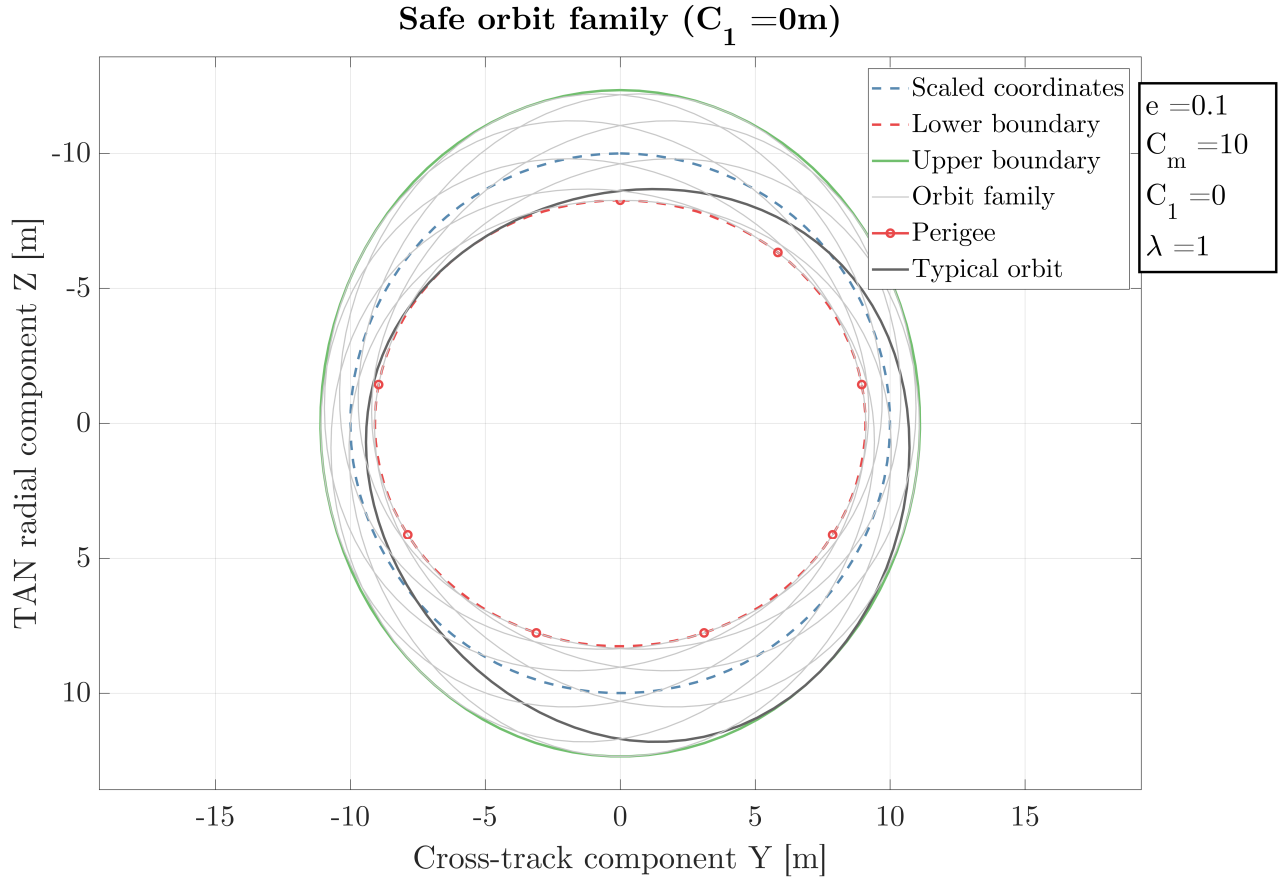


Figure 3.4: Safe orbit family: Scenario 1 ($C_1 = 0$).

As $C_1 = 0$, the every member of the family is an ellipse is centered at the origin.

II. B. Unbounded trajectory case ($C_1 \neq 0$).

The orbit family for this second case is shown in figure 3.5. The main difference now is that every orbit passes through the origin, as both boundaries collapse there.

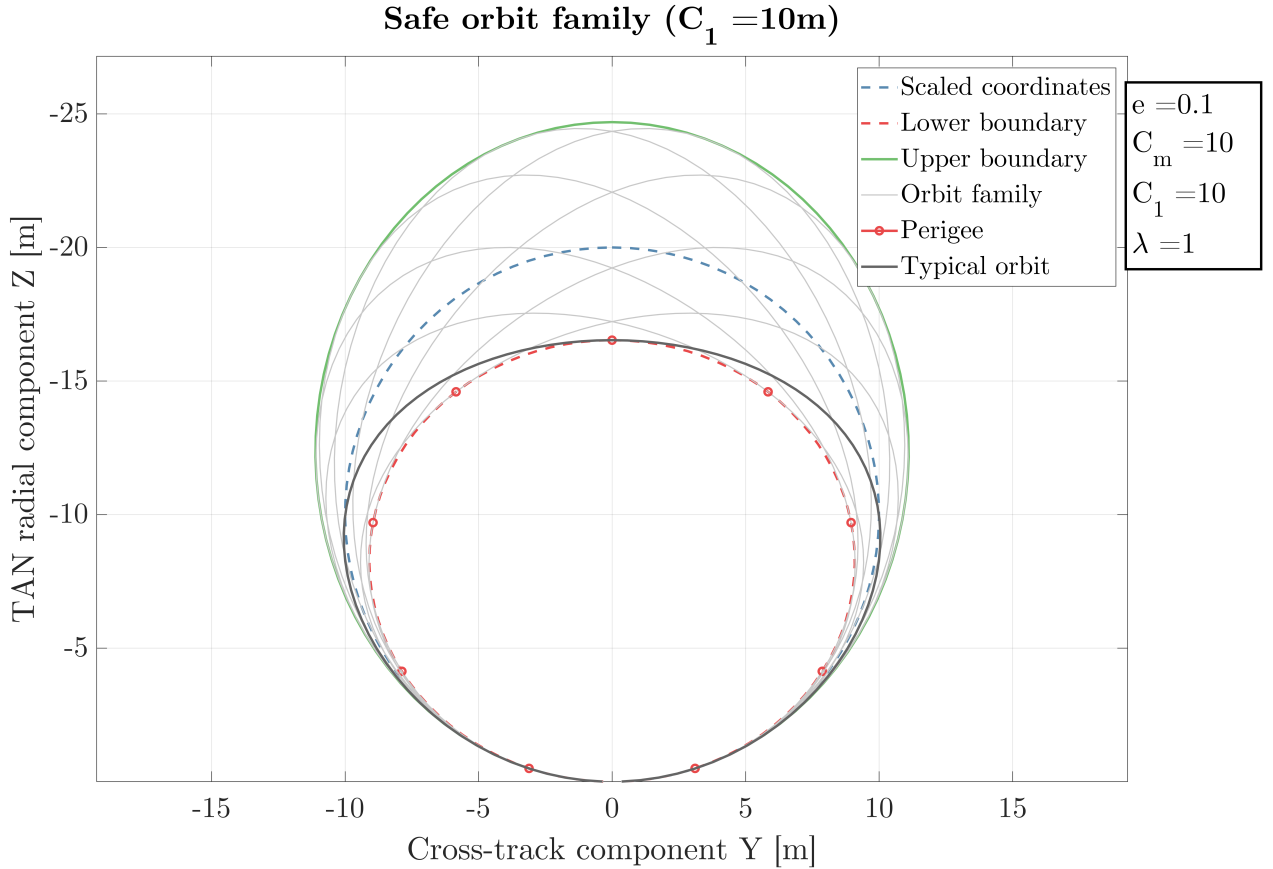


Figure 3.5: Safe orbit family: Scenario 2 ($C_1 = C_m$).

Besides analyzing the results by themselves, they can additionally be compared to a truth model (High-Fidelity). For this to be done, it is necessary to (a) convert the C ROEs into Keplerian and (b) define some dummy values of the chief's orbit. An example of this can be seen in figure 3.6, where some members of the previously graphed families are shown. The chief's orbit is defined by the first case specified in 3.1. The good correlation with the High-Fidelity propagation is enough to validate this theory, as it can be seen in figures 3.6(a) and 3.6(b)

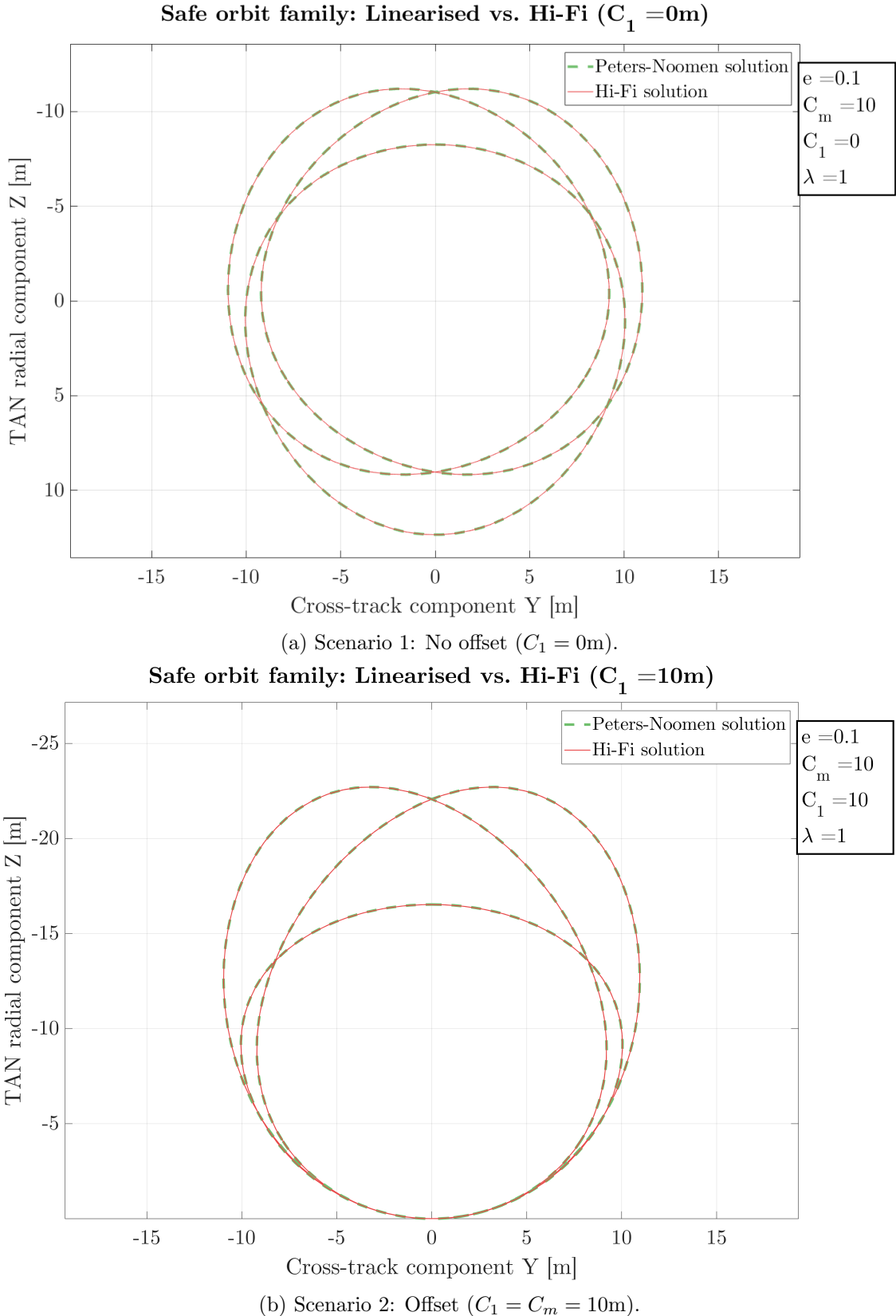


Figure 3.6: Comparison between Peters-Noomen approach and High-Fidelity propagation.

Perturbations: Non-spherical gravity.

4.1 Introduction.

Up until now, every single orbit has been propagated under the assumption of unperturbed motion. This hypothesis is essentially flawed: not a single celestial system in the nature is *exactly* a two body problem.

However, most of said systems are really close to the two-body configuration, deviating from it due to small perturbations. Of course, there are exceptions for that, as for example an interplanetary transfer, in which by definition two primary bodies are, at least at some point, equally important. The wide variety of perturbations and its notorious effect when needing accurate results induces the development of theories that (a) model and implement said perturbations and (b) yield insightful knowledge about them.

In any case, and for whatever theory that is formulated, one thing needs to be kept in mind: perturbation theories are built upon the assumption that perturbations remain small. The solutions that these theories may return are otherwise not valid nor useful [9].

Of all the perturbations that may be considered in spacecraft motion, one of the most relevant is the deviation of the gravity field from that of a central body. This is usually referred to as non-spherical gravity (NSG), and the goal is to accurately model the mass distribution of the central body and hence the gravity field induced by it. An example of overall knowledge is the Earth's oblateness (*i.e.* the Earth being flattened in its rotation direction). Although an oblate spheroid is usually a good enough approximation, the mathematical architecture behind some theories allows for a very accurate representation of the Earth's shape. This will undoubtedly improve the accuracy of the results.

The implementation of a non-spherical gravity model can be approached as a raw computation of its value – with a High-Fidelity propagation in mind – or as a way to further understand its effects and obtain closed-form solutions. Though the former improves the truth model, it is the latter who yields more knowledge and fewer computational cost.

This chapter intends to (a) provide an outlook on how to model perturbations in general through

averaging methods and (b) focus on the non-spherical gravity field analysis and implementation. Its structure is outlined with that in mind, starting by analyzing which perturbations should be considered and introducing general averaging methods. That is followed by a general description of the non-spherical gravity field, which leads to the two main sections of the chapter. The first one is about mean and osculating elements: its definition, how they simplify orbit propagation and how they are actually calculated for the oblate Earth. The second one deals with Kaula's theory, which provides a different insight on the spherical harmonic formulation of the gravity field.

4.1.1 Relevant perturbations in spacecraft motion.

Figure 4.1, remastered from Montenbruck [3], provides a very visual and insightful idea about usually considered perturbations in Earth orbits, as a function of the orbital radius. Besides the obvious central body term (GM), which remains the biggest effect for every considered radius, Low Earth Orbits (LEO) are most notably affected by Earth's oblateness (J_2) and aerodynamic drag. Moving on to higher orbits, other perturbations may escalate in importance and in value, such as the third-body effects of the Moon and the Sun. It is important to note though that the nonlinear effect of the oblateness (J_2^2) still rises above other NSG first-order harmonics (such as J_6). However, other smaller effects such as the solar radiation pressure (SRP) or other third-bodies may need to be considered in higher orbits. Nonetheless, if the orbit scope is enlarged, the aforementioned terms may become relevant, such as in the case of interplanetary trajectories.

The nature of SRP and drag makes them very body-dependent, in the sense that each body's surface, drag or reflective coefficient makes a huge difference in the disturbance. This fact becomes specially relevant when considering the relative motion of two different bodies, as the differential effect is what matters the most.

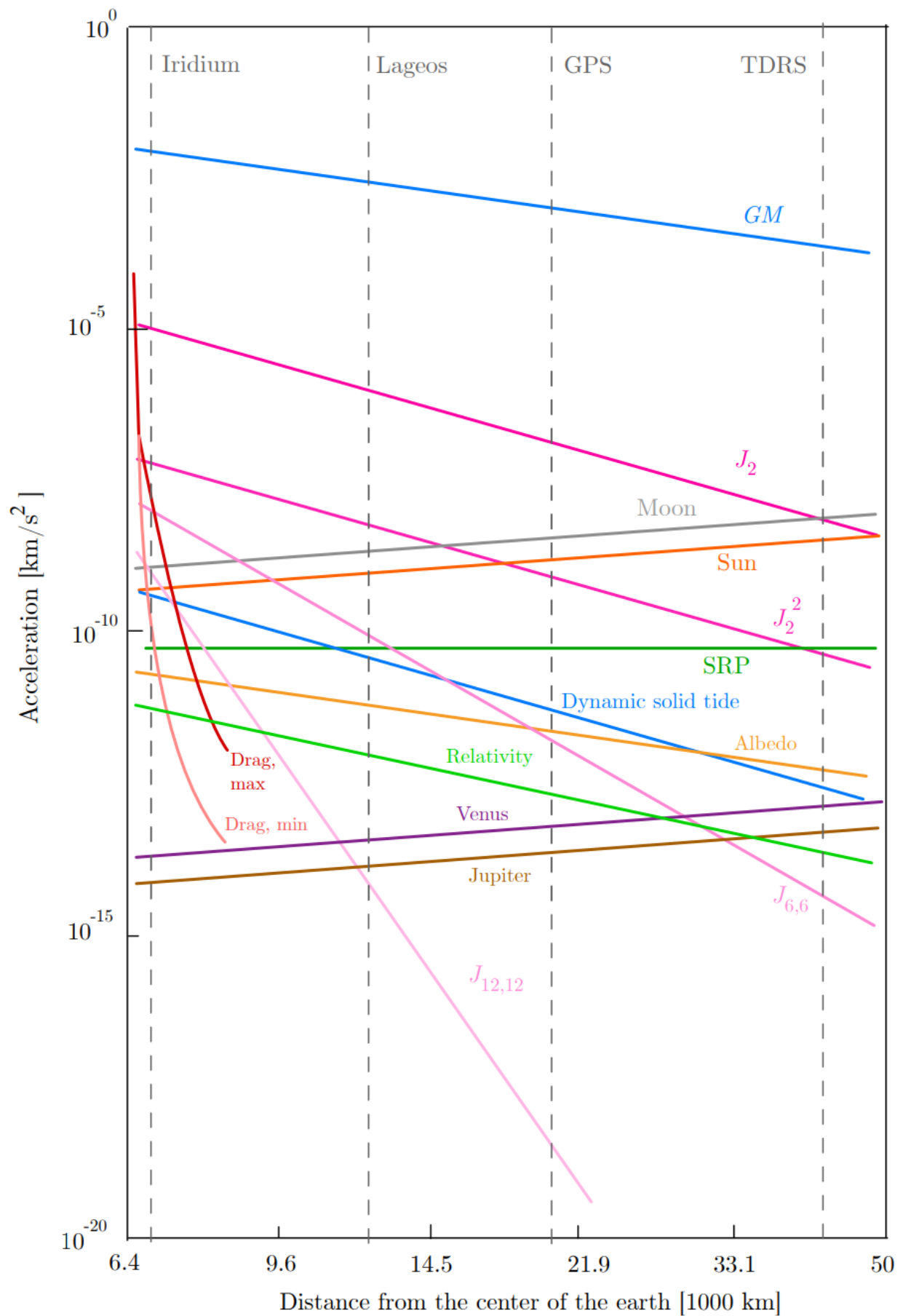


Figure 4.1: Order of magnitude of various perturbations of a satellite orbit. [3]

For low altitude Earth-centered relative motion, non-spherical gravity and aerodynamic drag become the main concern. During this chapter, the spotlight will be put on the former, whose scientific branch is known as satellite geodesy.

4.1.2 Variational formulation of perturbed motion: Averaging methods.

Perturbed problems are usually nonlinear and initially unsolvable, meaning that no closed-form solution can be directly derived. Before figuring out how to approach this issue, it is necessary to consider the type of effects these perturbations lead to. Considering the periodicity, perturbations cause three types of alterations:

- A. Secular: Non-periodic effects, which generate a net variation over time. In other words, those which long-term average is non zero.
- B. Short-period: Oscillations which feature a period equal or directly proportional to the fastest time-varying state variable. For example, in the case of a spacecraft, that variable may be the mean anomaly M .
- C. Long-period: Periodic oscillations with a period considerably greater than that of the short-period effects. Their long-term average is still zero. In the case of celestial motion, this may be the argument of perigee ω or the ascending node Ω .

The facet one is usually more concerned about is the secular or mean motion. Taking the example of a drag-affected orbit, the final target is to get the long-term motion, rather than the short-term oscillations. These oscillations may nonetheless be important, as they might determine other aspects of the motion.

In light of this, it would be interesting to separate the state variables into these three components, so as to analyse each by its own. Initially, one is faced with a problem expressed in instantaneous or osculating variables, which comprise all the motion components and are the “real” variables, in the sense that they can be measured and have a physical definition. The question now is, how can one go from these variables to the mean or averaged variables. This would lead to a closed-form, approximate solution of the original problem.

The target is now to reach a transformation from osculating to mean elements and vice versa. These methods range from raw averaging of the equations, to more sophisticated and insightful theories. The latter will be the main topic of this section, as two of them will be presented. A practical application of them will be later discussed, while here a mere theoretical introduction is made.

The two methods later described are based on a variational formulation, using concepts presented in appendix C. They seek for arriving at successively higher order solutions of the unsolvable, perturbed problem starting from the solvable, unperturbed problem (solution of order 0). This is done by generating a differential problem in which the unknown (*i.e.* the solution of order n) is expressed in terms of the lower order solutions (*i.e.* the solutions of order $n - 1, n - 2, \dots, 0$). In this way, increasingly accurate closed-form solutions are reached.

A common trait among the two surveyed methods is that they are based on canonical transformations. These are used to find a phase space in which the problem becomes trivial, making the generating function the true solution (and sought variable) of the problem. The difference between the two approaches is how this generating function is formulated.

4.1.2.1 Von Zeipel's method.

I. Problem statement.

Von Zeipel's method is the oldest of the two surveyed methods, though its relevance cannot be underestimated. A more formal approach is presented by Nayfeh [22], whereas the simplified viewpoint here developed is based on Wiesel [9]. It starts with the Hamilton-Jacobi equation, which is expressed as:

$$K(Q_i, P_i, t) = H(q_i, p_i, t)|_{Q_i, P_i} + \frac{\partial S}{\partial t} \quad (4.1)$$

where H is the original Hamiltonian, S is the generating function (or Hamilton principal function) and K is the transformed Hamiltonian. S is assumed to be of type 2, that is, $S = S(q_i, P_i, t)$. The original, perturbed Hamiltonian can be expressed as:

$$H(q_i, p_i, t) = H_0(q_i, p_i) + \varepsilon H_1(q_i, p_i, t) \quad (4.2)$$

where H_0 represents the solvable part of the problem, H_1 the perturbation part and $\varepsilon \ll 1$ a small parameter. The target is now to obtain the generating function S that nullifies the new Hamiltonian K , that is:

$$K(Q_i, P_i, t) = 0 = H\left(q_i, p_i = \frac{\partial S}{\partial q_i}, t\right) + \frac{\partial S}{\partial t} \quad (4.3)$$

II. Transformation.

Von Zeipel assumes that the generating function S can be expanded in powers of the parameter ε

as:

$$S(q_i, P_i, t) = S_0(q_i, P_i, t) + \varepsilon S_1(q_i, P_i, t) + \frac{1}{2} \varepsilon^2 S_2(q_i, P_i, t) + \dots \quad (4.4)$$

This formulation leads to the following form of the old momenta p_i :

$$p_i = \frac{\partial S}{\partial q_i} = \frac{\partial S_0}{\partial q_i} + \varepsilon \frac{\partial S_1}{\partial q_i} + \frac{1}{2} \varepsilon^2 \frac{\partial S_2}{\partial q_i} + \dots \quad (4.5)$$

Inserting (4.5) into (4.3) leads to:

$$K = 0 = H_0(q_i, \partial S / \partial q_i) + \varepsilon H_1(q_i, \partial S / \partial q_i) + \frac{\partial S}{\partial t} \quad (4.6)$$

Equation (4.6) features three terms which can be expanded in powers of ε around $\partial S_0 / \partial q_i$ through (4.5):

- H_0 :

$$\begin{aligned} H_0(q_i, \partial S / \partial q_i) &= H_0 \left(q_i, \frac{\partial S_0}{\partial q_i} + \varepsilon \frac{\partial S_1}{\partial q_i} + \frac{1}{2} \varepsilon^2 \frac{\partial S_2}{\partial q_i} + \dots \right) = H_0 \left(q_i, \frac{\partial S_0}{\partial q_i} + \delta p_i \right) \\ &\approx H_0(q_i, \partial S_0 / \partial q_i) + \sum_i \frac{\partial H_0}{\partial p_i} \delta p_i + \frac{1}{2!} \sum_i \sum_j \frac{\partial^2 H_0}{\partial p_i \partial p_j} \delta p_i \delta p_j + \mathcal{O}(\varepsilon^3) \end{aligned} \quad (4.7)$$

where $\delta p_i = \varepsilon \frac{\partial S_1}{\partial q_i} + \frac{1}{2} \varepsilon^2 \frac{\partial S_2}{\partial q_i} + \mathcal{O}(\varepsilon^3)$. Substituting this into (4.7) and retaining only elements up to second order in ε :

$$\begin{aligned} H_0(q_i, \partial S / \partial q_i) &\approx H_0(q_i, \partial S_0 / \partial q_i) + \sum_i \frac{\partial H_0}{\partial p_i} \left(\varepsilon \frac{\partial S_1}{\partial q_i} + \frac{1}{2} \varepsilon^2 \frac{\partial S_2}{\partial q_i} \right) \\ &\quad + \frac{1}{2!} \sum_i \sum_j \frac{\partial^2 H_0}{\partial p_i \partial p_j} \varepsilon^2 \frac{\partial S_1}{\partial q_i} \frac{\partial S_1}{\partial q_j} + \mathcal{O}(\varepsilon^3) \end{aligned} \quad (4.8)$$

- H_1 : In an analogue manner to H_0 , and considering that this factor is already of order ε :

$$\varepsilon H_1(q_i, \partial S / \partial q_i) = \varepsilon H_1 \left(q_i, \frac{\partial S_0}{\partial q_i} \right) + \varepsilon^2 \sum_i \frac{\partial H_1}{\partial p_i} \frac{\partial S_1}{\partial q_i} + \mathcal{O}(\varepsilon^3) \quad (4.9)$$

- $\partial S / \partial t$: Simply substituting (4.4) yields:

$$\frac{\partial S}{\partial t} \approx \frac{\partial S_0}{\partial t} + \varepsilon \frac{\partial S_1}{\partial t} + \frac{1}{2} \varepsilon^2 \frac{\partial S_2}{\partial t} \quad (4.10)$$

III. Substitution in Hamilton-Jacobi equation.

If one is to substitute equations (4.8), (4.9) and (4.10) into (4.6), a quite cumbersome expression arises. Nonetheless, applying the uniqueness of the coefficients of the ε expansion, a separate PDE for each order of can be reached. In particular:

$$\left\{ \begin{array}{l} \varepsilon^0 : H_0(q_i, \partial S_0 / \partial q_i) + \frac{\partial S_0}{\partial t} = 0 \\ \varepsilon^1 : \sum_i \frac{\partial H_0}{\partial p_i} \frac{\partial S_1}{\partial q_i} + H_1\left(q_i, \frac{\partial S_0}{\partial q_i}\right) + \frac{\partial S_1}{\partial t} = 0 \\ \varepsilon^2 : \frac{1}{2} \sum_i \frac{\partial H_0}{\partial p_i} \frac{\partial S_2}{\partial q_i} + \end{array} \right. \quad (4.11)$$

$$\left. \begin{array}{l} \frac{1}{2!} \sum_i \sum_j \frac{\partial^2 H_0}{\partial p_i \partial p_j} \frac{\partial S_1}{\partial q_i} \frac{\partial S_1}{\partial q_j} + H_2\left(q_i, \frac{\partial S_0}{\partial q_i}\right) + \frac{\partial S_2}{\partial t} = 0 \end{array} \right. \quad (4.12)$$

$$\left. \begin{array}{l} \frac{1}{2!} \sum_i \sum_j \frac{\partial^2 H_0}{\partial p_i \partial p_j} \frac{\partial S_1}{\partial q_i} \frac{\partial S_1}{\partial q_j} + H_2\left(q_i, \frac{\partial S_0}{\partial q_i}\right) + \frac{\partial S_2}{\partial t} = 0 \end{array} \right. \quad (4.13)$$

Equation (4.11) is the unperturbed, solvable problem, whose solution is reached by solving for S_0 in the PDE. S_0 provides the zeroth-order transformation $(p_i, q_i) \rightarrow (P_i, Q_i)$, hence the old variables in terms of the new. Once this is done, the first order problem (4.12) can be tackled, where again a PDE in terms of S_1 is to be solved. This will lead to a first-order approximation of the perturbed problem, which is in turn substituted in (4.13) to find the second-order solution. This is then a recursive scheme, in which increasingly higher order approximations are derived.

Remarks.

The described approach is based on the Hamilton-Jacobi equation, which seeks to find a state space in which the solution of the dynamics is trivial. The solution process consists of attaining increasingly better approximations of the generating function that simplifies the original dynamics.

Nonetheless, a somewhat different approach is to choose the generating function S in a way that it simplifies the problem in other ways. For example, if one wishes to just analyse the mean evolution of the system, choosing S such that it cancels the periodic terms in the Hamiltonian is a possible approach. The new Hamiltonian will be (by choice) non-zero. This will be discussed in more detail later, in a particularization of the perturbed two-body problem.

4.1.2.2 Lie series method.

Von Zeipel's method features a considerable disadvantage: the independent variables of the generating function S are a mix of the old and the new generalized coordinates and momenta. Hori

[23] and Deprit [24, 25] develop more sophisticated methods relying on the Lie theorem and Lie series expansions. The general Lie series method is explained in [22], specifying every detail of its mathematical grounds. This theory will not be implemented throughout this thesis. Nevertheless, a brief introduction is made, so as to have a starting point for future work. In particular, Hori's approach will be introduced [2].

Hori's method.

This approach starts by imposing that the generating function W depends only on the new generalized coordinates and momenta. Expanding said function until first order:

$$W(Q_i, P_i) = W_1(Q_i, P_i) + \varepsilon W_2(Q_i, P_i) + \mathcal{O}(\varepsilon^3) \quad (4.14)$$

The modified Hamiltonian K is expanded up to second order in ε so that:

$$K(Q_i, P_i) = K_0(Q_i, P_i) + \varepsilon K_1(Q_i, P_i) + \frac{1}{2}\varepsilon^2 K_2(Q_i, P_i) + \dots \quad (4.15)$$

On the other hand, the original Hamiltonian is defined as:

$$H(q_i, p_i) = H_0(q_i, p_i) + \varepsilon H_1(q_i, p_i) \quad (4.16)$$

Up until here, the only difference with respect to Von Zeipel's method is that the generating function depends only on the new variables. It is now where the main procedural difference appears, as the Lie theorem is applied, which states that:

$$H(q_i, p_i) = H(Q_i, P_i) + \varepsilon [H(Q_i, P_i), W] + \frac{1}{2}\varepsilon^2 [[H(Q_i, P_i), W], W] + \mathcal{O}(\varepsilon^3) \quad (4.17)$$

where $[\bullet, \bullet]$ represents the Poisson bracket. Substituting (4.16) and (4.14) into (4.17):

- $\varepsilon [H, W] = \varepsilon [H_0 + \varepsilon H_1, W_1 + \varepsilon W_2] = \varepsilon [H_0, W_1] + \varepsilon^2 ([H_0, W_2] + [H_1, W_1]) + \mathcal{O}(\varepsilon^3)$
- $\frac{1}{2}\varepsilon^2 [[H, W], W] = \frac{1}{2}\varepsilon^2 [[H_0, W_1], W_1] + \mathcal{O}(\varepsilon^3)$

The original Hamiltonian hence becomes:

$$H(q_i, p_i) = H_0(Q_i, P_i) + \varepsilon (H_1(Q_i, P_i) + [H_0, W_1]) + \varepsilon^2 \left([H_0, W_2] + [H_1, W_1] + \frac{1}{2} [[H_0, W_1], W_1] \right) \quad (4.18)$$

Additionally, Hamilton-Jacobi equation states that:

$$K(Q_i, P_i) = H(q_i, p_i)$$

Considering (4.18) and (4.15), and by virtue of the uniqueness of the coefficients of the expansion, one equation can be stated for each order of ε , that is:

$$\varepsilon^0 : K_0(Q_i, P_i) = H_0(Q_i, P_i) \quad (4.19)$$

$$\varepsilon^1 : K_1(Q_i, P_i) = H_1(Q_i, P_i) + [H_0, W_1] \quad (4.20)$$

$$\varepsilon^2 : K_2(Q_i, P_i) = [H_0, W_2] + [H_1, W_1] + \frac{1}{2} [[H_0, W_1], W_1] \quad (4.21)$$

Equation (4.19) can be understood as “go solve the unperturbed problem”, which in principle should be straightaway (as for the two-body problem). The first order differential equation (4.20) can be solved in different ways, as it has two unknowns (W_1 and K_1). In general, the first order modified Hamiltonian is selected to have a certain value or expression, and then the generating function is obtained. A quite common approach is to make K_1 to comprise just the secular part of the perturbations H_1 , making W_1 absorb the periodic part. For higher order equations, the procedure is similar: choose K_i and solve for W_i .

4.2 Non-spherical gravity: General concepts.

As shown in figure 4.1, the asphericity of the Earth induces some perturbations on the easily solved two-body problem. Many theories have been developed for the treatment of Earth’s oblateness (J_2), due to its dominance over the effect of the rest of the irregularities. However, when a more accurate result is needed, a higher-fidelity Earth model has to be implemented. These theories can be later implemented in spacecraft dynamics models or, in particular, STMs, such as in [5] or [26].

In this section, classical theories for J_2 effects will be first described, all based in Brouwer’s theory [27]. Later on, a promising approach full for non-spherical gravity field description is detailed. Implementation and validation of both theories will also be performed, as the final target is to use

them in a dynamics model.

4.3 J_2 effect analysis.

4.3.1 Mean and osculating elements

As introduced in 4.1.2, the mean motion is usually the most important component of the full motion. A very important advantage of the mean element space is that the variational equations become very simple, as only long-term effects are taken into account. The problem is how to convert the variational equations in instantaneous/osculating variables into a mean element counterpart.

This is where mean to osculating transformations arise. They can be either obtained by pure averaging or through some kind of transformation. During this section, an example of the latter will be developed, based on the Von Zeipel's method and applied to the J_2 -perturbed two-body problem. It is commonly referred to as Brouwer's Theory, in reference to its author Dirk Brouwer [27]. An extensive survey on this exact topic can be found in Gaias et al. [28], where several classical and state-of-the-art methods (including the one here described) are presented and compared against each other.

4.3.2 Brouwer's theory.

Brouwer's theory seeks a closed-form of the J_2 -perturbed motion of a spacecraft, applying Von Zeipel's method for that purpose. This approach starts by formulating the equations of motion of the spacecraft in a favorable form (*i.e.* in Delaunay elements). The resulting differential problem can be reshaped through canonical transformations until the mean elements and secular equations of motion are reached. These can be easily integrated, after which an inverse transformation (*i.e.* mean to osculating) can be performed, so as to get the actual motion of the spacecraft.

Once this general results are outlined, the Lyddane modification [29] for near zero eccentricities and inclination angles will be introduced. Finally, a quick validation test is performed.

4.3.2.1 Grounds: Brouwer's theory outline.

I. Modification of the Hamiltonian F .

As shown in section E.2.1, the variational equations of the motion of a spacecraft in Delaunay

variables are:

$$\begin{cases} \frac{dL}{dt} = \frac{\partial F}{\partial l}, & \frac{dl}{dt} = -\frac{\partial F}{\partial L} \\ \frac{dG}{dt} = \frac{\partial F}{\partial g}, & \frac{dg}{dt} = -\frac{\partial F}{\partial G} \\ \frac{dH}{dt} = \frac{\partial F}{\partial h}, & \frac{dh}{dt} = -\frac{\partial F}{\partial h} \end{cases} \quad (4.22)$$

where (L, G, H, l, g, h) is the set of Delaunay elements (see section A.2.2.5) and F is the Hamiltonian function, denoted that way to avoid confusion with the third Delaunay element. For a J_2 perturbed orbit, the Hamiltonian is expressed as:

$$F = \frac{\mu^2}{2L^2} + \frac{\mu^4 a_e^2 J_2}{L^6} \left[\left(-\frac{1}{2} + \frac{3}{2} \frac{H^2}{G^2} \right) \frac{a^3}{r^3} + \left(\frac{3}{2} - \frac{3}{2} \frac{H^2}{G^2} \right) \frac{a^3}{r^3} \cos(2g + 2\theta) \right] \quad (4.23)$$

One obvious change to arrive to a closed-form solution is to achieve a right-hand side of (4.22) which only depends on the Delaunay variables. That leads to the need of expressing $(a/r)^3$ and $\cos(2g + 2\theta)$ in terms of L, G, H, l, g, h . This is done through elliptic motion expansions, using Fourier series in terms of the mean anomaly l , that is:

$$\begin{cases} \frac{a^3}{r^3} = \frac{L^3}{G^3} + \sum_{j=1}^{\infty} 2P_j \cos jl \equiv \frac{L^3}{G^3} + \sigma_1 \\ \frac{a^3}{r^3} \cos(2g + 2\theta) = \sum_{j=-\infty}^{\infty} Q_j \cos(2g + jl) \equiv \sigma_2 \end{cases}$$

Additionally, defining:

$$A = -\frac{1}{2} + \frac{3}{2} \frac{H^2}{G^2}$$

$$B = \frac{3}{2} - \frac{3}{2} \frac{H^2}{G^2}$$

the Hamiltonian becomes:

$$F = \frac{\mu^2}{2L^2} + \frac{\mu^4 a_e^2 J_2}{L^6} \left[A \left(\frac{L^3}{G^3} + \sigma_1 \right) + B \sigma_2 \right] = F(L, G, H, l, g, -) \quad (4.24)$$

where the $-$ emphasizes the absence of h in the Hamiltonian.

II. Von Zeipel's method application.

The Hamiltonian function is now better suited for a canonical transformation, which through the removal of variables from the Hamiltonian will simplify the solution process. In this respect, Hamilton-

Jacobi equation can be leveraged in two ways:

- A. Choose the generating function so that only L', G', H' appear on the Hamiltonian, leading to a simple solution.
- B. Choose the generating function otherwise, tailoring the Hamiltonian rather than just simplifying it.

The approach followed by Brouwer consists on first getting rid of the mean anomaly l , hence of the short-period effects, to then eliminate the argument of perigee g and remove the long-period effects with it. The Von Zeipel's method will be used for this purpose.

The first step is to identify the solvable and the perturbation part of the original Hamiltonian accordingly to (4.2):

$$\begin{cases} H_0 = \frac{\mu^2}{2L^2} \\ H_1 = \frac{\mu^4 a_e^2 J_2}{L^6} \left[A \left(\frac{L^3}{G^3} + \sigma_1 \right) + B\sigma_2 \right] \end{cases}$$

where the small parameter ε has been merged into H_1 .

II.A. Short-period effects removal.

The transformation function is expanded again as:

$$S = S_0 + S_1 + S_2 + \dots$$

From now on, the subindex of each function denotes its order in ε . In order to transform the problem into the two-body space and remove the mean anomaly from the Hamiltonian, the zeroth-order factor of the generating function S_0 is chosen to be:

$$S_0 \equiv L'l + G'g + H'h$$

The Hamilton-Jacobi equation becomes:

$$K(L', G', H', -, g', -) = F(L, G, H, l, g, -) \quad (4.25)$$

Substituting the original Hamiltonian $F = H_0 + H_1$ and expanding the new one up to second order, equation (4.25) becomes:

$$\begin{aligned} K_0 + K_1 \left(L', G', H', - , \frac{\partial S}{\partial G'} , - \right) + K_2 \left(L', G', H', - , \frac{\partial S}{\partial G'} , - \right) = \\ H_0 \left(\frac{\partial S}{\partial L} \right) + H_1 \left(\frac{\partial S}{\partial l}, \frac{\partial S}{\partial g}, \frac{\partial S}{\partial h}, l, g, - \right) \end{aligned} \quad (4.26)$$

Expanding up to the second power of $\varepsilon = J_2 a_e^2$:

$$\begin{aligned} K_0 + K_1 (L', G', H', - , g, -) + \frac{\partial K_1}{\partial g} \frac{\partial S_1}{\partial G'} + K_2 (L', G', H', - , g, -) = \\ H_0 (L') + \frac{\partial H_0}{\partial L'} \frac{\partial S_1}{\partial l} + \frac{\partial H_0}{\partial L'} \frac{\partial S_2}{\partial l} + \frac{1}{2} \frac{\partial^2 H_0}{\partial L'^2} \left(\frac{\partial S_1}{\partial l} \right)^2 + H_1 (L', G', H', l, g, -) + \\ \frac{\partial H_1}{\partial L'} \frac{\partial S_1}{\partial l} + \frac{\partial H_1}{\partial G'} \frac{\partial S_1}{\partial g} \end{aligned} \quad (4.27)$$

It is possible to associate elements of corresponding order in either side of the equation, by considering that each term's order is equal to the sum of the subindices of each factor. With this in mind:

$$\begin{cases} \varepsilon^0 : K_0(L') & = H_0(L') \end{cases} \quad (4.28)$$

$$\begin{cases} \varepsilon^1 : K_1 & = H_1 + \frac{\partial H_0}{\partial L'} \frac{\partial S_1}{\partial l} \end{cases} \quad (4.29)$$

$$\begin{cases} \varepsilon^2 : K_2 + \frac{\partial K_1}{\partial g} \frac{\partial S_1}{\partial G'} & = \frac{\partial H_0}{\partial L'} \frac{\partial S_2}{\partial l} + \frac{1}{2} \frac{\partial^2 H_0}{\partial L'^2} \left(\frac{\partial S_1}{\partial l} \right)^2 + \frac{\partial H_1}{\partial L'} \frac{\partial S_1}{\partial l} + \frac{\partial H_1}{\partial G'} \frac{\partial S_1}{\partial g} \end{cases} \quad (4.30)$$

This expansion could be carried out indefinitely, although it will be restricted to the zeroth and first-order PDEs. It is now when one can get rid of the short-period terms of the first-order original Hamiltonian, by separating it into the secular and the short-periodic part, *i.e.* :

$$H_1 = H_{1s} + H_{1p}$$

where H_{1s} and H_{1p} can be expressed as:

$$\begin{cases} H_{1s} = \frac{\mu^4 a_e^2 J_2}{L^3 G^3} A \\ H_{1p} = \frac{\mu^4 a_e^2 J_2}{L^6} (A\sigma_1 + B\sigma_2) \end{cases} \quad (4.31)$$

Substituting (4.31) into (4.29) splits it into two:

$$\begin{cases} \frac{\partial S_1}{\partial l} = \frac{\mu^2 a_e^2 J_2}{L'^3} (A\sigma_1 + B\sigma_2) \\ K_{1p} = \frac{\mu^4 a_e^2 J_2}{L'^3 G'^3} A \end{cases} \quad (4.32)$$

After some mathematical manipulations, the final form of S_1 can be expressed as:

$$S_1 = \frac{\mu^2 a_e^2 J_2}{G'^3} \left\{ A(\theta - l + e \sin \theta) + B \left[\frac{1}{2} \sin(2g + 2\theta) + \frac{e}{2} \sin(2g + \theta) + \frac{e}{6} \sin(2g + 3\theta) \right] \right\} \quad (4.33)$$

And finally, the conversion between the long-period and secular motion set L', G', H', l', g', h' and the full osculating set L, G, H, l, g, h can be expressed as:

$$\begin{cases} L = L' + \frac{\partial S_1}{\partial l} & l = l' - \frac{\partial S_1}{\partial L'} \\ G = G' + \frac{\partial S_1}{\partial g} & g = g' - \frac{\partial S_1}{\partial G'} \\ H = H' & h = h' - \frac{\partial S_1}{\partial H'} \end{cases} \quad (4.34)$$

Second-order effects are specified in section 4. of Brouwer [30].

II.B. Long-period effects removal.

In an analogue manner to what was done before, a further canonical transformation can be performed over the prime set (L', G', H', l', g', h') . The new generating function will be:

$$\tilde{S} = L''l' + G''g' + H''h' + \tilde{S}_1(L'', G'', H'', -, g', -)$$

where the target now is to obtain the function \tilde{S}_1 for which $L'', G'', H'', l'', g'', h''$ do not contain any periodic term. After a very similar process to the one performed before, the function \tilde{S}_1 results:

$$\tilde{S}_1 = G''\gamma_2 \left(\frac{L'^2}{G''^2} - \frac{L'^4}{G''^4} \right) \left[\frac{1}{16} \left(1 - 11 \frac{H^2}{G''^2} \right) - \frac{5}{2} \frac{H^4}{G''^4} \left(1 - 5 \frac{H^2}{G''^2} \right)^{-1} \right] \sin 2g'' \quad (4.35)$$

where $\gamma_2 = \frac{\mu^2 a_e^2 J_2}{L'^4}$. The new mean element set results:

$$\left\{ \begin{array}{l} L' = L'' \quad l' = l'' - \frac{\partial \tilde{S}_1}{\partial L'} \\ G' = G'' + \frac{\partial \tilde{S}_1}{\partial g'} \quad g = g' - \frac{\partial \tilde{S}_1}{\partial G''} \\ H' = H'' = H \quad h = h' - \frac{\partial \tilde{S}_1}{\partial H} \end{array} \right. \quad (4.36)$$

III. Variational equations for mean element set.

Finally, the variational equations for this mean element set are:

$$\left\{ \begin{array}{l} \frac{dL''}{dt} = 0, \quad \frac{dl''}{dt} = -\frac{\partial \tilde{K}}{\partial L} \\ \frac{dG''}{dt} = 0, \quad \frac{dl}{dt} = -\frac{\partial \tilde{K}}{\partial G} \\ \frac{dH''}{dt} = 0, \quad \frac{dl}{dt} = -\frac{\partial \tilde{K}}{\partial h} \end{array} \right. \quad (4.37)$$

where \tilde{K} is the new modified Hamiltonian. The exact equations can be seen again in Brouwer, eqs. 39-41.

IV. Final mean to osculating relations.

The concatenation of transformations (4.34) and (4.36) lead to some cumbersome expressions, which for the sake of tidiness, are here only quoted: they are present in Brouwer [30], section 9.

4.3.2.2 Lyddane approximation.

Brouwer's theory, though groundbreaking at the time, featured singularities. Besides the uncommon case of critical inclination (which does not need to be solved), the equations become singular null eccentricities or inclination angles. Lyddane [29] tackled this singularities and gets rid of them by using Poincaré variables instead of the Delaunay set. The actual formulas for the mean to osculating transformation are quoted in the next section.

4.3.2.3 Results: Transformations.

Schaub and Junkins [31] provide the mathematical formulae derived from Brouwer's theory with Lyddane's modification in its appendix G. An important thing to keep in mind is that, as it

is a first-order mapping, the direct (*i.e.* mean to osculating) and inverse (*i.e.* osculating to mean) transformations just differ by a sign, contained in the small parameter γ'_2 :

$$\gamma'_2 = \pm \frac{J_2}{2\eta^4} \left(\frac{a_e}{a} \right)^2$$

Said expressions will later be validated.

4.3.3 STM approach.

Brouwer's theory by itself is a powerful tool. Nonetheless, it has enabled the development of many derived theories. The STM developed by Gim and Alfriend [5] is a good example of this. It actually uses a linearization of the Lyddane's modification of Brouwer's theory, as its sole purpose is to build an STM (linear by definition). An important difference with respect to the original Lyddane's modification shown in [31] is that effects are separated in long and short period, which can in turn be used to validate other theories. Additionally, quasi-nonsingular elements are used instead of the Keplerian.

A brief description on the approach followed by these authors is found in section 5.2, where an emphasis is made on the linearised mean to osculating transformations.

4.3.4 Validation.

Once the selected methods have been presented, it is time for validating their implementation. In this respect, the two surveyed methods are:

- A. Lyddane's modification of Brouwer's theory:** Explicit relation between mean and osculating elements, expressed in Keplerian OEs, and that can be inverted by merely changing the sign of the factor γ_2 . All the relations are shown in [31], appendix G, and this approach will be referred to as the Brouwer-Lyddane (BL) method.
- B. Gim-Alfriend's interpretation of Brouwer's theory:** Framed in the Gim-Alfriend STM paper, it is expressed in quasi-nonsingular elements, and approaches each of the individual effects separately (short/long period) through an alternative interpretation of Brouwer's theory. The inverse transformation is performed iteratively. This will be referred to as the Gim-Alfriend (GA) transformation, and its practical implementation is discussed in section 5.2.

The first validation test will be performed against the provided mean-osculating conversion by Alfriend et al. [2, section 3.4]. Once both formulations have been proven to match the benchmark,

the subdivided transformation will be tested against a High-Fidelity propagator, involving also the propagation of the mean elements.

4.3.4.1 Mean to osculating functions: Brouwer-Lyddane and GA vs truth.

The target is to validate both the direct and inverse transformations through the two different methods (BL and GA). The *truth* is obtained from example 3.1. of reference [2], which is expressed in quasi-nonsingular OEs:

$$\text{Truth} \left\{ \begin{array}{ll} \text{Mean } \underline{\text{OE}} & \left\{ \begin{array}{l} \bar{a} = 7100 \text{ km} \quad \bar{u} = 0 \text{ rad} \quad \bar{i} = 70 \text{ deg} \\ \bar{q}_1 = 0.05 \quad \bar{q}_2 = 0.05 \quad \bar{\Omega} = 45 \text{ deg} \end{array} \right. \\ \text{Osc. } \underline{\text{OE}} & \left\{ \begin{array}{l} a = 7109.31795 \text{ km} \quad u = 0.00005 \text{ rad} \quad i = 1.22196 \text{ rad} \\ q_1 = 0.05063 \quad q_2 = 0.05003 \quad \Omega = 0.78547 \text{ rad} \end{array} \right. \end{array} \right. \quad (4.38)$$

Table 4.1 shows the mentioned results, expressing the difference between the obtained sets and the truth.

Method	Transf.	δa [m]	δq_1 [-]	δq_2 [-]	δi [rad]	$\delta \Omega$ [rad]	δu [rad]
BL	Direct	$8.4138 \cdot 10^{-2}$	$5.5785 \cdot 10^{-6}$	$1.7288 \cdot 10^{-6}$	$2.6111 \cdot 10^{-6}$	$2.7143 \cdot 10^{-6}$	$1.5803 \cdot 10^{-5}$
	Inverse	4.0796	$6.1613 \cdot 10^{-6}$	$1.7465 \cdot 10^{-6}$	$3.1437 \cdot 10^{-6}$	$1.1636 \cdot 10^{-6}$	$1.5006 \cdot 10^{-5}$
GA	Direct	$8.3737 \cdot 10^{-2}$	$9.1123 \cdot 10^{-5}$	$8.3773 \cdot 10^{-5}$	$2.6235 \cdot 10^{-6}$	$2.8420 \cdot 10^{-3}$	$1.7263 \cdot 10^{-3}$
	Inverse	$1.6106 \cdot 10^{-1}$	$9.0807 \cdot 10^{-5}$	$8.1354 \cdot 10^{-5}$	$2.5994 \cdot 10^{-6}$	$2.8429 \cdot 10^{-3}$	$1.7263 \cdot 10^{-3}$

Table 4.1: Results of the mean to osculating transformation for both surveyed methods.

4.3.4.2 Comparison against High-Fidelity propagation.

A very useful way to leverage the mean to osculating theory is to propagate the variational equations in mean elements, retaining only the secular terms. The truth benchmark will be a High-Fidelity cartesian propagator (see appendix D), although alternatively, it could be the direct integration of the Gauss Variational Equations with J_2 effect in osculating elements. The required inputs for this test are only the chief's reference orbit at $t = t_0$ and the usual propagation parameters (number of orbits, propagation method . . .). The reference orbit is defined by the previous test, using the true values of the osculating quasi-nonsingular elements, and the orbit will be propagated along ten full revolutions.

Before showing the results, it is necessary to sketch out the propagation through the mean to osculating transformation. This procedure is performed following the next steps:

1st Convert the osculating elements (*i.e.* the reference orbit) to mean elements.

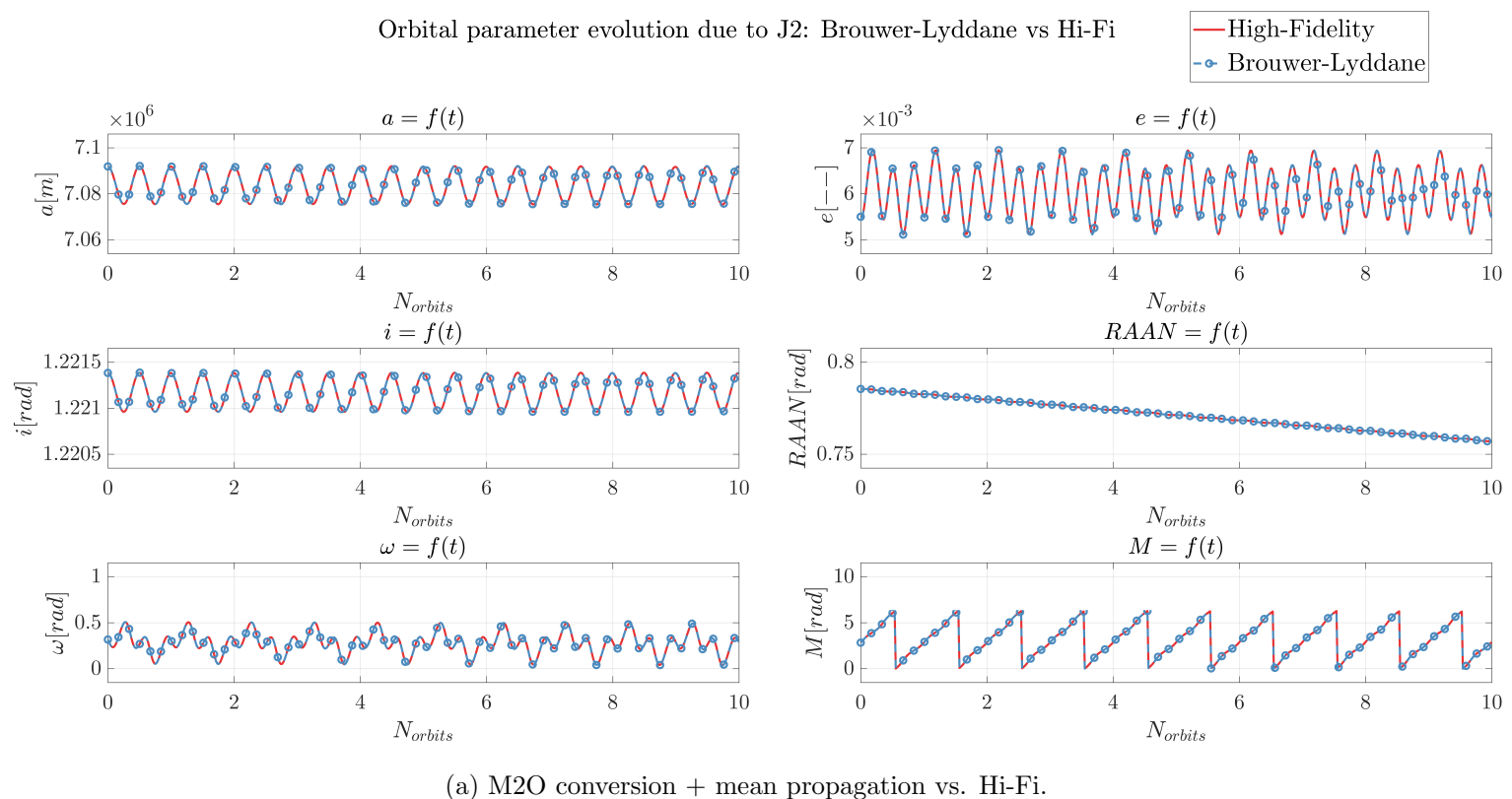
2nd Propagate the mean elements.

3rd Back-convert the mean elements to osculating.

It is insightful to now show the variational equations expressed in mean elements, which include the secular rates only (as it was expected). These equations for the Keplerian OEs are [5]:

$$\left\{ \begin{array}{l} \frac{da^{(s)}}{dt} = 0 \\ \frac{de^{(s)}}{dt} = 0 \\ \frac{di^{(s)}}{dt} = 0 \\ \frac{d\Omega^{(s)}}{dt} = -\frac{3}{2} \frac{J_2 a_e^2 n}{a^2 \eta^4} \cos i \\ \frac{d\omega^{(s)}}{dt} = \frac{3}{4} \frac{J_2 a_e^2 n}{a^2 \eta^4} (5 \cos^2 i - 1) \\ \frac{dM^{(s)}}{dt} = n + \frac{3}{4} \frac{J_2 a_e^2 n}{a^2 \eta^3} (3 \cos^2 i - 1) \end{array} \right. \quad (4.39)$$

Figure 4.2(a) shows the evolution of the Keplerian OEs as propagated by both approaches. The correlation is almost complete, which can be seen in more clarity in figure 4.2(b). All errors are almost negligible, being at least of four orders of magnitude smaller than the true value.



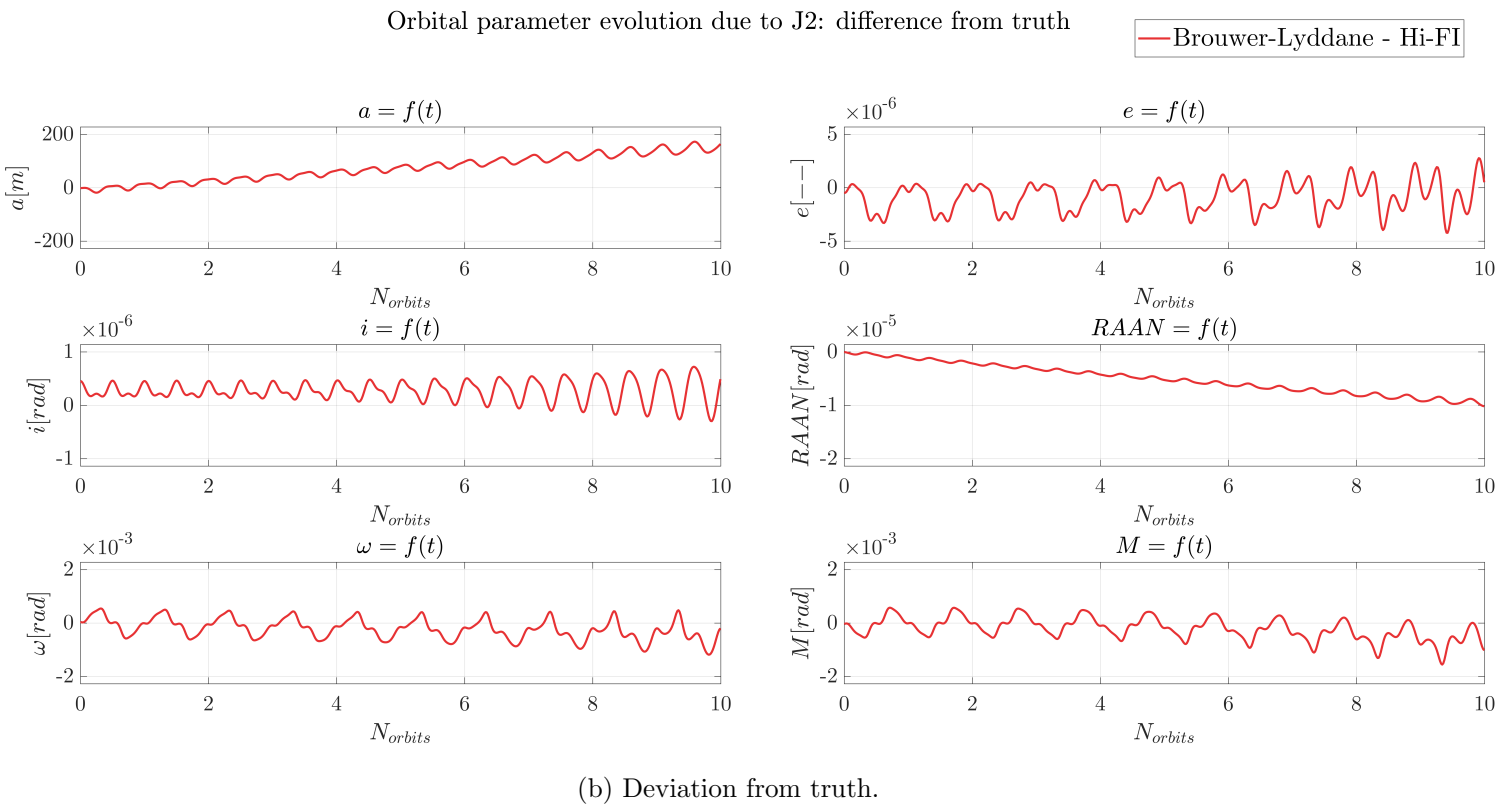


Figure 4.2: Mean to osculating theory versus High-Fidelity propagation.

Final comments.

Although J_2 is by far the biggest perturbation derived from Earth's asphericity, further spherical harmonics may be required –or at least useful– so as to generate more accurate models. It is important to note that, if harmonics of higher order are to be implemented, nonlinear perturbation theory should also be considered. This would be carried out through the already presented Von Zeipel's and Lie series methods, obtaining the second-order term of the expansions in the generating function (S_2) and the modified Hamiltonian (K_2). One must keep in mind that the J_2 term squared is of the order of any other term of the gravitational field.

As the grounds for nonlinear theories have been established, the next topic to tackle is the implementation of a more accurate gravity field model, ideally in a general form. In the following section, Kaula's theory is presented, developed and validated, as it is a very promising approach for the topic in question.

4.4 Kaula's theory.

The aim of this section is to provide a theory that extends the aforementioned variational approach for J_2 perturbed orbits to any given term of the gravity field. One remarkable problem with the spherical harmonic model of the gravity field is that it is not expressed in terms of the Keplerian OEs (or any kind really). That means that, when they are put into LPEs, cumbersome and hard to interpret terms arise. Kaula's theory [32] tries and solves this concern by mapping the spherical coordinates into the Keplerian element set, after a not at all trivial manipulation.

One application of this theory –among many others– is the development of a more accurate mean to osculating element transformation, which includes up to a desired number of harmonics. This can in turn be used for a linearised model of relative motion, in a similar manner as Gim and Alfriend do with their STM (see section 5.2). However, this theory enables many other analysis. For example, resonances for a certain kind of orbit can be studied as done by Chao [33].

Firstly, the mentioned mapping will be justified and developed. After that, its implementation will be discussed, and to conclude, it will be validated against a High-Fidelity propagation.

4.4.1 Approach: V_{lm} function rearrangement.

The general solution of the Laplace equation for the gravitational potential field in spherical coordinates is provided in equation 1.31 by Kaula [32]:

$$V = \sum_{l=0}^{\infty} \sum_{m=0}^l V_{lm} = \sum_{l=0}^{\infty} \sum_{m=0}^l \frac{\mu a_e^l}{r^{l+1}} P_{lm}(\sin \phi) (C_{lm} \cos m\lambda + S_{lm} \sin m\lambda) \quad (4.40)$$

where r, λ, ϕ are the spherical coordinates (radial distance, longitude and latitude, respectively), $P_{lm}(\sin \phi)$ is the Legendre function, C_{lm}, S_{lm} are the non-dimensional coefficients of the gravity field, a_e and μ are the equatorial radius and the gravitational parameter of the Earth. This expression could in principle be computed. Nonetheless, the target is to express this perturbing function in terms of the Keplerian OEs, as in that way, a closed form for the Gauss Variational Equations can be obtained.

The task at hand now is to obtain the expressions for r, ϕ and λ in terms of a, e, i, ω, Ω and M .

I. r in terms of the OEs: The orbital radius can easily be expressed in terms of orbital elements as:

$$r = \frac{a(1 - e^2)}{1 + e \cos \theta}$$

which is almost the desired expression. The only change that needs to be performed is the conversion from true anomaly θ to mean anomaly M in an analytical fashion. This will be achieved through the use of series expansions in terms of the eccentricity, which is a common topic in classical references. Hence, r has the following functional dependency:

$$r = g_1(a, e, M) \quad (4.41)$$

II. ϕ in terms of the OEs: The latitude conversion is not as straightforward. It requires the angular position of the spacecraft around the orbit –thus depending on the argument of perigee ω and true anomaly θ) and the orientation of the orbital plane with respect to the equatorial plane –hence depending on the inclination i . This can be achieved through the usage of spherical trigonometric relations, as shown in [see 32, p. 32, eq. 3.56]:

$$\sin \phi = \sin i \sin(\omega + \theta)$$

where the true anomaly needs again to be converted to mean through the mentioned elliptic expansions, so that:

$$\sin \phi = g_2(e, i, \omega, M) \quad (4.42)$$

III. λ in terms of the OEs: This is the most elaborated transformation of the three, as it depends not only on the angular position around the orbit, but also on the relative angular position of the orbit plane with respect to the Greenwich Meridian. This last consideration leads to a dependence on the ascending node Ω and the Greenwich Sidereal Time Θ . The decomposition of λ also requires to apply spherical trigonometry, as well as expansions of the sines and cosines in terms of its own powers (see [32], eqs. 3.50-3.52.). In conclusion, the longitude λ introduces dependencies on ω , θ , Ω and Θ , hence on all Keplerian elements but the semimajor axis:

$$(\cos m\lambda, \sin m\lambda) = g_3(e, i, \Omega, \omega, M, \Theta) \quad (4.43)$$

Combining all the prior transformations, and after some simplifications and regroupings, Kaula arrives to the following expression:

$$V_{lm} = \frac{\mu a_e^l}{a^{l+1}} \sum_{p=0}^l F_{lmp}(i) \sum_{q=-\infty}^{\infty} G_{lpq}(e) S_{lmpq}(\omega, M, \Omega, \Theta) \equiv \sum_{p=0}^l \sum_{q=-\infty}^{\infty} V_{lmpq} \quad (4.44)$$

where F_{lmp} , G_{lpq} , and S_{lmpq} are auxiliary functions that simplify the expression, each of which accounts for the influence of certain orbital elements.

4.4.2 Subfunctions F_{lmp} , G_{lpq} and S_{lmpq} .

4.4.2.1 Subfunction F_{lmp} .

The function $F_{lmp}(i)$ is built to concentrate the dependency on the inclination in one single function. It is defined as (see equation 3.62 [32]):

$$F_{lmp}(i) = \sum_t \frac{(2l - 2t)!}{t!(l-t)!(l-m-2t)!2^{2l-2t}} \sin^{l-m-2t} i \times \sum_{s=0}^m \binom{m}{s} \cos^s i \sum_c \binom{l-m-2t+s}{c} \binom{m-s}{p-t-c} (-1)^{c-k} \quad (4.45)$$

The summations are characterized by:

- I. Summation in t : t is summed from 0 to the lesser of p or k , that is: $p = \{0, 1, 2, \dots, \min(p, k)\}$, where k is defined as the integer part of $\frac{l-m}{2}$.
- II. Summation in s : s is summed from 0 to m .
- III. Summation in c : c is summed over all values that make the binomial coefficients nonzero. That is, those values for which the binomial coefficient does not turn into an infinite series. This condition is split in two: (A) both lower coefficients being lower or equal than the upper ones and (B) both lower coefficients must be greater or equal than zero.

$$\left\{ \begin{array}{l} \text{Condition A)} \\ \text{Condition B)} \end{array} \right\} \begin{cases} c \leq l - m - 2t + s \\ p - t - c \leq m - s \Rightarrow c \geq p - t - m + s \\ c \geq 0 \\ p - t - c \geq 0 \Rightarrow c \leq p - t \end{cases} \quad (4.46a)$$

$$\left\{ \begin{array}{l} \text{Condition A)} \\ \text{Condition B)} \end{array} \right\} \begin{cases} c \leq l - m - 2t + s \\ p - t - c \leq m - s \Rightarrow c \geq p - t - m + s \\ c \geq 0 \\ p - t - c \geq 0 \Rightarrow c \leq p - t \end{cases} \quad (4.46b)$$

Condition (4.46) is translated into limits for c , as:

$$\left\{ \begin{array}{l} \text{Lower limit: } c_{min} = \max(p - t - m + s, 0) \\ \text{Upper limit: } c_{max} = \min(l - m - 2t + s, p - t) \end{array} \right. \quad (4.47a)$$

$$\left\{ \begin{array}{l} \text{Lower limit: } c_{min} = \max(p - t - m + s, 0) \\ \text{Upper limit: } c_{max} = \min(l - m - 2t + s, p - t) \end{array} \right. \quad (4.47b)$$

This then leads to the more compact expression: $c = \{c_{min}, c_{min} + 1, c_{min} + 2, \dots, c_{max}\}$. Theoretically, c_{min} could be larger than c_{max} . In that case, no summation terms arise, thus being the summation zero, and also $F_{lmp}(i)$.

Example: Calculation of F_{321}

Equation (4.45), hand in hand with the summation limits definition (4.47), is undeniably far from intuitive. In order to show how the expression itself truly works, a particularization of it will now be developed. The calculation of F_{321} is explained in the following steps.

Step 1. Definition of auxiliary variables: Defining new constant coefficients (independent of the inclination) allows for a simpler mathematical notation:

$$F_{lmp}(i) = \sum_t C_t \sin^{l-m-2t}(i) \sum_s C_s \cos^s(i) \sum_c C_c \quad (4.48)$$

where:

$$\begin{cases} C_t(l, m, t) &= \frac{(2l - 2t)!}{t!(l-t)!(l-m-2t)!2^{2l-2t}} \\ C_s(m, s) &= \binom{m}{s} \\ C_c(l, m, p, t, s, c) &= \binom{l-m-2t+s}{c} \binom{m-s}{p-t-c} (-1)^{c-k} \end{cases} \quad (4.49)$$

Now, summations can be defined as:

$$\begin{cases} S_c(l, m, p, t, s) &= \sum_{c=c_{min}}^{c=c_{max}} C_c \\ S_s(l, m, p) &= \sum_{s=0}^m C_s S_c(l, m, p, t, s) \end{cases} \quad (4.50)$$

so that equation (4.48) can be reframed as:

$$F_{lmp}(i) = \sum_{t=0}^{\min p, k} C_t S_s \quad (4.51)$$

Step 2. Summation limits calculation: Starting with t :

$$t : \begin{cases} t_{min} &= 0 \\ t_{max} = \min \left(0, k = \int \left(\frac{l-p}{2} \right) \right) &= \min \left(0, \int \left(\frac{1}{2} \right) \right) = 0 \end{cases}$$

$$\Rightarrow t = \{0\} \quad (4.52)$$

Continuing with s :

$$s : \begin{cases} s_{min} = 0 \\ s_{max} = m = 2 \end{cases}$$

$$s = \{0, 1, 2\} \quad (4.53)$$

Lastly, the limits for the c summation are calculated:

$$t = 0 \rightarrow \begin{cases} s = 0 \rightarrow \begin{cases} c_{min} = \max(1 - 0 - 2 + 0, 0) = 0 \\ c_{max} = \min(3 - 2 - 2 \cdot 0 + 0, 1 - 0) = 1 \end{cases} \Rightarrow c = \{0, 1\} \\ s = 1 \rightarrow \begin{cases} c_{min} = \max(1 - 0 - 2 + 1, 0) = 0 \\ c_{max} = \min(3 - 2 - 2 \cdot 0 + 1, 1 - 0) = 1 \end{cases} \Rightarrow c = \{0, 1\} \\ s = 2 \rightarrow \begin{cases} c_{min} = \max(1 - 0 - 2 + 2, 0) = 1 \\ c_{max} = \min(3 - 2 - 2 \cdot 0 + 2, 1 - 0) = 1 \end{cases} \Rightarrow c = \{1\} \end{cases} \quad (4.54)$$

Step 3. Simplification of the general expressions: Particularizing (4.49):

$$\begin{cases} C_t &= \frac{(2 \cdot 3 - 2 \cdot 0)!}{0!(3-0)!(3-2-2 \cdot 0)!2^{2 \cdot 3 - 2 \cdot 0}} = \frac{15}{8} \\ C_s(s) &= \binom{2}{s} \\ C_c(s, c) &= \binom{3 - 2 - 2 \cdot 0 + s}{c} \binom{2 - s}{1 - 0 - c} (-1)^{c-0} = \binom{1+s}{c} \binom{2-s}{1-c} (-1)^c \end{cases} \quad (4.55)$$

Step 4. Calculation of the s summation:

$$S_s = C_s(s=0) \cos^0(i) S_c(s=0) + C_s(s=1) \cos(i) S_c(s=1) + C_s(s=2) \cos^2(i) S_c(s=2)$$

$$s=0 \left\{ \begin{array}{l} C_s(s=0) = \binom{2}{0} = 1 \\ S_c(s=0) = C_c(s=0, c=0) + C_c(s=1, c=1) = \\ \binom{1+0}{0} \binom{2-0}{1-0} (-1)^0 + \binom{1+0}{1} \binom{2-0}{1-1} (-1)^1 = 2 - 1 = 1 \end{array} \right.$$

$$\Rightarrow C_s(s=0) \cos^0(i) S_c(s=0) = 1 \quad (4.56)$$

$$s=1 \left\{ \begin{array}{l} C_s(s=1) = \binom{2}{1} = 2 \\ S_c(s=1) = C_c(s=1, c=0) + C_c(s=1, c=1) = \\ \binom{1+1}{0} \binom{2-1}{1-0} (-1)^0 + \binom{1+1}{1} \binom{2-1}{1-1} (-1)^1 = 1 - 2 = -1 \end{array} \right.$$

$$\Rightarrow C_s(s=1) \cos^1(i) S_c(s=1) = -2 \cos(i) \quad (4.57)$$

$$s = 2 \begin{cases} C_s(s=2) = \binom{2}{2} = 1 \\ S_c(s=2) = C_c(s=2, c=1) = \binom{1+2}{1} \binom{2-2}{1-1} (-1)^1 = -3 \end{cases}$$

$$\Rightarrow C_s(s=2) \cos^2(i) S_c(s=2) = -3 \cos^2(i) \quad (4.58)$$

$$\Rightarrow S_s(t=0) = 1 - 2 \cos i - 3 \cos^2 i \quad (4.59)$$

Step 5. Final calculation of F_{321} :

$$F_{321} = C_t(t=0) (\sin i)^{3-2-2\cdot0} S_s(t=0)$$

$$\Rightarrow F_{321}(i) = \frac{15}{8} \sin i (1 - 2 \cos i - 3 \cos^2 i) \quad (4.60)$$

which is exactly the same result as in Kaula's tables ([32, p.34-35]). The outlined procedure will be somehow mimicked by the computational approach later on.

4.4.2.2 Subfunction G_{lpq} .

This section focuses on the G_{lpq} function, which through elliptic expansions, converts true anomaly dependent functions into mean anomaly dependent. For this purpose, two approaches can be implemented: The one from Kaula, and its source, from Tisserand [34]. The former is the one that will here be tackled, as it is a somewhat simpler version of the latter.

The transformation one wishes to perform is:

$$\begin{aligned} & \frac{1}{r^{l+1}} \begin{Bmatrix} \cos \\ \sin \end{Bmatrix} [(l-2p)(\omega + f) + m(\Omega - \Theta)] \\ &= \frac{1}{a^{l+1}} \sum_q G_{lpq}(e) \begin{Bmatrix} \cos \\ \sin \end{Bmatrix} [(l-2p)\omega + (l-2p+q)M + m(\Omega - \Theta)] \end{aligned} \quad (4.61)$$

This expression can be averaged with respect to M in order to get long-period terms ([eq. 3.66 32]). Nonetheless, the target is to get the general expression for G_{lpq} , which will be done hereafter.

Kaula, quoting Tisserand, provides the result for G_{lpq} :

$$G_{lpq}(e) = (-1)^{|q|} (1 + \beta^2)^l \beta^{|q|} \sum_{k=0}^{\infty} P_{lpqk} Q_{lpqk} \beta^{2k} \quad (4.62)$$

where $\beta = \frac{e}{1 + \sqrt{1 - e^2}}$. Each of the sub-functions can now be analysed:

P_{lpqk} and Q_{lpqk} functions.

Kaula defines P_{lpqk} as:

$$P_{lpqk} = \sum_{r=0}^h \binom{2p' - 2l}{h - r} \frac{(-1)^r}{r!} \left(\frac{(l - 2p' + q')e}{2\beta} \right)^r \quad (4.63)$$

whereas Q_{lpqk} is defined as:

$$Q_{lpqk} = \sum_{r=0}^h \binom{-2p'}{h - r} \frac{1}{r!} \left(\frac{(l - 2p' + q')e}{2\beta} \right)^r \quad (4.64)$$

Both expressions feature two auxiliary indices p' and q' and the summation limit h . The first two are defined in terms of the input indices $lpqk$ as:

$$p' = \begin{cases} p & \text{if } p \leq l/2 \\ l - p & \text{if } p > l/2 \end{cases} \quad (4.65)$$

$$q' = \begin{cases} q & \text{if } p \leq l/2 \\ -q & \text{if } p > l/2 \end{cases} \quad (4.66)$$

and the summation limit h is defined as:

$$\text{For } P_{lpqk} : h = \begin{cases} k + q' & \text{if } q' > 0 \\ k & \text{if } q' < 0 \end{cases} \quad (4.67)$$

$$\text{For } Q_{lpqk} : h = \begin{cases} k & \text{if } q' > 0 \\ k - q' & \text{if } q' < 0 \end{cases} \quad (4.68)$$

Example: Calculation of G_{201}

Similarly to what has been done with F_{lmp} , a good way to break down the complexity of the G_{lpq} expression is to perform a by-hand substitution of the indices lpq . particularly, $l = 2$, $p = 0$ and $q = 1$.

Without further ado, the substitution proceeds as follows:

Step 1. Definition of auxiliary variables: A more compact form of G_{lpq} is achieved as:

$$G_{lpq}(e) = CS_k \quad (4.69)$$

where:

$$\begin{cases} C(l, q) = (-1)^{|q|} (1 + \beta^2)^l \beta^{|q|} \\ S_k(l, p, q) = \sum_{k=0}^{\infty} P_{lpqk} Q_{lpqk} \beta^{2k} \end{cases} \quad (4.70)$$

Additionally, the expressions of P_{lpqk} and Q_{lpqk} can also be redefined as:

$$\begin{cases} P_{lpqk} = \sum_{r=0}^h p_r (1 + \eta)^r \\ Q_{lpqk} = \sum_{r=0}^h q_r (1 + \eta)^r \end{cases} \quad (4.71)$$

where $\eta = \sqrt{1 - e^2}$ and:

$$\begin{cases} p_r(l, p, q, h, r) = \binom{2p' - 2l}{h - r} \frac{(-1)^r}{r!} \left(\frac{l - 2p' + q'}{2} \right)^r \\ q_r(l, p, q, h, r) = \binom{-2p'}{h - r} \frac{1}{r!} \left(\frac{l - 2p' + q'}{2} \right)^r \end{cases} \quad (4.72)$$

Step 2. Auxiliary indices and summation limits calculation:

$$\begin{cases} p = 0 < \frac{2}{2} = \frac{l}{2} \Rightarrow p' = p = 0 \\ q = 1 > 0 \Rightarrow q' = q = 1 \\ h = \begin{cases} \text{For } P_{lpqk} : q' = 1 > 0 \Rightarrow h = k + q' = k + 1 \\ \text{For } Q_{lpqk} : q' = 1 > 0 \Rightarrow h = k \end{cases} \end{cases} \quad (4.73)$$

Step 3. Simplification of the general expressions: With (4.73) in mind, and substituting the values into (4.72) and (4.70):

$$\begin{cases} C(l=2, q=1) & = (-1)^{|1|} (1 + \beta^2)^2 \beta^{|1|} = -\beta - 2\beta^3 - \beta^5 \\ p_r(l=2, p=0, q=1, h=k+1, r) & = \binom{-4}{k+1-r} \frac{(-1)^r}{r!} \left(\frac{3}{2}\right)^r \\ q_r(l=2, p=0, q=1, h=k+1, r) & = \binom{0}{k-r} \frac{1}{r!} \left(\frac{3}{2}\right)^r \end{cases} \quad (4.74)$$

Step 4. Analysis of eccentricity powers to retain: If, as Kaula, the aim is to get a fourth-order expansion in terms of the eccentricity, care must be taken to calculate just the necessary terms of the k summation. The factor $C(l, q)$ is a function of β , whose developments for different powers is provided in E.5.1. Substituting into C :

$$\begin{aligned} C(l=2, q=1)(e) &= -\left(\frac{1}{2}e + \frac{1}{8}e^3 + \mathcal{O}(e^5)\right) - 2\left(\frac{1}{8}e^3 + \mathcal{O}(e^5)\right) + \mathcal{O}(e^5) \\ \Rightarrow C(e) &= -\frac{1}{2}e - \frac{3}{8}e^3 + \mathcal{O}(e^5) = \mathcal{O}(e) \end{aligned} \quad (4.75)$$

As the coefficient C is of order $\mathcal{O}(e)$, the summation S_k shall only contain elements of order less or equal than $\mathcal{O}(e^3)$. The functions P_{lpqk} and Q_{lpqk} have a term of order zero, so terms of order up to three must be retained in β^{2k} . As powers of β (which is $\sim \mathcal{O}(e)$) grow by twos, only $k = 0$ and $k = 1$ must be considered.

Before diving into the calculation of S_k , it is necessary to arrive to a fourth-order version of η . Its MacLaurin series expansion can be calculated as:

$$\begin{aligned} \eta &= \sqrt{1 - e^2} = (1 - e^2)^{1/2} = \sum_{n=0}^{\infty} \binom{1/2}{n} (-1)^n e^{2n} = \\ &\quad \binom{1/2}{0} (-1)^0 e^0 + \binom{1/2}{1} (-1)^1 e^2 + \binom{1/2}{2} (-1)^2 e^4 + \mathcal{O}(e^6) = \\ &\quad \frac{(1/2)(-1/2)(-3/2)(-5/2)\dots}{1 \cdot (1/2)(-1/2)(-3/2)(-5/2)\dots} + \frac{(1/2)(-1/2)(-3/2)(-5/2)\dots}{1 \cdot (-1/2)(-3/2)(-5/2)\dots} (-1)e^2 + \\ &\quad + \frac{(1/2)(-1/2)(-3/2)(-5/2)\dots}{1 \cdot (-3/2)(-3/2)(-5/2)\dots} e^4 + \mathcal{O}(e^6) = 1 - \frac{e^2}{2} - \frac{e^4}{8} + \mathcal{O}(e^6) \end{aligned} \quad (4.76)$$

$$\Rightarrow 1 + \eta = 2 - \frac{e^2}{2} - \frac{e^4}{8} + \mathcal{O}(e^6) \quad (4.77)$$

In conclusion, $k = 0, 1$ and for each of those values, h is defined by (4.73).

Step 5. Computation of S_k :

$$S_k = P_{2010}Q_{2010}\beta^0 + P_{2011}Q_{2011}\beta^2 \quad (4.78)$$

$$k=0 \left\{ \begin{array}{l} P_{2010} = \sum_{r=0}^{0+1} p_r (1+\eta)^r = p_r(r=0) + p_r(r=1)(1+\eta) = \\ \qquad\qquad\qquad = \binom{-4}{1} \cdot 1 + \binom{-4}{0} (-1) \frac{3}{2}(1+\eta) = -4 - \frac{3}{2}(1+\eta) \\ Q_{2010} = \sum_{r=0}^{0+0} q_r (1+\eta)^r = q_r(r=0) = \binom{0}{0} \cdot 1 = 1 \end{array} \right.$$

$$k=1 \left\{ \begin{array}{l} P_{2011} = \sum_{r=0}^{1+1} p_r (1+\eta)^r = p_r(r=0) + p_r(r=1)(1+\eta) + p_r(r=2)(1+\eta)^2 = \\ \qquad\qquad\qquad = \binom{-4}{2} \cdot 1 + \binom{-4}{1} (-1) \frac{3}{2}(1+\eta) + \binom{-4}{0} \frac{9}{4}(1+\eta)^2 = 10 + 6(1+\eta) + \frac{9}{8}(1+\eta)^2 \\ Q_{2011} = \sum_{r=0}^{1+0} q_r (1+\eta)^r = q_r(r=0) + q_r(r=1)(1+\eta) = \\ \qquad\qquad\qquad = \binom{0}{1} \cdot 1 + \binom{0}{0} \frac{3}{2}(1+\eta) = \frac{3}{2}(1+\eta) \end{array} \right.$$

The “tricky” part starts now: The summation S_k now looks like:

$$S_k = \left[-4 - \frac{3}{2}(1+\eta) \right] + \left[\left(10 + 6(1+\eta) + \frac{9}{8}(1+\eta)^2 \right) \frac{3}{2}(1+\eta) \right] \beta^2 \quad (4.79)$$

As argued before, S_k must be expanded up to third order. The η in the first term in brackets can be expanded up to second order, as no additional eccentricity power exists. Conversely, in the right-hand side term, the fact that it is multiplied by $\beta^2 \sim \mathcal{O}(e^2)$ allows for expanding up to first order, which actually reduces to zeroth order (η has no linear term). In conclusion, $\eta \approx 1 - e^2/2$ for the left term and $\eta \approx 1$ for the right one:

$$S_k = \left[-4 - \frac{3}{2}(2 - e^2/2) \right] + \left[\left(10 + 6 \cdot 2 + \frac{9}{8} \cdot 2^2 \right) \frac{3}{2} \cdot 2 \right] \beta^2$$

Applying the β function expansion and retaining terms of up to second order:

$$S_k = -4 - 3 + \frac{3}{4}e^2 + \frac{53}{2} \frac{3}{4}e^2 = -7 + \frac{165}{8}e^2 \quad (4.80)$$

Step 6. Final calculation of G_{201} :

$$G_{201} = C S_k = \left(-\frac{1}{2}e - \frac{3}{8}e^3 \right) \left(-7 + \frac{165}{8}e^2 \right) =$$

$$\Rightarrow G_{201} = \frac{7}{2}e - \frac{123}{16}e^3 + \mathcal{O}(e^5) \quad (4.81)$$

expression which is exactly identical to the one from [Kaula 32, p.38].

4.4.2.3 Subfunction S_{lmpq} .

The subfunction S_{lmpq} embodies the longitude-dependent part of the spherical harmonic. This happens through the Keplerian OEs ω , M and Ω , and the Greenwich Mean Sidereal Time Θ . This function happens to be at the innermost loop in the V_{lm} function, depending on four indices. It is defined as:

$$S_{lmpq} = \begin{cases} \begin{bmatrix} C_{lm} \\ -S_{lm} \end{bmatrix}_{l-m \text{ odd}}^{l-m \text{ even}} & \cos [(l-2p)\omega + (l-2p+q)M + m(\Omega - \Theta)] \\ \begin{bmatrix} S_{lm} \\ C_{lm} \end{bmatrix}_{l-m \text{ odd}}^{l-m \text{ even}} & \sin [(l-2p)\omega + (l-2p+q)M + m(\Omega - \Theta)] \end{cases} \quad (4.82)$$

The shape of this function reveals some insights, depending on the values of the indices l, p and q :

- I. If $m = 0$, the sidereal angle Θ does not appear on the phase angle. This means that harmonics of the form V_{i0} (also known as zonal harmonics) do not depend on the Earth's rotational state. This makes sense, as said harmonics represent irregularities that present a rotational symmetry around the Earth's axis.
- II. If $l - 2p + q = 0$, no dependency on M arises. Hence, it is not a short-period effect: it is either long-period (depends on ω or Ω) or secular (null phase)
- III. If $l - 2p = 0$ and $m = 0$, ω , Ω and Θ do not appear in the phase angle. This means that it is either a secular or a short-periodic effect.

With this in mind, three different types of terms come to light:

- A. Secular terms: l, m, p and q such that: $l - 2p = 0$, $l - 2p + q = 0$ and $m = 0$.

- B. Long-period terms: l, m, p and q such that: $l - 2p + q = 0$ and $m \neq 0$, $l - 2p \neq 0$.
- C. Short-period terms: l, m, p and q such that: $l - 2p + q \neq 0$.

As a final remark, tables with F_{lmp} and G_{lpq} for $l = \{2, 3, 4\}$, $m = \{0, 1, 2, 3, 4\}$, $p = \{0, 1, 2, 3, 4\}$ and $q = \{-4, -3, -2, -1, 0, 1, 2, 3, 4\}$ are provided in appendix E

4.4.3 Implementation.

Once the gravity field has been re-parameterized, it is time to discuss its computational implementation. For now, the target is to obtain the effect of any component V_{lm} on the Keplerian OEs, which can be done through the LPEs. Nonetheless, the manipulation of each V_{lmpq} term and its summation turns out to be quite cumbersome, due to (a) the intrinsic uncomfortable expressions and (b) the summation of a considerable amount of individual terms. That is why a systematic approach is developed over the following sections.

4.4.3.1 Computation of V_{lm}

A priori, by looking at equation (4.44), there seem to be two ways to compute V_{lm} :

A : Compute $V_{lmpq} = F_{lmp}G_{lpq}S_{lmpq}$ and then do the summation on p and q .

B : Compute the summations on q and p successively, that is, compute $\sigma_q = \sum_q G_{lpq}S_{lmpq}$, then $\sigma_p = \sum_p F_{lmp}\sigma_q$ and finally obtain V_{lm} .

Both approaches are equally right. In this case, the first one will be used, whose general workflow can be seen in figure 4.3.

I. Subfunction F_{lmp} .

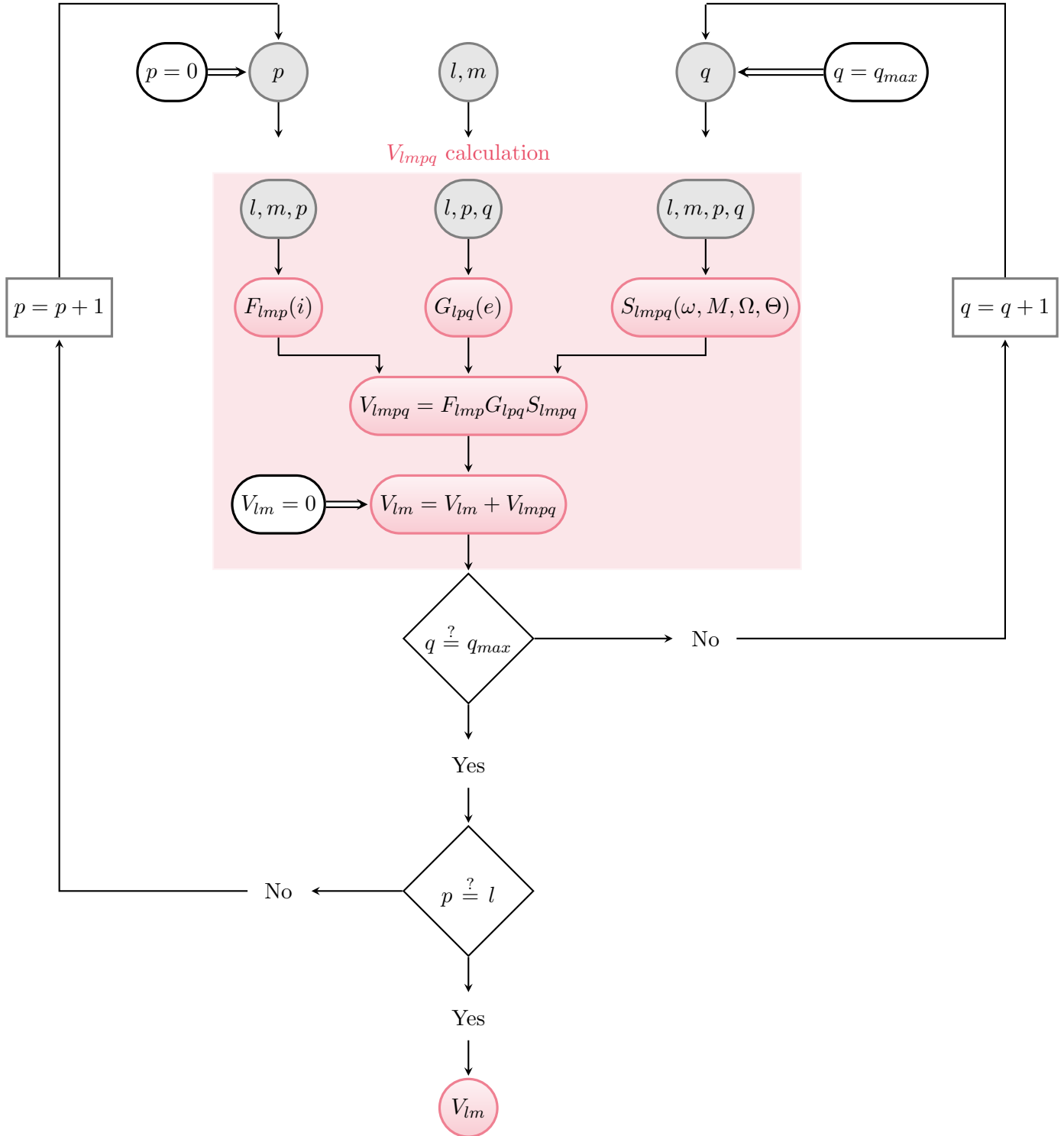
The function $F_{lmp}(i)$ has the structure shown in (4.45). As it can there be appreciated, there are three concatenated summations. The innermost will be called S_c onwards; the one in the middle, S_s , and the outer one is the function F_{lmp} itself. Mathematically:

$$S_c(i; l, m, t, s) = \sum_c \binom{l-m-2t+s}{c} \binom{m-s}{p-t-c} (-1)^{c-k} \equiv \sum_c C_c \quad (4.83)$$

$$S_s(i; l, m, t) = \sum_{s=0}^m \binom{m}{s} \cos^s i S_c(i; l, m, t, s) \equiv \sum_s C_s \cos^s i S_c \quad (4.84)$$

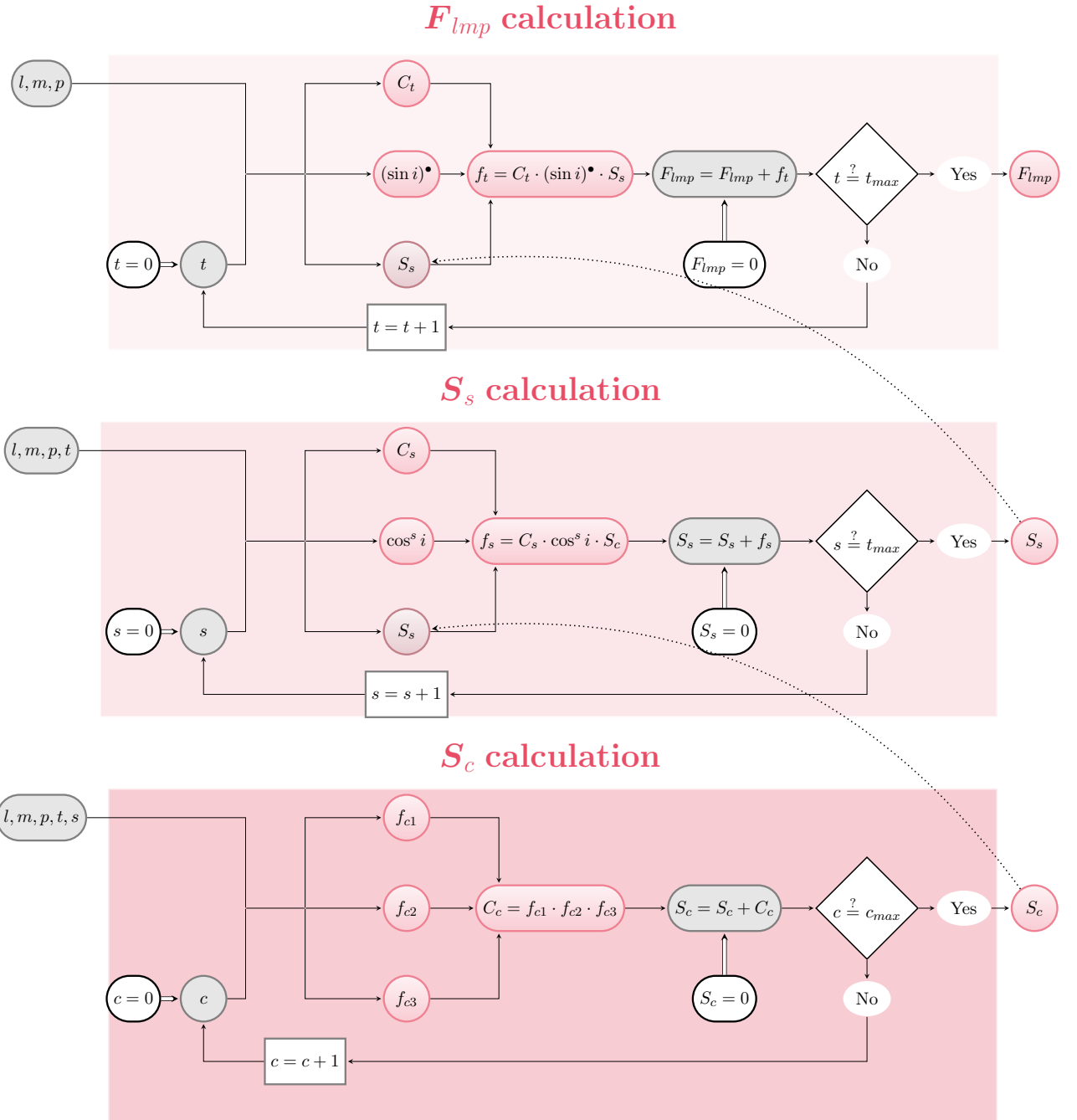
$$\Rightarrow F_{lmp}(i) = \sum_t \frac{(2l-2t)!}{t!(l-t)!(l-m-2t)!2^{2l-2t}} \sin^{l-m-2t} i S_s(i; l, m, t) \equiv \sum_t C_t (\sin i)^{l-m-2t} S_s \quad (4.85)$$

A simplified workflow of the procedure to compute F_{lmp} is shown in 4.4.

Figure 4.3: Workflow of the computation of V_{lm} .

II. Subfunction G_{lpq} .

The calculation of G_{lpq} can be carried out, as shown before, in two ways: the one developed by

Figure 4.4: Workflow of the computation of F_{lmp} .

Kaula and the one developed by Tisserand. Both are tightly related, though the second one seems to be more general. The results should be the same nevertheless. In order to have control on which method is used, a method argument will be fed into the function which computes G_{lpq} .

analogue to what was done for F_{lmp} , the computation of G_{lpq} can be separated into lower-level

components. Following equation (4.62):

$$S_k(e; l, p, q, k) = \sum_{k=0}^{k_{max}} P_{lpqk} Q_{lpqk} \beta^{2k} \quad (4.86)$$

$$G_{lpq}(e) = (-1)^{|q|} (1 + \beta^2)^l \beta^{|q|} S_k(e; l, p, q, k) \quad (4.87)$$

where P_{lpqk} and Q_{lpqk} are defined by (4.63) and (4.64), happening to be another nested summation in r . The workflow that embodies this method is shown in 4.5.

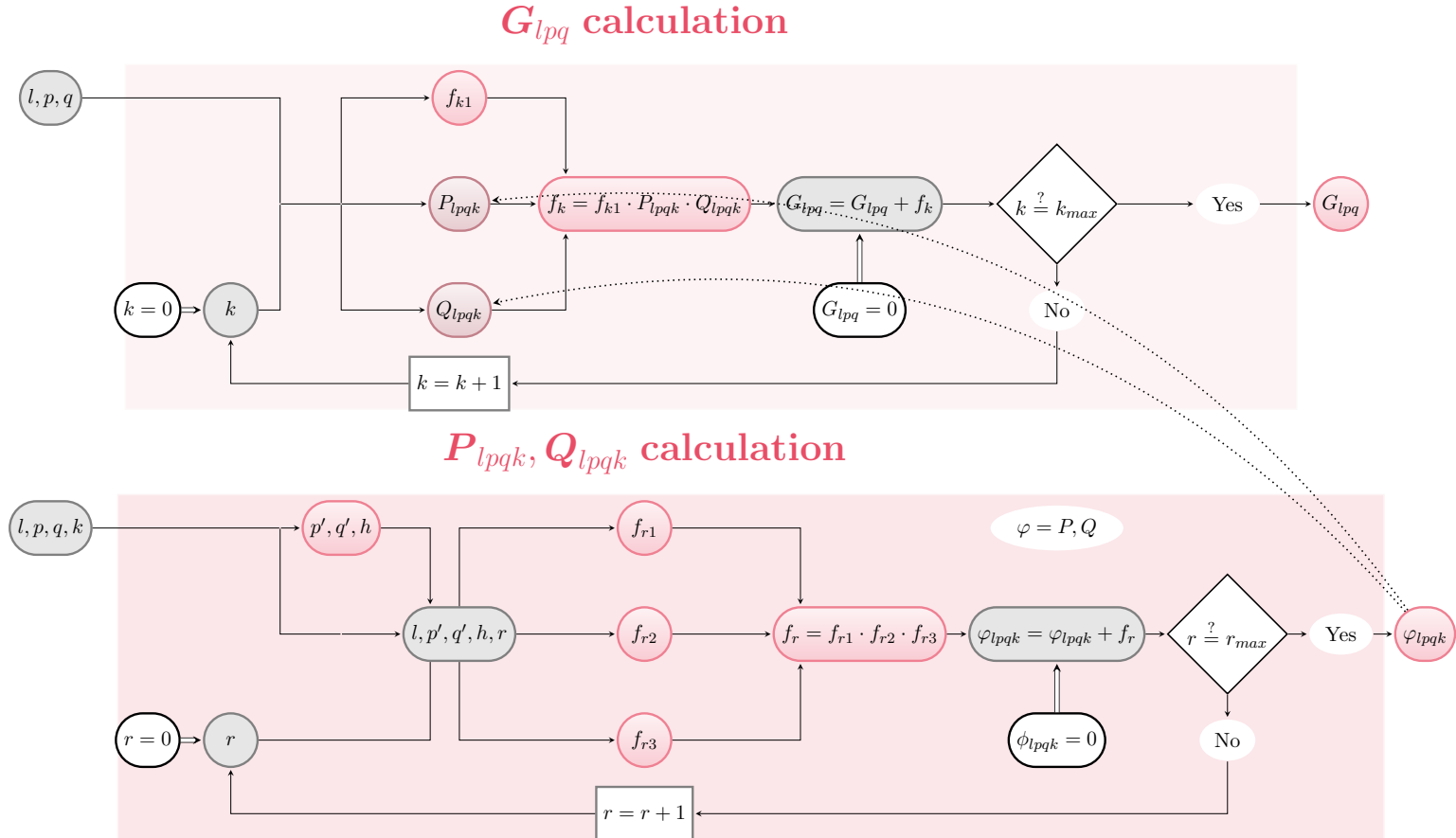


Figure 4.5: Workflow of the computation of G_{lpq} through Kaula's approach.

III. Subfunction S_{lmpq} .

The computation of S_{lmpq} cannot be simplified any further from the expression (4.82). The only

reformulation that can be useful for computational purposes is to obtain a case structure, that is:

$$S_{lmpq}(\omega, M, \Omega, \Theta; l, m, p, q) = \begin{cases} C_{lm} \cos \nu + S_{lm} \sin \nu & \text{if } \text{rem}(l - m, 2) = 0 \\ -S_{lm} \cos \nu + C_{lm} \sin \nu & \text{if } \text{rem}(l - m, 2) \neq 0 \end{cases} \quad (4.88)$$

where $\nu = (l - 2p)\omega + (l - 2p + q)M + m(\Omega - \Theta)$ and rem is the remainder function.

4.4.4 Validation.

4.4.4.1 Target and approach.

Once Kaula's theory has been implemented, it is time to validate its results against a truth model. There are two basic approaches to do this:

- A. Compare Kaula's form of V_{lm} with some other form: This validation process consists of comparing the results yielded by the expressions (4.40) and (4.44) or other expression provided in the literature. In the case of the spherical coordinate parametrization, it needs the implementation of a ECI to geodetic frame transformation, being actually a validation of Kaula's "happy thoughts" to arrive to a KOE-dependent expression of the gravitational field. However, a simplified version of this type of testing is achieved by comparing (4.44) for $l, m = 2, 0$ with the expression 5.48 from Wiesel [9], which is obtained through similar yet less general operations, and only second-order accurate.
- B. Compare a High-Fidelity orbit propagator with Kaula's LPEs: This approach basically means to implement the V_{lmpq} function into the general expression of the LPEs to then compare the output with a cartesian, High-Fidelity propagator. This leads to the need of derivatives of the functions F_{lmp} , G_{lpq} and S_{lmpq} , whose calculation might be more or less complex.

4.4.4.2 Validation of disturbing function.

This section focuses on the analysis of the validity of the V_{20} function itself, rather than its effect on the orbital elements. In order to test this, the analytical form of the J_2 disturbing function will be used. This function is shown in many references, such as [9], eq. 5.41 or [30]. It is equal to:

$$R_2 = -\frac{\mu a_e^2 J_2}{2r^3} (3 \sin^2 i \sin^2(\omega + \theta) - 1) \quad (4.89)$$

Wiesel [9] provides an approximation for this function in equation 5.48. It is obtained through similar though less general operations than Kaula, starting from (4.89). As before, the radial term

and the true anomaly must be converted into Keplerian OEs. For this purpose, the principal relation that is recurrently used is:

$$\theta \approx M + 2e \sin M + \frac{5}{4}e^2 \sin 2M + \mathcal{O}(e^3) \quad (4.90)$$

After performing some substitutions and expansions, the final form of R_2 correct up to second order in the eccentricity is:

$$\begin{aligned} R_2|_{e^2} = & -\frac{\mu a_e^2 J_2}{2a^3} \left(\frac{3}{2} \sin^2 i - 1 - \frac{3}{2} e^2 + \frac{9}{4} e^2 \sin^2 i - \frac{3}{2} \sin^2 i \cos(2M + 2\omega) \right. \\ & + \frac{3}{4} e \sin^2 i \cos(M + 2\omega) - \frac{21}{4} e \sin^2 i \cos(3M + 2\omega) + \frac{9}{2} e \sin^2 i \cos M \\ & - 3e \cos M - \frac{51}{4} e^2 \sin^2 i \cos(4M + 2\omega) + \frac{15}{4} e^2 \sin^2 i \cos(2M + 2\omega) \\ & \left. - \frac{9}{2} e^2 \cos(2M) + \frac{27}{4} e^2 \sin^2 i \cos 2M + \mathcal{O}(e^3) \right) \end{aligned} \quad (4.91)$$

Finally, Kaula computes this disturbing function as:

$$V_{20} = -\frac{\mu J_2}{a} \left(\frac{a_e}{a} \right)^2 \sum_p F_{20p} \sum_q G_{2pq} \cos [(2 - 2p)\omega + (2 - 2p + q)M] \quad (4.92)$$

expression which, in principle, should be accurate up to fourth order in the eccentricity. Now all it's needed to do is compare the expressions (4.89), (4.91) and (4.92). As the error should be dependent on the eccentricity value, two values will be used, without varying the rest of the orbital elements. The scenarios are defined by the true osculating values defined in (4.38) but expressed in Keplerian elements and, for the second scenario, increasing the eccentricity on purpose. To summarize:

$$\text{Scenarios} \left\{ \begin{array}{l} a_1 = a_2 = 7091870 \text{ km} \quad e_1 = 0.0055, e_2 = 0.2 \quad i_1 = i_2 = 1.22196 \text{ rad} \\ \Omega_1 = \Omega_2 = 0.78547 \text{ rad} \quad \omega_1 = \omega_2 = 0.31583 \text{ rad} \quad M_1 = M_2 = 2.82233 \text{ rad} \end{array} \right. \quad (4.93)$$

The results for each scenario are shown in 4.2. As expected, error grows steeply with the eccentricity. There are some unexpected results though: the second-order approximation of Wiesel yields better results than the one from Kaula, which should be fourth-order accurate. The explanation for this may hide in the fact that Kaula suggests to just retain terms from $q = -2$ to $q = 2$, although a deeper analysis would be more clear. Nonetheless, and as further and more meaningful validations will be performed, this is in principle unnecessary.

Method	Scenario 1		Scenario 2	
Truth (R_2 , eq. (4.89))	$2.42307 \cdot 10^4$		$1.41322 \cdot 10^4$	
Wiesel ($R_2 _{e^2}$, eq. (4.91))	$2.42307 \cdot 10^4$	$\Delta = 6.1731 \cdot 10^{-3}$	$2.42307 \cdot 10^4$	$\Delta = 4.76257 \cdot 10^2$
Kaula (V_{20} , eq. (4.92))	$2.42308 \cdot 10^4$	$\Delta = 4.9176 \cdot 10^{-2}$	$1.58803 \cdot 10^4$	$\Delta = 1.74815 \cdot 10^3$

Table 4.2: Approximations of the J_2 term of the geopotential expansion.

4.4.4.3 High-Fidelity propagation vs. Kaula's LPEs.

It is important to keep in mind the target, which is the validation of the expressions of V_{lm} for a given set of l and m . It is necessary then to validate each and every combination of l and m , so as to make sure that the effect of every harmonic is successfully taken into account. For the propagation of Kaula's LPEs this is easily achieved by just particularizing said values of l and m into the general expression. Conversely, for the Hi-Fi propagation, this is done in a “cheeky” way, by selectively nullifying the coefficients of the C and S matrices, leaving the only non-zero coefficient at C_{lm} , S_{lm} .

However, in a first approximation to the validation, doing so against a regular J_2 model may be enough. Further validations can easily be performed, by simply selecting any other value for l and m .

The LPEs particularized for Kaula's functions will be first developed, after which an approximated integration will be performed. Finally, the actual results of the comparison for a certain set of cases will be shown.

I. Kaula's LPEs for V_{lmpq} .

As shown in Kaula [32] (p. 29, eq. 3.38-3.40), the Gauss Variational Equations can be written as:

$$\left\{ \begin{array}{l} \frac{da}{dt} = \frac{2}{na} \frac{\partial R}{\partial M} \\ \frac{de}{dt} = \frac{\eta^2}{na^2 e} \frac{\partial R}{\partial M} - \frac{\eta}{na^2 e} \frac{\partial R}{\partial e} \\ \frac{di}{dt} = \frac{\cos i}{na^2 \eta \sin i} \frac{\partial R}{\partial \omega} - \frac{1}{na^2 \eta \sin i} \frac{\partial R}{\partial \Omega} \\ \frac{d\Omega}{dt} = \frac{1}{na^2 \eta \sin i} \frac{\partial R}{\partial i} \\ \frac{d\omega}{dt} = -\frac{\cos i}{na^2 \eta \sin i} \frac{\partial R}{\partial i} + \frac{\eta}{na^2 e} \frac{\partial R}{\partial e} \\ \frac{dM}{dt} = n - \frac{\eta^2}{na^2 e} \frac{\partial R}{\partial e} - \frac{2}{na} \frac{\partial R}{\partial a} \end{array} \right. \quad (4.94)$$

These equations can be particularized for the case $R = V_{lmpq}$: that is, when the disturbing function is the effect of the contribution p, q of the harmonic l, m . Substituting relation (4.44) into (E.11) and rearranging terms:

$$\left\{ \begin{array}{l} \frac{da_{lmpq}}{dt} = \frac{2\mu a_e^l}{na^{l+2}} F_{lmp} G_{lpq} (l - 2p + q) \frac{dS_{lmpq}}{d\nu} \\ \frac{de_{lmpq}}{dt} = \frac{\mu a_e^l \eta}{na^{l+3} e} F_{lmp} G_{lpq} \frac{dS_{lmpq}}{d\nu} [(l - 2p + q) \eta - (l - 2p)] \\ \frac{di_{lmpq}}{dt} = \frac{\mu a_e^l}{na^{l+3} \eta \sin i} F_{lmp} G_{lpq} \frac{\partial S_{lmpq}}{\partial \nu} [(l - 2p) \cos i - m] \\ \frac{d\Omega_{lmpq}}{dt} = \frac{\mu a_e^l}{na^{l+3} \eta \sin i} G_{lpq} S_{lmpq} \frac{dF_{lmp}}{di} \\ \frac{d\omega_{lmpq}}{dt} = \frac{\mu a_e^l}{na^{l+3} \eta} S_{lmpq} \left(\frac{\eta^2}{e} F_{lmp} \frac{dG_{lpq}}{de} - \frac{\cos i}{\sin i} G_{lpq} \frac{dF_{lmp}}{di} \right) \\ \frac{dM_{lmpq}}{dt} = \frac{\mu a_e^l}{na^{l+3}} F_{lmp} S_{lmpq} \left[2(l + 1) G_{lpq} - \frac{\eta^2}{e} \frac{dG_{lpq}}{de} \right] \end{array} \right. \quad (4.95)$$

where the elements on the right-hand side of the equation are the mean OEs, calculated with the secular rates. This is of course an approximation, without which the solution cannot be obtained. Anyway, in order to calculate the variation of the orbital elements, it is necessary then to calculate the derivatives of F_{lmp} , G_{lpq} and S_{lmpq} :

I.A. Derivative of F_{lmp} .

The derivative of F_{lmp} is directly calculated from (4.48) as:

$$\frac{dF_{lmp}}{di} = \sum_t (l - m - 2t) C_t \cos^{l-m-2t-1}(i) \sum_s C_s \cos^s(i) \sum_c C_c - \sum_t C_t \sin^{l-m-2t}(i) \sum_s s C_s \sin^{s-1}(i) \sum_c C_c \quad (4.96)$$

This expression can be computed in an analogue manner to F_{lmp} .

I.B. Derivative of G_{lpq} .

Expression G_{lpq} is clearly a messy expression to differentiate. For the sake of simplicity, the derivatives will be taken on the polynomial expansions derived from the original expression, that is, for a

general G_{lpq} approximated by:

$$G_{lpq} = g_0 + g_1 e + g_2 e^2 + g_3 e^3 + g_4 e^4 + g_5 e^5 + \mathcal{O}(e^6)$$

its derivative is calculated as:

$$\frac{dG_{lpq}}{de} \approx g_1 + 2g_2 e + 3g_3 e^2 + 4g_4 e^3 + 5g_5 e^4 \quad (4.97)$$

I.C. Derivative of S_{lmpq} .

Finally, it is time to calculate the derivative of S_{lmpq} with respect to its argument ν . It can be easily calculated by differentiating (4.88) as:

$$\frac{dS_{lmpq}}{d\nu} = \begin{cases} -C_{lm} \sin \nu + S_{lm} \cos \nu & \text{if } \text{rem}(l - m, 2) = 0 \\ S_{lm} \sin \nu + C_{lm} \cos \nu & \text{if } \text{rem}(l - m, 2) \neq 0 \end{cases} \quad (4.98)$$

II. Effect of V_{lm} in the Keplerian OEs.

Up to now a closed-form for the variation of the orbital elements due to V_{lmpq} has been reached. The effect of the harmonic V_{lm} is just a double summation on p and q of the obtained derivatives $\frac{d}{dt}(a, e, i, \omega, \Omega, M)$ (4.95), that is:

$$\left\{ \begin{array}{lcl} \frac{da_{lm}}{dt} & = & \sum_{p=0}^l \sum_{q=-\infty}^{\infty} \frac{da_{lmpq}}{dt} \\ \frac{de_{lm}}{dt} & = & \sum_{p=0}^l \sum_{q=-\infty}^{\infty} \frac{de_{lmpq}}{dt} \\ \frac{di_{lm}}{dt} & = & \sum_{p=0}^l \sum_{q=-\infty}^{\infty} \frac{di_{lmpq}}{dt} \\ \frac{d\Omega_{lm}}{dt} & = & \sum_{p=0}^l \sum_{q=-\infty}^{\infty} \frac{d\Omega_{lmpq}}{dt} \\ \frac{d\omega_{lm}}{dt} & = & \sum_{p=0}^l \sum_{q=-\infty}^{\infty} \frac{d\omega_{lmpq}}{dt} \\ \frac{dM_{lm}}{dt} & = & n + \sum_{p=0}^l \sum_{q=-\infty}^{\infty} \frac{dM_{lmpq}}{dt} \end{array} \right. \quad (4.99)$$

III. Periodic effects.

Equation (4.95) can be integrated with respect to time. The variational equation of the semimajor axis equation is used as an example. As stated before, the mean elements are substituted in the right-hand side of the equation. As a first order approximation, those mean elements are calculated under a J_2 perturbed gravity field (through equation (4.39)).

Integrating (4.95) with respect to time leads to:

$$\begin{aligned} da_{lmpq} &= \frac{2\mu a_e^l}{na^{l+2}} F_{lmp} G_{lpq} (l - 2p + q) \frac{dS_{lmpq}}{d\nu} dt \\ \xrightarrow{\int} \Delta a_{lmpq} &= \frac{2\mu a_e^l}{na^{l+2}} F_{lmp} G_{lpq} (l - 2p + q) \int \left(\frac{d\nu}{dt} \right)^{-1} dS_{lmpq} \end{aligned} \quad (4.100)$$

The secular motions are known to be the dominant perturbation in most Earth satellites. That leads to the approximation that the rate of change of the phase angle ν is due mainly to the secular rates, that is:

$$\frac{d\nu}{dt} \approx (l - 2p)\dot{\omega}^{(s)} + (l - 2p + q)\dot{M}^{(s)} + m(\dot{\Omega}^{(s)} - \dot{\Theta}^{(s)}) \quad (4.101)$$

Substituting (4.101) into (4.100) and integrating dS_{lmpq} into S_{lmpq} yields:

$$\Delta a_{lmpq} = \frac{2\mu a_e^l}{na^{l+2}} \frac{F_{lmp} G_{lpq} (l - 2p + q) S_{lmpq}}{(l - 2p)\dot{\omega} + (l - 2p + q)\dot{M} + m(\dot{\Omega} - \dot{\Theta})} \quad (4.102)$$

where the superscript (s) has been dropped for simplicity. Proceeding in the same way with the rest of the equations lead to:

$$\left\{ \begin{array}{l} \Delta a_{lmpq} = \frac{2\mu a_e^l}{na^{l+2}} \frac{F_{lmp}G_{lpq}(l-2p+q)S_{lmpq}}{[(l-2p)\dot{\omega} + (l-2p+q)\dot{M} + m(\dot{\Omega} - \dot{\Theta})]} \\ \Delta e_{lmpq} = \frac{\mu a_e^l \eta}{na^{l+3}e} \frac{F_{lmp}G_{lpq}[(l-2p+q)\eta - (l-2p)]S_{lmpq}}{[(l-2p)\dot{\omega} + (l-2p+q)\dot{M} + m(\dot{\Omega} - \dot{\Theta})]} \\ \Delta i_{lmpq} = \frac{\mu a_e^l}{na^{l+3}\eta \sin i} \frac{F_{lmp}G_{lpq}S_{lmpq}[(l-2p)\cos i - m]}{[(l-2p)\dot{\omega} + (l-2p+q)\dot{M} + m(\dot{\Omega} - \dot{\Theta})]} \\ \Delta \Omega_{lmpq} = \frac{\mu a_e^l}{na^{l+3}\eta \sin i} \frac{G_{lpq}\bar{S}_{lmpq} \frac{dF_{lmp}}{di}}{[(l-2p)\dot{\omega} + (l-2p+q)\dot{M} + m(\dot{\Omega} - \dot{\Theta})]} \\ \Delta \omega_{lmpq} = \frac{\mu a_e^l}{na^{l+3}\eta} \frac{\bar{S}_{lmpq} \left(\frac{\eta^2}{e} F_{lmp} \frac{dG_{lpq}}{de} - \frac{\cos i}{\sin i} G_{lpq} \frac{dF_{lmp}}{di} \right)}{[(l-2p)\dot{\omega} + (l-2p+q)\dot{M} + m(\dot{\Omega} - \dot{\Theta})]} \\ \Delta M_{lmpq} = \frac{\mu a_e^l}{na^{l+3}} \frac{F_{lmp}\bar{S}_{lmpq} \left[2(l+1)G_{lpq} - \frac{\eta^2}{e} \frac{dG_{lpq}}{de} \right]}{[(l-2p)\dot{\omega} + (l-2p+q)\dot{M} + m(\dot{\Omega} - \dot{\Theta})]} \end{array} \right. \quad (4.103)$$

A quick look at the equations reveal two inconvenient cases:

- I. Secular terms: Their indices are such that the phase angle derivative is not defined (zero), and as that lies in the denominator, it makes the solution divergent. This is tackled in more detail in [32], section 3.6. and in [33], sections 4.4-4.6.
- II. Near equatorial or near circular orbits: If any of e or i is close to zero, the ascending node, argument of perigee and mean anomaly perturbations become absurdly large and meaningless. This concern will be approached later, in the conclusions

However, these equations, when summed up in p and q (for a given l and m) can be understood as the oscillating part of the osculating elements. That is, if one adds up the already computed mean elements with these contributions, the osculating elements are obtained. To establish a parallelism with Brouwer's theory, the contributions $\Delta \bullet_{lmpq}$ can be understood as the derivative of the generating function in some way: that is, the difference between the osculating and the mean elements expressed as a function of the latter. Mathematically, denoting just for this case the mean elements with an overline:

$$\xi = \bar{\xi} + \sum_{p,q}^{\text{periodic}} \Delta\xi_{lmpq}(\bar{a}, \bar{e}, \bar{i}, \bar{\Omega}, \bar{\omega}, \bar{M}, \bar{\Theta}) \quad (4.104)$$

where ξ denotes any of $a, e, i, \Omega, \omega, M$. Equation (4.104) is nothing but a linear mean to osculating transformation.

IV. Results: Kaula vs Brouwer-Lyddane and High-Fidelity.

Kaula's theory can be leveraged to derive a mean to osculating transformation, which can be used in a similar form to the one shown before in section 4.3.4.2. In this case, and in order to analyse the effect only of the mean to osculating transformation, the process is the following:

1st : Convert the osculating elements to mean through the Brouwer-Lyddane transformation.

2nd : Propagate the mean elements.

3rd : Calculate each of the contributions (*i.e.* $\Delta\xi_{lmpq}$) and add them up to the mean elements, getting hence the osculating.

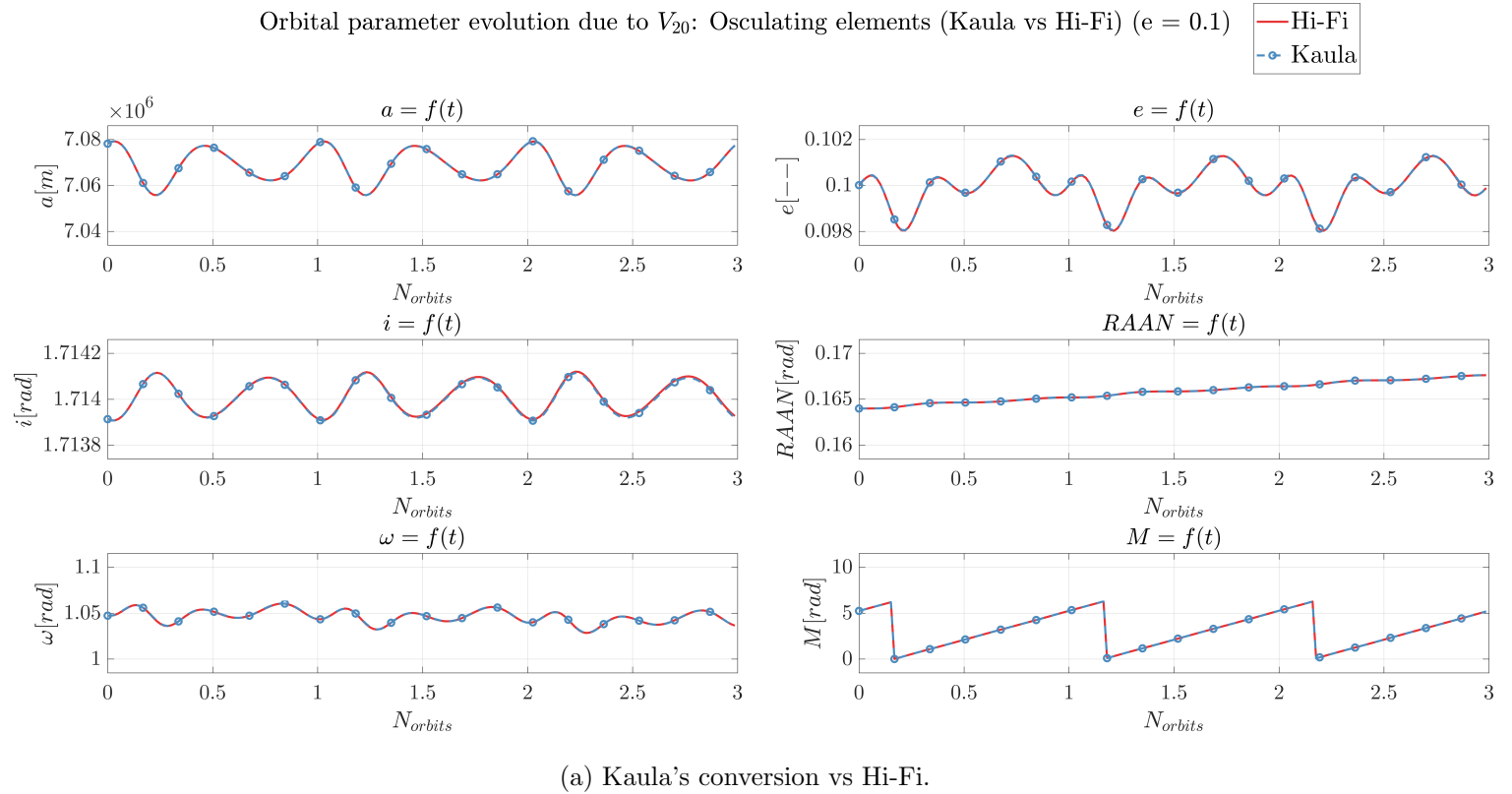
This conversion will be compared firstly against a High-Fidelity propagation of the same scenario, and afterwards, the deviation from truth will be compared with the one obtained through the Brouwer theory with Lyddane's modification. Three scenarios will be evaluated: one in which the eccentricity is not too low (so as to avoid the aforementioned singularity) and two with specially low eccentricity, in order to evaluate the effects of this situation. All of them are specified in 4.3:

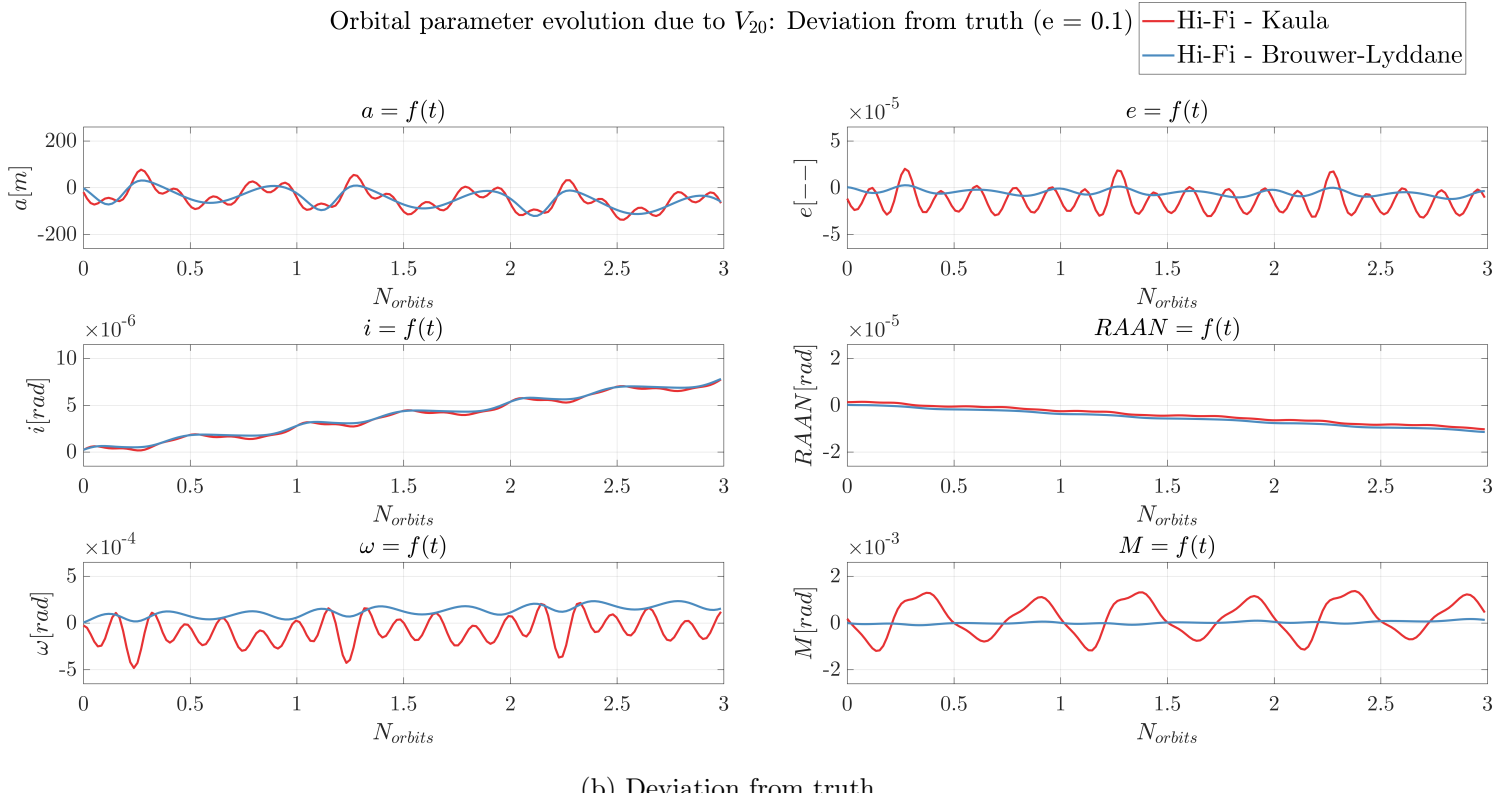
Scenario	a [m]	e [-]	i [rad]	Ω [rad]	ω [rad]	M [rad]
1 (elliptic)	7078135	0.1	1.7139	0.1640	1.0472	5.2377
2 (near-circular)	7078135	0.01	1.7139	0.1640	1.0472	5.2377
2 (near-circular)	7078135	0.001	1.7139	0.1640	1.0472	5.2377

Table 4.3: Scenarios for testing Kaula's theory.

IV.A. Scenario 1: $e = 0.1$.

Figure 4.6 shows a very tight correlation between Kaula's theory and the truth. The error is of the same order as the one obtained by Brouwer's theory (except for the mean anomaly), but in any case, it is always below an acceptable threshold (lower than 0.1%). Although more scenarios should be tested, the generality of this scenario (retrograde, eccentric, non-zero orbital elements) suggests that the theory works, at least for nonsingular cases.



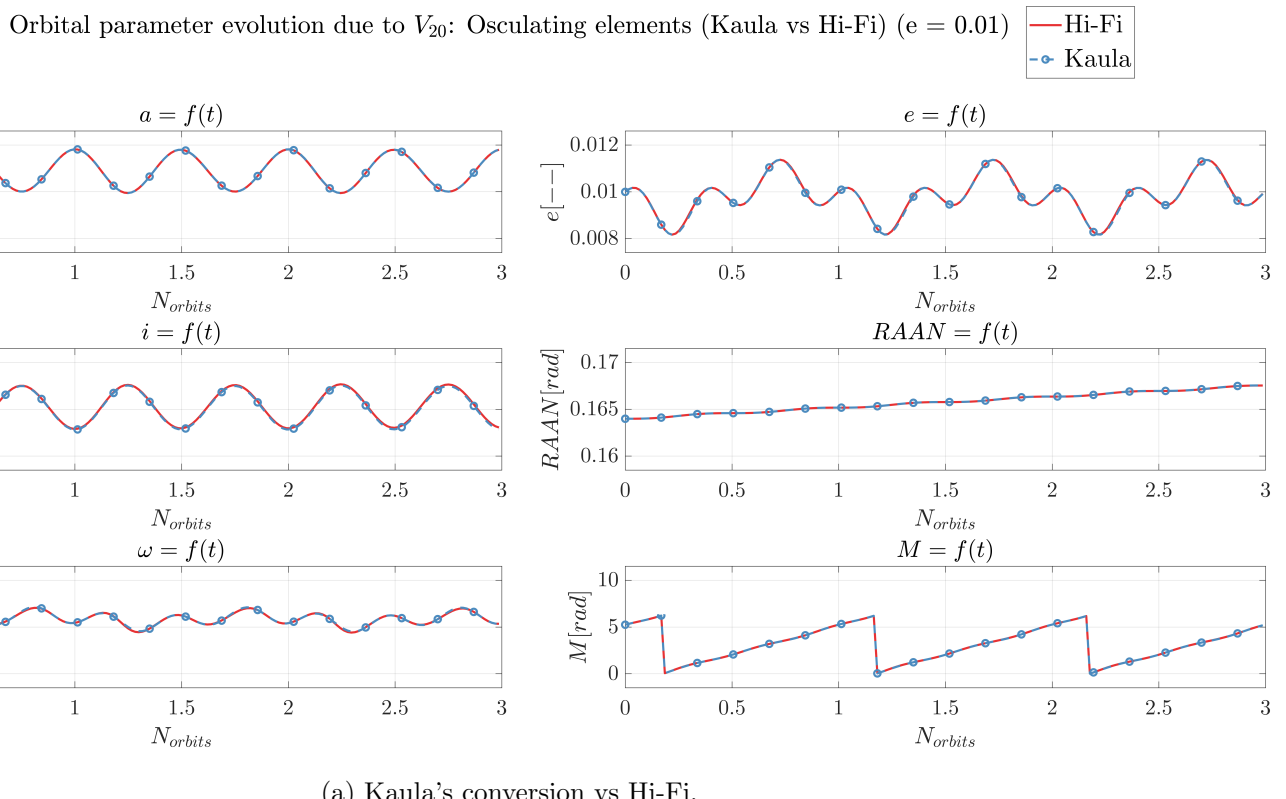


(b) Deviation from truth.

Figure 4.6: Results of Kaula's conversion for scenario 1 ($e = 0.1$).

IV.B. Scenario 2: $e = 0.01$.

However, the results for $e = 0.01$, shown in figure 4.7 are not as good. Error in mean anomaly and argument of perigee grow by at least one order of magnitude ($\approx 1\%$), and although it might be acceptable, it shows the nature of the behaviour of this model: low eccentricities make it inaccurate.



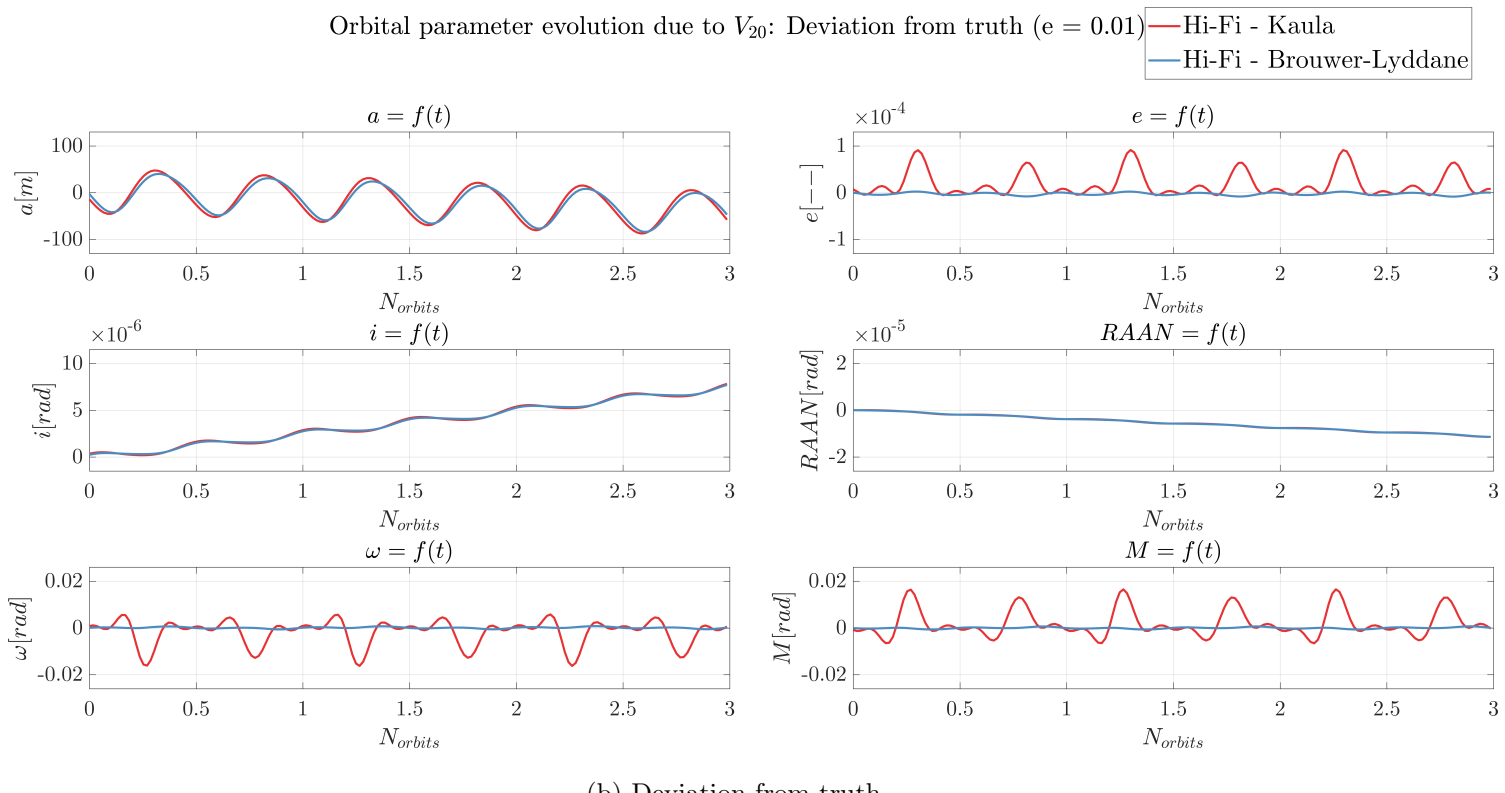
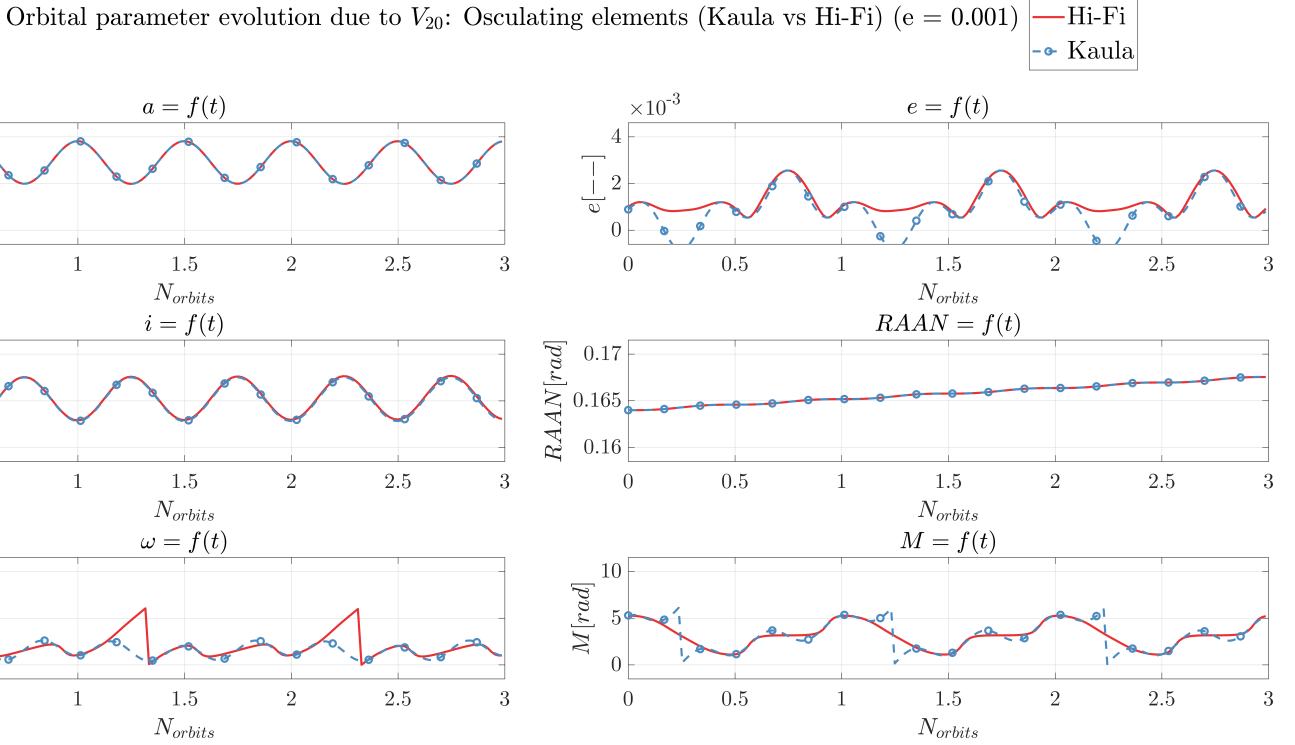


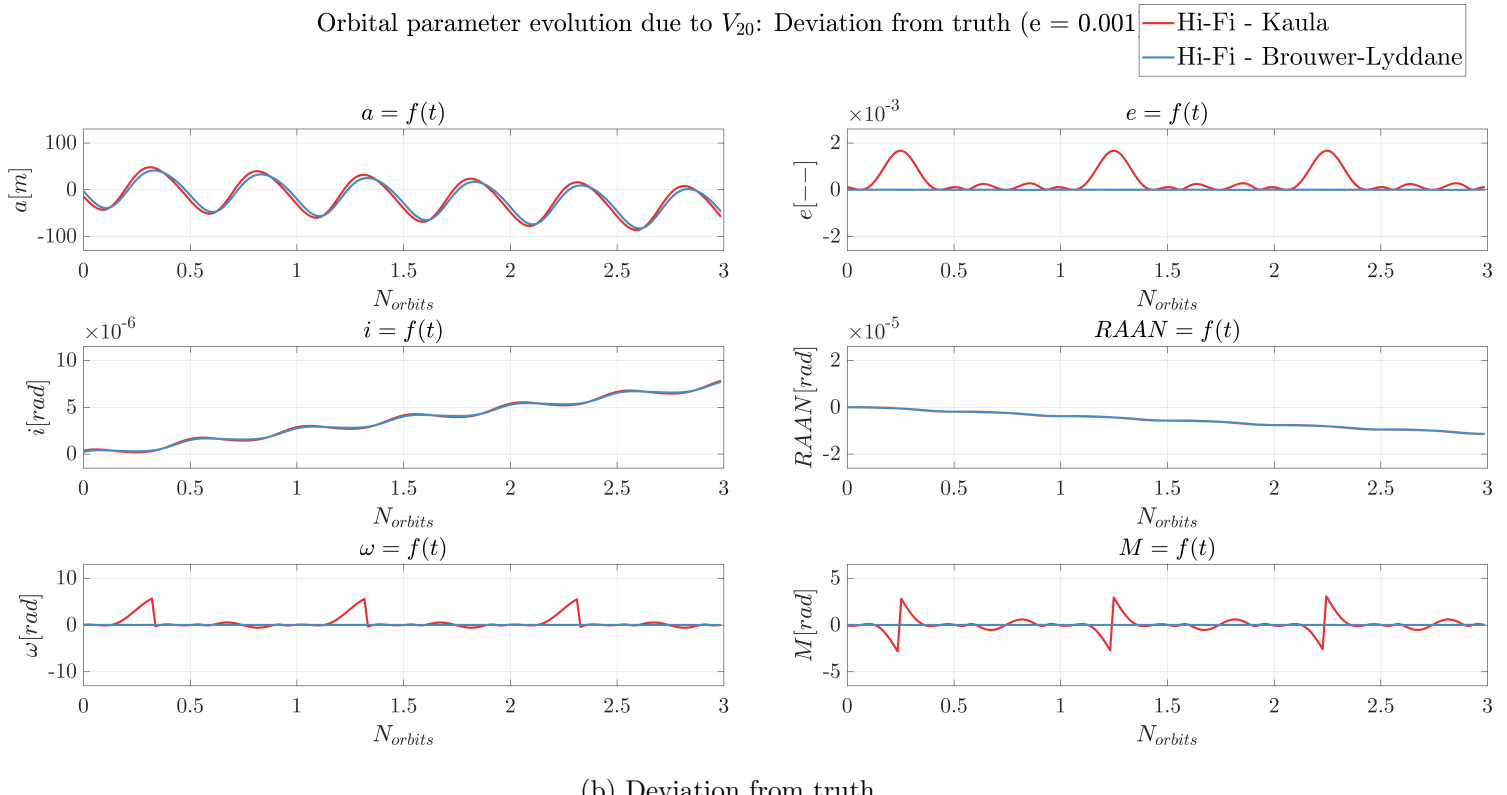
Figure 4.7: Results of Kaula's conversion for scenario 2 ($e = 0.01$).

IV.C. Scenario 3: $e = 0.001$

As it could be expected from the previous results, the scenario with the lowest eccentricity yields the worst results. It is the first time that it can be clearly seen in the first figure (4.8(a)), with huge deviations in eccentricity, argument of perigee and mean anomaly, which are unsurprisingly the ones that feature the inverse of the eccentricity in their oscillations. One remarkable defect is that eccentricity reaches negative values, which lacks any physical meaning whatsoever.



(a) Kaula's conversion vs Hi-Fi.



(b) Deviation from truth.

Figure 4.8: Results of Kaula's conversion for scenario 3 ($e = 0.001$).

4.4.4.4 Conclusions.

Kaula's theory has been validated, with the only setback of the singularities for null eccentricity or inclination. However, this should be somewhat easily tackled by the usage of nonsingular elements, such as Delaunay's or equinoctials. It seems like the functions G_{lpq} and F_{lmp} have no issue with this, so the source of this inconvenience is the inherent singularities of the Keplerian elements (through the LPEs).

Future work should then first focus on the implementation of a equinoctial form of the LPEs, to then move on to the usage of this transformation as a mean to construct a more accurate STM. This involves of course the inclusion of higher order harmonics, although that should not be any big issue.

Perturbed relative motion.

5.1 Introduction.

Once the perturbation theory and some relevant models have been discussed and validated, it is time to apply it to the main topic of the thesis. This chapter is devoted to perturbed relative motion, and in particular, linear formulations of it (*i.e.* STMs).

It is unsurprising how better dynamics models lead to more accurate results. Furthermore, when a linear model is implemented upon this type of theories, a warming balance between said increased accuracy and computational efficiency is obtained. When perturbation effects' modelling (specially the secular) is improved, two important by-products in the relative dynamics field are:

- I. Better guidance, which leads to a more fuel-efficient operation (less corrections).
- II. Enhanced understanding of the perturbations, allowing for more educated orbit design (*e.g.* safe orbits).

Firstly, a small introduction on the workflow of these orbit propagation methods is presented, to later show a particular example on the J_2 -perturbed Gim-Alfriend STM. Afterwards, a succinct research of the state-of-the-art STM formulations of relative motion is performed, and finally, a brief analysis of orbit safety in J_2 -perturbed orbits is carried out.

5.1.1 Relative orbit propagation in perturbed relative motion.

Generally, orbit propagation can be understood as a process in which, when feeding the initial state of one or more celestial bodies, it returns the updated state/s at a latter epoch. When dealing with the relative motion between two bodies, the initial states can be expressed in different ways: both in an absolute fashion (*i.e.* completely defined by itself) or the chief in absolute and the deputy in relative terms. The latter option is the most usual, as in relative motion, the relative state is the most meaningful.

These inputs are generally processed prior to its propagation, so as to have them in a favourable phase space. This is particularly true for perturbed orbits, as some element descriptions greatly simplify the computation. Once propagated, a back-transformation must be made, in order to return to the same structure as that of the inputs. However, the output might only be the relative state, not including the reference orbit.

The variety of how these processes may be expressed, with different and a greater or lower number of transformations, makes it impossible to go any further in general terms. Sullivan [18] provides a good example on this. Nonetheless, in order to have an insight on an example, an orbit propagation diagram is shown in 5.1 for the process followed as in this thesis. Additionally, the sub-processes of converting to and from mean elements is specified in 5.2.

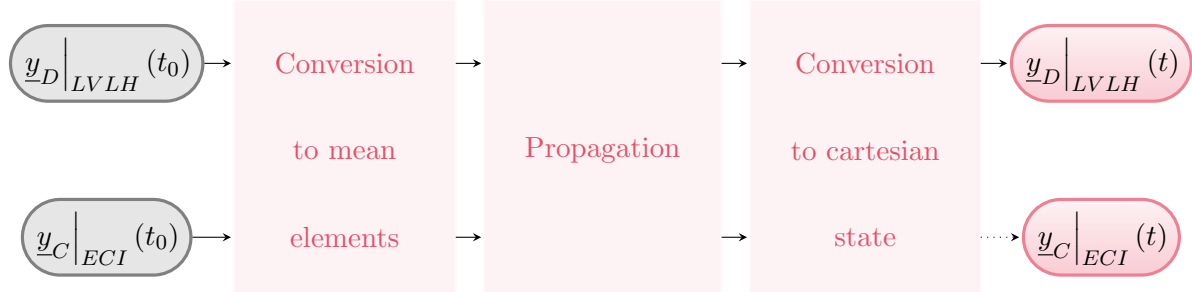


Figure 5.1: Workflow of mean element propagation from and to cartesian states.

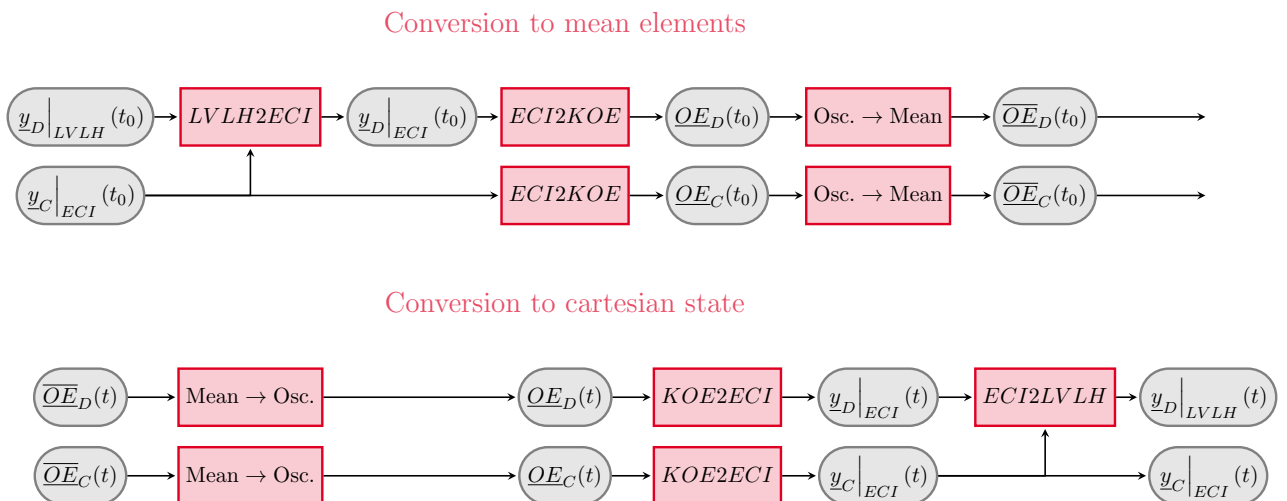


Figure 5.2: Workflows of the conversions from cartesian states to mean elements and vice versa.

5.2 Gim-Alfriend STM.

5.2.1 Gim-Alfriend STM structure.

Gim and Alfriend [5] came up with a precise analytic solution for the relative motion in elliptic and perturbed orbits, accounting specifically for the differential effect of the equatorial bulge J_2 . It is a STM-oriented method, performing some clever transformations to the mean element space.

The approach of the authors is to map the LVLH state vector (which is the physical magnitude of interest) into the relative osculating element space δOE . This is then mapped into the mean orbital element space $\delta\overline{\text{OE}}$, after which it is propagated and brought back to a cartesian state. Each of the aforementioned transformations is presented next:

1st LVLH to δOE : Gim and Alfriend make use of the so-called Geometric Method, which is represented by:

$$\underline{y}_{LVLH}(t) = [A(t) + \alpha B(t)] \delta\text{OE} \equiv \Sigma(t) \delta\text{OE} \quad (5.1)$$

This mapping effectively separates the effects of δOE in two parts: the ones caused by the pure difference in orbital elements, however they may vary (through the matrix $A(t)$) and the effects caused by the J_2 perturbation (through $\alpha B(t)$). The first matrix is exactly the same in the unperturbed case, though the second one obviously vanishes. Their expressions can be found in [5], appendices A and B. With this mapping, the STM can be formulated as:

$$\phi_{J2}(t, t_0) = \Sigma(t) \phi_e(t, t_0) (\Sigma(t_0))^{-1} \iff \underline{y}_{LVLH}(t) = \phi_{J2}(t, t_0) \underline{y}_{LVLH}(t_0) \quad (5.2)$$

2nd δOE to $\delta\overline{\text{OE}}$ (osculating to mean): Equation (5.2) involves the direct propagation of relative osculating OEs, which turns out to lead to a very much complicated form of the matrix ϕ_e . This is where Brouwer's theory comes into play: the authors suggest a mapping to and from mean elements as:

$$\delta\text{OE}_{osc} = D(t) \delta\text{OE}_{mean} \Leftrightarrow \delta\text{OE} = D(t) \delta\overline{\text{OE}} \quad (5.3)$$

The mean elements are from now on referred to either through an overline or the subindex *mean*, if extra clarity is required. This leads to the following decomposition of ϕ_e :

$$\phi_e(t, t_0) = D(t) \overline{\phi}_e(t, t_0) D^{-1}(t_0) \quad (5.4)$$

So that the final form of the state transition matrix becomes:

$$\phi_{J2}(t, t_0) = \Sigma(t)D(t)\bar{\phi}_e(t, t_0)D^{-1}(t_0)\Sigma(t_0) \quad (5.5)$$

Although the structure of the matrix and the geometric method are quite interesting topics, the spotlight is now on the $D(t)$ matrix, and how it relates to the previously introduced Brouwer's theory.

5.2.2 Linearised mean to osculating transformation.

The matrix D is the linearised form of a mean to osculating transformation. Mathematically:

$$D = \frac{\partial \underline{OE}_{osc}}{\partial \underline{OE}_{mean}} \quad (5.6)$$

The osculating elements are by definition the addition of the mean elements plus the periodic oscillations, that is:

$$\underline{OE} = \overline{\underline{OE}} + \Delta \underline{OE}^{(p)} \quad (5.7)$$

Lie theorem provides the following expression for the oscillations $\Delta \underline{OE}^{(p)}$:

$$\Delta \underline{OE}^{(p)} = \varepsilon [\underline{OE}, W] \quad (5.8)$$

where $\varepsilon = -J_2 a_e^2$ is the small parameter, and W is the generating function of the mean to osculating elements transformation. This generating function can be decomposed into three components, each linked to one of the subsequent transformations that get rid of the short and long-period oscillations. Mathematically:

$$W = W^{(sp1)} + W^{(sp2)} + W^{(lp)} \quad (5.9)$$

It is important to note that $W = W_1$ is the first order component of the full generating function. If (5.9) is substituted into (5.8), a similar separation comes up:

$$\Delta \underline{OE}^{(p)} = \Delta \underline{OE}^{(sp1)} + \Delta \underline{OE}^{(sp2)} + \Delta \underline{OE}^{(lp)} \quad (5.10)$$

where $\Delta \underline{OE}_i = \varepsilon[\underline{OE}, W^{(i)}]$. If this is now introduced into the D matrix definition (5.6), it follows that:

$$\begin{aligned} D &= \frac{\partial}{\partial \underline{OE}} \left(\underline{OE} + \Delta \underline{OE}^{(sp1)} + \Delta \underline{OE}^{(sp2)} + \Delta \underline{OE}^{(lp)} \right) = \\ &= \mathbb{I}_{6x6} + \varepsilon \left(\frac{\partial [\underline{OE}, W^{(sp1)}]}{\partial \underline{OE}} + \frac{\partial [\underline{OE}, W^{(sp2)}]}{\partial \underline{OE}} + \frac{\partial [\underline{OE}, W^{(lp)}]}{\partial \underline{OE}} \right) \\ \Rightarrow D &= \mathbb{I}_{6x6} - J_2 a_e^2 \left(D^{(sp1)} + D^{(sp2)} + D^{(lp)} \right) \end{aligned} \quad (5.11)$$

A particularity from this article is that quasi-nonsingular elements are used. However, the expressions for the oscillations (*i.e.* $\delta \underline{OE}^{(i)}$) and the D matrices (*i.e.* $D^{(i)}$) are provided. The former were carefully implemented, though the latter are numerically calculated, due to its uncomfortably long expressions.

To summarize, Gim and Alfriend provide a new approach on J_2 -perturbed, non-circular orbit linear propagation. They do so through two essential steps:

- I.** A new proposal (*i.e.* the geometric method) to map relative, quasi-non-singular elements into relative cartesian curvilinear coordinates.
- II.** The implementation of a mean to osculating transformation (*i.e.* Lyddane's modification of Brouwer's theory) to propagate mean elements rather than osculating.

5.2.3 Inverse transformation.

Gim and Alfriend do not tackle the osculating to mean transformation explicitly. Brouwer's theory, due to its first-order truncation nature, can be “inverted” by simply switching the sign of the small parameter. Nonetheless, there is also a more general method that allows for performing a osculating to mean transformation by only having the direct one (*i.e.* mean to osc.). This is done through an iterative numeric scheme, which is next outlined:

Input: Osculating elements.

1st : Initialize the mean elements with the osculating.

2nd : Compute the oscillations ($\Delta \underline{OE}^{(lp)}, \Delta \underline{OE}^{(sp1)}, \Delta \underline{OE}^{(sp2)}$) with the approximation of the mean elements.

3rd : Compute the new mean elements by subtracting the oscillations from the osculating.

4th : Convergence evaluation: If the variation between the last and the current iteration is below the threshold, stop iterating. Come back to the second step otherwise, with the updated mean element estimation.

The approximation herewith presented can be mathematically described as:

$$\left\{ \begin{array}{ll} \text{Direct: } & \underline{OE} = \overline{\underline{OE}} + \Delta\underline{OE}^{(p)}(\overline{\underline{OE}}) \Rightarrow \underline{OE} = f(\overline{\underline{OE}}) \\ \text{Inverse: } & \overline{\underline{OE}} = \underline{OE} - \Delta\underline{OE}^{(p)}(\underline{OE}) \approx \underline{OE} - \Delta\underline{OE}^{(p)}(\overline{\underline{OE}}) \Rightarrow \overline{\underline{OE}} = f^{-1}(\underline{OE}) \end{array} \right. \quad (5.12)$$

where the actual approximation is assuming that the periodic contributions $\Delta\underline{OE}$ are approximately equal when calculated using the osculating elements. Of course, as more iteration cycles are performed, the accuracy of this approach rises.

In this way, there is no need for developing the inverse transformation. The main setback is that no exact result is obtained, and that the computational cost becomes greater. A simple diagram of the outlined workflow is shown in 5.3.

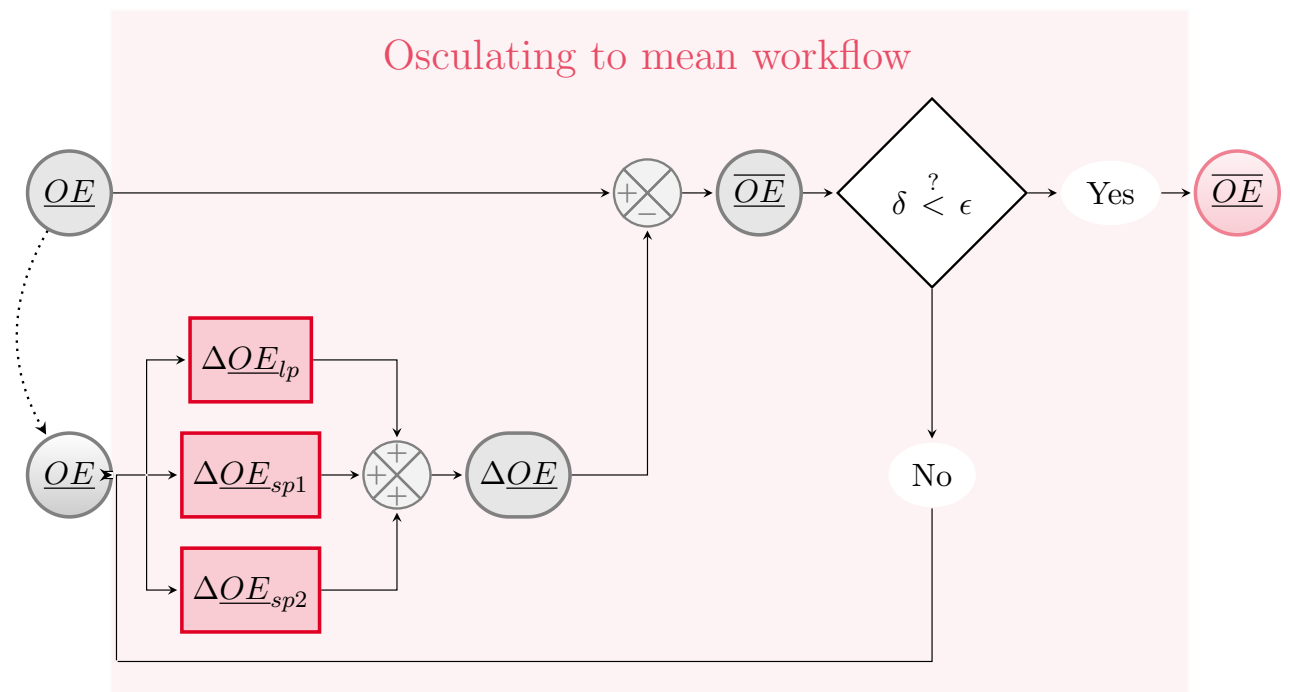


Figure 5.3: Workflow of iterative osculating-to-mean transformation.

5.3 State-of-the art perturbed STMs.

Although an in-depth analysis of this methods lies out of the scope of the thesis, it is nonetheless insightful to draft a quick survey of the state-of-the-art methods for perturbed STMs. A very useful

and well-structured classification of the historic and recent STMs is done by Sullivan et al. [18], yielding a very good outlook on how this field is structured. Going from unperturbed to perturbed and from circular to non-circular orbits, it also provides some very interesting results when comparing the models to a set truth model.

The considered perturbed models are the following:

- I. Gim-Alfriend STM: Already described. As it proposes two important changes (the geometric method and the mean elements propagation), two versions of it may be considered, so as to isolate the effect of the coordinate transformations. The first one uses the full STM provided by Gim and Alfriend, while the second one just uses the relative orbital element differences propagation (*i.e.* $\bar{\phi}_e(t, t_0)$) and makes use of the full non-linear Brouwer transformation for the mean-osculating transformations, and a regular transformation between osculating elements and LVLH frame. This one is referred to as the Gim-Alfriend core method.
- II. Yan-Alfriend STM: In an alternative approach, Yan and Alfriend [35] propose an expansion of the mean orbital element differences up to second-order, leading to a nonlinear model including second-order J_2 effects.
- III. GAM STM: Developed by Gaias et al. [36], it includes a time-varying differential drag as well as the J_2 effect for a more accurate relative motion model. The main setback is the assumption of near-circular reference orbits, which restricts this theory to a limited amount of scenarios
- IV. KGD STM: Constructed by Koenig et al. [37], it uses Floquet theory to arrive to a compact STM. It is developed for several types of OEs (singular, quasi-nonsingular and fully nonsingular) and can be generalized so as to incorporate any type of perturbations.
- V. Biria-Russell STM: Biria and Russell chose to incorporate Vinti's theory rather than Brouwer's, which through the usage of spheroidal coordinates allows for a simpler, more precise formulation. This theory is claimed (and proven) to provide a higher accuracy than Brouwer's.

These five models are compared against each other and a High-fidelity propagation with a full-force model (120x120 gravity field, atmospheric drag, SRP, Sun and Moon, relativistic and tidal effects) for three different scenarios. Depending on which scenario is considered, the supposedly best method changes, which leads to the conclusion that for each application there might be a different best method. In any case, for a small distance between the spacacrafts (*i.e.* small linearization error) all methods converge to an error of the same order. A more thorough analysis can be seen in the mentioned survey

[18], as well as a computational cost study.

A reference worth reading is Chihabi's approach to building an orbital element based STM [26]. It progressively specifies how to include some perturbations, including a NSG model of up to J_5 , third bodies and drag. Not only is it a thorough, complete reference, but also provides some compelling results.

5.4 Orbit safety in perturbed motion.

Finally, and in an analogue manner as done in chapters 2 and 3, a brief description of orbit safety in perturbed orbits is presented. Its roots are on the theory developed by D'Amico and Montenbruck [15], shown in chapter 2, thus being restricted to near-circular orbits.

The analysis of perturbations is usually eased by the utilisation of orbital elements, although in relative motion, the final motive or the sought variables are the relative cartesian position and velocity. For this purpose, the equivalence between the cartesian and the OE based formulation is first analyzed, as done by D'Amico [38], who is inspired by Eckstein's approach for the collocation of geostationary satellites [13]. After that, a short qualitative analysis on the effects of a non-spherical gravity field on relative OEs is performed, and finally, some applications of this approach are discussed.

5.4.1 Equivalence of cartesian coordinates and relative OEs.

5.4.1.1 Cartesian formulation: HCW equations.

D'Amico proposes a nondimensionalization of the Hill equations in RTN frame B.4.1. The relative position vector of the deputy in said frame is expressed as:

$$\delta\underline{r} = \underline{r}_D - \underline{r}_C = \delta r_R \underline{e}_R + \delta r_T \underline{e}_T + \delta r_N \underline{e}_N$$

This vector can be nondimensionalized with the chief's orbital radius r –which under the assumption of a circular reference orbit is constant and equal to the semimajor axis a . Effectively:

$$\underline{\rho} = \frac{\delta\underline{r}}{r} = \{x, y, z\}^T \quad (5.14)$$

Time can as well be nondimensionalized with the mean anomaly rate n as:

$$\frac{d}{d\tau} = \frac{1}{n} \frac{d}{dt} \quad (5.15)$$

The nondimensional version of Hill equations can be simply derived from (2.13), changing from the LVLH to the RTN frame and considering (5.14) and (5.15):

$$\begin{Bmatrix} \ddot{x} \\ \ddot{y} \\ \ddot{z} \end{Bmatrix} = \begin{Bmatrix} 2\dot{y} + 3x \\ -2\dot{x} \\ -z \end{Bmatrix} \quad (5.16)$$

where \dot{x}_i denotes the time derivative of x_i with respect to τ . D'Amico proposes an equivalent form to the Clohessy-Wiltshire solution, although with different integration constants, as:

$$\begin{Bmatrix} x \\ y \\ z \\ \dot{x} \\ \dot{y} \\ \dot{z} \end{Bmatrix} = \begin{bmatrix} 1 & 0 & -\cos \tau & -\sin \tau & 0 & 0 \\ -\frac{3}{2}(\tau - \tau_0) & 1 & 2\sin \tau & -2\cos \tau & 0 & 0 \\ 0 & 0 & 0 & 0 & \sin \tau & -\cos \tau \\ 0 & 0 & \sin \tau & -\cos \tau & 0 & 0 \\ -\frac{3}{2} & 0 & 2\cos \tau & 2\sin \tau & 0 & 0 \\ 0 & 0 & 0 & 0 & \cos \tau & \sin \tau \end{bmatrix} \begin{Bmatrix} a_1 \\ a_2 \\ a_3 \\ a_4 \\ a_5 \\ a_6 \end{Bmatrix} \quad (5.17)$$

The integration constants $(a_1, a_2, a_3, a_4, a_5, a_6)$ are related to the initial state vector $(x_0, y_0, z_0, \dot{x}_0, \dot{y}_0, \dot{z}_0)$ by:

$$\begin{Bmatrix} a_1 \\ a_2 \\ a_3 \\ a_4 \\ a_5 \\ a_6 \end{Bmatrix} = \begin{Bmatrix} 4x_0 + 2\dot{y}_0 \\ y_0 - 2\dot{x}_0 \\ 3x_0 + 2\dot{y}_0 \\ -\dot{x}_0 \\ \dot{z}_0 \\ -z_0 \end{Bmatrix} \quad (5.18)$$

The meaning of this integration constants will be duly explained later.

5.4.1.2 Relative OE formulation: GVEs.

Near-circular orbits feature an uncomfortable singularity, in that the argument of perigee is not defined. In order to avoid this, the quasi-non-singular element set (see A.2.2.3) is used.

Gauss Variational Equations (see E.2.2) express the evolution of the orbital elements as a function of the acceleration on the celestial body or spacecraft. That acceleration is now nondimensionalized as:

$$\underline{a} = \frac{r^2}{\mu} \underline{A} \quad (5.19)$$

where \underline{A} is the dimensional counterpart. With this in mind, and after some manipulation, the GVEs for the circular, non-equatorial case are:

$$\left\{ \begin{array}{l} \dot{a} \\ \dot{\lambda} \\ \dot{e}_x \\ \dot{e}_y \\ \dot{i} \\ \dot{\Omega} \end{array} \right\} = \left[\begin{array}{cccccc} 0 & 0 & 2a & 0 \\ 1 & -2 & 0 & -\sin \tau / \tan i \\ 0 & \sin \tau & 2 \cos \tau & 0 \\ 0 & -\cos \tau & 2 \sin \tau & 0 \\ 0 & 0 & 0 & \cos \tau \\ 0 & 0 & 0 & \sin \tau / \sin i \end{array} \right] \left\{ \begin{array}{l} 1 \\ a_R \\ a_T \\ a_N \end{array} \right\} \quad (5.20)$$

These equations can actually be integrated in both sides with respect to time, assuming an instantaneous velocity increment. Conceptually, this can be understood as the deviation of the deputy's orbital elements with respect to the chaser's due to a difference in velocity. Effectively:

$$\left\{ \begin{array}{l} \delta a/a \\ \delta \lambda \\ \delta e_x \\ \delta e_y \\ \delta i \\ \delta \Omega \end{array} \right\} = \left[\begin{array}{cccccc} 0 & 2a & 0 \\ -2 & 0 & -\sin \tau_0 / \tan i \\ \sin \tau_0 & 2 \cos \tau_0 & 0 \\ -\cos \tau_0 & 2 \sin \tau_0 & 0 \\ 0 & 0 & \cos \tau_0 \\ 0 & 0 & \sin \tau_0 / \sin i \end{array} \right] \left\{ \begin{array}{l} \delta v_R \\ \delta v_T \\ \delta v_N \end{array} \right\} \quad (5.21)$$

Finally, this equations can be transformed to use the eccentricity/inclination vectors element set, which has proven to be useful for trajectory safety purposes. By simply remembering the inclination vector definition:

$$\left\{ \begin{array}{l} \delta a/a \\ \delta \lambda \\ \delta e_x \\ \delta e_y \\ \delta i_x \\ \delta i_y \end{array} \right\} = \left[\begin{array}{cccccc} 0 & 2 & 0 \\ -2 & 0 & -\sin \tau_0 / \tan i \\ \sin \tau_0 & 2 \cos \tau_0 & 0 \\ -\cos \tau_0 & 2 \sin \tau_0 & 0 \\ 0 & 0 & \cos \tau_0 \\ 0 & 0 & \sin \tau_0 \end{array} \right] \left\{ \begin{array}{l} \delta v_R \\ \delta v_T \\ \delta v_N \end{array} \right\} \quad (5.22)$$

5.4.1.3 Equivalence.

Equation (5.17) can be inverted, hence expressing the integration constants in terms of the RTN state vector. If both spacecrafnts are assumed to be at the same position at $t = t_0$ (hence $\rho_0 = 0$), it reduces to:

$$\begin{Bmatrix} a_1 \\ a_2 \\ a_3 \\ a_4 \\ a_5 \\ a_6 \end{Bmatrix} = \begin{bmatrix} 0 & 2a & 0 \\ -2 & 0 & \\ \sin \tau & 2 \cos \tau & 0 \\ -\cos \tau & 2 \sin \tau & 0 \\ 0 & 0 & \cos \tau \\ 0 & 0 & \sin \tau \end{bmatrix} \begin{Bmatrix} \delta \dot{x}_0 \\ \delta \dot{y}_0 \\ \delta \dot{z}_0 \end{Bmatrix} \quad (5.23)$$

Equations (5.22) and (5.23) are clearly similar. This suggests the use of the integration constants a_i as dimensionless relative orbital elements, related to the E/I element set as:

$$\begin{cases} a_1 = \frac{a_D - a_C}{a} & = \frac{\delta a}{a} \\ a_2 = \lambda_D(\tau_0) - \lambda_C(\tau_0) + (\Omega_D - \Omega_C) \cos i & = \delta \lambda_0 + \delta \Omega \cos i \equiv \delta l_0 \\ a_3 = e_{x,D} - e_{x,C} & = \delta e_x \\ a_4 = e_{y,D} - e_{y,C} & = \delta e_y \\ a_5 = i_D - i_C & = \delta i_x \\ a_6 = (\Omega_D - \Omega_C) \sin i & = \delta i_y \end{cases} \quad (5.24)$$

The only different orbital element is the so-called modified relative mean longitude δl_0 .

5.4.1.4 Conclusion: HCW solution in terms of orbital elements.

Once the mapping between the integration constants a_i and the relative OEs has been established, equation (5.17) can be expressed in those terms as:

$$\begin{Bmatrix} x \\ y \\ z \\ \dot{x} \\ \dot{y} \\ \dot{z} \end{Bmatrix} = \begin{bmatrix} 1 & 0 & -\cos \tau & -\sin \tau & 0 & 0 \\ -\frac{3}{2}(\tau - \tau_0) & 1 & 2 \sin \tau & -2 \cos \tau & 0 & 0 \\ 0 & 0 & 0 & 0 & \sin \tau & -\cos \tau \\ 0 & 0 & \sin \tau & -\cos \tau & 0 & 0 \\ -\frac{3}{2} & 0 & 2 \cos \tau & 2 \sin \tau & 0 & 0 \\ 0 & 0 & 0 & 0 & \cos \tau & \sin \tau \end{bmatrix} \begin{Bmatrix} \delta a/a \\ \delta l_0 \\ \delta e_x \\ \delta e_y \\ \delta i_x \\ \delta i_y \end{Bmatrix} \quad (5.25)$$

The dimensional form of (5.25) is very widely used in orbit safety analysis. It is obtained after using the relations (5.14) and (5.15), leading to:

$$\left\{ \begin{array}{l} \frac{\delta r_R}{a} = \frac{\delta a}{a} - \delta e_x \cos \lambda - \delta e_y \sin \lambda \\ \frac{\delta r_T}{a} = \delta l_0 - \frac{3}{2} \frac{\delta a}{a} (\lambda - \lambda_0) - 2\delta e_y \cos \lambda + \delta e_x \sin \lambda \\ \frac{\delta r_N}{a} = -\delta i_y \cos \lambda + \delta i_x \sin \lambda \end{array} \right. \quad (5.26)$$

where τ has been substituted by λ , as:

$$\tau - \tau_0 = \int d\tau = \int n dt = \lambda - \lambda_0 - (\omega - \omega_0) = \lambda - \lambda_0$$

Equation (5.26) can be simplified for the case of non-drifting ($\delta a = 0$) centered (δl_0) relative orbits, leading to:

$$\left\{ \begin{array}{l} \frac{\delta r_R}{a} = -a\delta e \cos(\lambda - \varphi) \\ \frac{\delta r_T}{a} = 2a\delta e \sin(\lambda - \varphi) \\ \frac{\delta r_N}{a} = a\delta i \sin(\lambda - \psi) \end{array} \right. \quad (5.27)$$

where:

$$\delta e = \sqrt{\delta e_x^2 + \delta e_y^2} \quad \delta i = \sqrt{\delta i_x^2 + \delta i_y^2}$$

$$\varphi = \text{atan2}(\delta e_y, \delta e_x) \quad \psi = \text{atan2}(\delta i_y, \delta i_x)$$

are the amplitudes and phases of the in-plane and out-of-plane motion. These equations were already reached in (2.57), though in a less formal way.

The current formulation allows to easily implement any perturbation on the orbital elements, in order to then obtain the effect on the actual RTN coordinates. A small introduction about how to do so with the J_2 term is now discussed.

5.4.2 Effect of non-spherical gravity field: J_2 .

As discussed extensively before, perturbations induces two basic types of effects in spacecraft's motion: secular and periodic. Short-period effects are mainly dependent on the argument of latitude, which means that, for short baselines (δl_0), said effects can be neglected. Hence, only the secular effects will be considered.

The secular variations of the Keplerian elements is expressed as [5]:

$$\left\{ \begin{array}{l} \frac{da^{(s)}}{dt} = 0 \\ \frac{de^{(s)}}{dt} = 0 \\ \frac{di^{(s)}}{dt} = 0 \end{array} \right. \quad (5.28a)$$

$$\left\{ \begin{array}{l} \frac{d\Omega^{(s)}}{dt} = -\frac{\alpha}{2} \frac{n_0}{a_0^2 \eta_0^4} \cos i_0 \\ \frac{d\omega^{(s)}}{dt} = \frac{\alpha}{4} \frac{n_0}{a_0^2 \eta_0^4} (5 \cos^2 i_0 - 1) \end{array} \right. \quad (5.28b)$$

$$\left\{ \begin{array}{l} \frac{dM^{(s)}}{dt} = n_0 + \frac{\alpha}{4} \frac{n_0}{a_0^2 \eta_0^3} (3 \cos^2 i_0 - 1) \end{array} \right. \quad (5.28c)$$

$$\left\{ \begin{array}{l} \dot{a}^{(s)} = 0 \\ \dot{e}^{(s)} = 0 \\ \dot{i}^{(s)} = 0 \end{array} \right. \quad (5.29a)$$

$$\left\{ \begin{array}{l} \dot{\Omega}^{(s)} = -\frac{\alpha}{2} \frac{1}{a_0^2 \eta_0^4} \cos i_0 \\ \dot{\omega}^{(s)} = \frac{\alpha}{4} \frac{1}{a_0^2 \eta_0^4} (5 \cos^2 i_0 - 1) \end{array} \right. \quad (5.29b)$$

$$\left\{ \begin{array}{l} \dot{M}^{(s)} = 1 + \frac{\alpha}{4} \frac{1}{a_0^2 \eta_0^3} (3 \cos^2 i_0 - 1) \end{array} \right. \quad (5.29c)$$

$$\left\{ \begin{array}{l} \dot{a}^{(s)} = 0 \\ \dot{e}^{(s)} = 0 \\ \dot{i}^{(s)} = 0 \end{array} \right. \quad (5.29d)$$

$$\left\{ \begin{array}{l} \dot{\Omega}^{(s)} = -\frac{\alpha}{2} \frac{1}{a_0^2 \eta_0^4} \cos i_0 \\ \dot{\omega}^{(s)} = \frac{\alpha}{4} \frac{1}{a_0^2 \eta_0^4} (5 \cos^2 i_0 - 1) \end{array} \right. \quad (5.29e)$$

$$\left\{ \begin{array}{l} \dot{M}^{(s)} = 1 + \frac{\alpha}{4} \frac{1}{a_0^2 \eta_0^3} (3 \cos^2 i_0 - 1) \end{array} \right. \quad (5.29f)$$

The relative growth of the deputy with respect to the chief in E/I elements can be simply obtained by its definition:

$$\left. \begin{array}{l} \delta\dot{a}^{(s)} = \dot{a}_D^{(s)} - \dot{a}_C^{(s)} \\ \delta\dot{l}_0^{(s)} = \left[\left(\dot{\lambda}_0 \right)_D^{(s)} - \left(\dot{\lambda}_0 \right)_C^{(s)} \right] + \frac{d}{d\tau} \left[\left(\Omega_D^{(s)} - \Omega_C^{(s)} \right) \cos i \right] \\ \delta\dot{e}_x^{(s)} = \left(\dot{e}_x \right)_D^{(s)} - \left(\dot{e}_x \right)_C^{(s)} \\ \delta\dot{e}_y^{(s)} = \left(\dot{e}_y \right)_D^{(s)} - \left(\dot{e}_y \right)_C^{(s)} \\ \delta\dot{i}_x^{(s)} = \dot{i}_D^{(s)} - \dot{i}_C^{(s)} \\ \delta\dot{i}_y^{(s)} = \frac{d}{d\tau} \left[\left(\Omega_D^{(s)} - \Omega_C^{(s)} \right) \sin i \right] \end{array} \right\} \quad (5.30a)$$

$$\delta\dot{l}_0^{(s)} = \left[\left(\dot{\lambda}_0 \right)_D^{(s)} - \left(\dot{\lambda}_0 \right)_C^{(s)} \right] + \frac{d}{d\tau} \left[\left(\Omega_D^{(s)} - \Omega_C^{(s)} \right) \cos i \right] \quad (5.30b)$$

$$\delta\dot{e}_x^{(s)} = \left(\dot{e}_x \right)_D^{(s)} - \left(\dot{e}_x \right)_C^{(s)} \quad (5.30c)$$

$$\delta\dot{e}_y^{(s)} = \left(\dot{e}_y \right)_D^{(s)} - \left(\dot{e}_y \right)_C^{(s)} \quad (5.30d)$$

$$\delta\dot{i}_x^{(s)} = \dot{i}_D^{(s)} - \dot{i}_C^{(s)} \quad (5.30e)$$

$$\delta\dot{i}_y^{(s)} = \frac{d}{d\tau} \left[\left(\Omega_D^{(s)} - \Omega_C^{(s)} \right) \sin i \right] \quad (5.30f)$$

Substituting the definitions of the eccentricity vector and the secular rates of the Keplerian elements in equation (5.30) lead to:

$$\left. \begin{array}{l} \delta\dot{a}^{(s)} \approx 0 \\ \delta\dot{l}_0^{(s)} \approx -\frac{7}{4} \frac{\alpha}{a_0^2 \eta_0^4} \sin(2i_0) \delta i_{x0} \\ \delta\dot{e}_x^{(s)} \approx -\frac{\alpha}{4} \frac{1}{a_0^2 \eta_0^4} (5 \cos^2 i_0 - 1) \delta e_{y0} \\ \delta\dot{e}_y^{(s)} \approx \frac{\alpha}{4} \frac{1}{a_0^2 \eta_0^4} (5 \cos^2 i_0 - 1) \delta e_{x0} \\ \delta\dot{i}_x^{(s)} \approx 0 \\ \delta\dot{i}_y^{(s)} \approx \frac{\alpha}{2} \frac{1}{a_0^2 \eta_0^4} \sin^2 i_0 \delta i_{x0} \end{array} \right\} \quad (5.31a)$$

$$\delta\dot{l}_0^{(s)} \approx -\frac{7}{4} \frac{\alpha}{a_0^2 \eta_0^4} \sin(2i_0) \delta i_{x0} \quad (5.31b)$$

$$\delta\dot{e}_x^{(s)} \approx -\frac{\alpha}{4} \frac{1}{a_0^2 \eta_0^4} (5 \cos^2 i_0 - 1) \delta e_{y0} \quad (5.31c)$$

$$\delta\dot{e}_y^{(s)} \approx \frac{\alpha}{4} \frac{1}{a_0^2 \eta_0^4} (5 \cos^2 i_0 - 1) \delta e_{x0} \quad (5.31d)$$

$$\delta\dot{i}_x^{(s)} \approx 0 \quad (5.31e)$$

$$\delta\dot{i}_y^{(s)} \approx \frac{\alpha}{2} \frac{1}{a_0^2 \eta_0^4} \sin^2 i_0 \delta i_{x0} \quad (5.31f)$$

where second order terms in the relative OEs have been neglected. These equations can finally be integrated with respect to τ , leading to:

$$\left. \begin{array}{l} \delta a \approx \delta a_0 \\ \delta l_0 \approx \delta l_0(\tau_0) - \frac{7}{4} \frac{\alpha}{a_0^2 \eta_0^4} \sin(2i_0) \delta i_{x0} (\lambda - \lambda_0) \\ \delta e_x \approx \delta e_0 \cos(\varphi_0 + \varphi'(\lambda - \lambda_0)) \\ \delta e_y \approx \delta e_0 \sin(\varphi_0 + \varphi'(\lambda - \lambda_0)) \\ \delta i_x \approx \delta i_{x0} \\ \delta i_y \approx \delta i_{y0} - \frac{\alpha}{4} \frac{1}{a_0^2 \eta_0^4} \sin^2 i_0 \delta i_{x0} (\lambda - \lambda_0) \end{array} \right\} \quad (5.32)$$

$$\delta a \approx \delta a_0 \quad (5.32a)$$

$$\delta l_0 \approx \delta l_0(\tau_0) - \frac{7}{4} \frac{\alpha}{a_0^2 \eta_0^4} \sin(2i_0) \delta i_{x0} (\lambda - \lambda_0) \quad (5.32b)$$

$$\delta e_x \approx \delta e_0 \cos(\varphi_0 + \varphi'(\lambda - \lambda_0)) \quad (5.32c)$$

$$\delta e_y \approx \delta e_0 \sin(\varphi_0 + \varphi'(\lambda - \lambda_0)) \quad (5.32d)$$

$$\delta i_x \approx \delta i_{x0} \quad (5.32e)$$

$$\delta i_y \approx \delta i_{y0} - \frac{\alpha}{4} \frac{1}{a_0^2 \eta_0^4} \sin^2 i_0 \delta i_{x0} (\lambda - \lambda_0) \quad (5.32f)$$

where $\varphi' = \frac{\alpha}{4a_0^2 \eta_0^4} (5 \cos^2 i_0 - 1)$ is the derivative of the relative argument of perigee.

It is easy to lose track of what has been done until now. Firstly, an equivalence between the HCW formulation and the GVEs has been established, so that now, the RTN state vector is linked to the variation of the OEs. Going one step further, said variations of the OEs can be obtained for a given perturbation (J_2 in this case), so that the effect of that variation can be directly estimated on the RTN state vector. In conclusion, the effect of the J_2 term of the gravity field on the relative position of the deputy is now known.

Effect on the eccentricity and inclination vectors

Expression (5.32) provides the components of both eccentricity and inclination vectors along time. A simple derivation leads to the following expressions[15]:

$$\left. \begin{array}{l} \frac{d}{d\tau} \underline{\delta e} = \frac{d}{d\tau} (\delta e_0) \begin{Bmatrix} \cos(\varphi_0 + \varphi'(\lambda - \lambda_0)) \\ \sin(\varphi_0 + \varphi'(\lambda - \lambda_0)) \end{Bmatrix} = \delta e_0 \begin{Bmatrix} -\varphi' \sin(\varphi_0 + \varphi'(\lambda - \lambda_0)) \\ \varphi' \cos(\varphi_0 + \varphi'(\lambda - \lambda_0)) \end{Bmatrix} \\ \frac{d}{d\tau} \underline{\delta i} = \frac{d}{d\tau} \begin{Bmatrix} \delta i_{x0} \\ \delta i_{y0} - \frac{\alpha}{4} \frac{1}{a_0^2 \eta_0^4} \sin^2 i_0 \delta i_{x0} (\lambda - \lambda_0) \end{Bmatrix} = \begin{Bmatrix} 0 \\ -\frac{\alpha}{4} \frac{1}{a_0^2 \eta_0^4} \sin^2 i_0 \delta i_{x0} \end{Bmatrix} \end{array} \right\} \quad (5.33)$$

$$\left. \begin{array}{l} \frac{d}{d\tau} \underline{\delta e} = \frac{d}{d\tau} (\delta e_0) \begin{Bmatrix} \cos(\varphi_0 + \varphi'(\lambda - \lambda_0)) \\ \sin(\varphi_0 + \varphi'(\lambda - \lambda_0)) \end{Bmatrix} = \delta e_0 \begin{Bmatrix} -\varphi' \sin(\varphi_0 + \varphi'(\lambda - \lambda_0)) \\ \varphi' \cos(\varphi_0 + \varphi'(\lambda - \lambda_0)) \end{Bmatrix} \\ \frac{d}{d\tau} \underline{\delta i} = \frac{d}{d\tau} \begin{Bmatrix} \delta i_{x0} \\ \delta i_{y0} - \frac{\alpha}{4} \frac{1}{a_0^2 \eta_0^4} \sin^2 i_0 \delta i_{x0} (\lambda - \lambda_0) \end{Bmatrix} = \begin{Bmatrix} 0 \\ -\frac{\alpha}{4} \frac{1}{a_0^2 \eta_0^4} \sin^2 i_0 \delta i_{x0} \end{Bmatrix} \end{array} \right\} \quad (5.33a)$$

The results are quite clear: the relative eccentricity vector derivative induces a rotation in it, as it is perpendicular to it at every instant, without ever changing the module. Conversely, the inclination vector features a negative drift in the vertical component. These behaviours are shown in figure 5.4.

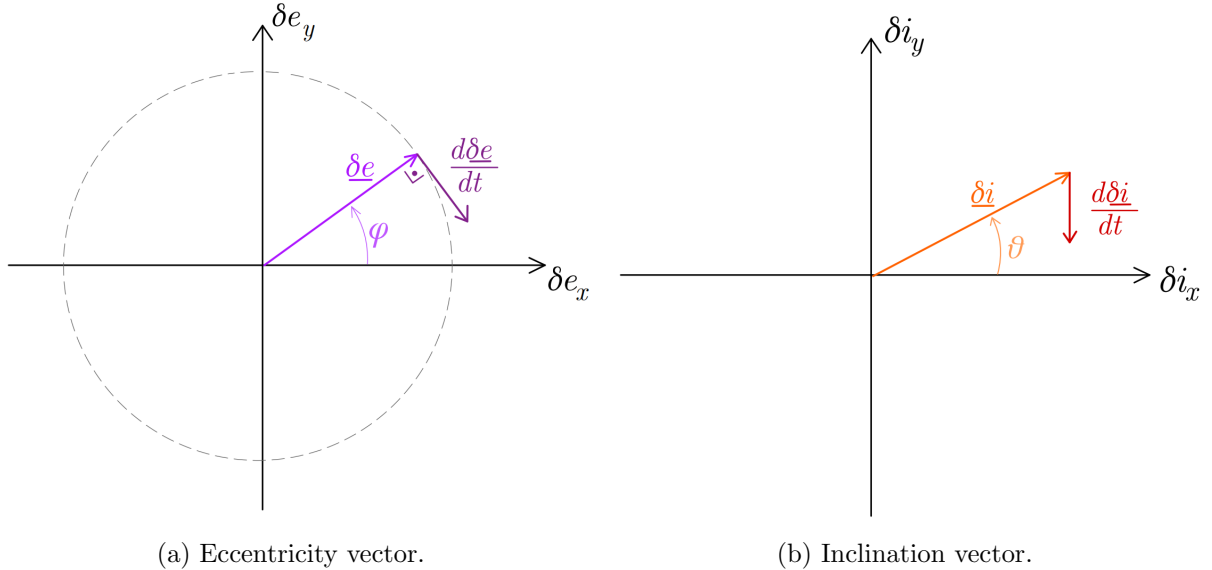


Figure 5.4: J_2 effect on the relative eccentricity and inclination vectors.

The concern now is how this will impact orbit safety. As explained in section 2.4.2, a useful strategy is the separation of the eccentricity and inclination vectors, so as to guarantee separation in either tangential or out-of-plane direction. This is done by imposing the same phase in both vectors ($\varphi = \psi$), which in the unperturbed problem was not much of a concern. However, now both vectors feature secular variations, which shatters this geometric condition. If the target is to maintain a parallel configuration of both vectors, correction manoeuvres need to be performed.

In view of this fact, a better approximation of the secular motion (through more accurate approximations) would lead to a better planning of the correction manoeuvres, hence more efficient.

Conclusions and research outlook.

The increasingly higher relevance of relative motion is beyond question. Satellite constellations, rendezvous operations and formation flying missions are becoming an everyday occurrence, and their growing success rates are no coincidence. Incrementally better models (*i.e.* truer-to-life, accounting for more effects) have an essential role in this.

In order to gain a comprehensible insight on this topic, this thesis has followed the same bottom-up structure, starting from the very simple Hill/Clohessy-Wiltshire equations up to the modelling of perturbations. The use of linear, closed-form models (through STMs) is an advantageous approach: firstly, computational cost drops, but even more importantly, deeper knowledge about the dynamics of the system is achieved. This allows for, among other things, the design of relative orbits with certain characteristics (*e.g.* safe orbits).

Any state-of-the-art model requires an analysis of the relevant perturbations to be carried out. For the case of Earth artificial satellites, this usually leaves the non-spherical gravity as the most important of them. Kaula's theory allows for the analysis of the effect of any spherical harmonic, which naturally leads for better accuracy models. Although it features certain singular cases (resonances and circular or equatorial orbits), these can be solved. Many applications can be branched from this theory, such as mean-to-osculating transformations, linearized relative motion models, resonance analysis ...

In conclusion, the modelling of perturbations is key for the construction of accurate linearised relative motion models as well as relative orbit design; both of which play a paramount role in the constantly growing discipline of distributed space systems.

Research outlook and future work.

The very wide horizon in which this topic is framed leads for countless possible research areas.

The evaluation of a robust implementation of Kaula's theory is the first on the list. This would be followed by an analysis of the resonant and secular terms, such as done by Chao [33]. The development of mean-to-osculating transformations through this theory is also considered, which could

derive into the development of linear relative motion models based on it.

In a somewhat more general sense, the survey, analysis and implementation of perturbed relative motion models (STMs) is to be tackled. A performance analysis of these models against a High-Fidelity and unperturbed models would be insightful, surely.

Orbit safety might also be an interesting topic to follow up on. A review of the existent models for non-circular, perturbed reference orbits would be insightful, and would continue on the here developed models for simpler cases (*i.e.* circular perturbed and elliptic unperturbed).

Further down the road, other types of perturbations might be analyzed, through the averaging methods here presented. Third bodies or drag are the most relevant ones, although second-order NSG effects are also to be considered.

Finally, real world scenarios may be analyzed, and eventually, a self-contained tool for this purpose could be regarded. Hopefully, this sort of roadmap looks as compelling as it does to the author.

Absolute and relative orbital element sets.

A.1 Introduction.

The description of a spacecraft's state is done via a state vector. While it can include several variables with other purposes (*e.g.* filtering), its only information throughout this thesis is the position and velocity. There are two main ways to describe them:

- A.** Through **cartesian coordinates**
- B.** Through **orbital elements**

While the first option yields a very explicit and graphic-ready description, the second one usually has two advantages over it. Firstly, orbital elements are generally more intuitive about both the orbit and the position on it. Secondly, as orbital elements are generally slow-varying, they allow for a bigger integration timestep without losing accuracy. This is quite clear when studying keplerian motion, as most of the elements remain constant. Variational formulation and Hamilton-Jacobi theory (with the notion of changing variables as the full solution of a problem) relate to this fact.

Throughout this thesis, several sets of orbital elements have been used. The goal of this appendix is to clarify on the definition and differences between them. Absolute orbital elements (OEs) will be described first, followed by relative OEs (ROEs).

A.2 Absolute element sets.

A.2.1 Workflow for transformations between absolute element sets.

Consider two different sets of OEs, denoted by \underline{OE} and \widetilde{OE} . The transformation function $G_{OE \rightarrow \widetilde{OE}}$ between them is defined by:

$$\widetilde{OE} = G_{OE \rightarrow \widetilde{OE}}(\underline{OE}) \quad (\text{A.1})$$

A numerous amount of element sets have been historically defined. Nevertheless, some of them are much more commonly used than others. Although this analysis will be restricted to a short number of sets (say n), the number of transformations becomes arduously large as n increases ($n(n - 1)$).

In order to reduce the number of transformation functions \mathbf{G} , the later defined Keplerian OEs (KOE) will be used as a pivot, that is, building only transformations to and from KOEs. This will in turn reduce the number of required functions to $2n$. The Keplerian set also has a further advantage: as it is the classical element set, almost every other set is defined explicitly in terms of it, so that transformations to and from them can be easily derived. A simple, graphical explanation of this is shown in figure A.1.



Figure A.1: Workflow for transforming between two arbitrary absolute element sets.

A.2.2 Element sets.

A.2.2.1 Keplerian orbital elements (KOE).

The Keplerian set of OEs (KOE) is one of the most widely used and classic options. An usual definition is the following:

$$\left\{ \begin{array}{lll} a & \equiv & \text{Semimajor axis} & [L] \\ e & \equiv & \text{Eccentricity} & [-] \\ i & \equiv & \text{Inclination} & [\text{rad}] \\ \Omega \text{ or } RAAN & \equiv & \text{Right ascension of the ascending node} & [\text{rad}] \\ \omega & \equiv & \text{Argument of periapsis} & [\text{rad}] \\ M & \equiv & \text{Mean anomaly} & [\text{rad}] \end{array} \right. \quad (\text{A.2})$$

The last element commonly varies across literature, being substituted by the true anomaly θ ; or, when tackling the variation of orbital parameters, by the mean anomaly at $t = 0$ (M_0) or the perigee time T_0 [9]. Mean anomaly is used due to the simplicity of its unperturbed variational equation, as it has a constant rate (denoted by n). The geometrical meaning and definition of these elements is out from the scope of this thesis. Nonetheless, figure A.2 shows a simple geometrical drawing of the involved angles.

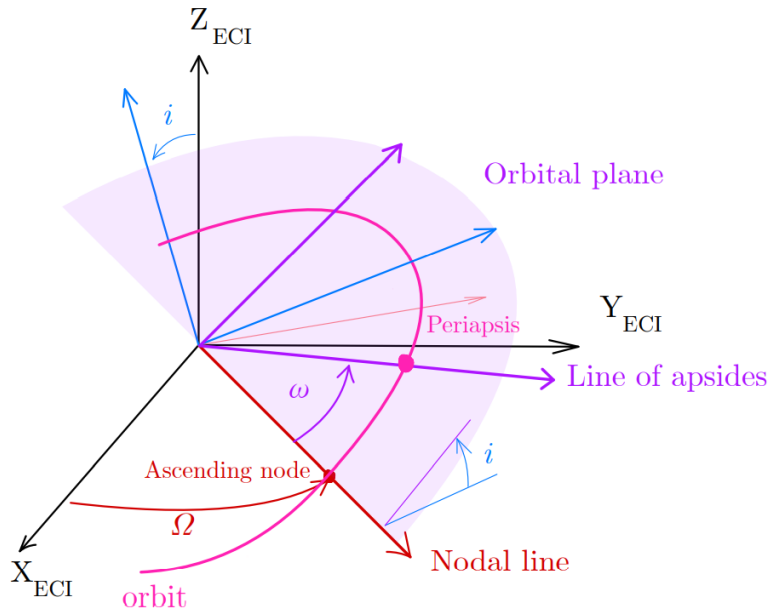


Figure A.2: Frame rotation from inertial to perifocal frame.

As it is seen in the figure before, the Keplerian elements become singular in two cases:

- A. If the **inclination** is null, the orbital plane is coincident with the inertial reference (ECI x-y) plane. The ascending node is hence undefined in this case.
- B. If the **eccentricity** is null, the periapsis is not defined, as it is the nearest point of the orbit around the central body. Thus, there is no angle defining its position, making the argument of periapsis singular.

These singularities are unfortunately quite common in orbit design. They correspond respectively with equatorial and circular orbits. In order to avoid this behaviour, many different elements sets have been defined. Wiesel [9] shows an intuitive approach in section 2.10, solving either problem with a graphic approach.

A.2.2.2 Eccentricity/inclination vectors orbital elements (EIOE).

This set, originally defined for geostationary orbits in absolute terms [13], is used mainly as a relative OE set. Though it is actually not used along this thesis, its definition is helpful for introducing the relative counterpart.

I. Eccentricity vector.

The notion of the eccentricity vector is quite basic, as it is, when in unperturbed motion, a constant

of the dynamic system. It is defined as the eccentricity-sized vector pointing towards the perigee. Nonetheless, for this purpose, the eccentricity vector is defined as [15]:

$$\underline{e} = \begin{Bmatrix} e_x \\ e_y \end{Bmatrix} = e \begin{Bmatrix} \cos \varpi \\ \sin \varpi \end{Bmatrix} \quad (\text{A.3})$$

where the argument of perigee ω might be substituted with the sum $\omega + \Omega$ [as in 13]. A graphical representation can be seen later in the relative definition A.5(a). As it arises from (A.3), it substitutes the eccentricity and argument of perigee from the Keplerian OE set.

II. Inclination vector.

The inclination vector is perpendicular to the orbital plane, similarly to the angular momentum, but inclination-sized. It is defined by its components as [13]:

$$\underline{i} = \begin{Bmatrix} i_x \\ i_y \end{Bmatrix} = i \begin{Bmatrix} \cos \Omega \\ \sin \Omega \end{Bmatrix}$$

The graphical interpretation is not as straightforward as for the eccentricity vector. It is clear that these components substitute the out-of-plane related elements i and Ω .

III. Element set.

The EI orbital element set is then composed of:

$$\left\{ \begin{array}{lcl} a & \equiv & \text{Semimajor axis} & [L] \\ e_x = e \cos \omega & \equiv & \text{x-projection of } \underline{e} & [-] \\ e_y = e \sin \omega & \equiv & \text{y-projection of } \underline{e} & [-] \\ i_x = i \cos \Omega & \equiv & \text{x-component of } \underline{i} & [-] \\ i_y = i \sin \Omega & \equiv & \text{y-component of } \underline{i} & [-] \\ \lambda = \omega + M & \equiv & \text{Mean argument of latitude} & [\text{rad}] \end{array} \right. \quad (\text{A.4})$$

A.2.2.3 Quasi-nonsingular orbital elements (QNSOE).

The quasi-nonsingular (QNS) orbital element set tackles the singularity existing in circular orbits [39], [38] [40]. It is quite similar to the formerly defined EI set, as it uses again the components

of the eccentricity vector to substitute e and ω . The set is then defined as:

$$\left\{ \begin{array}{lcl} a & \equiv & \text{Semimajor axis} & [L] \\ q_1 = e \cos \omega & \equiv & \text{x-projection of } \underline{e} & [-] \\ q_2 = e \sin \omega & \equiv & \text{y-projection of } \underline{e} & [-] \\ i & \equiv & \text{Inclination} & [\text{rad}] \\ \Omega & \equiv & \text{Right ascension of the ascending node} & [\text{rad}] \\ \lambda = \omega + M & \equiv & \text{Mean argument of latitude} & [\text{rad}] \end{array} \right. \quad (\text{A.5})$$

Though some authors use a different order, this is the one used in this thesis, so as to keep the time-varying element on the last place.

A.2.2.4 Equinoctial orbital elements (EOE).

The QNS set of elements only solved half of the singularity problem. To solve both, thus enabling the description of equatorial and polar orbits, the equinoctial set of elements is defined as:

$$\left\{ \begin{array}{lcl} a & \equiv & \text{Semimajor axis} & [L] \\ P_1 = e \cos \varpi & \equiv & \text{unclear physical meaning, similar to } e_x & [-] \\ P_2 = e \sin \varpi & \equiv & \text{unclear physical meaning, similar to } e_y & [-] \\ Q_1 = \tan \frac{i}{2} \cos \Omega & \equiv & \text{unclear physical meaning, similar to } i_x & [-] \\ Q_2 = \tan \frac{i}{2} \sin \Omega & \equiv & \text{unclear physical meaning, similar to } i_y & [-] \\ L = \Omega + \omega + \theta & \equiv & \text{True longitude} & [\text{rad}] \end{array} \right. \quad (\text{A.6})$$

where $\varpi = \Omega + \omega$. Not only does the order does change depending on the author, but also the symbols to refer to them. An example of its use is [39].

A.2.2.5 Delaunay orbital elements (DOE).

Delaunay elements arise when formulating the two-body problem through analytical mechanics E.2.1.1. Conversely to the previous element sets, who are clearly non-canonical (*i.e.* they do not satisfy Hamilton's equations), Delaunay elements are built based on the analytical perspective of the problem. Starting from the canonical set of elements (see appendix C), Delaunay elements are reached

after performing a canonical transformation, leading to the following definition:

$$\left\{ \begin{array}{lll} L = \sqrt{\mu a} & \equiv & \text{unclear physical meaning} & [L^{1/2}] \\ G = L\sqrt{1-e^2} & \equiv & \text{Angular momentum} & [L^{1/2}] \\ H = G \cos i & \equiv & \text{Polar component of angular momentum} & [L^{1/2}] \\ l = M & \equiv & \text{Mean anomaly} & [\text{rad}] \\ g = \omega & \equiv & \text{Argument of perigee} & [\text{rad}] \\ h = \Omega & \equiv & \text{Right ascension of ascending node} & [\text{rad}] \end{array} \right. \quad (\text{A.7})$$

This set is mainly used in the context of perturbations, as it yields a very convenient expression for the perturbed Hamiltonian (see section E.2.1.1).

A.3 Relative sets.

Relative elements are at the deepest roots of spacecraft relative motion, offering several advantages over cartesian relative states. First and foremost, they are more intuitive, but they also lead to a reduction of linearisation errors when expanding the deputy's movement around the chief's orbit [28]. In general, relative elements are defined as:

$$\delta \underline{OE} = \mathbf{f} (\underline{OE}_C, \underline{OE}_D) \quad (\text{A.8})$$

which is usually simplified by just taking the arithmetic difference between them, namely

$$\delta \underline{OE} = \underline{OE}_D - \underline{OE}_C \quad (\text{A.9})$$

where the subscripts denote respectively the deputy and chief spacecraft. The question now is, how do transformations between ROEs work.

A.3.1 Workflow for transformations between ROEs.

As for the absolute elements, Keplerian elements will be used as a pivot point. That means that only the transformations from and to RKOEs must be implemented. There are then two types of transformations:

A) From any ROE set to RKOE

While authors provide with scenarios expressed in their own ROE set, the element choice for this thesis is the Keplerian set. That leads to the need of implementing a transformation from the former set to the latter. The considered inputs and outputs are:

- **Inputs:**

- $\widetilde{ROE} = \delta\widetilde{OE}$: Any type of ROEs, whose absolute equivalents are known as a function of the KOEs ($\widetilde{OE} = f(KOE)$)
- KOE_C : Chief spacecraft/reference orbit KOEs

- **Output:**

- $RKOE = \delta KOE$: Keplerian ROEs

Taking equation (A.9) and particularizing it for KOEs:

$$\delta KOE = KOE_D - KOE_C \quad (\text{A.10})$$

while the second term is known (input), the second one must be calculated through a certain process:

1st Calculate chief's OEs in the source phase space (*i.e.* \widetilde{OE}_C)

$$\widetilde{OE}_C = G_{KOE \rightarrow \widetilde{OE}}(KOE_C)$$

2nd Compute deputy's OEs by direct addition

$$\widetilde{OE}_D = \widetilde{OE}_C + \delta\widetilde{OE}$$

3rd Compute deputy's KOEs by back-transformation

$$KOE_D = G_{\widetilde{OE} \rightarrow KOE}(\widetilde{OE}_D)$$

4th Subtract chief's KOEs from deputy's

$$\delta KOE = KOE_D - KOE_C$$

See graphic A.3 for a more visual explanation.

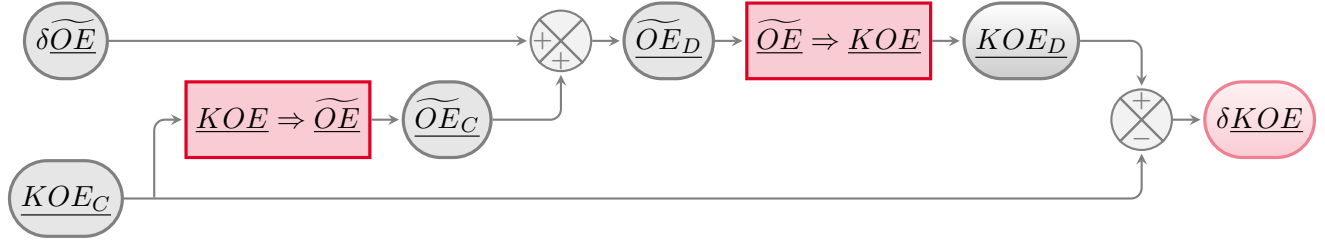


Figure A.3: Workflow for transforming any relative set into KOE.

B) From RKOE to any ROE set

In this case, the assumed inputs and outputs are:

- **Inputs:**

- $\underline{RKOE} = \delta\underline{KOE}$: Keplerian ROEs
- \underline{KOE}_C : Chief KOEs

- **Output:**

- $\underline{ROE} = \delta\underline{OE}$: Any type of ROEs, whose absolute equivalents are known as a function of the KOEs ($\underline{OE} = f(\underline{KOE})$)

For this transformation, the equation A.8 particularized for this case acquires the following shape:

$$\delta\underline{OE} = \underline{OE}_D - \underline{OE}_C \quad (\text{A.11})$$

Equation A.11 can be tackled in two main ways:

- A. Using the pertinent transformations, compute the absolute elements for both spacecrafts \underline{OE}_D , \underline{OE}_C , and then calculate the arithmetic difference (in a A.3.1). See graphic A.4.
- B. Expand the deputy absolute OEs (*i.e.* \underline{OE}_D) around the chief via a Taylor series expansion with respect to the Keplerian set of elements, retaining terms up to first order, achieving a linearised expression for the transformation. Mathematically:

$$\underline{OE}_D = \underline{OE}(KOE_D) = \underline{OE}(KOE_C + \delta\underline{KOE}) = \underline{OE}_C + \frac{\partial \underline{OE}}{\partial \underline{KOE}} \delta\underline{KOE} + \mathcal{O}(\delta\underline{KOE}^2)$$

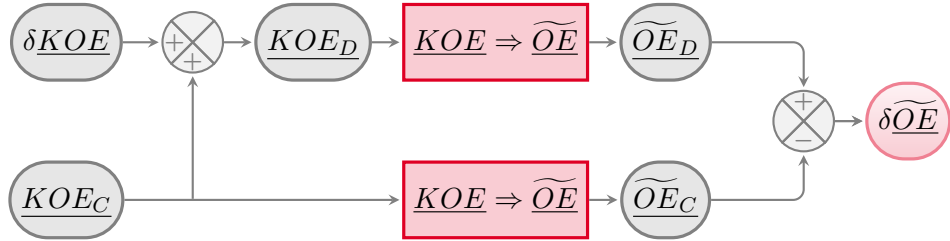


Figure A.4: Workflow for transforming RKOE into any other set.

hence,

$$\delta\widetilde{OE} \approx \widetilde{OE}_C + \frac{\partial\widetilde{OE}}{\partial\underline{KOE}}\delta\underline{KOE} - \widetilde{OE}_C = \frac{\partial\widetilde{OE}}{\partial\underline{KOE}}\delta\underline{KOE} \quad (\text{A.12})$$

where the Jacobian matrix is generally simple, as it usually only implies polynomic or trigonometric functions. Equation (A.12) is then a first order approximation of (A.11). Its validity is then reduced to a close proximity between both spacecrafts, which should be assessed.

A.3.2 Element sets.

Besides the ones derived directly from its absolute counterparts, a couple of additional ROE sets will be herewith defined and explained. This is due to one of two reasons. The first one is that some ROE sets are only defined in relative terms, lacking any absolute equivalent. The second one is that it might be interesting to dive in the meaning of the relative sets, deriving interesting relations that would otherwise be overlooked.

A.3.2.1 Relative eccentricity/inclination vectors orbital elements (REIOE).

This ROE set is the counterpart of the EI set (see A.2.2.2). It is nonetheless interesting to see the meaning and shape of it, as it is quite widely used in literature [15, 38, 40]. Firstly, the elements themselves are defined, to later analyze the meaning behind them:

$$\left\{ \begin{array}{lcl} \delta a & \equiv & \text{Relative semimajor axis} & [L] \\ \delta e_x & \equiv & \text{x-component of } \delta e & [-] \\ \delta e_y & \equiv & \text{y-component of } \delta e & [-] \\ \delta i_x & \equiv & \text{x-component of } \delta i & [-] \\ \delta i_y & \equiv & \text{y-component of } \delta i & [-] \\ \delta \lambda & \equiv & \text{Relative mean argument of latitude} & [\text{rad}] \end{array} \right. \quad (\text{A.13})$$

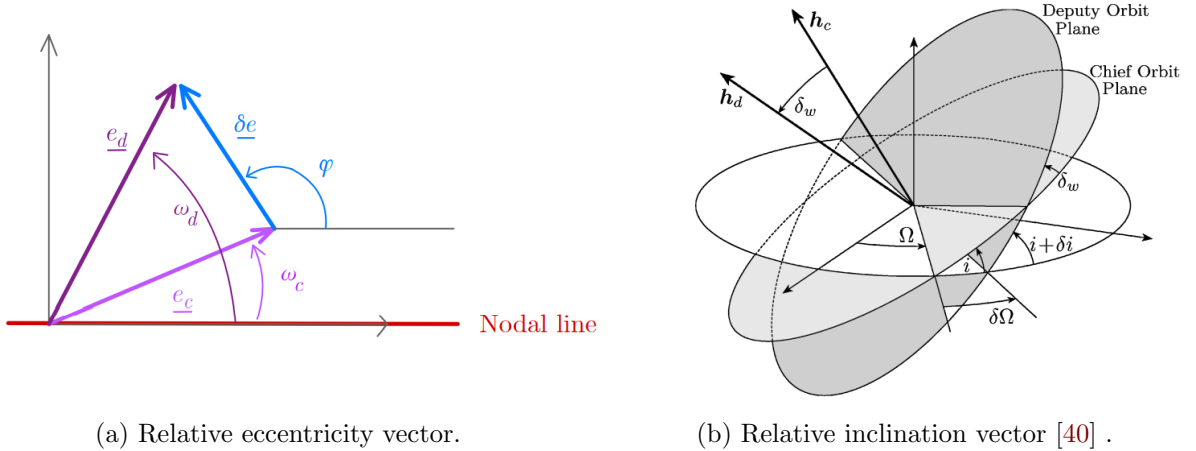


Figure A.5: Relative eccentricity & inclination vectors.

Concept & meaning

The relative eccentricity vector components substitute the relative eccentricity and the relative argument of perigee. It is based on the eccentricity vector definition (A.3), and a graphical representation can be seen in figure A.5(a). Mathematically:

$$\underline{\delta e} = \begin{Bmatrix} \delta e_x \\ \delta e_y \end{Bmatrix} = \delta e \begin{Bmatrix} \cos \varphi \\ \sin \varphi \end{Bmatrix}$$

where φ is referred to as the AOP of the relative orbit. This vector rules the in-plane relative motion (hand in hand with δa and $\delta\lambda$). There are two ways of tackling the transformation from RKOE to this set (see A.3.1). Besides the exact nonlinear form, a linear version can be derived. Assuming that the difference in the eccentricity vector is due to that of the eccentricity and argument of perigee (δe , $\delta\omega$), it follows that:

$$\underline{\delta e} \approx \begin{bmatrix} \cos \omega & -e \sin \omega \\ \sin \omega & e \cos \omega \end{bmatrix} \begin{Bmatrix} \delta e \\ \delta \omega \end{Bmatrix} \quad (\text{A.14})$$

where terms of second order and higher have been neglected. The relative inclination vector is defined in an alternative way [15] (comparing with the absolute counterpart). Mathematically:

$$\delta \underline{i} = \sin \delta i \begin{Bmatrix} \cos \theta \\ \sin \theta \end{Bmatrix}$$

where θ is the analogue angle to φ in the eccentricity vector, being commonly referred to as the RAAN of the relative orbit. Once again, the linearised transformation from RKOE to this set may be analysed, considering the differences δi and $\delta\Omega$. Applying the law of sines and the law of cosines for spherical trigonometry and assuming small values of δi and $\delta\Omega$, it follows that:

$$\delta \underline{i} = \begin{Bmatrix} \delta i \\ \sin i \delta\Omega \end{Bmatrix} \approx \begin{bmatrix} 1 & 0 \\ 0 & \sin i \end{bmatrix} \begin{Bmatrix} \delta i \\ \delta\Omega \end{Bmatrix} \quad (\text{A.15})$$

where i is the inclination of the chief's orbit. Combining the results of (A.14) and (A.15) with the definitions of the remaining elements, an expression analogue to (A.12) is reached:

$$\begin{Bmatrix} \delta a \\ \delta e_x \\ \delta e_y \\ \delta i_x \\ \delta i_y \\ \delta \lambda \end{Bmatrix} \approx \begin{bmatrix} 1 & 0 & 0 & 0 & 0 & 0 \\ 0 & \cos \omega & 0 & 0 & -e \sin \omega & 0 \\ 0 & \sin \omega & 0 & 0 & e \cos \omega & 0 \\ 0 & 0 & 1 & 0 & 0 & 0 \\ 0 & 0 & 0 & \sin i & 0 & 0 \\ 0 & 0 & 0 & 0 & 1 & 1 \end{bmatrix} \begin{Bmatrix} \delta a \\ \delta e \\ \delta i \\ \delta \Omega \\ \delta \omega \\ \delta M \end{Bmatrix} \quad (\text{A.16})$$

A graphical representation of this concept can be seen in figure A.5(b).

However, this definition is changed in some references. In particular, the mean argument of latitude λ is sometimes substituted by the modified relative mean longitude, which is defined as:

$$\delta l_0 \equiv \delta \lambda + \delta \Omega \cos i$$

The advantage of this formulation is that the in-plane motion becomes decoupled. This will also be done in the following set of relative elements.

A.3.2.2 C set of relative orbital elements (CROE).

Defined by Peters & Noomen in [21], this set is also closely related with the orbit safety notion. It arises from the analysis of the Gauss Variational Equations (GVEs) applied to the relative dynamics between a deputy and a chief spacecraft, when the former performs a cotangential transfer. The elements themselves are defined as:

$$\left\{ \begin{array}{lll} C_1 = \delta p = \eta^2 \delta a - 2 a e \delta e & \equiv & \text{Relative parameter of the orbit} \quad [L] \\ C_2 = e \delta p - p \delta e & \equiv & \text{unclear physical meaning} \quad [L] \\ C_3 = -e p (\delta \omega + \cos i \delta \Omega) & \equiv & \text{unclear physical meaning} \quad [L] \\ C_4 = a (\delta \omega + \cos i \delta \Omega + \eta^{-1} \delta M) & \equiv & \text{Modified relative mean longitude} \quad [L] \\ C_5 = -p (\cos \omega \delta i + \sin i \sin \omega \delta \Omega) & \equiv & \text{unclear physical meaning} \quad [L] \\ C_6 = p (\sin \omega \delta i - \sin i \cos \omega \delta \Omega) & \equiv & \text{unclear physical meaning} \quad [L] \end{array} \right. \quad (\text{A.17})$$

For a proper geometrical and conceptual description of the elements, please see [21]. As an introduction, the first four elements essentially determine the in-plane relative motion. C_1 , C_2 & C_3 arise from a very intelligent interpretation of the GVEs, with C_4 completing the element set. On the other hand, elements C_5 and C_6 describe the out-of-plane motion.

Cartesian reference systems.

B.1 Introduction.

Cartesian states are, as mentioned in appendix A, one of the two main alternatives to describe the state of a certain spacecraft (or celestial body). Though orbital elements (OEs) are generally more intuitive and meaningful, these states are quite critical for the description of both absolute and relative motion. Ultimately, and specially considering the latter, one wishes to know the relative orientation and linear distance between the involved bodies. During this appendix, a set of absolute and relative reference frames will be described and related through transformations, which have been used time and again along this thesis.

B.1.1 Inertial and rotating reference frames.

Technically, an inertial reference frame is one where Newton's law holds. Effectively, it is a frame which is not object of any acceleration whatsoever. It is then, when interpreted to the letter, an idealization, as there will always be any perturbation which disavows this assumption. Nonetheless, it is usual to neglect said perturbations up to a certain point, thus considering pseudo-inertial reference frames. From now on then, when inertial reference frames are mentioned they will be considered so, even though they are actually not. Along this thesis, both inertial and rotating frames will be considered, each bearing its different advantages and disadvantages.

B.1.2 Absolute and relative frames.

Another distinction that will be made is between absolute and relative frames. In this thesis, absolute frames are those who are centered in the Earth's center of mass, while relative frames are defined with respect to a reference orbit (the chief's generally). Again, they have different scopes, though relations between them need to be developed.

B.2 Transformations between reference systems.

In this section, two approaches for reference system transformations will be presented. These will prove quite useful later on, helping to clarify how different systems relate to each other.

For the sake of generality, two frames are considered: firstly an inertial and absolute reference frame, and secondly, a rotating, relative reference frame (see figure B.1). In case two absolute systems are considered, it is enough to just nullify the displacement between both frames' origins. The notation used is described below:

- Vectors: \underline{X} refers to a vector with respect an absolute frame, while \underline{x} is used for relative reference frames. Please, note that no reference system (*i.e.* vector base) is being used: the vector entity is considered as a mere object.
- Subscripts: Unless specified otherwise, denote the body: \bullet_C for the chief, \bullet_D for the deputy.
- Time derivatives and superscripts: As Coriolis' Theorem states, when non-inertial reference frames are involved, it is necessary to specify the frame with respect to which the derivative is calculated. $\frac{\mathcal{F}d\bullet}{dt}$ denotes the time derivative in the frame \mathcal{F} . An equally valid yet more compact notation is $\bullet^{\mathcal{F}}$.
- Right vertical bar subscript: Denotes the coordinate system in which one vector or matrix is described. For example, $\underline{u}|_1 = \sum_{i=1}^3 u_{xi} \hat{e}_{i1}$.

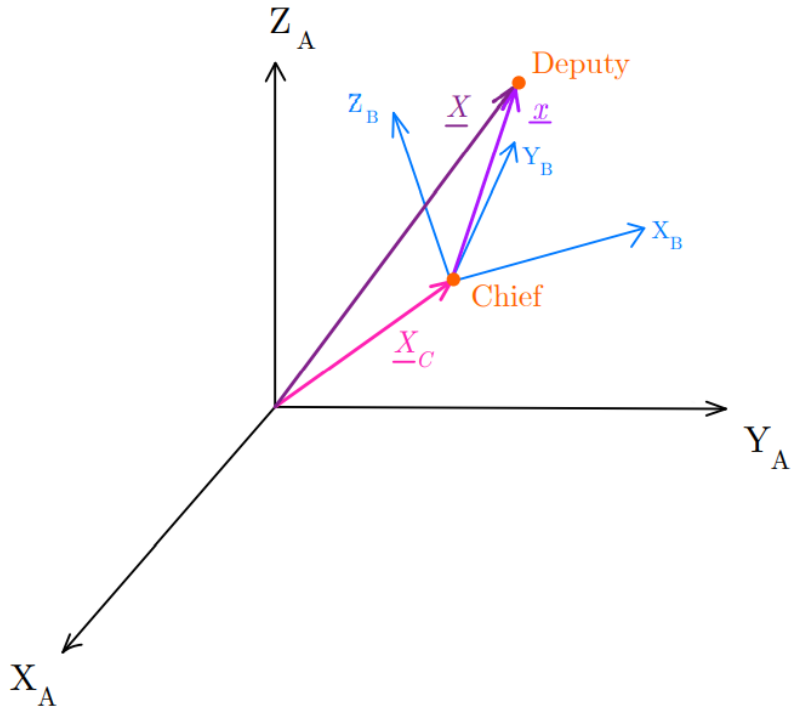


Figure B.1: Absolute and relative frames.

Consider the frames A and B from figure B.1. Firstly the transformation from $A \rightarrow B$ is addressed, that is, converting an absolute & inertial state vector expressed in coordinate system A to the relative, rotating frame B in its coordinates. What one would like to achieve is a relationship of the form:

$$\begin{cases} \underline{x}|_B = \mathbf{f}_1(\underline{X}|_A, \dots, \underline{X}_C|_A, \dots) \\ \dot{\underline{x}}^B|_B = \mathbf{f}_2(\underline{X}|_A, \dot{\underline{X}}^A|_A, \underline{X}_C|_A, \dot{\underline{X}}_C^A|_A) \end{cases}$$

As it turns out, this relation is actually linear on the inputs $\dot{\underline{X}}^A|_A$ and $\underline{X}|_A$. From this point on, two approaches are derived:

B.2.1 Direct analytical differentiation.

The first approach starts from the decomposition of the deputy's absolute position vector [41]:

$$\underline{X} = \underline{X}_C + \underline{x} \rightarrow \underline{x} = \underline{X} - \underline{X}_C$$

This vector can be expressed in both coordinate systems, namely $\underline{x}|_A$ and $\underline{x}|_B$. The transformation between them can be written as the following rotation:

$$\underline{x}|_B = R_{A \rightarrow B} \underline{x}|_A \quad (\text{B.1})$$

The rotation matrix $R_{A \rightarrow B}$ takes the following form:

$$R_{A \rightarrow B} = \begin{bmatrix} (\hat{e}_{xA} \cdot \hat{e}_{xB}) & (\hat{e}_{yA} \cdot \hat{e}_{xB}) & (\hat{e}_{zA} \cdot \hat{e}_{xB}) \\ (\hat{e}_{xA} \cdot \hat{e}_{yB}) & (\hat{e}_{yA} \cdot \hat{e}_{yB}) & (\hat{e}_{zA} \cdot \hat{e}_{yB}) \\ (\hat{e}_{xA} \cdot \hat{e}_{zB}) & (\hat{e}_{yA} \cdot \hat{e}_{zB}) & (\hat{e}_{zA} \cdot \hat{e}_{zB}) \end{bmatrix}$$

where each column is the coordinates of each base vector of the “origin” coordinate system (A) expressed in the “destination” system (B). This fact is specially useful when such vectors are characteristic of the problem at hand, as it is the case for the two body problem. In order to transform the velocity vector, the first step is to take the time derivative of B.1, yielding:

$$\dot{\underline{x}}|_B = \dot{R}_{A \rightarrow B} \underline{x}|_A + R_{A \rightarrow B} \dot{\underline{x}}|_A \quad (\text{B.2})$$

whose first derivative $\dot{R}_{A \rightarrow B}$ can be calculated by columns, simplifying the task at hand if the origin base $(\hat{e}_{xA}, \hat{e}_{yA}, \hat{e}_{zA})$ has been obtained in terms of the final one. For the sake of completeness, it is

necessary to keep in mind that [41]:

$$\frac{d}{dt}\hat{\underline{u}} = \frac{1}{u} [\dot{\underline{u}} - (\hat{\underline{u}} \cdot \dot{\underline{u}}) \hat{\underline{u}}] \quad (\text{B.3})$$

A final, more compact form of both B.1 and B.2 can be reached by rearranging terms:

$$\begin{Bmatrix} \underline{x}|_B \\ \dot{\underline{x}}^B|_B \end{Bmatrix} = \begin{bmatrix} R_{A \rightarrow B} & 0_{3 \times 3} \\ \dot{R}_{A \rightarrow B} & R_{A \rightarrow B} \end{bmatrix} \begin{Bmatrix} \underline{X}|_A - \underline{X}_C|_A \\ \dot{\underline{X}}^A|_A - \dot{\underline{X}}_C^A|_A \end{Bmatrix} \quad (\text{B.4})$$

and the inverse transformation can be expressed as:

$$\begin{Bmatrix} \underline{X}|_A \\ \dot{\underline{X}}^A|_A \end{Bmatrix} = \begin{bmatrix} R_{B \rightarrow A} & 0_{3 \times 3} \\ \dot{R}_{B \rightarrow A} & R_{B \rightarrow A} \end{bmatrix} \begin{Bmatrix} \underline{x}|_B \\ \dot{\underline{x}}^B|_B \end{Bmatrix} + \begin{Bmatrix} \underline{X}_C|_A \\ \dot{\underline{X}}_C^A|_A \end{Bmatrix} \quad (\text{B.5})$$

An example of this approach will be developed later on in B.4.2.2.

B.2.2 Classical motion composition.

This approach, rather on pure derivation, is based on the grounds of motion composition and Coriolis' Theorem. This theorem states that the derivative of a vector in an inertial frame is equivalent to the derivative in a rotating frame plus another contribution due to the rotation of this reference frame:

$$\frac{^A d\underline{u}}{dt} = \frac{^B d\underline{u}}{dt} + \underline{\omega}_{B||A} \times \underline{u}$$

The first term of the right-hand side is associated to the temporal variation of the coordinates of \underline{u} in the rotating frame, whereas the second one is purely related to the relative rotation between both frames. Applying this to B.1:

$$\begin{aligned} \frac{^A d\underline{X}}{dt} &= \frac{^A d\underline{X}_C}{dt} + \frac{^A d\underline{x}}{dt} = \frac{^A d\underline{X}_C}{dt} + \frac{^B d\underline{x}}{dt} + \underline{\omega}_{B||A} \times \underline{x} \\ \Rightarrow \dot{\underline{X}}^A &= \dot{\underline{X}}_C^A + \dot{\underline{x}}^B + \underline{\omega}_{B||A} \times \underline{x} \end{aligned} \quad (\text{B.6})$$

As before, the first step is to go from the inertial frame towards the rotating. For that purpose, one shall substitute (B.1) into (B.6), solving for $\dot{\underline{x}}^B$:

$$\dot{\underline{x}}^B = \dot{\underline{X}}^A - \dot{\underline{X}}_C^A - \underline{\omega}_{B||A} \times (\underline{X} - \underline{X}_C) \quad (\text{B.7})$$

Now, expressing every vector in its proper frame:

$$\dot{\underline{x}}^B|_B = R_{A \rightarrow B} \left[\dot{\underline{X}}^A|_A - \dot{\underline{X}}_C^A|_A + \underline{\omega}_{A||B}|_A \times (\underline{X}|_A - \underline{X}_C|_A) \right] \quad (\text{B.8})$$

Using the axial-dual vector form leads to:

$$\dot{\underline{x}}^B|_B = R_{A \rightarrow B} \left[\dot{\underline{X}}^A|_A - \dot{\underline{X}}_C^A|_A + \Omega_{A||B}|_A (\underline{X}|_A - \underline{X}_C|_A) \right] \quad (\text{B.9})$$

where $\Omega_{A||B}$ is the matrix dual form of $\underline{\omega}_{A||B}$, that is:

$$\Omega_{A||B} = \begin{bmatrix} 0 & -\omega_z & \omega_y \\ \omega_z & 0 & -\omega_x \\ -\omega_y & \omega_x & 0 \end{bmatrix}$$

It is possible now express the conversion in a far more compact form as:

$$\begin{Bmatrix} \underline{x}|_B \\ \dot{\underline{x}}^B|_B \end{Bmatrix} = \begin{bmatrix} R_{A \rightarrow B} & 0_{3x3} \\ R_{A \rightarrow B} \Omega_{A||B}|_A & R_{A \rightarrow B} \end{bmatrix} \begin{Bmatrix} \underline{X}|_A - \underline{X}_C|_A \\ \dot{\underline{X}}^A|_A - \dot{\underline{X}}_C^A|_A \end{Bmatrix} \quad (\text{B.10})$$

and its inverse can be easily derived, leading to:

$$\begin{Bmatrix} \underline{X}|_A \\ \dot{\underline{X}}^A|_A \end{Bmatrix} = \begin{bmatrix} R_{B \rightarrow A} & 0_{3x3} \\ R_{B \rightarrow A} \Omega_{B||A}|_B & R_{B \rightarrow A} \end{bmatrix} \begin{Bmatrix} \underline{x}|_B \\ \dot{\underline{x}}^B|_B \end{Bmatrix} + \begin{Bmatrix} \underline{X}_C|_A \\ \dot{\underline{X}}_C^A|_A \end{Bmatrix} \quad (\text{B.11})$$

Comparing (B.4) and (B.10), an interesting property of \dot{R} can be extracted, namely:

$$\dot{R}_{A \rightarrow B} = R_{A \rightarrow B} \Omega_{A||B}|_A$$

which is in turn quite useful, as time derivation of the rotation matrix itself might be quite costly and symbolically dense. This requires though to know the angular velocity vector, whose calculation might not be easy.

B.3 Absolute reference systems.

B.3.1 Earth-Centered-Inertial reference system (ECI).

As previously stated, any Earth-fixed reference system will in turn be non-inertial. That leads to the need of defining a common baseline, *i.e.* an epoch at which the reference system is known. The chosen epoch is denoted as J2000.0¹, which translates to January 1st, at 12:00:00.000 (midday) in Julian years [see 42, glossary]. Effectively, the ECI reference system, is geometrically defined as follows [43]:

$$ECI \equiv \begin{cases} \text{Origin} & \equiv \text{Earth's COM} \\ \text{X-axis} & \equiv \text{Earth's COM} \longrightarrow \text{Mean vernal equinox at epoch J2000.0} \\ \text{Z-axis} & \equiv \text{Normal to the mean equatorial plane at epoch J2000.0,} \\ & \quad \text{pointing towards the Northern Hemisphere} \\ \text{Y-axis} & \equiv \text{Perpendicular to the X and Z axes forming a right-handed system} \end{cases}$$

The main reason behind using this system is that it considerably simplifies the dynamics equation of any spacecraft. It is then the most adequate frame on which dynamics can be solved. Furthermore, when considering relative motion, the reference axis are not a critical axis, as one is rather focused on the motion between spacecrafts. On the other hand, this frame is not able to describe the position relative to Earth's surface, thus being useless in communications or visibility analysis. Moreover, the gravitational field rotates with the Earth, which means that an Earth-Fixed frame needs to be defined for that to be accounted for.

¹J2000 denotes a reference frame, being analog to ECI. J2000.0 refers to the mentioned epoch.

B.3.2 Earth-Centered, Earth-Fixed reference system (ECEF).

Due to the formerly mentioned concerns, another Earth-centered reference frame must be defined. In this case, that will be ECEF. Geometrically, it is defined as [43]

$$ECEF \equiv \begin{cases} \text{Origin} & \equiv \text{Earth's COM} \\ \text{X-axis} & \equiv \text{Earth's COM} \rightarrow \text{Intersection of prime meridian} \\ & \quad \text{with true equatorial plane} \\ \text{Z-axis} & \equiv \text{Earth's true angular velocity vector (rotation axis)} \\ \text{Y-axis} & \equiv \text{Perpendicular to the X and Z axes forming a right-handed system} \end{cases}$$

Once defined, it is turn to evaluate how ECI and ECEF frames differ.

B.3.2.1 Conversion from ECI to ECEF.

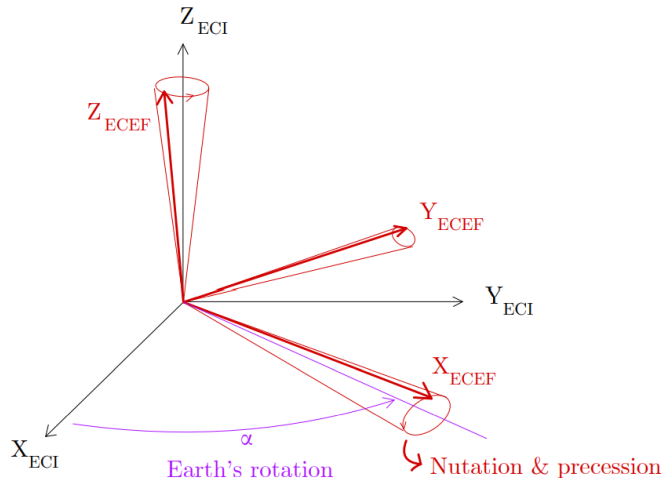


Figure B.2: ECI and ECEF reference frames.

Decomposition of the conversion.

There are four essential differences between ECI and ECEF frame, due to four motions that ECEF include due to it being fixed to Earth:

1. Precession of the equinoxes.
2. Nutations (small oscillations) of the equinoxes.

3. Earth's rotation around its axis.
4. Spin axis motion.

Each of this motions can be characterized by a rotation to an associated frame. That is, the conversion between ECI and ECEF may be decomposed in four rotations, which will now be analyzed.

I. Involved intermediate frames & rotations.

I.A. ECI(J2000) to Mean of Date.

The equinoxes rotate at a slow, but relevant rate. That means that the vernal equinox today differs considerably from the one at J2000.0. The Mean of Date (MOD) frame arises from this notion, being defined as [43]:

$$MOD \equiv \begin{cases} \text{X-axis} & \equiv \text{Earth's COM} \longrightarrow \text{Mean vernal equinox at current epoch} \\ \text{Z-axis} & \equiv \text{Perpendicular to the mean equatorial plane at current epoch} \\ \text{Y-axis} & \equiv \text{Perpendicular to the X and Z axes forming a right-handed system} \end{cases}$$

The rotation matrix from J2000 to MOD results:

$$R_{ECI \rightarrow MOD} = \begin{bmatrix} C\zeta_A C\theta_A Cz_A - S\zeta_A S z_A & -S\zeta_A C\theta_A Cz_A - C\zeta_A S z_A & -S\theta_A Cz_A \\ C\zeta_A C\theta_A S z_A + S\zeta_A Cz_A & -S\zeta_A C\theta_A S z_A + C\zeta_A Cz_A & -S\theta_A S z_A \\ C\zeta_A S\theta_A & -S\zeta_A S\theta_A & C\theta_A \end{bmatrix} \quad (\text{B.12})$$

where the precession angles ζ_A , θ_A and z_A , which are functions of the epoch, are shown in [43], page 519. S and C are abbreviations of the sine and cosine functions.

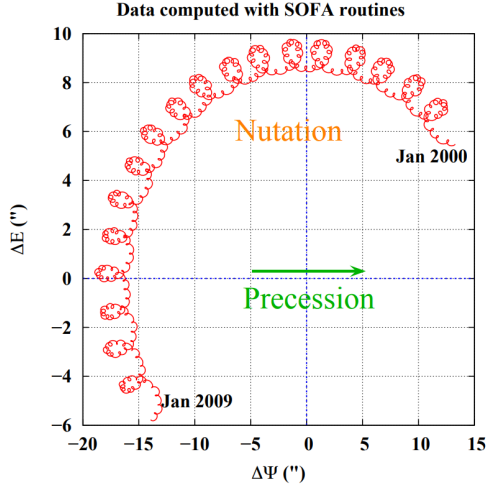


Figure B.3: Nutation and precession motion [44].

I.B. Mean of Date to True of Date.

Besides the “long-term” precession motion, equinoxes suffer also short-period, small oscillations, which are denoted as nutations. For more clarity, see figure B.3. The True of Date (TOD) frame is thus defined as:

$$TOD \equiv \begin{cases} \text{X-axis} & \equiv \text{Earth's COM} \longrightarrow \text{True vernal equinox at current epoch} \\ \text{Z-axis} & \equiv \text{Perpendicular to the true equatorial plane at current epoch} \\ \text{Y-axis} & \equiv \text{Perpendicular to the X and Z axes forming a right-handed system} \end{cases}$$

The rotation matrix now has the following shape:

$$R_{MOD \rightarrow TOD} = \begin{bmatrix} C\Delta\psi & -C\epsilon_m S\Delta\psi & -S\epsilon_m S\Delta\psi \\ C\epsilon_t S\Delta\psi & C\epsilon_m C\epsilon_t C\Delta\psi + S\epsilon_m S\epsilon_t & S\epsilon_m C\epsilon_t C\Delta\psi - C\epsilon_m S\epsilon_t \\ S\epsilon_t S\Delta\psi & C\epsilon_m S\epsilon_t C\Delta\psi - S\epsilon_m C\epsilon_t & S\epsilon_m S\epsilon_t C\Delta\psi + C\epsilon_m C\epsilon_t \end{bmatrix} \quad (\text{B.13})$$

where four angles appear. Firstly, the mean obliquity, which is the angle between the mean ecliptic and the mean equatorial plane ($\approx 23.5^\circ$). For an analytic expression, see [43], page 519. Moreover, two nutations arise: one in longitude and one in obliquity ($\Delta\psi$ and $\Delta\epsilon$, respectively). These angles are computed by a summation of a large number of sinusoidal functions, whose construction and coefficients are shown in [45]. Lastly, the true obliquity is simply the addition of its mean counterpart and the nutation ($\epsilon_t = \epsilon_m + \Delta\epsilon$).

I.C. True of Date to Pseudo-Body-Fixed.

Perhaps the biggest and most intuitive difference between ECI and ECEF is Earth's rotation around its axis. The pseudo-body-fixed is simply a clockwise rotation (seen from north pole towards the Earth's COM) around said axis from the True of Date frame:

$$PBF \equiv \begin{cases} \text{X-axis} & \equiv \text{Earth's COM} \longrightarrow \text{Intersection between prime meridian .} \\ & \quad \text{with true equatorial plane (not accounting for the axis' displacement).} \\ \text{Z-axis} & \equiv \text{Perpendicular to the true equatorial plane at current epoch} \\ \text{Y-axis} & \equiv \text{Perpendicular to the X and Z axes forming a right-handed system} \end{cases}$$

The rotation matrix is now as simple as:

$$R_{TOD \rightarrow PBF} = \begin{bmatrix} C\alpha_G & S\alpha_G & 0 \\ -S\alpha_G & C\alpha_G & 0 \\ 0 & 0 & 1 \end{bmatrix} \quad (\text{B.14})$$

where α_G is referred to as the Greenwich Mean Sidereal Time (GMST). $\dot{\alpha}_G$ is then the rotation rate of the Earth. An analytical expression for this angle is provided in [43], page 520 (eq. H.4.3).

I.D. Pseudo-Body-Fixed to Body-Fixed (ECEF).

The last, and surely most subtle transformation, is the one that accounts for the displacement in Earth's axis of rotation. This displacement is parametrized with the polar angles x_p and y_p , which can again be found at [45]. As these angles are sufficiently small, the rotation matrix from PBF to ECEF is:

$$R_{PBF \rightarrow BF} = \begin{bmatrix} 1 & 0 & x_p \\ 0 & 1 & -y_p \\ -x_p & y_p & 1 \end{bmatrix} \quad (\text{B.15})$$

II. Full rotation matrix $R_{ECI \rightarrow ECEF}$.

By simply successively composing rotations, the full rotation matrix from ECI to ECEF is computed as:

$$R_{ECI \rightarrow ECEF} = R_{PBF \rightarrow ECEF} R_{TOD \rightarrow PBF} R_{MOD \rightarrow TOD} R_{ECI \rightarrow MOD}$$

B.3.3 Perifocal (PQW) reference frame.

B.3.3.1 Definition.

The perifocal reference frame is defined as:

$$PQW \equiv \begin{cases} \text{Origin} & \equiv \text{Central body's COM} \\ \text{X-axis} & \equiv \text{Origin} \rightarrow \text{Periapsis.} \\ \text{Z-axis} & \equiv \text{Perpendicular to the osculating orbital plane (out-of-plane)} \\ \text{Y-axis} & \equiv \text{Perpendicular to the X and Z axes forming a right-handed system} \end{cases}$$

This frame takes advantage of the motion being contained in the orbital plane (when using osculating elements, see section 4.3.1). That means that usually, the problem reduces to evaluating two components of the position and velocity. It also allows for a quite straightforward description of the motion in terms of the Keplerian OEs, assuming elliptical motion. In this case, and using \underline{q} and $\dot{\underline{q}}$ to denote perifocal position and velocity, the perifocal state vector is expressed as:

$$\underline{q} = \begin{Bmatrix} r \cos \theta \\ r \sin \theta \\ 0 \end{Bmatrix} = \begin{Bmatrix} a(\cos E - e) \\ a \sin E \\ 0 \end{Bmatrix}, \quad \dot{\underline{q}} = \frac{na}{\sqrt{1-e^2}} \begin{Bmatrix} -\sin \theta \\ e + \cos \theta \\ 0 \end{Bmatrix}$$

where E is the eccentric anomaly, r is the orbital radius, n is the mean orbital rate and the remaining parameters are the regular Keplerian OEs. r and n can be expressed as a function of them as:

$$r = \frac{a(1-e^2)}{1+e \cos \theta} = a(1-e \cos E); \quad n = \sqrt{\frac{\mu}{a^3}}$$

with $\mu = GM$ being the gravitational parameter of the central body.

B.3.3.2 State vector transformation.

The target is to get an expression analogous to (B.10). As both frames are Earth-centered, $\underline{X}_C = 0$, so that only the rotation and angular velocity matrices are to be found.

I. Rotation matrix from & to ECI.

As done with the ECI to ECEF transformation, this one can also be decomposed in three rotations, each associated with one Keplerian angle.

The first rotation is associated to Ω , being done around the Z ECI axis. The resulting frame will be named I1 (intermediate 1), and the rotation matrix from ECI is:

$$R_{ECI \rightarrow I1}(\Omega) = \begin{bmatrix} \cos \Omega & \sin \Omega & 0 \\ -\sin \Omega & \cos \Omega & 0 \\ 0 & 0 & 1 \end{bmatrix}$$

Afterwards, a rotation around X axis of I1 (nodal line) of value i is performed, leading to frame I2. The rotation matrix is simply:

$$R_{I1 \rightarrow I2}(\Omega) = \begin{bmatrix} 1 & 0 & 0 \\ 0 & \cos i & \sin i \\ 0 & -\sin i & \cos i \end{bmatrix}$$

Finally, a rotation around Z axis of I2 (out-of-plane direction) of value ω is done, yielding the desired perifocal frame (which will be denoted as PQW):

$$R_{I2 \rightarrow PQW}(\Omega) = \begin{bmatrix} \cos \omega & \sin \omega & 0 \\ -\sin \omega & \cos \omega & 0 \\ 0 & 0 & 1 \end{bmatrix}$$

By composition, the matrix $R_{ECI \rightarrow PQW}$ can easily be calculated:

$$R_{ECI \rightarrow PQW} = R_{I2 \rightarrow PQW} R_{I1 \rightarrow I2} R_{ECI \rightarrow I1} = \begin{bmatrix} C\Omega C\omega - S\Omega CiS\omega & S\Omega C\omega + C\Omega CiS\omega & SiS\omega \\ -C\Omega S\omega - S\Omega Cic\omega & C\Omega CiC\omega + S\Omega S\omega & SiC\omega \\ S\Omega Si & -C\Omega Si & Ci \end{bmatrix}$$

II. Angular velocity.

In order to fully transform the system, it is necessary to calculate the relative angular velocity between both frames. Again, that can be done by composing the angular motions:

$$\underline{\omega}_{PQW||ECI} = \dot{\Omega} \hat{k}_{I1} + i \dot{i} \hat{k}_{I2} + \dot{\omega} \hat{k}_{PQW}$$

Expressing everything in PQW frame:

$$\underline{\omega}_{PQW||ECI}|_{PQW} = \begin{Bmatrix} \omega_x \\ \omega_y \\ \omega_z \end{Bmatrix} = \dot{\Omega} R_{ECI \rightarrow PQW} \begin{Bmatrix} 0 \\ 0 \\ 1 \end{Bmatrix} + i R_{I2 \rightarrow PQW} R_{I1 \rightarrow I2} \begin{Bmatrix} 1 \\ 0 \\ 0 \end{Bmatrix} + \dot{\omega} R_{I2 \rightarrow PQW} \begin{Bmatrix} 0 \\ 0 \\ 1 \end{Bmatrix}$$

In virtue of the axial dual form principle, there exists one matrix that, when applied to a certain vector, yields the same result as doing the cross product between $\underline{\omega}$ and that vector. This matrix has the following shape:

$$\Omega_{PQW||ECI}|_{PQW} = \begin{bmatrix} 0 & -\omega_z & \omega_y \\ \omega_z & 0 & -\omega_x \\ -\omega_y & \omega_x & 0 \end{bmatrix}$$

III. Transformation matrices $T_{PQW \rightarrow ECI}$, $T_{ECI \rightarrow PQW}$.

The transformation matrices can easily be built as in (B.10):

$$T_{PQW \rightarrow ECI} = \begin{bmatrix} R_{PQW \rightarrow ECI} & 0_{3x3} \\ R_{PQW \rightarrow ECI} \Omega_{PQW||ECI}|_{PQW} & R_{PQW \rightarrow ECI} \end{bmatrix}$$

whose inverse counterpart can be obtained in terms of the same components, as:

$$T_{ECI \rightarrow PQW} = \begin{bmatrix} R_{PQW \rightarrow ECI}^T & 0_{3x3} \\ -\Omega_{PQW||ECI}|_{PQW} R_{PQW \rightarrow ECI}^T & R_{PQW \rightarrow ECI}^T \end{bmatrix}$$

It is important to note that, as the rotation angles are Keplerian OEs, the unperturbed assumption leads to a null angular velocity (as the orbital plane remains unchanged along time). That greatly simplifies the transformation, turning into a trivial rotation of the position and velocity vectors, which can be expressed as:

$$\begin{cases} \underline{x}_{ECI} = R_{PQW \rightarrow ECI} \underline{q} \\ \dot{\underline{x}}_{ECI} = R_{PQW \rightarrow ECI} \dot{\underline{q}} \end{cases} \quad (\text{B.16})$$

where the functional dependencies are separated, as $R_{PQW \rightarrow ECI}(\Omega, i, \omega)$ and $[\underline{q}, \dot{\underline{q}}] = f(a, e, M)$. This fact will prove useful later on.

B.4 Relative reference systems.

It is time now to address relative reference frames. For each of them, a description is provided, followed by a conversion to and from the ECI reference frame.

B.4.1 RTN reference frame.

B.4.1.1 Definition.

The Radial-Tangential-Normal (RTN) reference frame is defined as [38]:

$$RTN \equiv \begin{cases} \text{Origin} & \equiv \text{Chief SC COM} \\ \text{X-axis}(\underline{e}_R) & \equiv \text{Radial direction (positive outwards)} \\ \text{Z-axis}(\underline{e}_N) & \equiv \text{Normal to the orbit plane (positive with orbit momentum)} \\ \text{Y-axis}(\underline{e}_T) & \equiv \text{Perpendicular to the X and Z axes forming a right-handed system} \\ & (\approx \text{tangent to the trajectory}) \end{cases}$$

A graphical representation of this frame is shown in figure B.4.



Figure B.4: RTN frame [38].

B.4.1.2 State vector transformation.

As before, one needs to build two matrices: The rotation matrix and the angular velocity matrix.

I. Rotation matrix from ECI.

When paying close attention to both PQW and RTN frames, it arises that the rotation matrix is

virtually the same, only changing the value of the last rotation from ω to $u = \theta + \omega$. That is:

$$R_{I2 \rightarrow RTN} = R_{I2 \rightarrow RTN}|_{\omega \rightarrow u} \Rightarrow R_{ECI \rightarrow RTN} = R_{ECI \rightarrow PQW}|_{\omega \rightarrow u}$$

which leads to the following expression:

$$R_{ECI \rightarrow RTN} = \begin{bmatrix} C\Omega Cu - S\Omega CiSu & S\Omega Cu + C\Omega CiSu & SiSu \\ -C\Omega Su - S\Omega CiCu & -S\Omega Su + C\Omega CiCu & SiCu \\ S\Omega Si & -C\Omega Si & Ci \end{bmatrix}$$

II. Angular velocity.

Assuming unperturbed motion, the only time-varying angle is u through the true anomaly. Its rate is in fact:

$$\dot{\theta} = \dot{M} \frac{\rho^2}{\eta^3} = \frac{n\rho^2}{\eta^3}$$

where $\rho = 1 + e \cos \theta$ and $\eta = \sqrt{1 - e^2}$. With this in mind, the angular velocity matrix takes the following form:

$$\Omega_{RTN||ECI}|_{RTN} = \begin{bmatrix} 0 & -\dot{\theta} & 0 \\ \dot{\theta} & 0 & 0 \\ 0 & 0 & 0 \end{bmatrix}$$

III. Transformation matrices $T_{RTN \rightarrow ECI}$, $T_{ECI \rightarrow RTN}$.

The transformation matrices are composed as follows:

$$T_{ECI \rightarrow RTN} = \begin{bmatrix} R_{ECI \rightarrow RTN} & 0_{3x3} \\ -\Omega_{RTN||ECI}|_{RTN} R_{ECI \rightarrow RTN} & R_{ECI \rightarrow RTN} \end{bmatrix}$$

whose inverse counterpart can be obtained in terms of the same components, as:

$$T_{RTN \rightarrow ECI} = \begin{bmatrix} R_{ECI \rightarrow RTN}^T & 0_{3x3} \\ R_{ECI \rightarrow RTN}^T \Omega_{RTN||ECI}|_{RTN} & R_{ECI \rightarrow RTN}^T \end{bmatrix}$$

B.4.2 LVLH reference frame.

B.4.2.1 Definition.

The Local Vertical-Local Horizontal frame (LVLH) may be understood as a different interpretation of the RTN frame. It basically differs from it in the naming and direction of the axis, namely:

$$LVLH \equiv \begin{cases} \text{Origin} & \equiv \text{Chief SC COM} \\ \text{Z-axis}(-\underline{e}_R) & \equiv \text{Radial direction (positive inwards)} \\ \text{Y-axis}(-\underline{e}_N) & \equiv \text{Normal to the orbit plane (cross-track)} \\ & \quad (\text{negative with orbit momentum}) \\ \text{X-axis}(\underline{e}_T) & \equiv \text{Perpendicular to the Y and Z axes (along-track)} \\ & \quad \text{forming a right-handed system } (\approx \text{tangent to the trajectory}) \end{cases}$$

B.4.2.2 State vector transformation.

There are two main ways to obtain the ECI to LVLH frame transformation:

A) Using reference orbit's Keplerian OEs.

This method is the one used for the PQW and the RTN frame. It is as easy as performing yet another rotation from the RTN frame, being consistent with the angular velocity.

I. Rotation matrix from ECI.

The additional rotation from RTN to LVLH is:

$$R_{RTN \rightarrow LVLH} = \begin{bmatrix} 0 & 1 & 0 \\ 0 & 0 & -1 \\ -1 & 0 & 0 \end{bmatrix}$$

leading to the full rotation matrix:

$$R_{ECI \rightarrow LVLH} = R_{ECI \rightarrow RTN} R_{RTN \rightarrow LVLH} = \begin{bmatrix} -C\Omega Su - S\Omega Ci Cu & C\Omega Ci Cu - S\Omega Su & Cu Si \\ -S\Omega Si & C\Omega Si & -Ci \\ -C\Omega Cu + S\Omega Ci Su & -C\Omega Ci Su - S\Omega Cu & -Su Si \end{bmatrix}$$

II. Angular velocity.

Although one could rotate either the vector or the matrix itself, it is actually easier to graphically derive the angular velocity (assuming of course unperturbed motion). Doing this, it can easily be seen that the only angular velocity component is the one in Y-axis, of value $-\dot{\theta}$. The angular velocity matrix then becomes:

$$\Omega_{LVLH||ECI}|_{LVLH} = \begin{bmatrix} 0 & 0 & -\dot{\theta} \\ 0 & 0 & 0 \\ \dot{\theta} & 0 & 0 \end{bmatrix}$$

B) Using reference ECI state vector.

This approach is based on [41], and was introduced in B.2.1. For this transformation to be performed, the rotation matrix and its derivative have to be calculated. With this approach, that is analogous to get the unitary vectors expressed in ECI frame. As the inputs are actually the ECI coordinates and velocity of the chief spacecraft, this is almost already done. The unitary vectors of the rotating frame in this case are:

$$\left\{ \begin{array}{l} \hat{e}_z = -\hat{r} \\ \hat{e}_y = -\hat{h} \\ \hat{e}_x = \hat{e}_y \times \hat{e}_z \end{array} \right. \quad (\text{B.17})$$

where $\hat{h} = \frac{\underline{r} \times \underline{v}}{|\underline{r} \times \underline{v}|}$. \underline{r} and \underline{v} are respectively the position and velocity of the chief spacecraft.

I. Rotation matrix from ECI.

The rotation matrix $R_{ECI \rightarrow LVLH}$ is then:

$$R_{ECI \rightarrow LVLH} = \begin{bmatrix} \hat{e}_x^T \\ \hat{e}_y^T \\ \hat{e}_z^T \end{bmatrix}$$

that is, each unitary vector is transposed into one row of the matrix.

II. Rotation matrix derivative.

By using equation (B.3), the vectors' time derivatives are:

$$\left\{ \begin{array}{lcl} \frac{d}{dt} (\hat{\underline{e}}_z) & = & \frac{d}{dt} (-\hat{\underline{r}}) \\ \frac{d}{dt} (\hat{\underline{e}}_y) & = & \frac{d}{dt} (-\hat{\underline{h}}) \\ \frac{d}{dt} (\hat{\underline{e}}_x) & = & \frac{d}{dt} (\hat{\underline{e}}_y \times \hat{\underline{e}}_z) \end{array} \right. = \begin{array}{l} -\frac{1}{r} [\underline{v} - (\hat{\underline{r}} \cdot \underline{v}) \hat{\underline{r}}] \\ -\frac{1}{h} [\dot{\underline{h}} - (\hat{\underline{h}} \cdot \dot{\underline{h}}) \hat{\underline{h}}] \\ \frac{d}{dt} (\hat{\underline{e}}_y) \times \hat{\underline{e}}_z + \hat{\underline{e}}_y \times \frac{d}{dt} (\hat{\underline{e}}_z) \end{array}$$

where all entities are known except for $\dot{\underline{h}}$, which is in turn:

$$\dot{\underline{h}} = \frac{d}{dt} (\underline{r} \times \underline{v}) = \underline{r} \times \underline{a}$$

Hence, the acceleration of the chief spacecraft needs to be provided when it is not radial. As that is the case with the unperturbed two-body problem, the rotation matrix is significantly simplified:

$$\left\{ \begin{array}{lcl} \frac{d}{dt} (\hat{\underline{e}}_z) & = & -\frac{1}{r} [\underline{v} - (\hat{\underline{r}} \cdot \underline{v}) \hat{\underline{r}}] \\ \frac{d}{dt} (\hat{\underline{e}}_y) & = & \underline{0} \\ \frac{d}{dt} (\hat{\underline{e}}_x) & = & -\hat{\underline{h}} \times \frac{d}{dt} (\hat{\underline{e}}_z) \end{array} \right.$$

The construction of $\dot{\underline{R}}_{ECI \rightarrow LVLH}$ is identical to its primitive. The transformation matrices can now be built, following equations B.4 and B.5.

B.4.3 TAN reference frame.

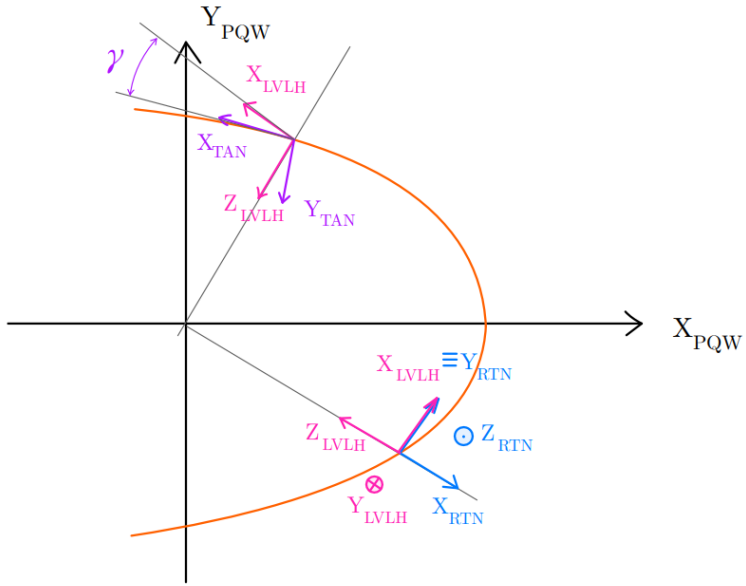


Figure B.5: Relative reference frames.

B.4.3.1 Definition.

The Tangent reference frame (TAN) is quite similar to the LVLH frame, but instead of featuring an axis pointing towards *nadir* (Earth), this frame includes an axis pointing always in the velocity direction. This involves a simple rotation from the LVLH frame, of an angle γ called flight path angle (see figure B.5). It is then unsurprisingly defined as the angle between the horizon (local horizontal) and the velocity vector. The transformation from the LVLH frame is now described [21].

B.4.3.2 State vector transformation.

I. Rotation matrix from LVLH.

In this case, it is a simple clockwise rotation around LVLH Y-axis, that is:

$$R_{LVLH \rightarrow TAN} = \begin{bmatrix} \cos \gamma & 0 & -\sin \gamma \\ 0 & 1 & 0 \\ \sin \gamma & 0 & \cos \gamma \end{bmatrix}$$

II. Angular velocity.

As it has been explained before, the angular velocity matrix can be written as:

$$\Omega_{LVLH \rightarrow TAN}|_{LVLH} = \begin{bmatrix} 0 & 0 & -\dot{\gamma} \\ 0 & 0 & 0 \\ \dot{\gamma} & 0 & 0 \end{bmatrix}$$

There is something remaining: γ and its derivative must be calculated. Starting with the angle itself, its sine and cosine satisfy:

$$\begin{cases} \sin \gamma = \frac{e \sin \theta}{\Theta} \\ \cos \gamma = \frac{\rho}{\Theta} \end{cases}$$

where $\Theta = \sqrt{2\rho - \eta^2}$. γ is simply calculated as:

$$\gamma = \text{atan2}(\sin \gamma, \cos \gamma)$$

On the other hand, $\dot{\gamma}$ can be calculated as:

$$\dot{\gamma} = n \frac{\rho^2 (\rho - \eta^2)}{\eta^3 \Theta^2}$$

Therefore, the transformation is complete.

B.5 Conversions from OEs to cartesian coordinates.

B.5.1 Keplerian OEs to ECI and vice versa.

B.5.1.1 KOE to ECI transformation.

By considering the perifocal coordinates $(\underline{q}, \dot{\underline{q}})$ (see B.3.3), an explicit relation from Keplerian OEs to the ECI state vector can easily be derived:

$$\begin{cases} x = (\cos \Omega \cos u - \sin \Omega \cos i \sin u) r \\ y = (\sin \Omega \cos u + \cos \Omega \cos i \sin u) r \\ z = (\sin i \sin u) r \\ \dot{x} = (\cos \Omega \cos u - \sin \Omega \cos i \sin u) v_R - (\cos \Omega \sin u + \sin \Omega \cos i \cos u) v_T \\ \dot{y} = (\sin \Omega \cos u + \cos \Omega \cos i \sin u) v_R - (\sin \Omega \sin u - \cos \Omega \cos i \cos u) v_T \\ \dot{z} = (\sin i \sin u) v_R + (\cos u \sin i) v_T \end{cases}$$

where v_R and v_T are the radial and tangential velocities, namely:

$$\begin{cases} v_R = \dot{r} = \frac{h}{p} e \sin \theta \\ v_T = r\dot{\theta} = \frac{h}{p} \rho \end{cases}$$

B.5.1.2 ECI to KOE transformation.

This transformation is considerably more complex. For that reason, the relations will not be entirely justified. These are the following:

- Semimajor axis: Directly from energy equation:

$$a = \frac{r}{2 - \frac{rv^2}{\mu}}$$

- Eccentricity: Prior relations arise from (a) the dot product of velocity and position and (b) the polar equation of the ellipse:

$$\begin{cases} e \sin \theta = \frac{h}{\mu r} \mathbf{r} \cdot \mathbf{v} \\ e \cos \theta = \frac{p}{r} - 1 \end{cases} \Rightarrow e = \sqrt{(e \sin \theta)^2 + (e \cos \theta)^2}$$

- Inclination From the orientation of the angular momentum vector:

$$i = \text{atan2}(h_{xy}, h_z)$$

$$\text{where } h_{xy} = \sqrt{h_x^2 + h_y^2}$$

The remaining elements (Ω , ω and M) depend on the type of the orbit. If the orbit is equatorial ($i = 0$), Ω and ω are not defined by themselves. Furthermore, if the orbit is circular, not even ω is defined, and therefore it is necessary to make some adjustments. In the first case, $\varpi = \omega + \Omega$ is assumed as our fifth element, and the fourth will be null. In the second case, all values will be merged into the mean anomaly, assuming both ω and Ω to be null.

Case A) Non-singular eccentricity or inclination.

$$\begin{cases} \Omega = \text{atan2}(h_x, -h_y) \\ u = \text{atan2}(h \cdot z, y \cdot h_x - x \cdot h_y) \\ \theta = \text{atan2}(e \sin \theta, e \cos \theta) \\ \omega = u - \theta \end{cases}$$

Case B) Null inclination, non-singular eccentricity.

$$\begin{cases} \Omega = 0 \\ u = \text{atan2}(y, x) \cdot \text{sign}(h_z) \\ \theta = \text{atan2}(e \sin \theta, e \cos \theta) \\ \omega = u - \theta \end{cases}$$

Case C) Null eccentricity, non-singular inclination.

Auxiliary definitions:

$$\begin{cases} \underline{N} = \hat{\underline{e}}_z \times \underline{h} \\ N_{xy} = \sqrt{N_x^2 + N_y^2} \\ S = \text{sign}((\underline{e} \times \underline{r}) \cdot \underline{h}) \end{cases}$$

Element computation:

$$\begin{cases} \Omega = \text{atan2}(h_x, -h_y) \\ \omega = 0 \\ \theta = S \cdot \arccos\left(\frac{\underline{r}}{r}, \frac{\underline{N}}{N_{xy}}\right) \end{cases}$$

Case D) Null eccentricity and inclination.

$$\begin{cases} \Omega = 0 \\ \omega = 0 \\ \theta = \text{atan2}(y, x) \cdot \text{sign}(h_z) \end{cases}$$

B.5.2 Relative Keplerian OEs to RTN.

Although one can technically go from RKOEs to RTN coordinates in several steps already described, there is a direct mapping between them, developed by H. Schaub [40]. Without further

ado, the position mapping is expressed as follows:

$$\begin{cases} x \approx \frac{r}{a} \delta a + \frac{ae \sin \theta}{\eta} \delta M - a \cos \theta \delta e \end{cases} \quad (\text{B.18a})$$

$$\begin{cases} y \approx \frac{r \rho^2}{\eta^3} \delta M + r \delta \omega + \frac{r \sin \theta}{\eta^2} (\rho + 1) \delta e + r \cos i \delta \Omega \end{cases} \quad (\text{B.18b})$$

$$\begin{cases} z \approx r (\sin u \delta i - \cos u \sin i \delta \Omega) \end{cases} \quad (\text{B.18c})$$

Nonetheless, the mapping for the velocity is expressed in terms of relative quasi-non-singular OEs [46]. For the conversion from RKOEs to these, please see [A](#):

$$\begin{cases} \dot{x} \approx -\frac{V_r}{2a} \delta a + \left(\frac{1}{r} - \frac{1}{p} \right) h \delta u \\ + (V_r a q_1 + h \sin u) \frac{\delta q_1}{p} + (V_r a q_2 - h \cos u) \frac{\delta q_2}{p} \end{cases} \quad (\text{B.19a})$$

$$\begin{cases} \dot{y} \approx -\frac{3V_t}{2a} \delta a - V_r \delta u + (3V_t a q_1 + 2h \cos u) \frac{\delta q_1}{p} \\ + (3V_t a q_2 + 2h \sin u) \frac{\delta q_2}{p} + V_r \cos i \delta \Omega \end{cases} \quad (\text{B.19b})$$

$$\begin{cases} \dot{z} \approx (V_t \cos u + V_r \sin u) \delta i \\ + (V_t \sin u - V_r \cos u) \sin i \delta \Omega \end{cases} \quad (\text{B.19c})$$

The mapping represented by equations (B.18) and (B.19) is a linear approximation, in which it is assumed that the relative distance between spacecrafts is much smaller than the chief's orbital radius. For more in-depth content about this transformation, please see [40, 46].

Analytical mechanics applied to the two-body problem.

C.1 Introduction.

Lagrangian and Hamiltonian mechanics are the two most widely used approaches to analytical mechanics, which constitute a generalization of the classical Newtonian mechanics. These formalisms are closely related to each other, and they usually lead to the same solution. Both approaches will be here succinctly described, as they embody significant advantages for the treatment of some problems of relative motion. For more in-depth content on this topic, please see [2, 9].

C.2 Lagrangian formulation.

C.2.1 Generalized coordinates & energy of a dynamical system.

Consider any given dynamical system. Lagrangian mechanics deal with a configuration space Q , which is parametrized by a set of generalized coordinates $q_i \in Q$ and generalized velocities \dot{q}_i . It is through (q_i, \dot{q}_i) how said dynamical system will be described.

The equations that describe the evolution of the system can be reached through two main approaches. The first one is the Lagrangian formulation, which is described next.

C.2.2 Lagrangian function.

For a conservative system, the Lagrangian function \mathcal{L} is a function of the time and the generalized coordinates and velocity, and it is defined as:

$$\mathcal{L}(q_i, \dot{q}_i, t) = T - U$$

where T and U are respectively the kinetic and potential energy of the system.

C.2.3 Lagrange equations.

Hamilton's variational principle states that the variation of the integral of the Lagrangian must be zero, that is:

$$\delta \int_a^b \mathcal{L}(q_i, \dot{q}_i, t) dt = 0 \quad (\text{C.1})$$

The differential counterpart of (C.1) can be reached by using calculus of variations, leading to:

$$\frac{d}{dt} \frac{\partial \mathcal{L}}{\partial \dot{q}_i} - \frac{\partial \mathcal{L}}{\partial q_i} = 0 \quad (\text{C.2})$$

C.3 Hamiltonian formulation.

C.3.1 Hamiltonian function.

Hamiltonian formulation is a very widely used alternative to the Lagrangian one. The Hamiltonian function H is defined as:

$$H(q_i, \dot{q}_i, t) = \sum_i p_i \dot{q}_i - \mathcal{L}(q_i, \dot{q}_i, t) \quad (\text{C.3})$$

where p_i are the so-called conjugate momenta, who are defined as:

$$p_i = \frac{\partial \mathcal{L}}{\partial \dot{q}_i} \quad (\text{C.4})$$

C.3.2 Hamilton equations.

The Hamiltonian definition (C.3) can be substituted into (C.2). Identifying coefficients leads to Hamilton's equations:

$$\begin{cases} \dot{q}_i = \frac{\partial H}{\partial p_i} \\ \dot{p}_i = -\frac{\partial H}{\partial q_i} \end{cases} \quad (\text{C.5})$$

C.3.3 Canonical transformations.

As with many mathematical problems, a change of variable might simplify the solution process of Hamilton equations. Nonetheless, this must be done carefully, as the variables must remain canonical. Canonical variables are those for which Hamilton's equations (C.5) are satisfied. Assuming the original set (q_i, p_i) is canonical, a different canonical set (Q_i, P_i) is obtained through a so-called canonical transformation.

A new Hamiltonian function appears by merely substituting the variable change $(Q_i, P_i) = f(q_i, p_i, t)$ into (C.3), which is denoted by $K(Q_i, P_i, t)$. Hamilton's equations will by definition be obeyed:

$$\begin{cases} \dot{Q}_i = \frac{\partial K}{\partial P_i} \\ \dot{P}_i = -\frac{\partial K}{\partial Q_i} \end{cases} \quad (\text{C.6})$$

Applying Hamilton's principle (C.1) for both sets and substituting (C.3), leads to:

$$\delta \int_a^b \left(\sum_{i=1}^N p_i \dot{q}_i - H \right) dt = 0 \quad (\text{C.7a})$$

$$\delta \int_a^b \left(\sum_{i=1}^N P_i \dot{Q}_i - K \right) dt = 0 \quad (\text{C.7b})$$

The variation of both integrals is identically zero, and although the integrands describe the same dynamical system, they may not be equal. Anyway, it is derived that they can only differ by the total derivative of an arbitrary function F , so that:

$$\delta \int_a^b \left(\sum_{i=1}^N p_i \dot{q}_i - H(p_i, q_i, t) - \sum_{i=1}^N P_i \dot{Q}_i + K(Q_i, P_i, t) - \frac{dF}{dt} \right) dt = 0 \quad (\text{C.8})$$

The function F is the so-called generating function of the transformation. It provides a time-dependent relation between the old (q_i, p_i) and the new (Q_i, P_i) phase spaces. There are four possibilities, depending on which generalized coordinates and/or conjugate momenta are selected as independent variables. The actual relations for the canonical transformation for each of the four cases is provided in table C.1.

$F_1(q_i, Q_i, t)$	$F_2(q_i, P_i, t)$	$F_3(p_i, Q_i, t)$	$F_4(p_i, P_i, t)$
$p_i = \frac{\partial F_1}{\partial q_i}$	$p_i = \frac{\partial F_2}{\partial q_i}$	$q_i = -\frac{\partial F_3}{\partial p_i}$	$q_i = -\frac{\partial F_4}{\partial p_i}$
$P_i = -\frac{\partial F_1}{\partial Q_i}$	$Q_i = \frac{\partial F_2}{\partial P_i}$	$P_i = -\frac{\partial F_3}{\partial Q_i}$	$Q_i = \frac{\partial F_4}{\partial P_i}$

Table C.1: Canonical transformation relations [9].

A further relationship, which is common for all the types of generating functions F , allows to

get the new hamiltonian K in terms of the old one H and the generating function itself:

$$K(Q_i, P_i, t) = H(q_i, p_i, t) + \frac{\partial F}{\partial t} \quad (\text{C.9})$$

C.3.4 Hamilton-Jacobi theory.

It is clear that expressing a problem in a certain choice of coordinates can dramatically help with its solution. A possible approach would be to find the transformation which leads to the most simple form of the problem. In this case, the more coordinates or momenta that are missing in the transformed Hamiltonian (C.9), the more momenta or coordinates are constant. The most advantageous situation then would be that the Hamiltonian itself is null, which translates into a constant set of generalized coordinates and conjugate momenta. This is expressed mathematically as:

$$H(q_i, p_i, t) + \frac{\partial F}{\partial t} = 0 \quad (\text{C.10})$$

which is called the Hamilton-Jacobi equation. It is valid for all kinds of transforming functions, although generally, it is applied for $F_2(q_i, P_i)$, meaning:

$$H\left(q_i, \frac{\partial F_2}{\partial q_i}, t\right) + \frac{\partial F_2}{\partial t} = 0 \quad (\text{C.11})$$

This last equation is a partial differential equation for F_2 , which is also known as Hamilton's principal function, denoted by S . Now, the approach to the problem has changed. The direct variant seeks to achieve the transformed Hamiltonian once the generating function has been built. Conversely, the Hamilton-Jacobi approach goes the opposite way: knowing what it is to be achieved (a null hamiltonian), the generating function is calculated. This is a staggering fact: deeply, it means that the solution to the dynamical system in the original phase space (q_i, p_i) involves a new phase space (Q_i, P_i) in which all of the coordinates and conjugate momenta are constant.

Additionally, in the common case that the hamiltonian is not an explicit function of time:

$$H\left(q_i, \frac{\partial S}{\partial q_i}\right) + \frac{\partial S}{\partial t} = 0 \quad (\text{C.12})$$

Separating the variables of Hamilton's principal function:

$$S(q_i, P_i, t) = W(q_i, P_i) + S_t(t) \quad (\text{C.13})$$

where W is called Hamilton's characteristic function. Substituting (C.13) into (C.12):

$$H \left(q_i, \frac{\partial W}{\partial q_i} \right) + \frac{dS}{dt} = 0 \quad (\text{C.14})$$

This way, two different terms that are functions of different variables arise. It is clear that if two functions of different variables are equal, both must be constant, so that:

$$\begin{cases} \frac{dS_t}{dt} = -P_1 \Rightarrow S_t(t) = -P_1 t \end{cases} \quad (\text{C.15a})$$

$$\begin{cases} H \left(q_i, \frac{\partial W}{\partial q_i} \right) = P_1 \end{cases} \quad (\text{C.15b})$$

Hamilton-Jacobi theory is object of a very wide range of application. Nonetheless, the next section focuses on how it transforms and simplifies the two-body problem.

C.4 Application to the two-body problem.

Wiesel [9] provides a succinct variational approach for the two body problem. In particular, the Hamiltonian function of a certain body rotating within the gravity a central body can be expressed as:

$$H = \frac{1}{2} \left(p_r^2 + \frac{1}{r^2} p_\theta^2 + \frac{1}{r^2 \sin^2 \theta} p_\phi^2 \right) - \frac{\mu}{r} \quad (\text{C.16})$$

where r is the radial distance, θ is the latitude and ϕ is the longitude. As H is not an explicit function of the time, the Hamilton-Jacobi equation follows directly to the next expression:

$$\frac{1}{2} \left(\left(\frac{\partial W}{\partial r} \right)^2 + \frac{1}{r^2} \left(\frac{\partial W}{\partial \theta} \right)^2 + \frac{1}{r^2 \sin^2 \theta} \left(\frac{\partial W}{\partial \phi} \right)^2 \right) - \frac{\mu}{r} \equiv P_E \quad (\text{C.17})$$

where P_E is the first conjugante momentum of the new canonical variables, and corresponds with the total energy of the orbit. As it can be seen, equation (C.17) is separable, that is, each derivative can be isolated and assumed to be constant (alone or together with a coefficient).

Firstly, it is assumed that the generating function W is of the following form:

$$W = W_r(r) + W_\theta(\theta) + W_\phi(\phi)$$

Substituting this into (C.17), it is possible to separate to one side of the equation all dependence on ϕ . This leads, after some manipulation, to:

$$\frac{dW_\phi}{d\phi} \equiv P_\phi = p_\phi \quad (\text{C.18})$$

which leads to:

$$\frac{1}{2} \left(\left(\frac{\partial W}{\partial r} \right)^2 + \frac{1}{r^2} \left\{ \left(\frac{\partial W}{\partial \theta} \right)^2 + \frac{1}{r^2 \sin^2 \theta} (P_\phi)^2 \right\} \right) - \frac{\mu}{r} = P_E \quad (\text{C.19})$$

It can be easily identified that the only θ -dependent part of the equation is enclosed by the braces, which leads to:

$$\left(\frac{\partial W}{\partial \theta} \right)^2 + \frac{1}{r^2 \sin^2 \theta} (P_\phi)^2 \equiv P_3^2 \quad (\text{C.20})$$

As of now, three new constant conjugate momenta have been reached. Half of the problem is now solved, as the actual form of the generating function W is still to be found, which allows the calculation of the generalized coordinates Q_i . This involves a much more arduous manipulation which will not be herewith developed: just quoted.

The constant coordinate Q_E conjugate to the total energy P_E needs to be a constant time, as its time derivative has to be non-dimensional. This time turns out to be the perigee passage time T_0 , or most commonly, its negative $-T_0$. P_3 represents the total angular momentum, whose conjugate coordinate is the argument of perigee ω . Finally, the conjugate coordinate to the z-angular momentum P_ϕ is the RAAN Ω .

As imposed, the new Hamiltonian function $K(Q_i, P_i)$ is null, which then again means that both the coordinates and the conjugate momenta are conserved along the motion.

Software & simulator.

D.1 Software tool: Matlab

Software development represents a very large and meaningful part of this thesis. It allows to understand, replicate, compare and analyze the results that are provided in the literature. As this involves a fast prototyping approach, non-compiled programming languages are the most rewarding choice. In this case, the particular choice is MATLAB in its 2017a release. The selection of said release is due to its stability and relatively long period of usage, assuring up to a certain grade that unfound errors are unlikely to appear.

While being a commercial software tool, MATLAB also provides a sharing platform (MATLAB exchange) in which many useful libraries and functionalities can be found. As it will later be explained, the code repository developed for this thesis includes some MATLAB exchange files, which will be duly quoted.

D.2 Code repository.

D.2.1 Purpose and approach.

The purpose of this code repository is to comprehend a self-contained tool which can simulate a variety of relative dynamics models as well as perturbation theories, not forgetting all the utilities and libraries that support them. The followed approach is to implement incrementally more complex models in both topics, developing or including on the go the required auxiliary functions.

A version control system has been implemented, in order to keep track of changes and develop new features in a structured way. In the future, a Continuous Integration workflow should be integrated, in order to streamline the development, testing and integration of the new features or the solution of known issues.

D.2.2 General structure.

D.2.2.1 Relative dynamics models.

In line with the developed theory throughout the thesis, the following relative dynamics models have been implemented:

- I. High-fidelity cartesian propagator: Explained in more detail in section D.2.4, this model consists on the direct integration of Newton's equations considering a certain amount of effects (central body, third bodies, non-spherical gravity, . . .). It provides a truth value for any orbit propagation model, acting as a benchmark for testing them.
- II. Circular unperturbed model: Includes all the methods of propagating Hill/Clohessy-Wiltshire equations, as shown in chapter 2.
- III. Eccentric unperturbed model: Refers to the Yamanaka-Ankersen [4] model and the safe orbit theory developed by Peters and Noomen [21], both explained in chapter 3.
- IV. Perturbed model: A simplified perturbed model has been implemented following D'Amico [38], which is restricted to near-circular orbits. Future work should also focus on the implementation of the later described perturbation models into relative dynamics, enlarging this section.

D.2.2.2 Perturbation models.

The implemented perturbation models are listed below:

- I. Gauss Variational Equations (GVEs): Truth model based on the implementation of GVEs (see appendix E.2) for different accelerations, mainly related to Earth's asphericity.
- II. Lagrange Planetary Equations (LPEs): Another truth model that in this case considers the LPEs, which can be understood as a potential form of the GVEs.
- III. Gim-Alfriend model[5]: Derived from Brouwer's theory [30], involves a mean to osculating element transformation that allows for a very simple integration of GVEs.
- IV. Kaula's theory [32]: Includes the implementation of Kaula's functions and its testing against LPEs.

D.2.2.3 Input.

Besides the surveyed models themselves, a vital part of the repository lies on the input folder. It basically contains two types of things: Body data and orbit scenarios. Each of them is next described:

1. Body Data: This subfolder includes three types of parameters: celestial body data (*e.g.* radii, gravitational parameter, …, based on SPICE database), physical constants (*e.g.* AU, solar constant, …) and spacecraft data (*e.g.* ID, mass, …). These three types of data can be held in the same file, as it will later be shown.
2. Scenarios: Includes several files with the needed data for propagating certain scenarios under certain assumptions. It includes the following data:
 - Scenario ID: Identifier of the scenario.
 - Force flags: Used to select the effects to take into account for the High-Fidelity simulation.
 - Propagation parameters: Includes all the data related to time propagation (*e.g.* timestep, initial epoch, …)
 - Initial conditions: Contains the reference orbit’s orbital elements and the relative state between chief and deputy.
 - Graphics settings: Comprises the setup of the figure computation (*e.g.* title, save path, legend, …).

Computationally, this data is accessed within MATLAB as a structure, which means that it can be accessed as `BodyData.EarthData.mu`, for example, or `Scenario.force_flags.J2`. This allows for a very intuitive manipulation, rather than having a large number of individual variables.

The question now is, how to load said parameters into MATLAB. This can be done by running a MATLAB function that returns the structure file after loading each value one by one or, alternatively, through a JSON file. A JSON file stores simple data structures and objects in JavaScript Object Notation (JSON), and its main advantages are their light weight, the easy human read and the very fast computer read. Although MATLAB has some interfaces to work with this type of files, a in-house set of functions has been developed.

D.2.2.4 Utilities.

Orbit propagation as well as its pre- and postprocessing require a decent amount of auxiliary functions, which can be more or less related to orbital mechanics. The Utilities folder gives place to those that are either used in more than one topic (*e.g.* element conversion) or that are not strictly related to orbital mechanics (*e.g.* Graphics, mathematical functions). The folder itself is structured as:

- I. Angle conversions: Includes the functions that convert between absolute and relative anomalies (true, eccentric and mean), and between date and sidereal angle.
- II. Element conversions: Contains the functions that compute the transformations between the different state descriptions of a spacecraft (cartesian or orbital element based). These are explained in more detail in appendix A and B.
- III. Graphics: This folder comprises the main and the auxiliary functions used for graphic representation, allowing for a much sleeker data evaluation in code prototyping.
- IV. Input-Output (I-O): Contains the functions used for input data preprocessing and for file generation (except figures, which is handled by the preceding subfolder).
- V. Math functions: Includes general math functions (dot product, angle wrapping...) and numerical propagators, which act more of a template to be tailored for different purposes.
- VI. Miscellaneous: Gives place to functions related to MATLAB manipulation (strings, paths, ...)

D.2.3 General orbit propagation workflow.

The usual workflow followed to simulate an orbit or a relative dynamics scenario goes as follows:

I. Parameter load and scenario preprocessing

This preprocessing stage consists on accessing and manipulate the data contained in the Input folder. First, the `DynStruct` variable is loaded through its namesake JSON file, which contains the celestial body data, constants and spacecraft data. Afterwards, the `Scenario` is loaded and preprocessed, procedure in which the following things are done:

- 1st** JSON file is read.
- 2nd** Reference orbit's OEs are converted to Keplerian.
- 3rd** Deputy's relative state is converted to LVLH frame (*Only in relative dynamics*).
- 4th** Keplerian orbital period is computed (for representation purposes).
- 5th** Initial epoch is converted to MJD2000 format.
- 6th** Required number of timesteps is calculated (for variable allocation).

II. Trajectory propagation

In this stage, each spacecraft's orbit is computed, or in case of pure relative dynamics models, the relative motion is directly computed.

III. Graphical representation

The desired results are plotted through the use of graphics functions.

D.2.4 High-Fidelity simulator.

As it is not explained elsewhere in the thesis, this section is dedicated to briefly describe how the High-Fidelity simulator works. Firstly, the computation of a single orbit will be introduced, to later explain how relative dynamics are derived from individual orbits.

D.2.4.1 Single orbit propagation.

I. Main function: propRK4_HiFi

This main function is in charge of, given a scenario, a set of parameters and the hierarchy of the spacecraft (chief/target or deputy/chaser), returning the spacecraft's ECI state vector along time. It mainly consists of a time loop in which the trajectory is integrated through a Runge-Kutta 4-step algorithm. A graphical representation of the workflow this function goes through is shown in figure D.1.

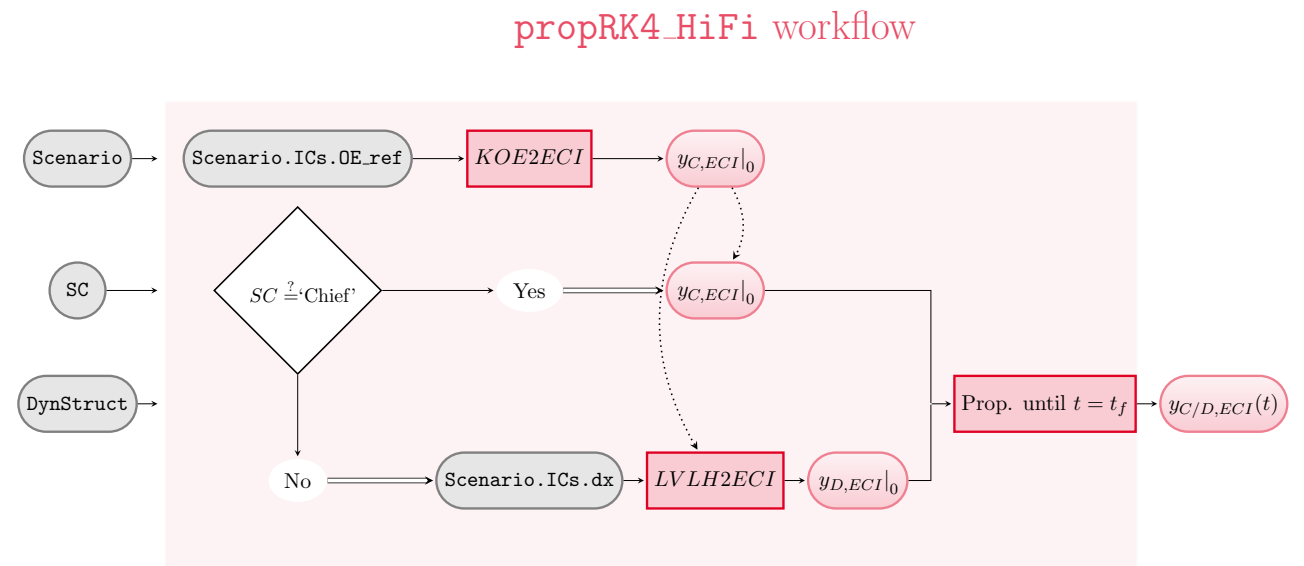


Figure D.1: Workflow of the High-Fidelity propagator.

II. Dynamics function: SCDynamicsMatlab

The Runge-Kutta method (and any integrator really) requires a function that calculates the time derivative of the variable vector (the ECI state vector in this case). For the High-Fidelity integrator, this function – called `SCDynamicsMatlab` – adds up every considered force for this scenario. This is done through the previously described force flags, which enable or not the calculation of each effect. The available effects to consider are:

- Central body acceleration.
- Non-spherical gravity of the Earth: Either a full gravity model or a J_2 model.
- Third body perturbations from Sun and Moon.
- Solar radiation pressure.

D.2.4.2 Relative dynamics propagation.

The dynamics of a deputy around a chief spacecraft are represented through a LVLH state vector. As one would expect, this can be done by simply propagating both spacecrafts as explained before to then, somehow, transform the deputy's state vector to a chief-centered LVLH frame. This is simply shown in D.2.

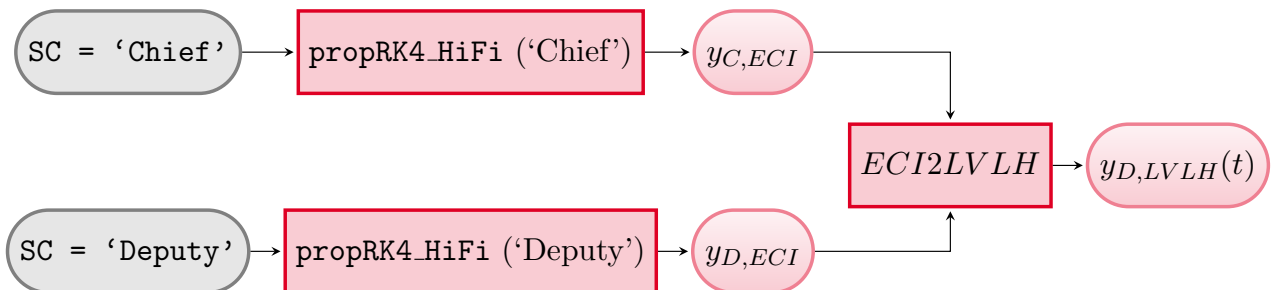


Figure D.2: Workflow of the relative dynamics computation through the Hi-Fi simulator.

D.2.5 Matlab Exchange libraries.

The MATLAB Exchange libraries used in this repository are cited in the bibliography. They mainly have to do with either graphics or input/output operations, involving no technical knowledge that should be herewith described.

Miscellaneous

E.1 State Transition Matrices.

E.1.1 STM for circular, unperturbed reference orbit.

As analyzed in chapter 2, out of the four surveyed HCW methods, only two of them provide a true closed-form expression for the STM. Furthermore, as these two are mere different approaches or decompositions of the same matrix, the simplest result will be here shown: that is, the Clohessy-Wiltshire solution STM:

$$\Phi(t, t_0) = \begin{bmatrix} 1 & 0 & 6(\omega\tau - \sin \omega\tau) & \frac{4}{\omega} \sin \omega\tau - 3\tau & 0 & \frac{2}{\omega}(1 - \cos \omega\tau) \\ 0 & \cos \omega\tau & 0 & 0 & \frac{1}{\omega} \sin \omega\tau & 0 \\ 0 & 0 & 4 - 3 \cos \omega\tau & \frac{2}{\omega}(\cos \omega\tau - 1) & 0 & \frac{1}{\omega} \sin \omega\tau \\ 0 & 0 & 6\omega(1 - \cos \omega\tau) & 4 \cos \omega\tau - 3 & 0 & 2 \sin \omega\tau \\ 0 & -\omega \sin \omega\tau & 0 & 0 & \cos \omega\tau & 0 \\ 0 & 0 & 3\omega \sin \omega\tau & -2 \sin \omega\tau & 0 & \cos \omega\tau \end{bmatrix} \quad (\text{E.1})$$

E.1.2 STM for elliptic, unperturbed reference orbit.

The one and only implementation is the state-of-the-art Yamanaka-Ankersen STM, which is computed through:

$$\Phi_{\theta_0}^\theta = \Phi_\theta (\Phi_{\theta_0})^{-1} \quad (\text{E.2})$$

where:

$$\Phi_\theta = \begin{bmatrix} 1 & 0 & -c(1 + \rho^{-1}) & s(1 + \rho^{-1}) & 0 & 3\rho^2 J \\ 0 & \cos\theta & 0 & 0 & \sin\theta & 0 \\ 0 & 0 & s & c & 0 & 2 - 3esJ \\ 0 & 0 & 2s & 2c - e & 0 & 3(1 - 2esJ) \\ 0 & -\sin\theta & 0 & 0 & \cos\theta & 0 \\ 0 & 0 & s' & c' & 0 & -3e(s'J + s/\rho^2) \end{bmatrix} \quad (\text{E.3a})$$

$$\Phi_{\theta_0}^{-1} = \frac{1}{1 - e^2} \times \begin{bmatrix} 1 - e^2 & 0 & 3e(s/\rho)(1 + \rho^{-1}) & -es(1 + \rho^{-1}) & 0 & 2 - ec \\ 0 & (1 - e^2)\cos\theta & 0 & 0 & -(1 - e^2)\sin\theta & 0 \\ 0 & 0 & -3(s/\rho)(1 + e^2/\rho) & s(1 + \rho^{-1}) & 0 & c - 2e \\ 0 & 0 & -3(c/\rho + e) & c(1 + \rho^{-1}) + e & 0 & -s \\ 0 & (1 - e^2)\sin\theta & 0 & 0 & (1 - e^2)\cos\theta & 0 \\ 0 & 0 & 3\rho + e^2 - 1 & -\rho^2 & 0 & es \end{bmatrix} \quad (\text{E.3b})$$

It shall be remarked that this matrices operates on the modified LVLH state vector, derived from the original LVLH state vector. If one wishes to have an expression for the STM in which a true LVLH state vector is fed and returned, a slight modification must be performed:

$$\Phi(t, t_0) = (T_\theta(\theta))^{-1} \Phi_\theta (\Phi_{\theta_0})^{-1} T_\theta(\theta_0) \quad (\text{E.4})$$

where $T_\theta(\theta)$ is the matrix that converts a regular LVLH state vector into the modified form.

E.1.3 STM for elliptic, J2-perturbed orbit.

Outlined in section 5.2, the Gim-Alfriend STM components is specified in [5], appendices A to E.

E.2 Variational equations.

The equations of motion of a spacecraft immersed in a potential field V can be expressed, in an inertial reference frame, as:

$$\ddot{\underline{x}} = \nabla V = \underline{a}$$

These equations can be converted, as usual, to a system of six first-order equations, by treating the velocity components as variables. Accordingly:

$$\begin{cases} \frac{d}{dt}x_i = \dot{x}_i \\ \frac{d}{dt}\dot{x}_i = \frac{\partial V}{\partial x_i} = a_i \end{cases} \quad i = 1, 2, 3 \quad (\text{E.5})$$

One can expect that these coordinates and velocities change rapidly, requiring a smaller integration timestep. However, it is known that there are some phase spaces in which the state vector does not change so quickly, if it change at all. The obvious example for this is the Keplerian Orbital Elements, which for the two body problem remain constant (except for the mean anomaly, which grows linearly). If the target is to analyze a problem that differs very slightly from the two body problem, an interesting approach would be to use the Keplerian Elements as a parametrization, as they would change slowly. The question now is, how to express the equations of motion in terms of the orbital elements (Keplerian in this case).

This is where the variational equations appear, as they are (by construction) said equations. There are two approaches, depending on whether it is desirable to work with perturbation potentials (V) or perturbation accelerations (a), which are the so-called Lagrange Planetary Equations (LPEs) and the Gauss Variational Equations (GVEs) respectively.

E.2.1 Lagrange Planetary Equations.

The procedure followed herewith is derived from Kaula [32]. Firstly, the rates of change of position and velocity are assumed to be functions of the rates of change of the Keplerian OEs ds_k/dt , where s_k represents any of $a, e, i, \Omega, \omega, M$. Equation (E.5) can be then reformulated as:

$$\sum_{k=1}^6 \frac{\partial x_i}{\partial s_k} \cdot \frac{ds_k}{dt} = \frac{\partial x_i}{\partial s_k} \cdot \frac{ds_k}{dt} = \dot{x}_i, \quad i = 1, 2, 3 \quad (\text{E.6})$$

$$\sum_{k=1}^6 \frac{\partial \dot{x}_i}{\partial s_k} \cdot \frac{ds_k}{dt} = \frac{\partial \dot{x}_i}{\partial s_k} \cdot \frac{ds_k}{dt} = \frac{\partial V}{\partial x_i}, \quad i = 1, 2, 3 \quad (\text{E.7})$$

where the partial derivatives $\frac{\partial x_i}{\partial s_k}$ and $\frac{\partial \dot{x}_i}{\partial s_k}$ can be computed through (B.16). Furthermore, if one adds the multiplication of (E.6) times $-\frac{\partial \dot{x}_i}{\partial s_k}$ plus the product of (E.7) times $\frac{\partial x_i}{\partial s_k}$, it follows that:

$$-\frac{\partial \dot{x}_i}{\partial s_l} \cdot \frac{\partial x_i}{\partial s_k} \cdot \frac{ds_k}{dt} + \frac{\partial x_i}{\partial s_l} \cdot \frac{\partial \dot{x}_i}{\partial s_k} \cdot \frac{ds_k}{dt} = -\frac{\partial \dot{x}_i}{\partial s_l} \dot{x}_i + \frac{\partial x_i}{\partial s_l} \cdot \frac{\partial V}{\partial x_i} \quad (\text{E.8})$$

which can be more succinctly written as:

$$[s_l, s_k] \frac{ds_k}{dt} = \frac{\partial F}{\partial s_l} \quad (\text{E.9})$$

where two new concepts appear. The first one is the Lagrange brackets, which are defined as:

$$[s_l, s_k] = \frac{\partial x_i}{\partial s_l} \cdot \frac{\partial \dot{x}_i}{\partial s_k} - \frac{\partial \dot{x}_i}{\partial s_l} \cdot \frac{\partial x_i}{\partial s_k} \quad (\text{E.10})$$

and the function F , which is equal to:

$$F = V - T = V - \frac{1}{2} \dot{x}_i \dot{x}_i$$

Solving for ds_k/dt in (E.9) leaves exactly what one was looking for: an initial value problem expressed in terms of the Keplerian OEs. Skipping the mathematical specifics of the development (detailed in [32], eqs. 3.34-3.37), the final form of the equations is:

$$\left\{ \begin{array}{l} \frac{da}{dt} = \frac{2}{na} \frac{\partial F}{\partial M} \\ \frac{de}{dt} = \frac{\eta^2}{na^2 e} \frac{\partial F}{\partial M} - \frac{\eta}{na^2 e} \frac{\partial F}{\partial e} \\ \frac{di}{dt} = \frac{\cos i}{na^2 \eta \sin i} \frac{\partial F}{\partial \omega} - \frac{1}{na^2 \eta \sin i} \frac{\partial F}{\partial \Omega} \\ \frac{d\omega}{dt} = -\frac{\cos i}{na^2 \eta \sin i} \frac{\partial F}{\partial i} + \frac{\eta}{na^2 e} \frac{\partial F}{\partial e} \\ \frac{d\Omega}{dt} = \frac{1}{na^2 \eta \sin i} \frac{\partial F}{\partial i} \\ \frac{dM}{dt} = -\frac{\eta^2}{na^2 e} \frac{\partial F}{\partial e} - \frac{2}{na} \frac{\partial F}{\partial a} \end{array} \right. \quad (\text{E.11})$$

It is common to express the force function F as:

$$F = \frac{\mu}{r} + R - T = \frac{\mu}{2a} + R$$

where R is the disturbing function, and comprises all terms except the central body acceleration (\approx the two body part of the problem). Hence, the usual form of Lagrange Planetary Equations is:

$$\left\{ \begin{array}{l} \frac{da}{dt} = \frac{2}{na} \frac{\partial R}{\partial M} \\ \frac{de}{dt} = \frac{\eta^2}{na^2 e} \frac{\partial R}{\partial M} - \frac{\eta}{na^2 e} \frac{\partial R}{\partial e} \\ \frac{di}{dt} = \frac{\cos i}{na^2 \eta \sin i} \frac{\partial R}{\partial \omega} - \frac{1}{na^2 \eta \sin i} \frac{\partial R}{\partial \Omega} \\ \frac{d\omega}{dt} = -\frac{\cos i}{na^2 \eta \sin i} \frac{\partial R}{\partial i} + \frac{\eta}{na^2 e} \frac{\partial R}{\partial e} \\ \frac{d\Omega}{dt} = \frac{1}{na^2 \eta \sin i} \frac{\partial R}{\partial i} \\ \frac{dM}{dt} = n - \frac{\eta^2}{na^2 e} \frac{\partial R}{\partial e} - \frac{2}{na} \frac{\partial R}{\partial a} \end{array} \right. \quad (\text{E.12})$$

As a side note, Wiesel [9] provides yet another approach to obtain these equations in section 3.8.

E.2.1.1 Delaunay elements from the LPEs.

The structure of equation (E.9) as well as the symmetry of the Lagrangian brackets suggests that a simpler form of the LPEs may be reached, when using an adequate set of elements. In particular, consider a set of elements L, G, H such that:

$$\begin{aligned} [M, L] &= 1, & [M, G] &= 0, & [M, H] &= 0, \\ [\omega, L] &= 0, & [\omega, G] &= 1, & [\omega, H] &= 0, \\ [\Omega, L] &= 0, & [\Omega, G] &= 0, & [\Omega, H] &= 1, \end{aligned} \quad (\text{E.13})$$

In order to derive the expressions for L, G and H , it is necessary to apply the definition of the Lagrangian brackets and the chain rule. For the case of H , and considering the already known bracket $[\Omega, i]$:

$$\begin{aligned} [\Omega, i] &= [\Omega, L] \frac{\partial L}{\partial i} + [\Omega, G] \frac{\partial G}{\partial i} + [\Omega, H] \frac{\partial H}{\partial i} = [\Omega, H] \frac{\partial H}{\partial i} = \frac{\partial H}{\partial i} \\ &\Rightarrow \frac{\partial H}{\partial i} = [\Omega, i] = -na^2 \eta \sin i \\ &\Rightarrow H = na^2 \eta \cos i \end{aligned}$$

As a check, the brackets $[\Omega, e]$ and $[\Omega, a]$ can be computed, while it is also possible to derive H

directly from them. Proceeding in an analog manner with G and L leads to:

$$G = na^2\eta, \quad L = na^2$$

The set $L, G, H, l = M, g = \omega, h = \Omega$ is the so-called Delaunay element set, matching the definition provided in appendix A. To conclude, the LPEs for this set of elements become (by design):

$$\left\{ \begin{array}{l} \frac{dL}{dt} = \frac{\partial F}{\partial l}, \quad \frac{dl}{dt} = -\frac{\partial F}{\partial L} \\ \frac{dG}{dt} = \frac{\partial F}{\partial g}, \quad \frac{dg}{dt} = -\frac{\partial F}{\partial G} \\ \frac{dH}{dt} = \frac{\partial F}{\partial h}, \quad \frac{dh}{dt} = -\frac{\partial F}{\partial H} \end{array} \right. \quad (\text{E.14})$$

E.2.2 Gauss Variational Equations.

A possible drawback or limitation of the LPEs is that it assumes the existence of a force potential whose functional form is known. Nonetheless, there are some cases in which either only the force is modelled or it does not come from a potential field, as it happens with aerodynamic drag. Gauss Variational Equations involve only the components of the perturbing acceleration, allowing to model a wider spectrum of forces. Its derivation is also mathematically dense, as it can be seen in Wiesel [9], section 3.3. It involves several “happy thoughts” to reach the following expression:

$$\left\{ \begin{array}{l} \frac{da}{dt} = \frac{2e \sin \theta}{n\eta} a_r + \frac{2a\eta}{nr} a_\theta \\ \frac{de}{dt} = \frac{\eta \sin \theta}{na} a_r + \frac{\eta}{na^2 e} \left(\frac{a^2 \eta^2}{r} - r \right) a_\theta \\ \frac{di}{dt} = \frac{r \cos(\omega + \theta)}{na^2 \eta} a_N \\ \frac{d\Omega}{dt} = \frac{r \sin(\omega + \theta)}{na^2 \eta \sin i} a_N \\ \frac{d\omega}{dt} = -\frac{\eta \cos \theta}{nae} a_r - \frac{r \cot i \sin(\omega + \theta)}{na^2 \eta} a_N + \frac{\eta}{nae} \left(1 + \frac{1}{1 + e \cos \theta} \right) \sin \theta a_\theta \\ \frac{dM}{dt} = n - \frac{1}{na} \left(\frac{2r}{a} - \frac{\eta^2}{e} \cos \theta \right) a_r - \frac{\eta^2}{nae} \left(1 + \frac{1}{1 + e \cos \theta} \right) \sin \theta a_\theta \end{array} \right. \quad (\text{E.15})$$

where a_r, a_θ and a_N are the radial, azimuthal and normal (RTN) components of the acceleration on the spacecraft. These equations allow for a very intuitive evaluation of the quantitative effects of a

certain kind of acceleration. For example, it is clear that only an out-of-plane acceleration is able to change the inclination or the ascending node of the orbit. The problem of equation (E.15) is that, as it involves the use of the true anomaly θ , it requires the solution of Kepler's equation at every timestep. Another option is to substitute the variational equation of the mean anomaly by its true anomaly equivalent, or even integrate the seven of them.

To finalize, it should be remarked that both LPEs and GVEs as here presented become singular for null eccentricity and for equatorial/polar orbits, due to the in some sense poor election of the OEs. There are though several alternatives in the literature, in which LPEs and GVEs are expressed for non-singular elements, such as the Equinoctial elements or the Delaunay elements.

E.3 Elliptic anomaly mapping.

The parametrization of the elliptic motion of a spacecraft in its orbit plane may involve the use of three different angles: the true anomaly, the eccentric anomaly and the mean anomaly. Without stopping in its academic definitions, let's remark that the true anomaly is the most physically meaningful one, while the eccentric and the mean are basically mathematical constructs that simplify the motion parametrization.

That being said, it is usually impossible – or at least uncomfortable – to use just one of them. That is why a mapping between them is required, as it is also recurrently used in the software side.

E.3.1 Angles.

E.3.1.1 Eccentric to mean and viceversa.

The relation between mean and eccentric anomalies is more of a definition, as Kepler's equation states:

$$M = E - \sin E \tag{E.16}$$

It is quite clear that the direct transformation (*i.e.* $E \rightarrow M$) is trivial. The inverse transformation is a bit more tricky. There is no closed-form solution for $E = E(M)$, so an alternative way must be developed. A common exact solution of said equation consists of an infinite series of Bessel functions, which is not handy or worth the calculation. However, a simple iterative scheme can be obtained, solving for the linear term E and substituting the precedent value in the \sin function. A usually good initial approximation is $E_0 = M$, although for highly eccentric orbit, $E_0 = \pi$ yields

better results. In summary, this numeric method can be written as:

$$[P] \equiv \begin{cases} E_{i+1} = M + e \sin E_i \\ E_0 = M \end{cases} \quad (\text{E.17})$$

This is called a fixed-point iteration. Of course, several other methods can be implemented (*e.g.* Newton's Method).

E.3.1.2 True to eccentric and viceversa.

The position of the spacecraft in the perifocal frame can be parametrized by both the true and the eccentric anomaly:

$$\begin{cases} X = r \cos \theta = \frac{a\eta^2 \cos \theta}{1 + e \cos \theta} = a(\cos E - e) \\ Y = r \sin \theta = \frac{a\eta^2 \sin \theta}{1 + e \cos \theta} = b \sin E = a\eta \sin E \end{cases} \quad (\text{E.18})$$

These lead to a handy pair of equations for $\sin E$ and $\cos E$:

$$\cos E = \frac{e + \cos \theta}{1 + e \cos \theta} \quad (\text{E.19})$$

$$\sin E = \frac{\eta \sin \theta}{1 + e \cos \theta} \quad (\text{E.20})$$

In the seeking of a more concise relation between E and θ , they are substituted by their half angles, which after a little manipulation, leads to:

$$2 \cos^2 E/2 = 1 + \cos E = \frac{(1 + e)(1 + \cos \theta)}{1 + e \cos \theta} = \frac{(1 + e)2 \cos^2 \theta/2}{1 + e \cos \theta} \quad (\text{E.21})$$

$$\sin E = 2 \sin E/2 \cos E/2 = \eta \frac{2 \sin \theta/2 \cos \theta/2}{1 + e \cos \theta} \quad (\text{E.22})$$

Dividing (E.22) by (E.21) and simplifying:

$$\tan \frac{E}{2} = \sqrt{\frac{1 - e}{1 + e}} \tan \frac{\theta}{2} \quad (\text{E.23})$$

The inverse transformation is again trivial, by just solving for $\tan \theta/2$.

E.3.1.3 True to mean and viceversa.

As simple or absurd as it sounds, and although a closed form exists for the direct transformation (*i.e.* $\theta \rightarrow M$), the simplest procedure is to just concatenate the transformations (E.23) and (E.16).

E.3.2 Angle rates.

The eccentric and true anomaly rates are usually required, although the fact that they vary along any eccentric orbit makes them unpleasant to manipulate or integrate. In order to tackle their conversion to mean anomaly rate (or mean motion, which is constant along any unperturbed eccentric orbit) it is enough to calculate the time derivatives of the already prescribed equations, that is [31, appendix E]:

- A. Mean to eccentric rate: By differentiating in (E.16), the sensitivity is obtained:

$$\frac{dM}{dE} = 1 - e \cos E = \frac{\eta^2}{\rho} = \frac{r}{a} \quad (\text{E.24})$$

where $\rho = 1 + e \cos \theta$ as usual. The relation between the mean and eccentric rates is obtained by simply using the chain rule:

$$\frac{dM}{dt} = \dot{M} = n = \frac{dM}{dE} \frac{dE}{dt} = \frac{\eta^2}{\rho} \frac{dE}{dt} \Rightarrow \dot{E} = \frac{\rho}{\eta^2} n \quad (\text{E.25})$$

- B. Mean to true rate: Differentiating (E.19) and rearranging terms, the sensitivity of the true anomaly with respect to the eccentric is obtained[31]:

$$\frac{d\theta}{dE} = \frac{\eta}{1 - e \cos E} = \frac{\rho}{\eta} = \frac{b}{r} \quad (\text{E.26})$$

Combining (E.26) and (E.24), and taking time derivatives, it is pretty much straightaway to get $\dot{\theta}$:

$$\frac{d\theta}{dt} = \frac{d\theta}{dE} \left(\frac{dM}{dE} \right)^{-1} \frac{dM}{dt} \Rightarrow \dot{\theta} = \frac{\rho^2}{\eta^3} n \quad (\text{E.27})$$

E.3.3 Relative anomalies.

Relative motion may be expressed through relative elements, hence relative anomalies. In order to convert them, one must keep in mind that the aforementioned transformations are defined for absolute values. That is, when converting relative anomalies, firstly the absolute values must be computed before they are transformed. For example, consider the transformation from relative

eccentric anomaly to relative mean anomaly, assuming as inputs the relative value δE and the absolute value of the chief E_C . The diagram shown in E.1 shows the process of this conversion.

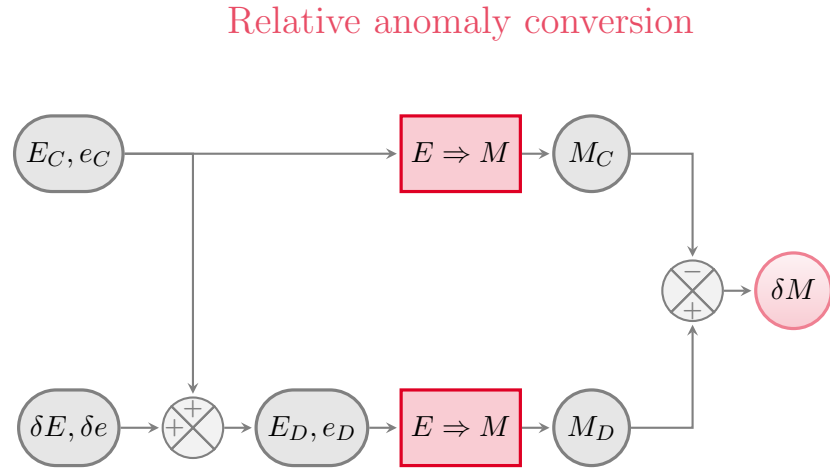


Figure E.1: Workflow of the relative anomaly transformation (eccentric to mean).

E.4 Kaula's functions.

The developments of Kaula's theory, in particular, equations (4.45) and (4.62), as well as its derivatives (4.96) and (4.97), can be computed for a given set of indices $lmpq$. Tables E.1, E.2 and E.3 include these functions for $l = \{2, 3, 4\}$, $m = \{0, 1, 2, 3, 4\}$, $p = \{0, 1, 2, 3, 4\}$ and $q = \{-4, -3, -2, -1, 0, 1, 2, 3, 4\}$.

l	m	p	$F_{lmp}(i)$
2	0	0	$-(3 \sin i^2)/8$
2	0	1	$(3 \sin i^2)/4 - 1/2$
2	0	2	$-(3 \sin i^2)/8$
2	1	0	$\sin i((3 \cos i)/4 + 3/4)$
2	1	1	$-(3 \cos i \sin i)/2$
2	1	2	$\sin i((3 \cos i)/4 - 3/4)$
2	2	0	$(3 \cos i)/2 + (3 \cos i^2)/4 + 3/4$
2	2	1	$3/2 - (3 \cos i^2)/2$
2	2	2	$(3 \cos i^2)/4 - (3 \cos i)/2 + 3/4$
3	0	0	$-(5 \sin i^3)/16$
3	0	1	$(15 \sin i^3)/16 - (3 \sin i)/4$
3	0	2	$(3 \sin i)/4 - (15 \sin i^3)/16$
3	0	3	$(5 \sin i^3)/16$
3	1	0	$-\sin i^2((15 \cos i)/16 + 15/16)$
3	1	1	$\sin i^2((45 \cos i)/16 + 15/16) - (3 \cos i)/4 - 3/4$
3	1	2	$(3 \cos i)/4 - \sin i^2((45 \cos i)/16 - 15/16) - 3/4$
3	1	3	$\sin i^2((15 \cos i)/16 - 15/16)$
3	2	0	$\sin i((15 \cos i)/4 + (15 \cos i^2)/8 + 15/8)$
3	2	1	$-\sin i((15 \cos i)/4 + (45 \cos i^2)/8 - 15/8)$
3	2	2	$-\sin i((15 \cos i)/4 - (45 \cos i^2)/8 + 15/8)$
3	2	3	$-\sin i((15 \cos i^2)/8 - (15 \cos i)/4 + 15/8)$
3	3	0	$(45 \cos i)/8 + (45 \cos i^2)/8 + (15 \cos i^3)/8 + 15/8$
3	3	1	$(45 \cos i)/8 - (45 \cos i^2)/8 - (45 \cos i^3)/8 + 45/8$
3	3	2	$(45 \cos i^3)/8 - (45 \cos i^2)/8 - (45 \cos i)/8 + 45/8$
3	3	3	$(45 \cos i^2)/8 - (45 \cos i)/8 - (15 \cos i^3)/8 + 15/8$
4	0	0	$(35 \sin i^4)/128$
4	0	1	$(15 \sin i^2)/16 - (35 \sin i^4)/32$
4	0	2	$(105 \sin i^4)/64 - (15 \sin i^2)/8 + 3/8$
4	0	3	$(15 \sin i^2)/16 - (35 \sin i^4)/32$
4	0	4	$(35 \sin i^4)/128$
4	1	0	$-\sin i^3((35 \cos i)/32 + 35/32)$
4	1	1	$\sin i^3((35 \cos i)/8 + 35/16) - \sin i((15 \cos i)/8 + 15/8)$
4	1	2	$(15 \cos i \sin i)/4 - (105 \cos i \sin i^3)/16$
4	1	3	$\sin i^3((35 \cos i)/8 - 35/16) - \sin i((15 \cos i)/8 - 15/8)$
4	1	4	$-\sin i^3((35 \cos i)/32 - 35/32)$
4	2	0	$-\sin i^2((105 \cos i)/16 + (105 \cos i^2)/32 + 105/32)$
4	2	1	$\sin i^2((105 \cos i)/8 + (105 \cos i^2)/8) - (15 \cos i^2)/8 - (15 \cos i)/4 - 15/8$
4	2	2	$(15 \cos i^2)/4 - \sin i^2((315 \cos i^2)/16 - 105/16) - 15/4$
4	2	3	$(15 \cos i)/4 - (15 \cos i^2)/8 - \sin i^2((105 \cos i)/8 - (105 \cos i^2)/8) - 15/8$
4	2	4	$-\sin i^2((105 \cos i^2)/32 - (105 \cos i)/16 + 105/32)$
4	3	0	$\sin i((315 \cos i)/16 + (315 \cos i^2)/16 + (105 \cos i^3)/16 + 105/16)$
4	3	1	$-\sin i((315 \cos i^2)/8 + (105 \cos i^3)/4 - 105/8)$
4	3	2	$-\sin i((315 \cos i)/8 - (315 \cos i^3)/8)$
4	3	3	$-\sin i((105 \cos i^3)/4 - (315 \cos i^2)/8 + 105/8)$
4	3	4	$\sin i((315 \cos i)/16 - (315 \cos i^2)/16 + (105 \cos i^3)/16 - 105/16)$
4	4	0	$(105 \cos i)/4 + (315 \cos i^2)/8 + (105 \cos i^3)/4 + (105 \cos i^4)/16 + 105/16$
4	4	1	$(105 \cos i)/2 - (105 \cos i^3)/2 - (105 \cos i^4)/4 + 105/4$
4	4	2	$(315 \cos i^4)/8 - (315 \cos i^2)/4 + 315/8$
4	4	3	$(105 \cos i^3)/2 - (105 \cos i)/2 - (105 \cos i^4)/4 + 105/4$
4	4	4	$(315 \cos i^2)/8 - (105 \cos i)/4 - (105 \cos i^3)/4 + (105 \cos i^4)/16 + 105/16$

Table E.1: Inclination functions $F_{lmp}(i)$

l	m	p	$dF_{lmp}/di(i)$
2	0	0	$-(3 \sin 2i)/8$
2	0	1	$(3 \sin 2i)/4$
2	0	2	$-(3 \sin 2i)/8$
2	1	0	$(3 \cos i)/4 + (3 \cos i^2)/2 - 3/4$
2	1	1	$3 \sin i^2 - 3/2$
2	1	2	$(3 \cos i^2)/2 - (3 \cos i)/4 - 3/4$
2	2	0	$-(3 \sin 2i)/4 - (3 \sin i)/2$
2	2	1	$(3 \sin 2i)/2$
2	2	2	$(3 \sin i)/2 - (3 \sin 2i)/4$
3	0	0	$(15 \cos i(\cos i^2 - 1))/16$
3	0	1	$-(3 \cos i(15 \cos i^2 - 11))/16$
3	0	2	$(3 \cos i(15 \cos i^2 - 11))/16$
3	0	3	$-(15 \cos i(\cos i^2 - 1))/16$
3	1	0	$-(15 \sin i(2 \cos i + 3 \cos i^2 - 1))/16$
3	1	1	$(15 \sin 2i)/16 + (135 \sin 3i)/64 + (3 \sin i)/64$
3	1	2	$(15 \sin 2i)/16 - (135 \sin 3i)/64 - (3 \sin i)/64$
3	1	3	$-(15 \sin i(2 \cos i - 3 \cos i^2 + 1))/16$
3	2	0	$(15(\cos i + 1)^2(3 \cos i - 2))/8$
3	2	1	$(105 \cos i)/8 - (15 \cos i^2)/2 - (135 \cos i^3)/8 + 15/4$
3	2	2	$(135 \cos i^3)/8 - (15 \cos i^2)/2 - (105 \cos i)/8 + 15/4$
3	2	3	$-(15(\cos i - 1)^2(3 \cos i + 2))/8$
3	3	0	$-(45 \sin 2i)/8 - (45 \sin 3i)/32 - (225 \sin i)/32$
3	3	1	$(45 \sin 2i)/8 + (135 \sin 3i)/32 - (45 \sin i)/32$
3	3	2	$(45 \sin 2i)/8 - (135 \sin 3i)/32 + (45 \sin i)/32$
3	3	3	$(45 \sin 3i)/32 - (45 \sin 2i)/8 + (225 \sin i)/32$
4	0	0	$(35 \cos i \sin i^3)/32$
4	0	1	$(35 \sin 4i)/64 - (5 \sin 2i)/32$
4	0	2	$-(15 \sin 2i)/64 - (105 \sin 4i)/128$
4	0	3	$(35 \sin 4i)/64 - (5 \sin 2i)/32$
4	0	4	$(35 \cos i \sin i^3)/32$
4	1	0	$-(35 \sin i^2(3 \cos i + 4 \cos i^2 - 1))/32$
4	1	1	$(75 \cos i)/16 + (145 \cos i^2)/8 - (105 \cos i^3)/16 - (35 \cos i^4)/2 - 5/2$
4	1	2	$(105 \sin i^4)/4 - (435 \sin i^2)/16 + 15/4$
4	1	3	$(145 \cos i^2)/8 - (75 \cos i)/16 + (105 \cos i^3)/16 - (35 \cos i^4)/2 - 5/2$
4	1	4	$(35 \sin i^2(3 \cos i - 4 \cos i^2 + 1))/32$
4	2	0	$-(105 \sin i(\cos i + 1)^2(2 \cos i - 1))/16$
4	2	1	$(15 \sin 2i)/8 + (315 \sin 3i)/32 + (105 \sin 4i)/16 + (15 \sin i)/32$
4	2	2	$(45 \sin 2i)/16 - (315 \sin 4i)/32$
4	2	3	$(15 \sin 2i)/8 - (315 \sin 3i)/32 + (105 \sin 4i)/16 - (15 \sin i)/32$
4	2	4	$-(105 \sin i(\cos i - 1)^2(2 \cos i + 1))/16$
4	3	0	$(105(\cos i + 1)^2(\cos i + 4 \cos i^2 - 3))/16$
4	3	1	$-(105 \cos i(\cos i + 1)^2(8 \cos i - 7))/8$
4	3	2	$(315 \sin i^2(4 \sin i^2 - 3))/8$
4	3	3	$-(105 \cos i(\cos i - 1)^2(8 \cos i + 7))/8$
4	3	4	$-(105(\cos i - 1)^2(\cos i - 4 \cos i^2 + 3))/16$
4	4	0	$-(735 \sin 2i)/16 - (315 \sin 3i)/16 - (105 \sin 4i)/32 - (735 \sin i)/16$
4	4	1	$(105 \sin i(\cos i + 1)^2(2 \cos i - 1))/2$
4	4	2	$(315 \sin 2i)/8 - (315 \sin 4i)/16$
4	4	3	$(105 \sin i(\cos i - 1)^2(2 \cos i + 1))/2$
4	4	4	$(315 \sin 3i)/16 - (735 \sin 2i)/16 - (105 \sin 4i)/32 + (735 \sin i)/16$

Table E.2: Derivatives of the inclination functions $dF_{lmp}/di(i)$

l	p	q	$G_{lpq}(e)$	dG_{lpq}/de
2	0	-2	0	0
2	0	-1	$(e(e^2 - 8))/16$	$(3e^2)/16 + (65e^4)/384 - 1/2$
2	0	0	$(13e^4)/16 - (5e^2)/2 + 1$	$(13e^3)/4 - 5e$
2	0	1	$-(e(123e^2 - 56))/16$	$(2355e^4)/128 - (369e^2)/16 + 7/2$
2	0	2	$-(e^2(115e^2 - 51))/6$	$17e - (230e^3)/3$
2	1	-2	$(e^2(7e^2 + 9))/4$	$(9e)/2 + 7e^3$
2	1	-1	$(3e(9e^2 + 8))/16$	$(81e^2)/16 + (1275e^4)/128 + 3/2$
2	1	0	$(3e^2)/2 + (15e^4)/8 + 1$	$3e + (15e^3)/2$
2	1	1	$(3e(9e^2 + 8))/16$	$(81e^2)/16 + (1275e^4)/128 + 3/2$
2	1	2	$(e^2(7e^2 + 9))/4$	$(9e)/2 + 7e^3$
2	2	-2	$-(e^2(115e^2 - 51))/6$	$17e - (230e^3)/3$
2	2	-1	$-(e(123e^2 - 56))/16$	$(2355e^4)/128 - (369e^2)/16 + 7/2$
2	2	0	$(13e^4)/16 - (5e^2)/2 + 1$	$(13e^3)/4 - 5e$
2	2	1	$(e(e^2 - 8))/16$	$(3e^2)/16 + (65e^4)/384 - 1/2$
2	2	2	0	0
3	0	-3	0	0
3	0	-2	$(e^2(e^2 + 6))/48$	$(e(e^2 + 3))/12$
3	0	-1	$(5e^3)/4 - e$	$(15e^2)/4 - (25e^4)/96 - 1$
3	0	0	$(423e^4)/64 - 6e^2 + 1$	$(423e^3)/16 - 12e$
3	0	1	$5e - 22e^3$	$(6025e^4)/48 - 66e^2 + 5$
3	0	2	$-(e^2(3065e^2 - 762))/48$	$-(e(3065e^2 - 381))/12$
3	0	3	$(163e^3)/4$	$-(3e^2(4295e^2 - 652))/16$
3	1	-3	$(23e^3)/12$	$(e^2(445e^2 + 138))/24$
3	1	-2	$(e^2(49e^2 + 22))/16$	$(e(49e^2 + 11))/4$
3	1	-1	$e + (5e^3)/2$	$(15e^2)/2 + (175e^4)/8 + 1$
3	1	0	$2e^2 + (239e^4)/64 + 1$	$4e + (239e^3)/16$
3	1	1	$3e + (11e^3)/4$	$(33e^2)/4 + (2405e^4)/96 + 3$
3	1	2	$(e^2(39e^2 + 106))/16$	$(e(39e^2 + 53))/4$
3	1	3	$(77e^3)/6$	$-(e^2(125e^2 - 1848))/48$
3	2	-3	$(77e^3)/6$	$-(e^2(125e^2 - 1848))/48$
3	2	-2	$(e^2(39e^2 + 106))/16$	$(e(39e^2 + 53))/4$
3	2	-1	$3e + (11e^3)/4$	$(33e^2)/4 + (2405e^4)/96 + 3$
3	2	0	$2e^2 + (239e^4)/64 + 1$	$4e + (239e^3)/16$
3	2	1	$e + (5e^3)/2$	$(15e^2)/2 + (175e^4)/8 + 1$
3	2	2	$(e^2(49e^2 + 22))/16$	$(e(49e^2 + 11))/4$
3	2	3	$(23e^3)/12$	$(e^2(445e^2 + 138))/24$
3	3	-3	$(163e^3)/4$	$-(3e^2(4295e^2 - 652))/16$
3	3	-2	$-(e^2(3065e^2 - 762))/48$	$-(e(3065e^2 - 381))/12$
3	3	-1	$5e - 22e^3$	$(6025e^4)/48 - 66e^2 + 5$
3	3	0	$(423e^4)/64 - 6e^2 + 1$	$(423e^3)/16 - 12e$
3	3	1	$(5e^3)/4 - e$	$(15e^2)/4 - (25e^4)/96 - 1$
3	3	2	$(e^2(e^2 + 6))/48$	$(e(e^2 + 3))/12$
3	3	3	0	0

l	p	q	$G_{lpq}(e)$	dG_{lpq}/de
4	0	-4	0	0
4	0	-3	$-e^3/48$	$-(e^2(35e^2 + 48))/768$
4	0	-2	$-(e^2(2e^2 - 3))/6$	$e - (4e^3)/3$
4	0	-1	$(3e(25e^2 - 8))/16$	$(225e^2)/16 - (1875e^4)/128 - 3/2$
4	0	0	$(199e^4)/8 - 11e^2 + 1$	$(199e^3)/2 - 22e$
4	0	1	$-(e(765e^2 - 104))/16$	$(189175e^4)/384 - (2295e^2)/16 + 13/2$
4	0	2	$-(3e^2(107e^2 - 17))/2$	$51e - 642e^3$
4	0	3	$(3751e^3)/48$	$-(e^2(1764595e^2 - 180048))/768$
4	0	4	$(4943e^4)/24$	$(4943e^3)/6$
4	1	-4	$(67e^4)/48$	$(67e^3)/12$
4	1	-3	$(49e^3)/48$	$(e^2(12725e^2 + 2352))/768$
4	1	-2	$(3e^2(7e^2 + 2))/8$	$(3e(7e^2 + 1))/2$
4	1	-1	$(e(33e^2 + 8))/16$	$(99e^2)/16 + (9415e^4)/384 + 1/2$
4	1	0	$e^2 + (65e^4)/16 + 1$	$2e + (65e^3)/4$
4	1	1	$-(3e(e^2 - 24))/16$	$(4725e^4)/128 - (9e^2)/16 + 9/2$
4	1	2	$-(e^2(179e^2 - 318))/24$	$-(e(179e^2 - 159))/6$
4	1	3	$(1541e^3)/48$	$-(e^2(117395e^2 - 73968))/768$
4	1	4	$(555e^4)/8$	$(555e^3)/2$
4	2	-4	$(745e^4)/48$	$(745e^3)/12$
4	2	-3	$(145e^3)/16$	$(5e^2(4715e^2 + 1392))/256$
4	2	-2	$(5e^2(31e^2 + 12))/12$	$10e + (155e^3)/3$
4	2	-1	$(5e(27e^2 + 8))/16$	$(405e^2)/16 + (36335e^4)/384 + 5/2$
4	2	0	$5e^2 + (105e^4)/8 + 1$	$10e + (105e^3)/2$
4	2	1	$(5e(27e^2 + 8))/16$	$(405e^2)/16 + (36335e^4)/384 + 5/2$
4	2	2	$(5e^2(31e^2 + 12))/12$	$10e + (155e^3)/3$
4	2	3	$(145e^3)/16$	$(5e^2(4715e^2 + 1392))/256$
4	2	4	$(745e^4)/48$	$(745e^3)/12$
4	3	-4	$(555e^4)/8$	$(555e^3)/2$
4	3	-3	$(1541e^3)/48$	$-(e^2(117395e^2 - 73968))/768$
4	3	-2	$-(e^2(179e^2 - 318))/24$	$-(e(179e^2 - 159))/6$
4	3	-1	$-(3e(e^2 - 24))/16$	$(4725e^4)/128 - (9e^2)/16 + 9/2$
4	3	0	$e^2 + (65e^4)/16 + 1$	$2e + (65e^3)/4$
4	3	1	$(e(33e^2 + 8))/16$	$(99e^2)/16 + (9415e^4)/384 + 1/2$
4	3	2	$(3e^2(7e^2 + 2))/8$	$(3e(7e^2 + 1))/2$
4	3	3	$(49e^3)/48$	$(e^2(12725e^2 + 2352))/768$
4	3	4	$(67e^4)/48$	$(67e^3)/12$
4	4	-4	$(4943e^4)/24$	$(4943e^3)/6$
4	4	-3	$(3751e^3)/48$	$-(e^2(1764595e^2 - 180048))/768$
4	4	-2	$-(3e^2(107e^2 - 17))/2$	$51e - 642e^3$
4	4	-1	$-(e(765e^2 - 104))/16$	$(189175e^4)/384 - (2295e^2)/16 + 13/2$
4	4	0	$(199e^4)/8 - 11e^2 + 1$	$(199e^3)/2 - 22e$
4	4	1	$(3e(25e^2 - 8))/16$	$(225e^2)/16 - (1875e^4)/128 - 3/2$
4	4	2	$-(e^2(2e^2 - 3))/6$	$e - (4e^3)/3$
4	4	3	$-e^3/48$	$-(e^2(35e^2 + 48))/768$
4	4	4	0	0

Table E.3: Eccentricity functions and its derivatives $G_{lpq}(e)$

E.5 Series expansions for β and e/β .

In order to match the convenient formulation from Kaula for G_{lpq} results, the series expansions for $\beta = e/(1+\eta)$ and e/β are now provided, as they appear recurrently in the P_{lpqk} and G_{lpqk} functions.

E.5.1 β series expansion.

Brouwer and Clemence [30, page 63] show the series development of β up to the seventh power (β^7) in terms of the eccentricity, retaining terms of up to seventh power (e^7). The results are:

$$\left. \begin{array}{l} \beta = \frac{1}{2}e + \frac{1}{8}e^3 + \frac{1}{16}e^5 + \frac{5}{128}e^7 + \mathcal{O}(e^9) \\ \beta^2 = \frac{1}{4}e^2 + \frac{1}{8}e^4 + \frac{5}{64}e^6 + \mathcal{O}(e^8) \end{array} \right\} \quad (\text{E.28a})$$

$$\left. \begin{array}{l} \beta^3 = \frac{1}{8}e^3 + \frac{3}{32}e^5 + \frac{9}{128}e^7 + \mathcal{O}(e^9) \\ \beta^4 = \frac{1}{16}e^4 + \frac{1}{16}e^6 + \mathcal{O}(e^8) \end{array} \right\} \quad (\text{E.28b})$$

$$\left. \begin{array}{l} \beta^5 = \frac{1}{32}e^5 + \frac{5}{128}e^7 + \mathcal{O}(e^9) \\ \beta^6 = \frac{1}{64}e^6 + \mathcal{O}(e^8) \end{array} \right\} \quad (\text{E.28c})$$

$$\left. \begin{array}{l} \beta^7 = \frac{1}{128}e^7 + \mathcal{O}(e^9) \end{array} \right\} \quad (\text{E.28d})$$

$$\left. \begin{array}{l} \beta^8 = \frac{1}{256}e^8 + \mathcal{O}(e^{10}) \end{array} \right\} \quad (\text{E.28e})$$

$$\left. \begin{array}{l} \beta^9 = \frac{1}{512}e^9 + \mathcal{O}(e^{11}) \end{array} \right\} \quad (\text{E.28f})$$

$$\left. \begin{array}{l} \beta^{10} = \frac{1}{1024}e^{10} + \mathcal{O}(e^{12}) \end{array} \right\} \quad (\text{E.28g})$$

E.5.2 e/β series expansion.

This series expansion is not explicitly mentioned, though it is necessary, as it is not directly derived from the β expansion (at least in MATLAB). Using (E.28), we arrive to the following result:

$$\left. \begin{array}{l} \left(\frac{e}{\beta}\right)^1 = 2 - \frac{1}{2}e^2 - \frac{5}{16}e^4 + \mathcal{O}(e^6) \end{array} \right\} \quad (\text{E.29a})$$

$$\left. \begin{array}{l} \left(\frac{e}{\beta}\right)^2 = 4 - 2e^2 - \frac{9}{8}e^4 + \mathcal{O}(e^6) \end{array} \right\} \quad (\text{E.29b})$$

$$\left. \begin{array}{l} \left(\frac{e}{\beta}\right)^3 = 8 - 6e^2 - \frac{27}{4}e^4 + \mathcal{O}(e^6) \end{array} \right\} \quad (\text{E.29c})$$

$$\left. \begin{array}{l} \left(\frac{e}{\beta}\right)^4 = 16 - 16e^2 - 8e^4 + \mathcal{O}(e^6) \end{array} \right\} \quad (\text{E.29d})$$

$$\left. \begin{array}{l} \left(\frac{e}{\beta}\right)^5 = 32 - 40e^2 - 25e^4 + \mathcal{O}(e^6) \end{array} \right\} \quad (\text{E.29e})$$

$$\left. \begin{array}{l} \left(\frac{e}{\beta}\right)^6 = 64 + \mathcal{O}(e^6) \end{array} \right\} \quad (\text{E.29f})$$

$$\left. \begin{array}{l} \left(\frac{e}{\beta}\right)^7 = 128 + \mathcal{O}(e^6) \end{array} \right\} \quad (\text{E.29g})$$

Bibliography

General

Books

- [1] W. Fehse. *Automated Rendezvous and Docking of Spacecraft*. Cambridge Aerospace Series. Cambridge: Cambridge University Press, 2003. DOI: [10.1017/CBO9780511543388](https://doi.org/10.1017/CBO9780511543388) (cit. on pp. 2, 3, 19, 20).
- [2] K. T. Alfriend and Srinivas. *Spacecraft Formation Flying*. 1st ed. Oxford, United Kingdom: Elsevier, 2010 (cit. on pp. 3, 13, 14, 72, 80, 81, 169).
- [3] O. Montenbruck and E. Gill. *Satellite Orbits: Models, Methods and Applications*. 1st ed. Wessling, Germany: Springer, 2001 (cit. on pp. 4, 21, 66, 67).
- [9] W. E. Wiesel. *Modern Astrodynamics*. 2nd ed. Beavercreek, Ohio: Aphelion Press, 2010 (cit. on pp. 14, 65, 69, 101, 134, 135, 169, 171, 173, 185, 186).
- [16] R. H. Battin. *An Introduction to the Mathematics and Methods of Astrodynamics, Revised Edition*. 1st ed. Reston, Virginia: American Institute of Aeronautics and Astronautics, 1999 (cit. on p. 35).
- [30] D. Brouwer and G. M-Clemence. *Methods of Celestial Mechanics*. Brackley Square House, London: Academic Press, 1961 (cit. on pp. 78, 79, 101, 176, 195).
- [31] H. Schaub and J. L. Junkins. *Analytical Mechanics of Space Systems*. Reston, VA: AIAA Education Series, Oct. 2003. DOI: [10.2514/4.861550](https://doi.org/10.2514/4.861550) (cit. on pp. 79, 80, 189).
- [42] P. K. S. Dennis D. McCarthy. *Time: From Earth Rotation to Atomic Physics*. Wiley-VCH, 2009. ISBN: 3527407804; 9783527407804 (cit. on p. 150).
- [43] B. D. Tapley, B. E. Schutz, and G. H. Born. *Statistical Orbit Determination*. 1st ed. Amsterdam, Netherlands: Elsevier, 2004 (cit. on pp. 150–154).

Articles

- [8] G. W. Hill. “Researches in the Lunar Theory”. In: *American Journal of Mathematics* 1.2 (1878), pp. 129–147. DOI: [10.2307/2369304](https://doi.org/10.2307/2369304) (cit. on pp. 11, 17).

- [10] W. H. Clohessy and R. S. Wiltshire. “Terminal Guidance System for Satellite Rendezvous”. In: *Journal of the Aerospace Sciences* 27.9 (1960), pp. 653–658. DOI: [10.2514/8.8704](https://doi.org/10.2514/8.8704) (cit. on p. 20).
- [14] O. Montenbruck, M. Kirschner, and S. D’Amico. “E/I-vector separation for safe switching of the GRACE formation”. In: *Aerospace Science and Technology* 10 (2006), pp. 628–635. DOI: [10.1016/j.ast.2006.04.001](https://doi.org/10.1016/j.ast.2006.04.001) (cit. on pp. 34, 39).
- [18] J. Sullivan, S. Grimberg, and S. D’Amico. “Comprehensive Survey and Assessment of Spacecraft Relative Motion Dynamics Models”. In: *Journal of Guidance, Control & Dynamics* 40.8 (2017), pp. 1837–1859. DOI: [10.2514/1.G002309](https://doi.org/10.2514/1.G002309) (cit. on pp. 43, 116, 121, 122).
- [40] H. Schaub. “Relative Orbit Geometry Through Classical Orbit Element Differences”. In: *Journal of Guidance, Control & Dynamics* 27.5 (2004), pp. 839–848. DOI: [10.2514/1.12595](https://doi.org/10.2514/1.12595) (cit. on pp. 136, 141, 142, 166, 167).
- [46] H. Schaub and K. T. Alfriend. “Hybrid Cartesian and Orbit Element Feedback Law for Formation Flying Spacecraft”. In: *Journal of Guidance, Control & Dynamics* 25.2 (2002), pp. 387–393. DOI: [10.2514/2.4893](https://doi.org/10.2514/2.4893) (cit. on p. 167).
- [47] N. Capitaine. “The Celestial Pole Coordinates”. In: *Celestial Mechanics and Dynamical Astronomy* 48 (1990), pp. 127–143.

Eccentric Dynamics

Articles

- [4] K. Yamanaka and F. Ankersen. “New State Transition Matrix for Relative Motion on an Arbitrary Elliptical Orbit”. In: *Journal of Guidance, Control & Dynamics* 25.1 (2002), pp. 60–66. DOI: [10.2514/2.4875](https://doi.org/10.2514/2.4875) (cit. on pp. 5, 15, 43, 46, 51, 52, 176).
- [13] M. Eckstein, C. Rajasingh, and P. Blumer. “Colocation Strategy and Collision Avoidance for the Geostationary Satellites at 19 Degrees West”. In: *CNES International Symposium on Space Dynamics*. Vol. 25. Oberpfaffenhofen, Germany: DLR GSOC, Nov. 1989, pp. 60–66 (cit. on pp. 33, 34, 122, 135, 136).
- [15] S. D’Amico and O. Montenbruck. “Proximity Operations of Formation-Flying Spacecraft Using an Eccentricity/Inclination Vector Separation”. In: *Journal of Guidance, Control & Dynamics* 29.3 (2006), pp. 554–563. DOI: [10.2514/1.15114](https://doi.org/10.2514/1.15114) (cit. on pp. 34, 122, 129, 136, 141, 143).

- [19] J. Tschauner and P. Hempel. “Optimale Beschleunigungsprogramme für das Rendezvous-Manöver”. In: *Astronautica Acta* 10 (1964), pp. 296–307 (cit. on p. 43).
- [20] T. Carter. “State Transition Matrices for Terminal Rendezvous Studies: Brief Survey and New Example”. In: *Journal of Guidance Control and Dynamics* 21 (Jan. 1998), pp. 148–155. DOI: [10.2514/2.4211](https://doi.org/10.2514/2.4211) (cit. on p. 43).
- [21] T. Vincent Peters and R. Noomen. “Linear Cotangential Transfers and Safe Orbits for Elliptic Orbit Rendezvous”. In: *Journal of Guidance, Control & Dynamics* 44.4 (2021), pp. 732–748. DOI: [10.2514/1.G005152](https://doi.org/10.2514/1.G005152) (cit. on pp. 44, 56–58, 60, 144, 163, 176).
- [48] R. Broucke. “On the Matrizant of the Two-Body Problem”. In: *Astronomy and Astrophysics* 6 (June 1970), p. 173.

Perturbations

Books

- [22] A. H. Nayfeh. *Perturbation Methods*. Weinheim, Germany: Wiley-VCH, 2004 (cit. on pp. 69, 72).
- [32] W. M. Kaula. *Theory of Satellite Geodesy*. Mineola, New York: Dover Publications, 2013 (cit. on pp. 85–87, 91, 96, 103, 107, 176, 183, 184).
- [34] F. Tisserand. *Traité de Mécanique Céleste*. Vol. 1. Paris, 1889 (cit. on p. 91).

Articles

- [5] D.-W. Gim and K. Alfriend. “State Transition Matrix of Relative Motion for the Perturbed Noncircular Reference Orbit”. In: *Journal of Guidance Control and Dynamics* 26 (Nov. 2003), pp. 956–971. DOI: [10.2514/2.6924](https://doi.org/10.2514/2.6924) (cit. on pp. 5, 73, 80, 82, 117, 127, 176, 182).
- [27] D. Brouwer. “Solution of the problem of artificial satellite theory without drag”. In: *Astronomical Journal* 64.5 (Nov. 1959), p. 378. DOI: [10.1086/107958](https://doi.org/10.1086/107958) (cit. on pp. 73, 74).
- [28] G. Gaias, C. Colombo, and M. Lara. “Accurate Osculating/Mean Orbital Elements Conversions for Spaceborne Formation Flying”. In: (Feb. 2018). https://www.researchgate.net/publication/340378956_Accurate_OsculatingMean_Orbital_Elements_Conversions_for_Spaceborne_Formation_Flying (cit. on pp. 74, 138).
- [29] R. H. Lyddane. “Small eccentricities or inclinations in the Brouwer theory of the artificial satellite”. In: *Astronomical Journal* 68 (Oct. 1963), p. 555. DOI: [10.1086/109179](https://doi.org/10.1086/109179) (cit. on pp. 74, 79).

- [35] K. Alfriend and H. Yan. “An Orbital Elements Based Approach to the Nonlinear Formation Flying Problem”. In: Toulouse, France, Feb. 2016 (cit. on p. 121).
- [36] G. Gaias, J. Ardaens, and O. Montenbruck. “Model of J2 Perturbed Satellite Relative Motion with Time-Varying Differential Drag”. In: *Celestial Mechanics and Dynamical Astronomy* (2015) (cit. on p. 121).
- [37] A. Koenig, T. Guffanti, and S. D’Amico. “New State Transition Matrices for Relative Motion of Spacecraft Formations in Perturbed Orbits”. In: Sept. 2016. DOI: [10.2514/6.2016-5635](https://doi.org/10.2514/6.2016-5635) (cit. on p. 121).
- [38] S. D’Amico. *Relative Orbital Elements as Integration Constants of Hill’s Equations*. TN 05-08. Oberpfaffenhofen, Germany: Deutsches Zentrum für Luft- und Raumfahrt (DLR), 2005 (cit. on pp. 122, 136, 141, 158, 176).
- [39] D.-W. Gim and K. T. Alfriend. “Satellite Relative Motion Using Differential Equinoctial Elements”. In: *Celestial Mechanics and Dynamical Astronomy* 92.4 (2005), pp. 295–336. DOI: [10.1007/s10569-004-1799-0](https://doi.org/10.1007/s10569-004-1799-0) (cit. on pp. 136, 137).
- [49] G. Gaias, J.-S. Ardaens, and C. Colombo. “Precise line-of-sight modelling for angles-only relative navigation”. In: *Advances in Space Research* 67.11 (2021). Satellite Constellations and Formation Flying, pp. 3515–3526. DOI: [10.1016/j.asr.2020.05.048](https://doi.org/10.1016/j.asr.2020.05.048).
- [50] G. Gaias, C. Colombo, and M. Lara. “Analytical Framework for Precise Relative Motion in Low Earth Orbits”. In: *Journal of Guidance, Control, and Dynamics* 43.5 (2020), pp. 915–927. DOI: [10.2514/1.G004716](https://doi.org/10.2514/1.G004716).
- [51] A. Biria and R. Russell. “A Satellite Relative Motion Model Including J2 and J3 via Vinti’s Intermediary”. In: Feb. 2016.

Matlab Exchange libraries

- [52] F. G. Nievinski. *subtightplot*. <https://www.mathworks.com/matlabcentral/fileexchange/39664-subtightplot>. 2013.
- [53] J. C. Lansey. *linspecer*. <https://www.mathworks.com/matlabcentral/fileexchange/42673-beautiful-and-distinguishable-line-colors-colormap>. 2015.
- [54] Jan. *WindowAPI*. <https://www.mathworks.com/matlabcentral/fileexchange/31437-windowapi>. 2013.

- [55] T. Davis. *Arrow3*. <https://www.mathworks.com/matlabcentral/fileexchange/14056-arrow3>. 2022.
- [56] E. Duenisch. *latexTable*. <https://www.mathworks.com/matlabcentral/fileexchange/44274-latextable>. 2016.

Websites & others

- [6] S.-S. Exchange. *Practical Uses of an STM*. 2019. URL: <https://space.stackexchange.com/questions/32916> (cit. on p. 6).
- [7] ESA. *Precise Orbit Determination*. 2011. URL: https://gssc.esa.int/navipedia/index.php/Precise_Orbit_Determination (cit. on p. 6).
- [11] Mathworks. *Convert complex diagonal form into real diagonal form*. 2022. URL: <https://www.mathworks.com/help/matlab/ref/cdf2rdf.html> (cit. on p. 24).
- [44] M. R. Delgado. *Lecture notes: Basics of Orbital Mechanics I*. Apr. 2008 (cit. on p. 153).